Università degli studi di Padova

Dipartimento di ingegneria civile, edile e ambientale

Department of civil, environmental and architectural engineering

Corso di Laurea Magistrale in Ingegneria civile

Tesi di Laurea.

Assessment of grouted rock-bolts behaviour subjected to axial loads

Relatore:
Chiar.mo PROF. Fabio Gabrieli
Corelatore:
Chiar.mo PROF. Yannick Fargier

Laureando: Mohamed Labrag
Matricola:1239041

Anno accademico 2021/2022

Contents

List of Figures

List of Tables

1 Acknowledgements

I wanted to show my deepest appreciation to all the members of the RRo laboratory, who welcomed me to develop my thesis. I am really grateful to each one of you, you've all been great examples of professionalism and hard work. I wanted to thank you all for creating a great working environment that made me enjoy each single one of my working days. I will always remember you all as a great working team. Each one of you will always have my deepest gratitude.
In particularly I would love to thank my supervisor Yannick Fargier who has been a great mentor for me during these months in Lyon. I am deeply grateful to him for all the things that he has taught me, the insights he has given me and all the time that he has dedicated to me and to my internship work. I strongly believe that under his supervision I have grown both professionally and personally. I will always be thankful to him, as I can not forget how his door was always open each time I had a doubt or a question. I am really appreciative that I had the great pleasure of working under his guidance during these months.

I can not write these acknowledgements, without thanking in particular my office colleagues. Thank you for sharing this experience with me. I am extremely delighted that during these months I had the pleasure to know you both as friends and as colleagues. Working with you has been such a pleasing experience. I sincerely hope that our paths will get to cross again in the future.

A special acknowledgement goes also to my professor Fabio Gabrieli, without him this experience would have never been possible. I want to thank him and show him my deepest recognition for his extreme availability: he would always find the time and attention to support and advice his students no matter what, and no one can deny his great dedication to his work and to his students.

A special thank you goes also to you, who have always been by my side, giving me all the support that I needed during and before this experience.

And finally I want to thank my family, particularly my parents who have made many sacrifices for me to get at this point and I will never forget that.

2 Introduction

In mountain environments an important aspect, both from an economical and from a technical point of view, is the protection against gravitational hazards. Rock-falling in fact can cause tragic events not only to engineering and architectural works but also to human lives. These are some among the reasons that make the mitigation measures and protection structures, like rock-bolts and cable nets for example, extremely important .

It becomes then very critical for us, as geotechnical and civil engineers, to understand properly the behaviour of these structures, and of the elements they are composed by.

It is not a case, in fact, that the testing campaigns that will be presented in this work were commissioned by SNCF (Société Nationale des Chemins de fer Français), which acknowledges that a better understanding of these structures can lead to an improvement in the design approach, which can translate in a signification gain, not only economical but also in the safety of human lives.

The aim of this thesis is to study the foundations of rockfall nets, which are usually made by grouted rock-bolts. Studying the behaviour of these elements is not an easy task, in fact, they are not only influenced by the characteristics of the steel bar and the grout, but also by the ones of the surrounding rock, and by its state. As it will be presented in this work, in fact, the state of the rock massif can change the reaction of these elements: a fractured rock and a non-fractured one react differently.

To accomplish this objective and study how these elements act once loaded, the rock-bolts were monitored with the use of fibre optic and sensors in the head of the anchorage that measured the displacements and the loading.

During this work the applied loads were axial ones, which were applied with the use of a hydraulic jack on a three meters bar, which had only the last meter grouted. This was done on three different sites : Seyssel, Bourg-d'Oisans and Mongalgon.

The behaviour of these elements has been studied also with some numerical tools. With the use of the software Abaqus, in fact, an axisymmetric model that represents a pull-out test, with the same geometry as the one realized for the in situ tests, was developed. This model has enabled us to compare its results to the ones obtained from the campaign tests.

In addiction to this model a FEM software, called ANCHOR, was developed by Jean-Pierre Rajot to study the influence of the system stiffness on the reaction of the anchorage. This software also was very important to have a comparison with the in situ tests.

3 Introduction to the rock-bolts

Rock-bolts were introduced in the end of the 1800s and they have been employed in different sectors since then. They were used in the beginning of the 20^{th} century in coal mines and since then they become a prominent instrument in the rock support for underground mines and tunnels.
Since its introduction this technique has been important in different domains:

- Tunnelling: rock-bolts can be an important tool for the sustain of the excavation.
- Excavations: this technique can be used during excavation for the realisation of retaining walls.
- Foundations: the use of the rock-bolts can produce an improvement in the soil features; we can improve the resistance and decrease the deformability of the ground.
- Protection structures against gravitational hazards: rock-bolts are usually used as a foundation for these structures.

According to Windsor (1997) we can identify four principal elements in a reinforcement system:

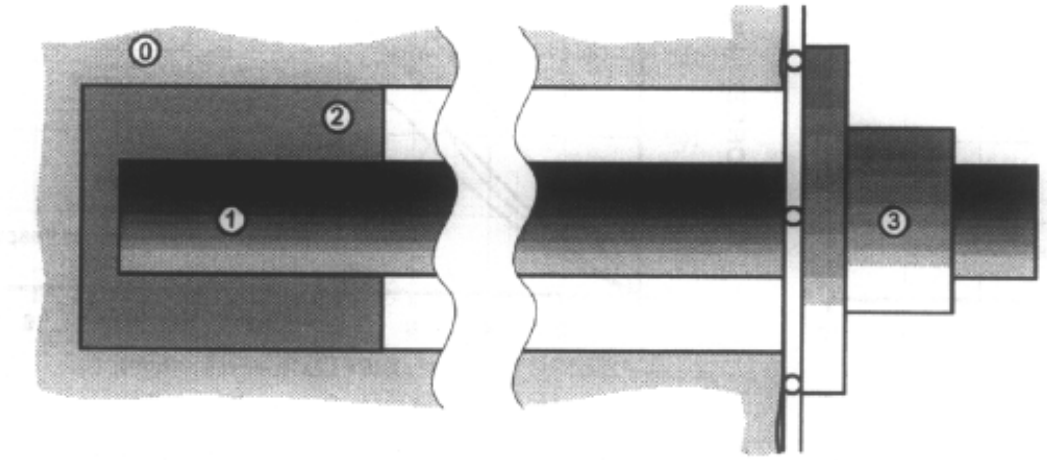

Figure 3.1: The principal components of a reinforcement system, according to Windsor (1997)

- (0), the rock.
- (1), the reinforcement element(for example a steel bar, a cable etc.).
- (2), the internal fixture.
- (3), the external fixture.

This can schematically represent the design of an anchorage. We drill a cavity in the rock, put a rigid element inside it and fix this element to the rock somehow. Inside this general procedure we can have different distinctions for each type of anchorage.

- Active anchorage: the interaction between the performed system and the soil arise immediately after its construction, there is no need of a relative displacement between soil and element to load the latter. An example are the cable-bolts which are pre-stressed elements.
- Passive anchorage: the interaction between the element and the soil is possible only if there is a relative displacement between the two. Examples of techniques where we use passive anchorages are soil nailing and rock bolting.

As previously introduced in this thesis we will analyse the behaviour of grouted rock-bolts.

3.1 Application of grouted rock-bolts

As already introduced, different types of structures in civil engineering might need the use of fully grouted rock-bolts: underground structures (tunnels, mines and quarries), foundations, slope and landslide stabilisation, excavations (road trenches, open-air mines and quarries).
The success of these elements is linked to the many advantages they have:

- The simple realisation: the construction of these elements is in fact particularly easy and a team of three people is generally sufficient for the job.
- The low installation price: the facility and rapidity of the realisation, combined with the use of cheap materials, make these structures quite competitive from an economical point of view.
- The flexibility in the application: they can be an independent geotechnical structure or combined with other structures, like the projected concrete, cable nets or wire meshes to create lightweight supports.
- A non bulky device: these devises are buried in the soil for the 90% of their length.
- An important durability of these structures.
- An ease in maintenance: compared to active anchorages, in fact, the conservation of these elements is far easier.

In the underground applications, the cavity excavation decompresses the rock and causes displacements toward the interior of the hole. To resist this movement, anchorages are implanted perpendicularly to the perimeter of the cavity, going inside the rock for several meters. The application of the rock-bolts combined with shotcrete reinforces the rock massif, and decreases the deformations.

In the case of foundations on rock, especially large-scale works , sustained with piles of large height, or for more modest works made on slopes with adverse

discontinuities, then the usual solutions (superficial and semi-deep foundations) are not sufficient. It becomes usually mandatory to reinforce the ground with fully grouted anchorages.

In open-air excavations, to confine and reinforce the ground, anchorages are used similarly to underground works, always in combination with a confinement (like reinforced shotcrete).

For the stabilization of natural slopes, pre-stressed cable anchors can be a valid solution, because the pre-stressing force reduces the displacements of the unstable blocks. Although the use of passive fully-grouted anchorages is surely economically convenient, but can also be technically interesting because they are stressed only when a displacement is registered. So even if they enable bigger displacements compared to the active anchorages, the lack of prestressing avoids the presence of creep and relaxation which are effects of the pretentioning. These elements can also be used for the reinforcement of slopes before the beginning of an excavation.

These elements can be used also to fix the passive protection structures against gravitational hazard, these structures, such as cable nets, are used to stop falling rocks. We can observe an example of these elements in the figure 3.2.

Figure 3.2: Example of protection structures against gravitational hazard

3.2 Anchorages role

In their different field of applications anchorages can play different roles:

- Reinforcement: in fractured rocks , the anchorages help with the use of their rigidity and resistance, so they end up improving the resistance of the system and decrease its deformability. These anchorages work as a reinforcement in the rock, creating binding forces between the different blocks.
- rock confinement: the application of confinement stress to the soil with the use of anchorages has a local effect on the stresses around the rock-bolt, which

has the effect of improving the shear resistance. This is usually the role of active anchorages where pre-stressing the anchorage results in a compression of the surrounding soil. This compression decreases the aperture degree of the discontinuities and improves the soil's resistance. With the use of passive anchorages the confinement effect is always present but it is not controllable.

- Jointed rock mass stabilization: this role is applied when we use an anchorage to fix a structure or an unstable block to the stable rock behind. The anchorage is then stressed in the head or at the discontinuity with a traction force, a shear one or by a combination of both.

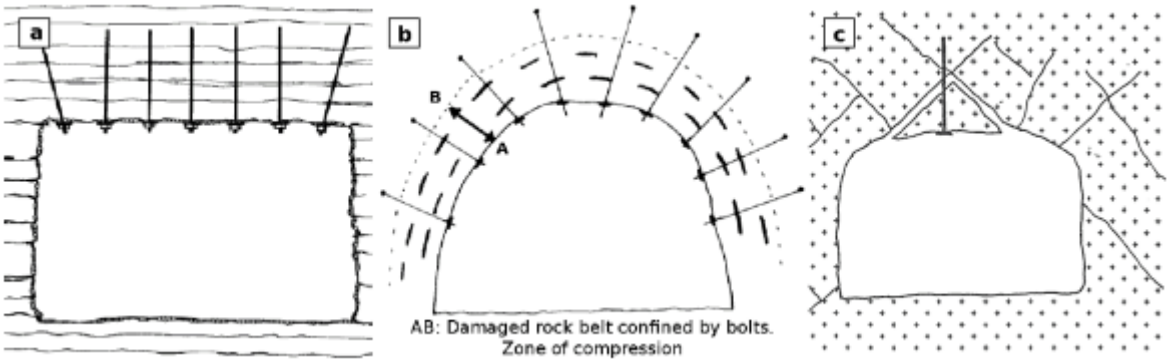

Figure 3.3: Anchorage roles (Blanco Martin, 2012)

The choice of the type of anchorage has to be compatible with its role. The mechanical anchorages are preferred for the confinement role for the possibility of pre-stressing them immediately, they can play the stabilization role too, but they can not be used as a reinforcement, because the lack of connection between rock and bolt in the free segment do not give the possibility of securing effectively the rock. On the other side the fully grouted, the frictional and the mixed anchorages can be used in all three roles.

The role of the anchorage is extremely important because it also changes the design approach. During the reinforcement or the confinement, it is necessary to consider a composite medium, where the rock-bolt contribute to the mechanical properties of the rock. While in a stabilization role the design process consists simply in proposing different failure mechanisms of the bolts and calculating the resistance of each anchorage.

In the gravitational hazard domain, the passive grouted anchorage, if used for the rock block support or as a foundation for active or passive protection structures, has a stabilization role, and is stressed on its head or in the joint between the unstable block and the rock mass, by a combination of shear-traction depending on its direction.

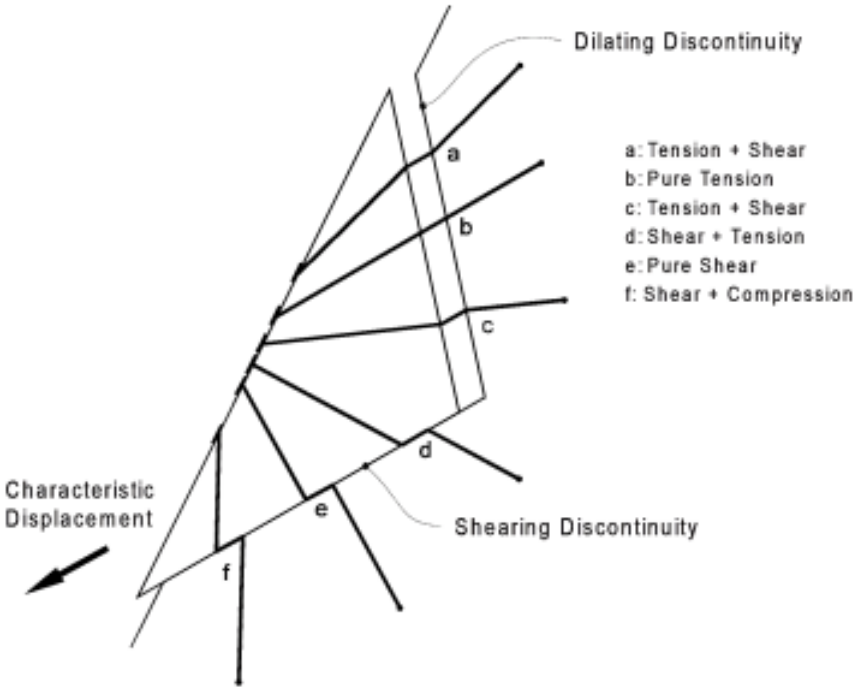

Figure 3.4: Types of solicitations in a passive grouted anchorage (Windsor, 1997)

4 Review of the different rock-bolts types

As already introduced an important aspect of the rock-bolt design is the identification of its role. Once this has been decided it is important to choose accordingly the type of the anchorage, to assure a good behaviour of the element.
We can define three kinds of rock-bolts, according to their functioning mechanisms:

- Mechanical rock-bolts.
- Grouted rock-bolts.
- Frictional rock-bolts.

4.1 Mechanical rock-bolt

These rock-bolts are anchored to the borehole through a mechanical locking between the end of the bolt and the rock.
Some examples of mechanical rock-bolts are:

- Expansion Shell Rock-bolt: this element is characterized by two threads in the two ends of the bar, in the distal end an expansion shell is attached, while a nut and a plate are disposed in the head end. By rotating the bolt the wedge is pulled toward the borehole collar, while the shell leaves are expanded and pushed against the borehole wall establishing a contact stress.
  In figure 4.1 we can observe one of the different types of shells that are available.

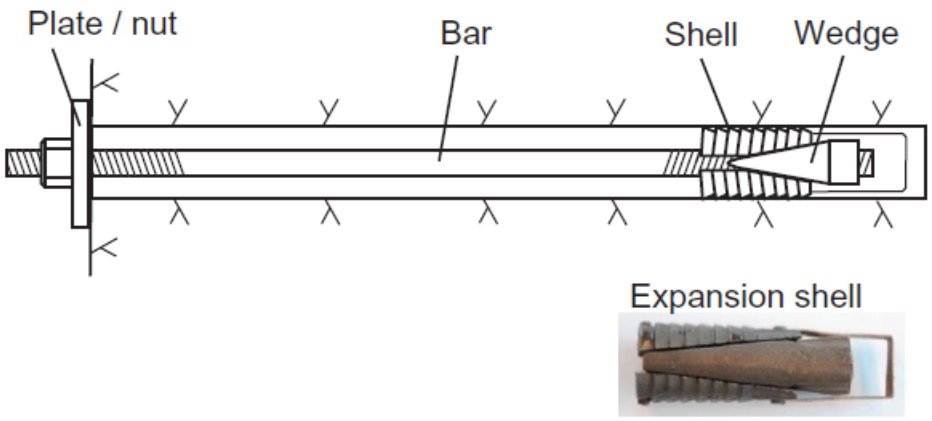

Figure 4.1: Expansion Shell Rockbolt

- Slot-and-Wedge Rockbolts: this rock-bolt has a slot longitudinally cut in the distal end of the bolt and a wedge inserted in the slot . During the installation the bolt is bushed inside the borehole until the wedge touched the end of the cavity. In figure 4.2 we can see a Slot-and-Wedge Rockbolt.

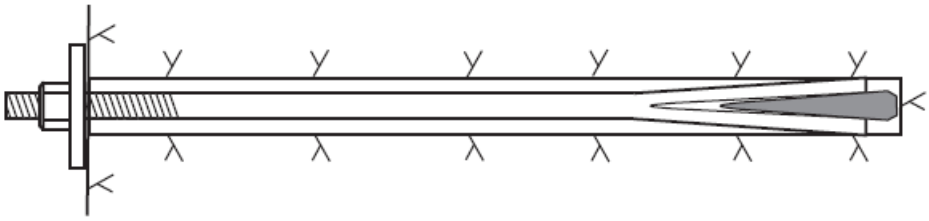

Figure 4.2: Slot-and-Wedge Rockbolt

4.2 Grouted rock-bolt

This anchorages are characterized by the use of a grout as an internal fixture, this grout could be made of resin or cement.
Some of the examples of this typology of rock-bolts are:

- Fully grouted rebar Rockbolts: This anchorage is completely wrapped along the bolt by the grout (see figure 4.3). The mechanical interlock between the ribs in the bolt's surface and the grout guarantees the interaction with the rock-mass.

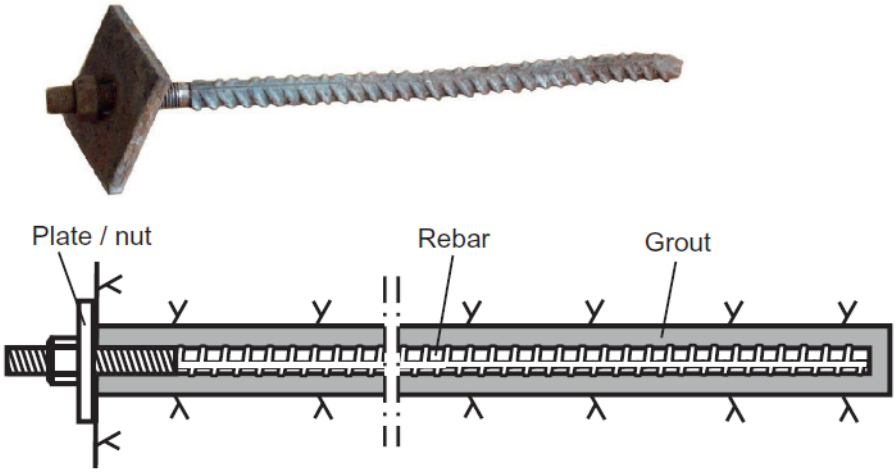

Figure 4.3: Fully grouted rebar Rockbolts

- Fully grouted Threadbar: this one is similar to rebar bolt, but its surface is made of coarse thread (see figure 4.4).

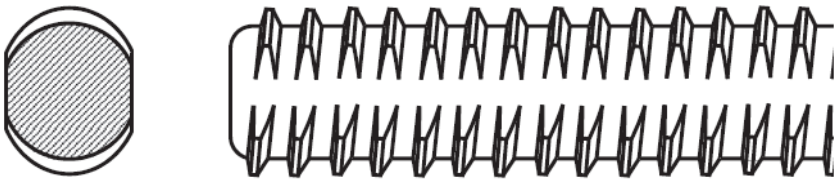

Figure 4.4: Threadbar

- End-grouted bolt: it is fixed only in the final segment of the bar; the shank can be either a rebar or a threadbar (see figure 4.5).

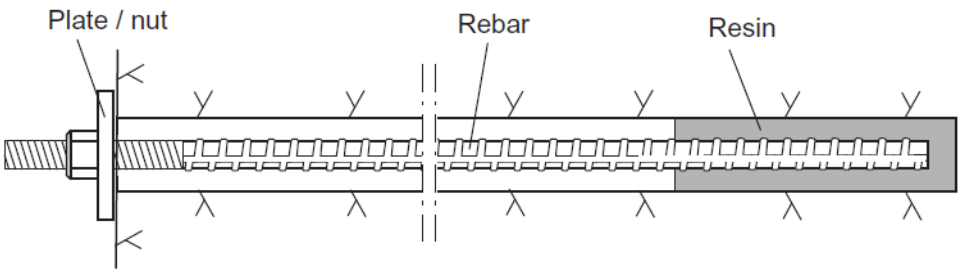

Figure 4.5: End-grouted bolt

- Fully grouted slot-and-wedge rockbolt: also called Kiruna bolt (see figure 4.6). Thins anchorage is made by a rebar with a wedge in its extremity. Once the cement grout is inside the borehole, the rebar is pushed in. This causes the expansion of the distal end when the wedge is pressed against the boreholes extremity.

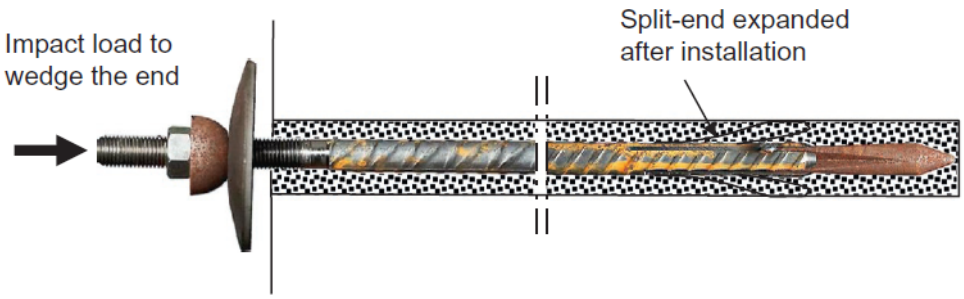

Figure 4.6: Fully grouted slot-and-wedge rockbolt

- Self-drilling rockbolts: this anchorage is composed by a hollow anchor rod with a drill bit attached to the distal end of the rod (see figure 4.7). The borehole is created with the sacrificial drill bit, then once once this phase is completed the grout is pumped in.

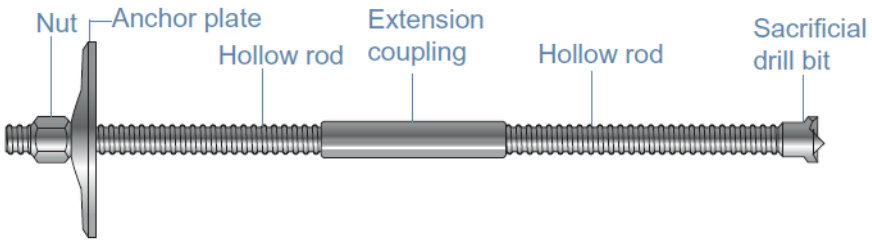

Figure 4.7: Self-drilling rockbolts

- Cablebolt: it could be made of single, twin or multiple strands, and they are usually fixed with cementitious grout in boreholes (see figure 4.8).

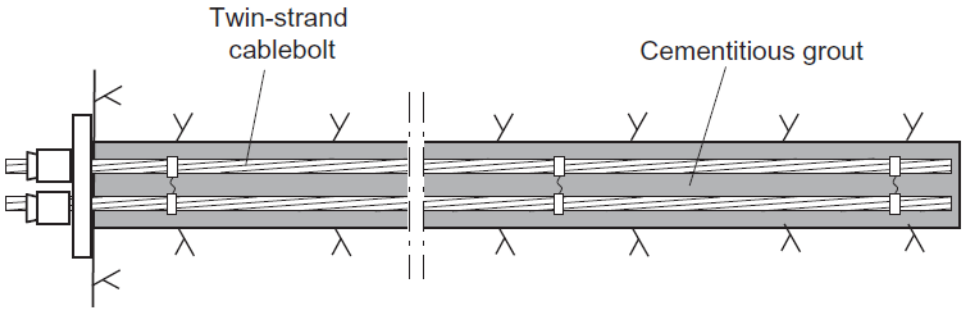

Figure 4.8: Cablebolt

4.3 Frictional rock-bolt

In this typology of rockbolts the interaction with the rock-mass is guaranteed by the friction between the anchorage and the rock. We can introduce several examples:

- Split Set: this rock bolt is composed by a steel sheet that is sealed by a welded ring (see figure 4.9). The bolt has generally a diameter that is 1-5mm larger than the borehole's.

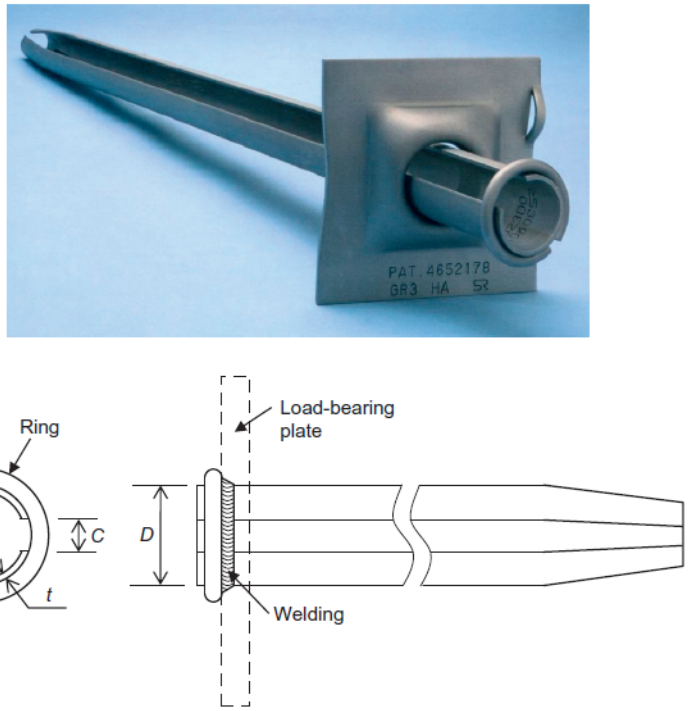

Figure 4.9: Split Set

- Inflatable Rockbolt: they are made of welded steel tube that is folded into an omega shape; during the installation we inject water at high pressure inside the bolt expanding it inside the borehole (see figure 4.10).

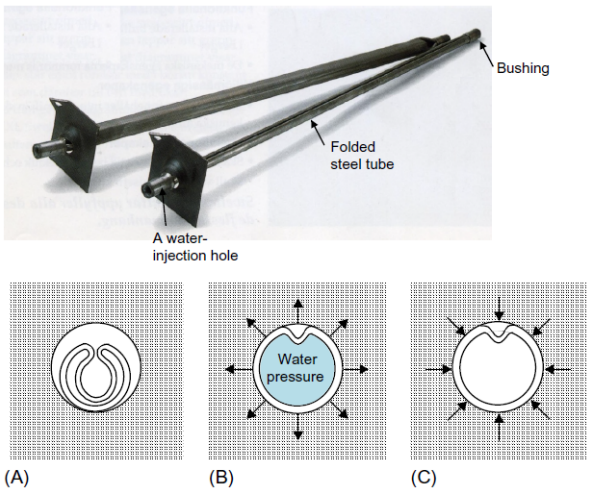

Figure 4.10: Inflatable Rockbolt

- Combined Rockbolt: this rock-bolt has an expansion shell that is used to prestress the bolt before the curing of the cement grout(see figure 4.11).

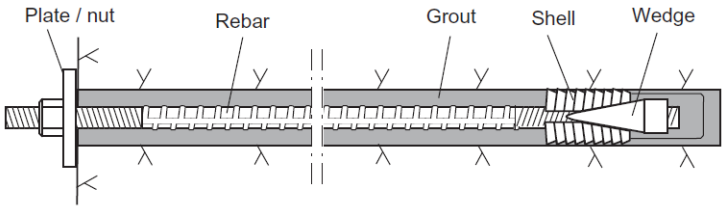

Figure 4.11: Combined Rockbolt

4.4 Energy-Absorbing Yield rockbolt

This typology of rockbolts is used to dissipate a part of the energy during the use of the element. Some example of these anchorages are:

- Cone bolt: this solution is made of a smooth steel bar with a conical outgrowth forged at the distal of the bolt (see figure 4.12).

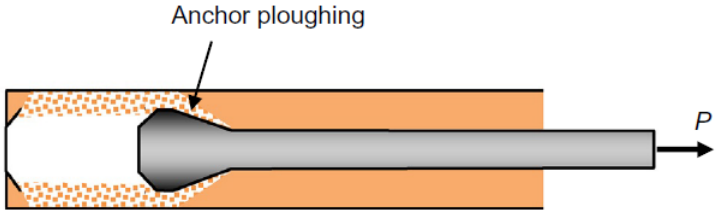

Figure 4.12: Cone bolt

- D-Bolt: this bolt absorbs the energy through the mobilization of the strength and the deformation capacity of the steel (see figure 4.13).

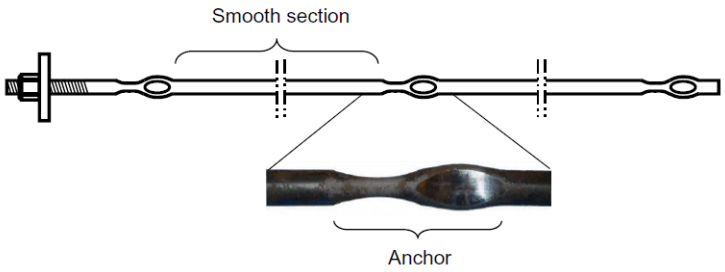

Figure 4.13: D-Bolt

- Garford Solid Bolt: this bolt is characterized by it's anchor, which inner diameter is smaller than the bar's shank (see figure 4.14).

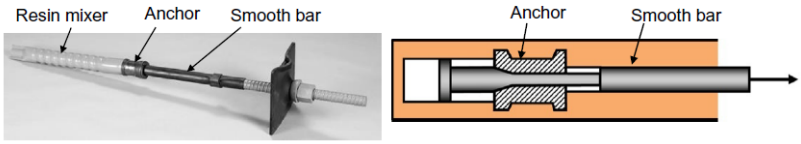

Figure 4.14: Garford Solid Bolt

- Yield-Lok: in this rockbolt the anchor is inside an engineered polymer coating (see figure 4.15).

Figure 4.15: Yield-Lok

- Durabar: this rockbolt is made with the use of a smooth bar with a sinusoidal waved portion (see figure 4.16).

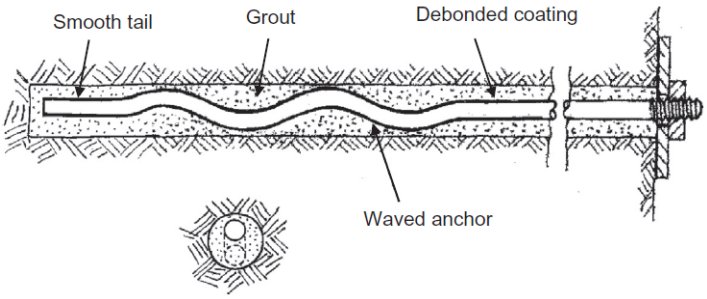

Figure 4.16: Durabar

- Roofex: this rockbolt is very similar to the Garford solit bolt; once installed the steel bar dissipates energy slipping through the anchor hole following the rock displacements (see figure 4.17).

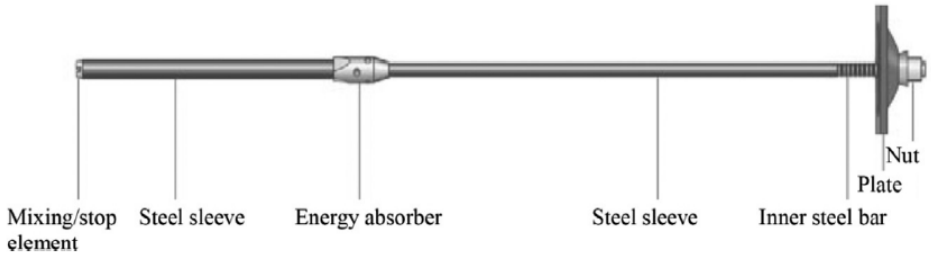

Figure 4.17: Roofex

- He Bolt: it is made of a steel bar, a cone shaped piston, a sleeve, a face plate, and a nut. We can observe in the figure 4.18 its functioning system.

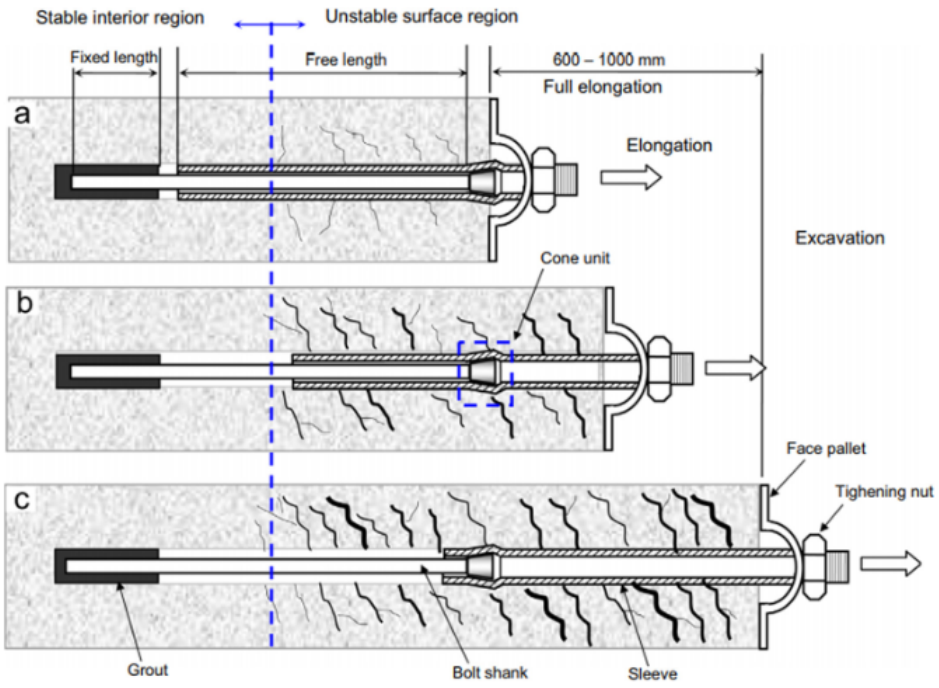

Figure 4.18: He Bolt

5 State of the art

When an anchorage is stressed in its head with an inclined force, this will be transmitted with two mechanisms:

- A bending reaction in the head of the bolt, in the "transmission length", where the reaction depends from the bolts resistance to bending and the reaction modules of grout and rock.
- A traction stress on the "dissipation length", where the traction force is progressively dissipated by the shear stress on the steel-grout interface.

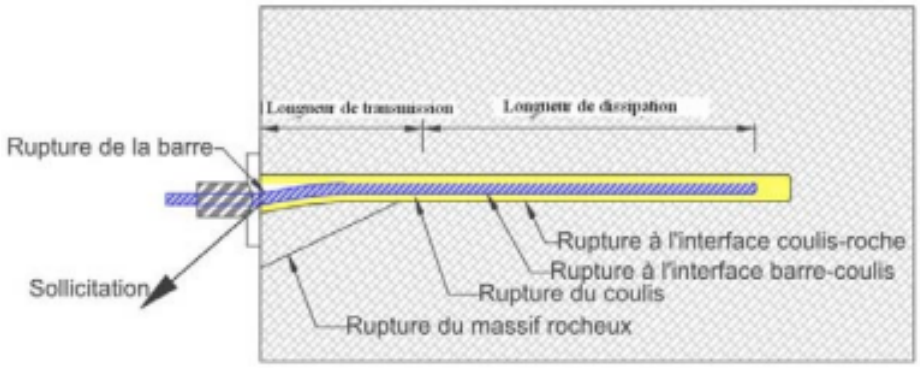

Figure 5.1: Failure types for a rock-bolt

The transmission length is usually considered to be around 5 times diameter of the steel bar for a shear stress, for rock with average or high resistance, according to the studies of Pellet(1993), Pellet and Egger (1996), Ferrero (1995) and Grasselli (2005). When a force is applied to the head of a rock bolt, as in figure 5.1, normally the superficial rock is damaged and can not contribute with the reaction. In this case the bolt will bend to be in the axis of the applied load, which has a positive effect because the shear resistance of the bar is 1.7 times inferior to the traction one. Consequently the inclined force is completely transmitted through traction. In any case, the length of the rock-bolt has to consider the dissipation length, and make sure that the load is dissipated in-depth.

In literature studies about the behaviour of the anchorage were made for different fields of applications and for different mechanisms:

- For reinforced concrete, steel bars are used as elements for the load transfer or to enhance the traction resistance of the material. As these reinforcements work prevalently in traction, we have different studies that analyse the behaviour of steel bars buried in concrete. This studies can help us to understand the transfer mechanism between steel and grout.
- For mining and tunnelling applications, here anchorages are used to assure a reinforcement and are stressed in traction by the tunnel convergence.

Differently than the case previously introduced when the applied force is parallel to the bar's axis the bolt is solicited only by a traction force, this force is transmitted firstly to the grout through the adherence between steel and grout, and then it is transmitted to the rock from the cement grout. This can lead to different failure types which are not exclusive :

- The failure of the grout-rock interface for a lack of adherence between the two.
- The failure of the steel-grout interface for the lack of adherence between the two.
- The failure of the grout.
- The failure of the rock.
- The failure of the bar.

The behaviour and the failure of the system, represent the interaction of different parameters associated to the characteristics of the bolt, the grout, the rock and also to the interfaces between them.

5.1 Steel-Grout interface

5.1.1 Experimental observations

An important aspect is understanding the local behaviour of the interface; in fact, studying the behaviour on a limited portion of the anchorage gives us the possibility of approaching the problem considering a uniform behaviour (both for stresses and deformations) along the considered segment. This is why different experimental studies were realized with a small grout length.

To study the behaviour of the local steel-grout interface, several devices can be used:

One of the first proposed pull-out tests was introduced by Fuller and Cox (1975) (figure 5.2 A) to study the load transfer between a cable and it's grout. In this device, a steel tube is used to represent the rock and reproduce the confinement conditions. Although the rigidity of a steel tube is too big to represent the rock. This is why Hyett et al.(1992) has modified this device using tubes of different materials like, PVC, aluminium, steel. This made possible to change the confinement conditions (figure 5.2 B).

The Benmokrane device for the pull-out testing (Benmokrane et al.1995) (figure 5.3), uses a concrete cylinder with a diameter of 200mm to represent the rock. Two situations were analysed:

- Tests to study the resistance of the anchorage according to the length of the grout, changing it from 7 to 20 times the diameter of the bar.
- A test to define a local model of behaviour at the interface grout-bar, with a short grout length that corresponds to 4 times of the bar's diameter.

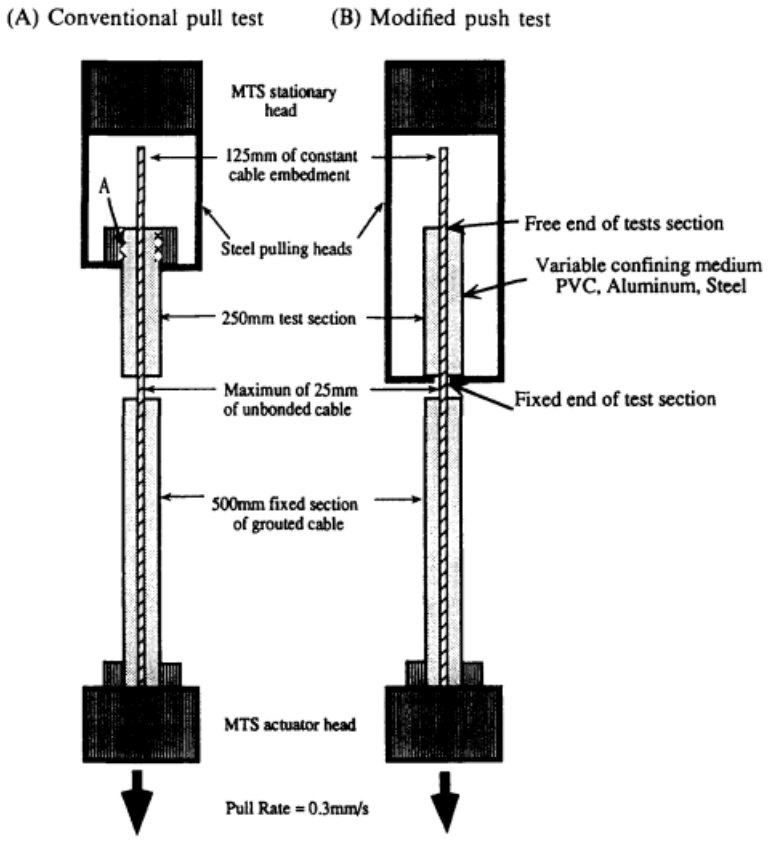

Figure 5.2: The two devices for the pull-out test of Fuller and Cox(1975) and Hyett et al.(1992)

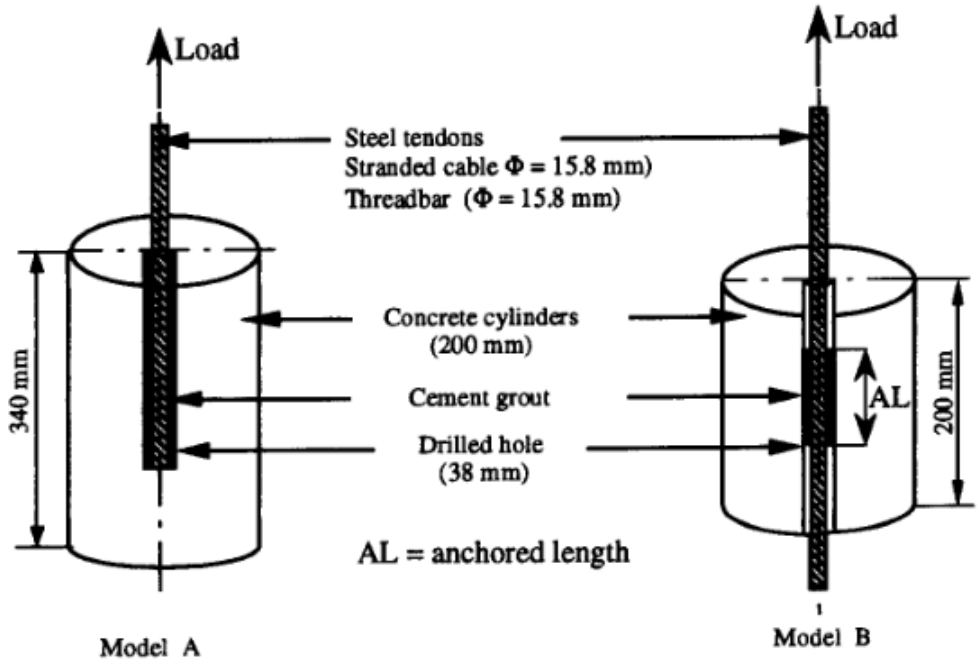

Figure 5.3: The two devices for the pull-out test of Benmokrane et al.(1995)

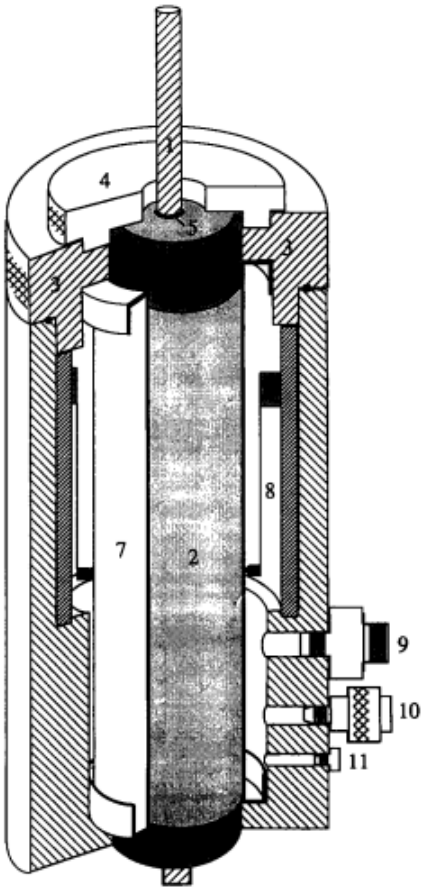

Figure 5.4: The modified Hoek cell (MHC): (1) 15.2 mm (0.6") seven-wire strand; (2) type 10 portland cement annulus; (3) pressure vessel endcap; (4) specimen endcap; (5) 15 mm PVC tube for debonding; (6) ABS pipe to support end of the specimen and overcome end-effects; (7) neoprene bladder; (8) cantilever strain gauge arms; (9) high pressure electrical feedthrough; (10) high pressure fitting; (I 1) pressure transducer. (Hyett et al.1995)

A triaxial cell has been performed by Hyett et al.(1995) (figure 5.4), starting from the triaxial cell of Hoek, to determine a behaviour model in the interface cable-concrete. This device was after used by Moosavi et al.(2005) to test the confinement effect on the interface.

A new testing cell has been developed by "Géosciences Mines-Paris Thech" in 2008 (figure 5.5). This device allows to apply hydraulic pressures on the sample. The applied pressures can be considered or not, which enables to realise tests under a constant confinement stress or a constant rigidity. To promote the failure along the interface steel-grout a plate of support is fixed on the head of the cell to block the shear on the grout or in the grout-rock interface. The rock's wall is slotted to improve the adherence.

With any device the pull-out test consists in applying a displacement in the head of the bar. During the test the value of the traction force and the displacement in the

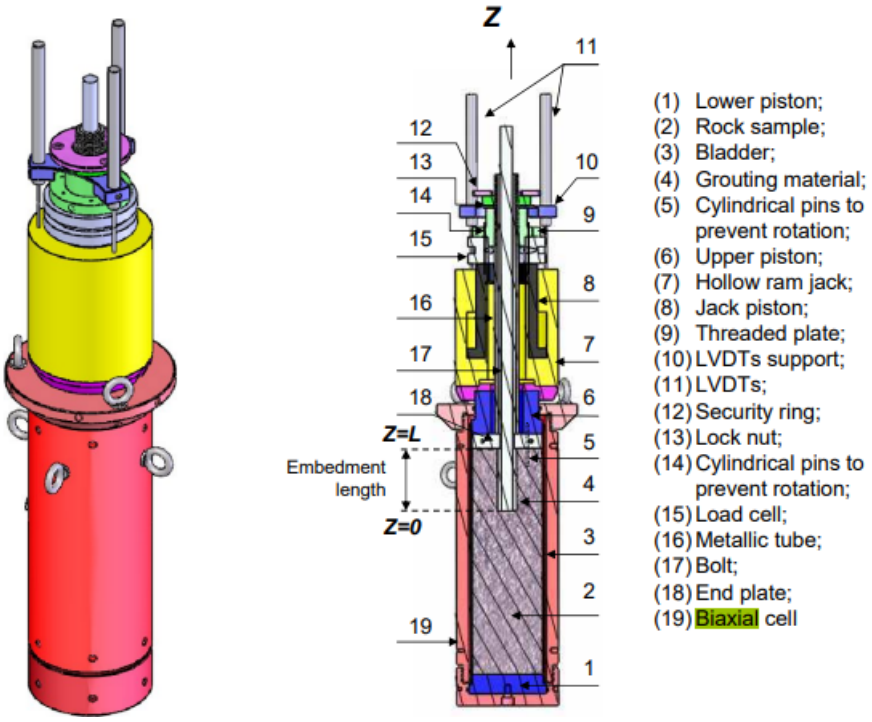

Figure 5.5: Biaxial cell (Blanco Martín 2012)

head of the bar are measured. For the biaxial devices it is also possible to measure the radial expansion of the cylindrical sample.

The displacements in the head are measured while having as a reference the unperturbed zone of the encasing medium, so it has two components: the relative slip between bar and grout, and the deformation of the surrounding medium, while the steel deformations can be neglected. If a support plate is applied, the measured displacement is composed only by the relative slipping on the interface. The value of the shear stress on the steel-grout surface can be the calculated considering a uniform distribution :

$$\tau^{s-g} = \frac{T}{\pi d_s L} \tag{5.1}$$

Where L is the length of the grout and d_s is the bar's diameter.

At the end of the test, the curve that represents the shear stresses τ^{b-g} calculated as a function of the displacements u of the bar (see figure 5.6). This curve is used to study the local behaviour in the bar grout interface.

In the figure 5.6 we can observe the local behaviour at the steel bar interface. These curves were obtained from reinforced concrete with different conditions of confinement. We can observe an almost linear increase in the beginning, then a softening behaviour once preached the peak value, and in the end a plateau.

This behaviour is justified by the presence of different reaction mechanisms, which contribute to the resistance at the interface. According to Lutz et al. (1967), Tepfers

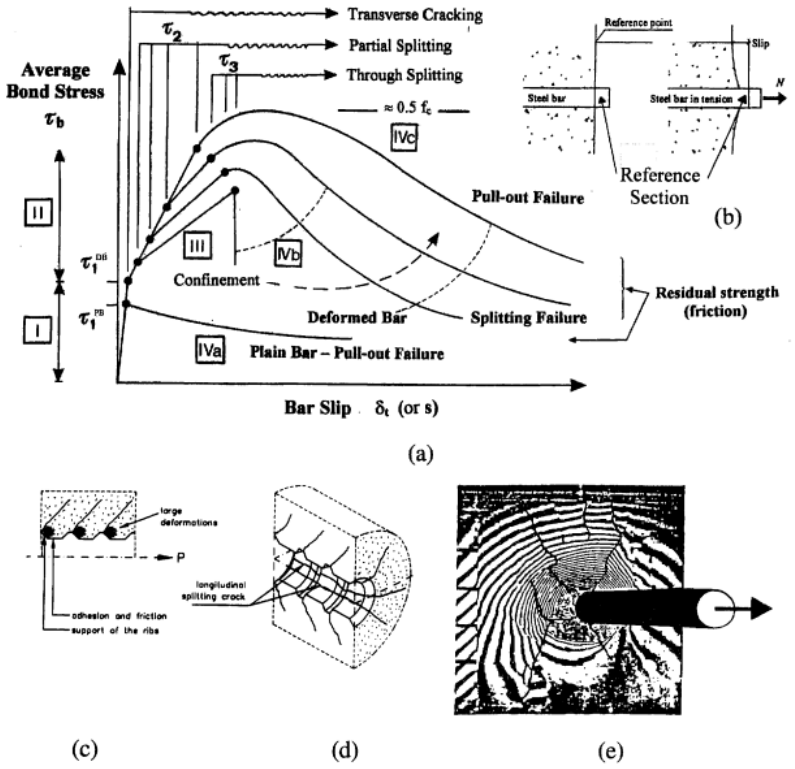

Figure 5.6: Local behaviour at the steel-grout interface (FIB, 2000)

(1979), Hyett et al. (1992) and Fib (2000), we can observe three mechanisms:

- chemical adhesion between steel and the grouting material. This force is generated by the cementation. Lutz and Gergely (1967) assign a range of values between 1.93 and 4.3 MPa, while the experimental studies of Aydan et al. (1990) reduced the range to 1.2 and 1.5 MPa. According to Hyett et al. (1992) this resistance is one tenth of the shear resistance which is around 12 MPa.

- mechanical interaction, this force is the result of reaction stresses of the grout pressing against the steel ribs.

- friction, this force is present only if a relative displacement between steel and grout has occurred.

These three mechanisms do not contribute necessarily in the same moment to the resistance of the system, but they can evolve during the loading.

According to Hyett et al.(1992) and FIB(2000), we can study the steel grout interface using four phases, as we can observe in the figure 5.6.

- First stage: in this phase the grout is uncracked, it is characterized by low bon-stress values, $\tau \leqslant \tau_1 = (0.2 - 0.8) f_{ct}$, The bond efficiency is mostly assured by the chemical adhesion, and there is no slipping in the interface. Along the lugs localized stresses arise as we can observe in figure 5.7 a. The chemical

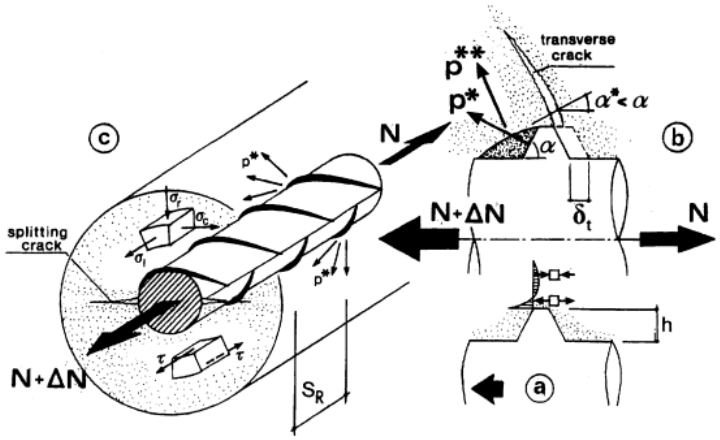

Figure 5.7: Reaction mechanisms (FIB, 2000)

adhesion is also accompanied by the micro-mechanical interaction associated with the microscopically rough steel surface, but on the whole chemical and physical adhesion plays a minor role. It is important to remember that the relative displacement is measured with reference to the undisturbed concrete, and it is made by two components, the relative slip between steel and grout, and the shear deformations in the concrete as we can observe in figure 5.6 b. Therefore, even if there is no slip, a certain displacement occurs.

- Second stage: this is the stage of the first cracking, in this stage the chemical adhesion breaks down. The deformed bar induce large bearing stresses to the concrete with the lugs (the pressure p*, in figure 5.7 b) , inducing transverse micro-cracks at the tip of the lugs allowing the bar to slip, in this phase the wedging effect of the lugs is still limited and there is no concrete splitting (figure 5.6 c).

- Third stage: for higher bonds of stress the longitudinal cracks spread radially, (splitting cracks, figure 5.6 d, and figure 5.7 c), this is caused by the wedging action of the lugs, that is enhanced that the crushed concrete which is blocked in front of the lugs. The presence of crushed concrete in front of the lugs changes the direction of the external component of the pressure (p**, figure 5.7b), which is resisted by the stresses in the concrete. As a consequence the grout exerts a confinement action on the bar, and the bond is assured thanks to the interlocking among the reinforcement, the concrete struts radiating from the bar and the undamaged outer ring.

- Stage IVa: in weak rocks , the grout dilatation is not prevented, cracks develop longitudinally along the bar in the grout spreading radially. The bar then is extracted by the slipping of the lugs on the decompressed and cracked grout. This behaviour can be seen also in plain bars.

- Stage IVb: In rocks with average rigidity, the failure of the steel grout interface involves at the same time the development of longitudinal cracks and the damage of the grout by compression and shear.

- Stage IVc: for rigid rocks , the dilatation of the grout and the development of longitudinal cracks is prevented. This causes important pressures in the interface between steel and cement, until the shear resistance is reached. The failure of the interface is due to the shear stresses.

These studies give us also the possibility of understanding the influence of the different parameters:

- Bar geometry: In reinforced concrete the inclination angle of the lugs has been examined in different studies (Rehm(1961), Lutz and Gergely (1967), Tepfers(1979) and FIB(2000)). These studies showed that ribs with a face angle between 40° and 105°, have the same behaviour during the pull-out test. This is explained because the damaged grout stored in front of the ribs changes the face angle to an effective one of 30°-40°.

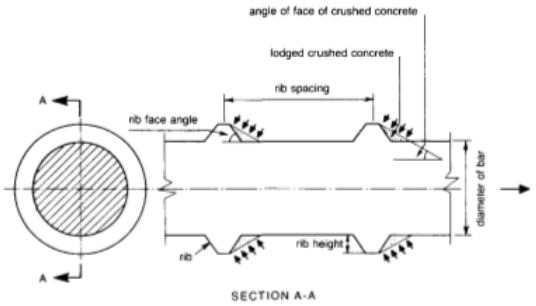

Figure 5.8: Bar geometry (Tepfers, 1979)

Regarding the height and the spacing of the ribs, considered in a coefficient called "bond index" or "relative rib area" which is the ratio between the transversal projected area of the ribs and the product between the nominal perimeter of the bar and the spacing between the ribs.

$$f_R = \frac{A_R}{\pi d_b s_R} \tag{5.2}$$

Rehm(1961) has discovered that the peak resistance in the interface a linear function of this coefficient.

- Mechanical characteristics: the resulting force on the steel-grout interface includes not only a longitudinal component which mobilises a shear stress in the grout, but also a radial component which equilibrates the ortho-radial stresses in the grout. The behaviour of the interface depends then on the compression resistance of the grout f_c and on the traction resistance f_t. Depending on the confinement applied by the rock one of the two can be more or less important. In a harder rock, which assures an important confinement f_c has a more predominant role than f_t, and vice versa.
  Benmokrane et al. (1995) have performed some pull-out tests on short lengths (figure 5.3 B). The steel bar has a 15.8 mm diameter with a 11.1 mm thick concrete around. The cement grout is made from the Portland cement and a ratio water cement of 0.45, the samples have the following properties:

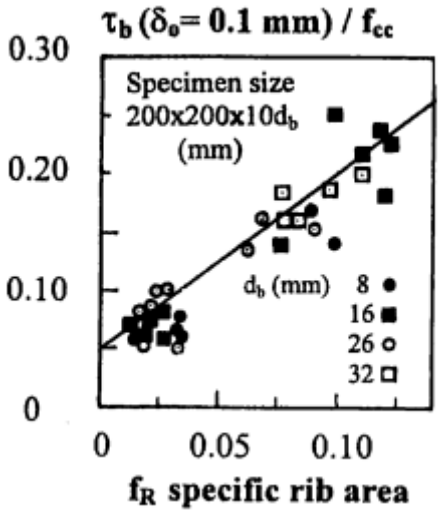

Figure 5.9: Resistance in the steel-grout interface in function of the relative rib area for a head displacement of 0.1mm (FIB, 2000)

- Sample CG1: Portland cement;W/C=0.45.
- Sample CG3: Portland cement;W/C=0.45; with an addition of 0.007% (relative to cement) of aluminium powder. This additive has swelling capacities which causes an increase of the grout porosity.
- Sample CG4: Portland cement;W/C=0.45; with a replacement of a 10% of the cement with Silica fume. This additive, which has very fine particles , increases the compactness of the grout, and then it increases also its compression resistance.
- Sample CG6: Portland cement;W/C=0.45; with an addition of 30% (relative to cement) of fine sand, which decreases the porosity, then also the compressibility of the grout.

Sample	f_c (Mpa)	f_t (Mpa)	E (GPa)	ν	τ_p^{s-g} (Mpa)
CG1	52.6	3.8	14.8	0.14	10.2
CG3	40.6	3.7	12.0	0.17	10.7
CG4	59.6	3.8	16.4	0.12	10.5
CG6	51.8	4.3	17.9	0.15	13.1

Table 5.1: Mechanical properties for the different samples after 28 days

From the results of the test (table 5.1) on the different samples, compared to CG1, we can conclude that the presence of additives has a positive effect of the peak resistance at the steal-grout interface τ_p^{s-g}. In CG3, the addition of aluminium powder decreases the compression resistance; but the swelling of the cement creates an increase in confining stresses, which is sufficient to improve the interface resistance. For CG4, the replacement of cement with silica fume has increased the compression resistance of the grout and then also

the interface resistance. In the case of CG6 the use of sand has not increased the compression resistance but the traction one and this has improved significantly the interface resistance.
Benmokrane (1995) has proposed a relation for calculating the interface resistance:

$$\tau_p^{s-g} = \alpha R_c^g \quad or \quad \tau_p^{s-g} = \beta\sqrt{R_c^g} \tag{5.3}$$

where $\alpha = (22.4 \pm 4)\%$ and $\beta = 1.5 \pm 0.2$ are experimental values obtained for different grouts and additives and R_c^g is the compressive resistance of the grout.

- Rock influence: The radial component of forces in the interface steel-grout create a pressure in this interface. These stresses are transmitted to the grout and then partially to the surrounding rock. According to the relative rigidity between the rock and the grout, the magnitude of the reactions and the radial dilatation of the rock's borehole wall, can be different.
To study these effects we can use two different types of tests:

  - Pull-out test at constant stiffness: the steel bar and the grout are subjected to confinement stresses which are proportional to the radial deformation during the test; the devices in figure 5.2, figure 5.3 and figure 5.5 can realise this test.
  - Pull-out test at constant confinement stresses: The steel bar and its grout are subjected to one confinement stress during the test. The devices that can realize this test are figure 5.4 and figure 5.5.

Pull-out test at constant stiffness: Hyett et al.(1992) have studied how the load transmission between bolt and grout is influenced by the surrounding rock; to do this they used as a container steel, aluminium and PVC tubes to represent the rock and they were able to find laboratory results that were relatable.
Jarred and Haberfield (1997) also have followed the same procedure to study the effect of the stiffness on the behaviour of the steel-grout interface.
The rock's stiffness is obtained with the use of Timoshenko's theory (1941) of a thick cylinder. If we suppose an elastic and linear behaviour of the rock with an infinite external diameter we have:

$$k^r = \frac{E^r}{1-\nu^r}\frac{1}{r^g} \tag{5.4}$$

where:

- E^r is the rock's Young Modulus.
- ν^r is the rock's Poission's ratio.
- r^g is the radius of the borehole.

During the tests the confinement stiffness is estimated with the use of the same theory (we can see some examples in table 5.2):

$$k = \frac{2E}{1+\nu} \times \frac{d_{ext}^2 - d_{int}^2}{d_{int}((1-2\nu)d_{int}^2 + d_{ext}^2)} \tag{5.5}$$

where:

- d_{int} is the internal diameter of the confining tube.
- d_{ext} is the external diameter of the confining tube.
- E is the Young Modulus of the tube's material.
- ν is the Poisson's ratio of the tube's material.

Material	d_{int}(mm)	d_{ext}(mm)	Stiffness(MPa/mm)	Rappresentative rock
PVC	67.00	71.20	11	Hard soils
Aluminium	73.70	74.84	63	Soft rocks
Steel	82.50	85.70	395	Gres
Steel	73.70	81.30	1061	Shiste
Steel	87.30	100.50	1241	Quartzite

Table 5.2: Stiffness of different tubes and their corresponding rocks (Jarred & Haberfield, 1997)

Jarred & Haberfield (1997) tested threaded steel bars with a 26 mm diameter, with a length diameter ratio of ten. These bars were grouted with concrete made with the use of Portland cement with a w/c ratio of 0.45.

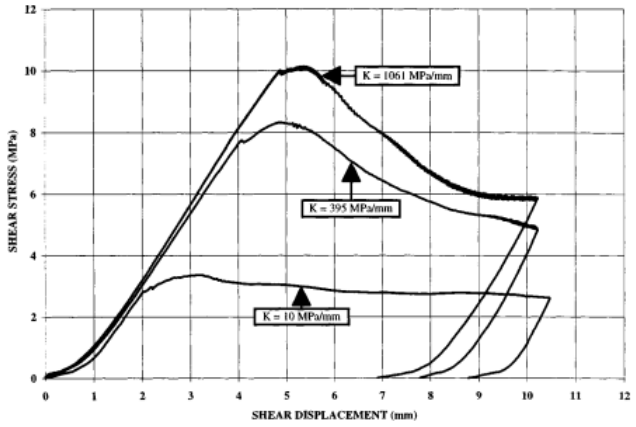

Figure 5.10: Shear stresses at the steel-grout interface with displacements for different confinement stiffnesses (Jarred & Haberfield, 1997)

We can observe in figure 5.10 that the peak resistance increases with the increase of the confinement stiffness. But this increase is not linear as we can see in figure 5.11.

We can also observe that starting for a certain value (around 10 MPa) the peak resistance becomes constant, this can be explained by the fact that an important confinement prevents the formation of radial crack and the failure of the interface can be obtained only reaching the shear resistance of the grout.

Pull-out tests at constant stresses: Moosavi et al. (2005) have made tests with a constant confinement to the grout with the use of the modified Hoek

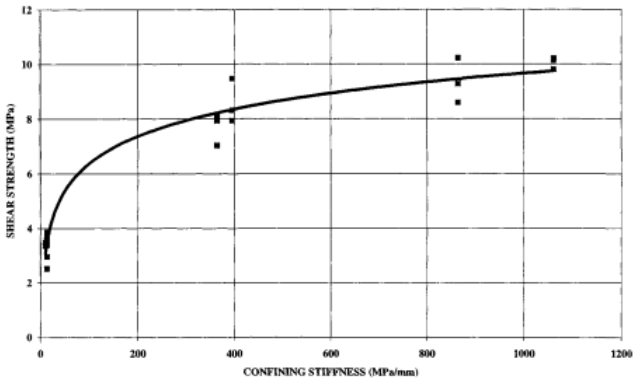

Figure 5.11: Peak shear strength vs confining stiffness (Jarred & Haberfield, 1997)

biaxial cell (figure 5.4). During the test the external dilatation of the grout, the traction force and the head displacements of the steel bar are measured.

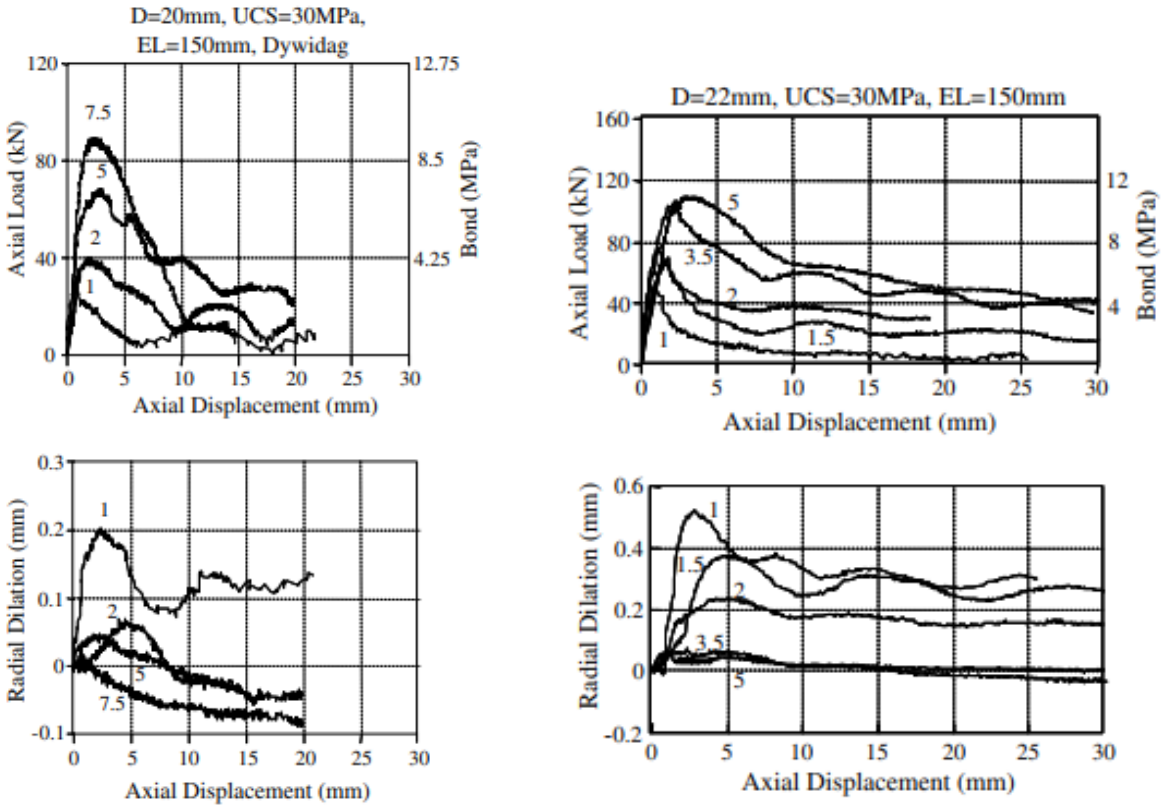

(a) 20mm Dywidag bar

(b) 22mm rebar P22

Figure 5.12: Shear stresses and radial dilatation in the results of Moosavi's tests (Moosavi et al. 2005)

We can see a clear influence of the confining pressure on the behaviour of the interface. We can observe how the peak resistance increases with the confining pressure and the radial dilatation decreases.

5.1.2 Local behaviour models in the steel-grout interface

Several models were developed to describe the behaviour of the steel-grout interface. For reinforced steel, Ciampi et al. (1981) and Eligehausen et al. (1983), have proposed a model that approximates the real behaviour as we can observe in figure 5.13.

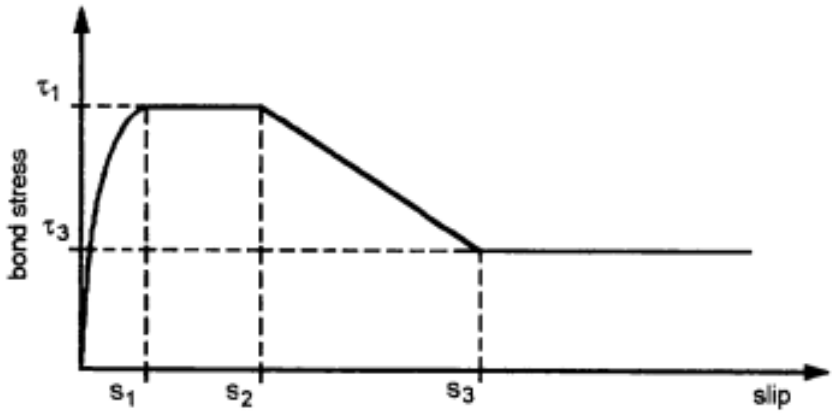

Figure 5.13: Analytical model for stress-slip relationship by Ciampi et al. (1981) and Eligehausen et al. (1983), (FIB, 2000)

And we can describe it with the following equations:

$$\tau_{s-g} = \begin{cases} \tau^p_{s-g}(\frac{\delta}{\delta_1})^\alpha & \text{if } 0 \leqslant \delta \leqslant \delta_1 \\ \tau^p_{s-g} & \text{if } \delta_1 < \delta \leqslant \delta_2 \\ \tau^p_{s-g} - \frac{\tau^p_{s-g}-\tau^r_{s-g}}{\delta_3-\delta_2}(\delta-\delta_2) & \text{if } \delta_2 \leqslant \delta \leqslant \delta_3 \\ \tau^r_{s-g} & \text{if } \delta_3 < \delta \end{cases} \tag{5.6}$$

This model has been used in the Model Code 1990 (Fib, 1993) and also in the Model Code for Concrete Structure 2010 (Fib, 2013) as a standard analytical model for the steel-grout interface.
This model is fully described with the use of six parameters ($\alpha; \tau^p_{s-g}; \tau^r_{s-g}; \delta_1; \delta_2; \delta_3$) which depend on the relative rib area coefficient, f_R, the physical and mechanical characteristics of the concrete and on the confining conditions.

For grouted rock-bolts, Benmokrane et al. (1995) proposed an empirical tri-linear model of the behaviour of the steel-grout interface (see 5.14).
Which can be described with the use of the following equations:

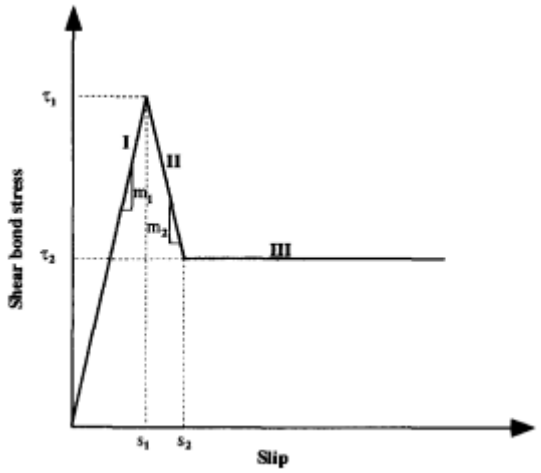

Figure 5.14: Idealized shear bond stress-slip model by Benmokrane (Benmokrane et al. 1995)

$$\tau_{s-g} = \begin{cases} \frac{\tau^p_{s-g}}{\delta^p_{s-g}}\delta & \text{if } 0 \leqslant \delta \leqslant \delta^p_{s-g} \\ \tau^p_{s-g} - \frac{\tau^p_{s-g}-\tau^r_{s-g}}{\delta^p_{s-g}-\delta^r_{s-g}}(\delta - \delta_p) & \text{if } \delta^p_{s-g} < \delta \leqslant \delta^r_{s-g} \\ \tau^r_{s-g} & \text{if } \delta^r_{s-g} < \delta \end{cases} \tag{5.7}$$

This model is defined by four parameters ($\tau^p_{s-g}; \tau^r_{s-g}; \delta^p_{s-g}; \tau^r_{s-g}$) which can be determined from pull-out tests.

5.1.3 Behaviour of the Steel-grout interface during a traction force

In the previously presented studies, for a short grouted length, the load transfer from the head of the bar to the grout is considered to be immediate, while the interface stresses and the displacements are considered the same along this interface. For a longer steel-grout interface these simplifications are not valid any more; in fact the load transfer takes place progressively, as the displacements and the shear stresses which also change with the depth.

The measured head displacement (see 5.15) includes the relative slip at the steel-grout interface, the deformations of the grout and of the rock and the relative slip between rock and grout, while we can neglect the displacements of the free bar in the head of the free segment of the bar at the head of the bolt. In axial-symmetrical coordinates we can obtain:

$$u_s = u_r + \delta_{g-r} + u_g + \delta_{s-g} \tag{5.8}$$

Or as strains:

$$\varepsilon_s = \varepsilon_r + \varepsilon_g + \frac{\delta_{g-r}}{dx} + \frac{\delta_{s-g}}{dx} \tag{5.9}$$

Where:

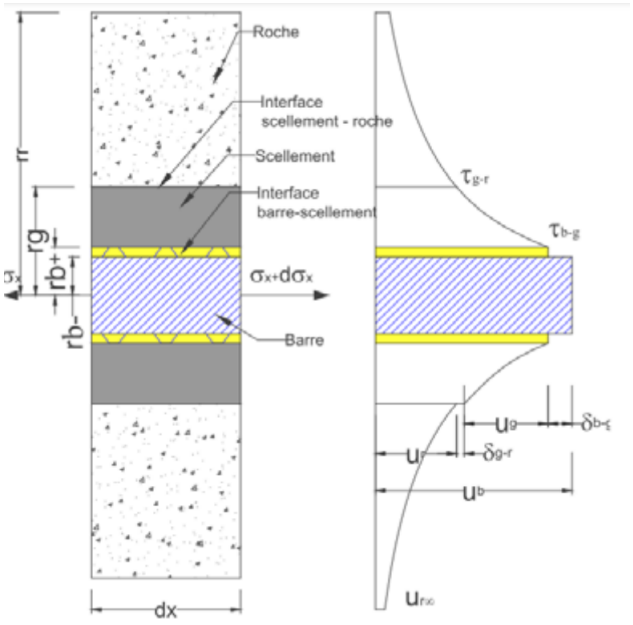

Figure 5.15: Displacements in the rock-bolt (Duc An Ho 2017)

- u_s, u_g, u_r are the displacements of the steel bolt, the grout and the rock.
- $\delta_{g-r}, \delta_{s-g}$ are the relative slips between rock and grout and between steel and grout.
- $\varepsilon_s, \varepsilon_g, \varepsilon_r$ are the strains of the steel bolt, the grout and the rock.

If we consider an elastic behaviour in the bar, we obtain the following equation of equilibrium of the grouted bar (see figure 5.16):

$$\pi r_s^2 \frac{d\sigma_s}{dx} - 2\pi r_s \tau_{s-g} = 0 \Rightarrow \frac{d\sigma_s}{dx} - \frac{2\tau_{s-g}}{r_s} = 0 \tag{5.10}$$

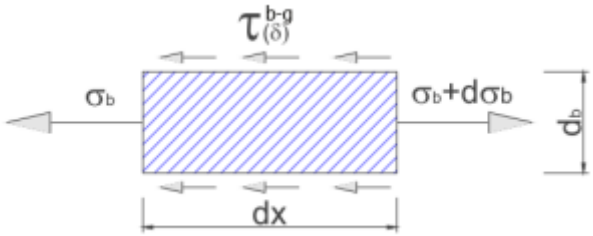

Figure 5.16: Stresses applied on the bar (Duc An Ho 2017)

The axial stresses in the bar is linked to the axial deformations:

$$\sigma_s = E_s \varepsilon_s = E_s \frac{du_s}{dx} \tag{5.11}$$

Using the equations 5.10 and 5.11 we obtain:

$$E_s \frac{d^2 u_s}{dx^2} - \frac{2\tau_{s_g}}{r_s} = 0 \tag{5.12}$$

This equation was the starting point for several studies to investigate the trend of the stresses.

Farmer (1975) was the first one to study analytically the trend of the shear stresses along a passive anchorage grouted with resin (see 5.17). The study was conducted assuming the following simplifications:

- An elastic behaviour in the steel bar and the grouting material.
- A rigid, non-deformable, behaviour of the rock (u_r).
- Bonded steel-grout and grout-rock interfaces ($\delta_{g-r} = \delta_{s-g} = 0$).

The bar displacement is then equal to the grout one ($u_s = u_g$).

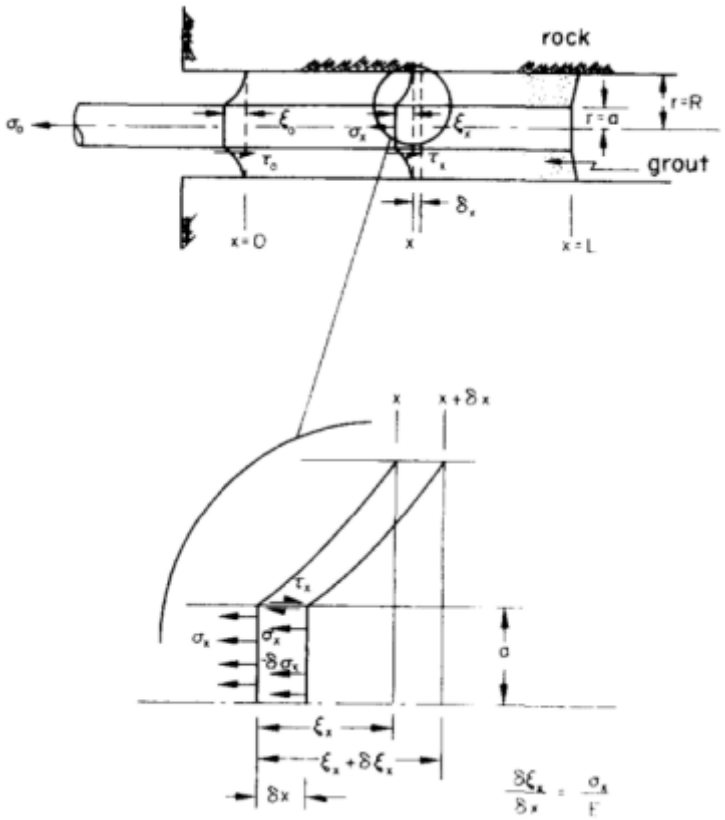

Figure 5.17: Stress trend in a grouted passive anchorage (Farmer, 1975)

If the annular space is small ($r_g < 2r_s$), the axial strains in the grout are considered uniform, the shear stresses on the steel-grout interface, then, can be calculated as:

$$\tau_{s-g} = G_g \frac{u_g}{r_g - r_s} \tag{5.13}$$

where G_g is the shear modulus of the grout.

While if the annular space is sufficiently big ($r_g > 2r_s$), the axial strains are considered linear in the grout, which means the shear stresses in the steel-grout interface can be calculated as:

$$\tau_{s-g} = \frac{G_g u_g}{r_s \times ln(\frac{r_g}{r_s})} \tag{5.14}$$

If we replace this equation in the 5.12 we obtain the equilibrium equation of the bar:

$$\frac{d^2 u_s}{dx^2} - \frac{\alpha^2}{r_s^2} u_s = 0 \tag{5.15}$$

where α is defined as:

$$\alpha = \begin{cases} \frac{2G_g}{E_s(\frac{r_g}{r_s}-1)} & if\ r_g < 2r_s \\ \frac{2G_g}{E_s ln(\frac{r_g}{r_s})} & if\ r_g > 2r_s \end{cases} \tag{5.16}$$

The equation can be resolved with the following boundary conditions:

- $\tau_{s-g} = \tau^0_{s-g}$ if $x = 0$.
- $\tau_{s-g} = 0$ if $x = L$.

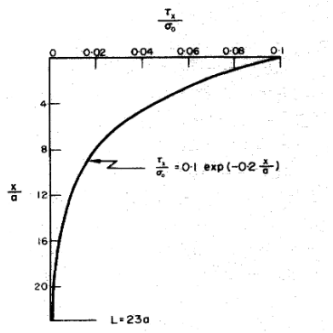

Figure 5.18: Theoretical stress distribution along a resin anchor in a rigid socket and having a thin resin annulus (Farmer, 1975)

we obtain then:

$$u_s = \frac{\tau^0_{s-g} r_b}{E_b \alpha} \frac{cosh\frac{\alpha}{r_b}(L-x)}{sinh\frac{\alpha}{r_b}L} \tag{5.17}$$

This equation can be simplified considering $\frac{L}{r_b} >> \frac{1}{\alpha}$:

$$u_s = \frac{\tau^0_{s-g} r_s}{E_s \alpha} exp(-\frac{\alpha}{r_b}x) \tag{5.18}$$

The shear stresses in the steel-grout interface are then determined as:

$$\tau_{s-g} = \frac{1}{2}\alpha\sigma^0_{s-g} exp(-\frac{\alpha}{r_r}x) = \tau^0_{s-g} exp(-\frac{\alpha}{r_b}x) \tag{5.19}$$

where σ^0_{s-g} is the axial stress in the steel bar in $x = 0$.

This trend has been confirmed for a cement grout by the study of Ballivy and Dupuis (1980). They have realized several laboratory and in situ tests with anchorages made of a steel bar with a diameter of $d_s = 9.5mm$, and a cement grout ($\frac{w}{c} = 0.4$) with a 5.25 mm thickness on a length of 10 diameters. Ballivy and Dupuis (1980) found, for hard rocks, that the failure takes place in the steel-grout interface and that shear stress trend is described by the following equation:

$$\tau_{s-g} = \tau^0_{s-g} exp(-\frac{\alpha}{r_b} x) \tag{5.20}$$

where:

- α is a parameter that represents the rock type. This value is calculated experimentally and it is normally in the range between 0.125 and 0.165 for hard rocks ($f_c \geqslant 70MPa$).
- τ^0_{s-g} is the shear resistance of the grout, and it can be calculated with the use of Brown's formula (1970): $\tau^0_{s-g} = 0.96\sqrt{R^g_c}$, where R^g_c is the cement's compression resistance.

However, according to Farmer (1975), this distribution is correct only for small loads. In the figure 5.19 we can observe the comparison between the results calculated analytically and those from in situ tests, using passive rock-bolts grouted to a concrete block with the use of resin. We can observe a correspondence between the two results only for smaller loads. Beyond a certain value we can observe an important difference between the results. An explanation could be the fact that for these values we are beyond the elastic limit of the materials used.

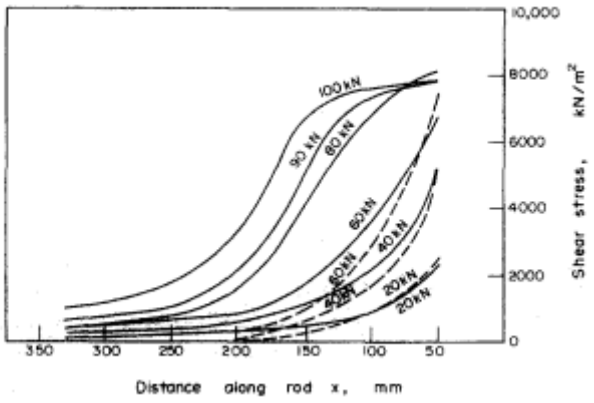

Figure 5.19: Measured shear stress distribution curves compared with the theoretical curves. The dashed lines are theoretical shear-stress distribution curves. The solid lines are computed from the strain distribution curves. (Farmer, 1975)

Li and Stillborg (1999) assumed that, with a traction force, the axial stresses in the bar are maximum in the head and decrease in depth along the bolt, with a trend that depends on the presence of a decoupling between grout and steel (see figure 5.20).

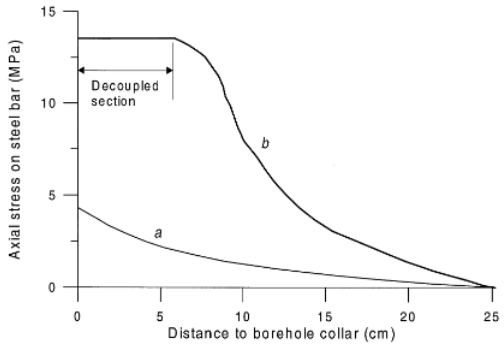

Figure 5.20: Distribution of the axial stress (a) Without decoupling and (b) with decoupling. (Li and Stillborg 1999)

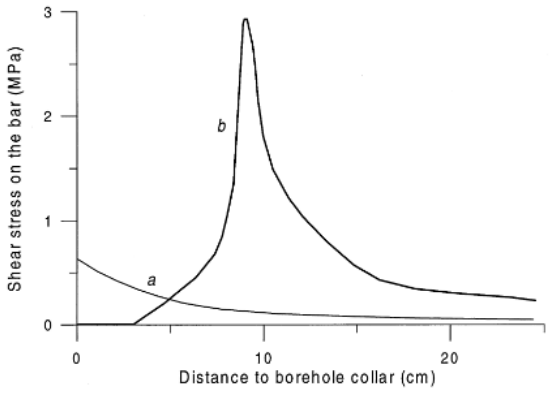

Figure 5.21: Distribution of the shear stress obtained from axial stress. (Li and Stillborg 1999)

Then starting from the axial stresses we can obtain the shear stresses as in figure 5.21.
Starting from these results, Li and Stillborg (1999) proposed a shear stress trend in the steel-grout interface divided in four sections (see figure 5.22).

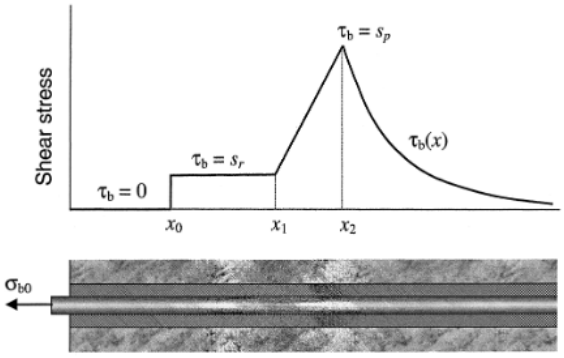

Figure 5.22: Distribution of shear stress along a fully grouted rock bolt subjected to an axial load. (Li and Stillborg 1999)

- The first segment has a length x_0 , in this length steel and grout are completely decoupled, and the opening is sufficiently big to annul the shear stresses.
- In the second segment, which goes from x_0 to x_1, there is a relative slip between steel and grout, the shear stresses are generated by the friction between bar and grout and they have a constant value τ_r.
- In the third part, which goes from x_1 to x_2, the steel-grout interface is partially decoupled. The shear stresses have a linear distribution starting from τ_r to τ_p.
- In the final segment the steel-grout interface is coupled and the shear stresses have an exponential trend according to the studies made by Farmer (1975). However Li and Stillborg(1999) have not considered the hypothesis on non-deformability of the rock, changing the parameter α to consider the elasticity of the rock with the following formula:

$$\alpha = \frac{2G_r G_g}{E_s[G_r ln(\frac{d_g}{d_s}) + G_g ln\frac{d_r}{d_g}]} \tag{5.21}$$

Considering x_0 as the position of first contact between steel and grout, and defining $\Delta = x_2 - x_1$ we need four parameters to define this model : τ_r , τ_p , Δ , and $x_1(\delta)$. The Li and Stillborg (1999) model can be defined using the following equation:

$$\tau_{s-g}(x,\delta) = \begin{cases} 0 & if\ x < x_0 \\ \tau^r_{s-g} & if\ x_0 \leqslant x < x_1 \\ \tau^r_{s-g} + \frac{\tau^p_{s-g} - \tau^r_{s-g}}{\Delta}(x - x_1) & if\ x_1 \leqslant x < x_2 \\ \tau^p_{s-g} exp(-\frac{2\alpha(x-x_2)}{d_s}) & if\ x_2 \leqslant x \end{cases} \tag{5.22}$$

The traction load applied in the head of the rock-bolt can be calculated as the integral of the shear stresses along the length of the grout L:

$$T_0(x_2) = \pi d_s \int_{x_0}^{L} \tau_{s-g} dx =$$

$$= \pi d_s [\tau^r_{s-g}(x_2 - \Delta - x_0) + \frac{1}{2}\tau^p_{s-g}\Delta(1 + \frac{\tau^r_{s-g}}{\tau^p_{s-g}}) + \tag{5.23}$$

$$+ \frac{d_s}{2\alpha}\tau^p_{s-g}(1 - e^{-\frac{2\alpha}{d_s}(L-x_2)})]$$

And from this equation we can obtain the maximum applicable force as:

$$\frac{\delta T_0(x_2)}{\delta x_2} = 0 \Rightarrow x_2 = L - \frac{d_b}{2\alpha} ln(\frac{\tau^p_{s-g}}{\tau^r_{s-g}})$$

$$T_0 = \pi d_s \tau^p_{s-g} [\frac{\tau^r_{s-g}}{\tau^p_{s-g}}(L + \frac{d_s}{2\alpha} ln(\frac{\tau^r_{s-g}}{\tau^p_{s-g}}) - \Delta) + \frac{1}{2}\Delta(1 + \frac{\tau^r_{s-g}}{\tau^p_{s-g}}) + \tag{5.24}$$

$$+ \frac{d_s}{2\alpha}\tau^p_{s-g}(1 - \frac{\tau^r_{s-g}}{\tau^p_{s-g}})]$$

5.2 Local behaviour and failure in the grout-rock interface

In a rock-bolt with tractions load applied the stress transfer toward the rock requires the developing shear stresses along the grout-rock interface. The failure in this interface is generally quite rare in situ, and it has been observed only in soft rocks (Ballivy and Dupuis, 1980), and it consists usually in the shear failure of the weakest material (rock or grout).

Cements	Specific surface area ($\frac{m^2}{kg}$)	Bond strength(MPa)			
		Quarts	Granite	Limestone	Marble
OPC,PC400	365.4	3.46	3.01	4.63	3.70
Sul. Res. PZ 2/30	371.3	3.32	3.13	3.42	3.30
Gypsfree ASTM type 0	309.0	5.49	4.83	8.85	4.26
Gypsfree ASTM type III	708.6	7.82	6.21	10.05	5.94
OPC PC400+ Plasticizer		3.69	3.86	4.12	3.70
PZ $\frac{2}{30}$+ Plasticizer		3.43	4.11	3.28	4.04

Table 5.3: Chemical adhesion between cement and rock. (Bazantova and Modry, 1998)

According to Bensted and Barns (2001), in concrete, the resistance of the interface between cement and aggregate interface is developed by physical and chemical processes, that take place during the hardening of the cement and they depend on the rock's surface and by it chemical and mineral composition. An increase in the cement's specific surface causes an increase in the chemical adhesion. While an increase in the porosity provokes an increase in the mechanical interaction, because the hydraulic binders penetrate in the pores before the hardening of the cement.

Ballivy and Dupuis (1980) have realized pull-out tests on several anchorages, both in situ and in laboratory, with the use of rocks with different stiffnesses, they discovered that the failure in the rock-grout interface is observed only in softer rocks, and that the shear stress trend is constant along this interface. They realized that the resistance along this interface can be approximated with the following formula:

$$\tau_{g-r,min} = 0.17\sqrt{f'_c} \quad and \quad \tau_{g-r,average} = 0.5\sqrt{f'_c} \tag{5.25}$$

where:

- $\tau_{g-r,min}$ and $\tau_{g-r,average}$ are the minimal and the average resistance in the interface.
- f'_c is the compression resistance of the weakest material(cement or rock).

The British standard BS 8081:1989, relative to anchorages, suggests some resistance values for the rock-grout interface (table 5.4). These values are obtained from experimental tests.

Rock type		Ultimate resistance (MPa)	Recommended resistance (MPa)
Igneous rock	Basalt	3.86	1.21 to 1.39
	Granite	4.83	1.38 to 1.55
	Alterated Granite	1.5 to 2.5	
	Serpentine	1.55	0.45 to 0.69
Metamorphic rock	Manhattan's schist	2.8	0.70
	Clay schist	0.83 to 1.38	
Sedimentary rocks	Limestone rock	2.83	1.00
	Soft Limestone rock	1.03 to 1.52	
	Grés	4.28	2.45
	Alterated Grés	0.69 to 0.85	
	Pelite	2.24	0.69 to 0.83
	Soft schist	0.35	

Table 5.4: Shear resistance in the rock-grout interface according to the British norm BS 8081:1989

According to Haberfield and Baycan (1997), the resistance in the rock-grout interface does not depend only on the mechanical properties of the rock or the grout, but also from the roughness of the walls, the borehole diameter and by the confining stresses applied initially on the rock-grout interface. Several in situ tests were realized to see the influence of the different parameters.
From the results it is possible to deduct how the roughness, the diameter of the borehole and the addition of expansive cement can influence the behaviour of the rock-bolts:

- The roughness of the borehole have not been proved particularly influential on the shear stresses during these tests.
- The borehole diameter: the shear resistance decreases with the increase of the borehole's diameter.
- The addition of expansive cement has been proven quite effective to improve the shear resistance. It has been observed that the shear resistance in the interface doubles with the addition of 200 $\frac{kg}{m^3}$ of expansive cement.

6 Material and methods

During this thesis a series of different experiments were analysed. The testing campaigns were conducted in three different locations (Seyssel, Oisans and Mongalgon) with the development sixteen rock-bolts.
In Figure 6.1 we can observe the geometry used during the testing campaigns. The reinforcement has a length of 3 m were the first meter is grouted inside the hole, the second meter is still inside the borehole but with no grouting and the final meter is outside .

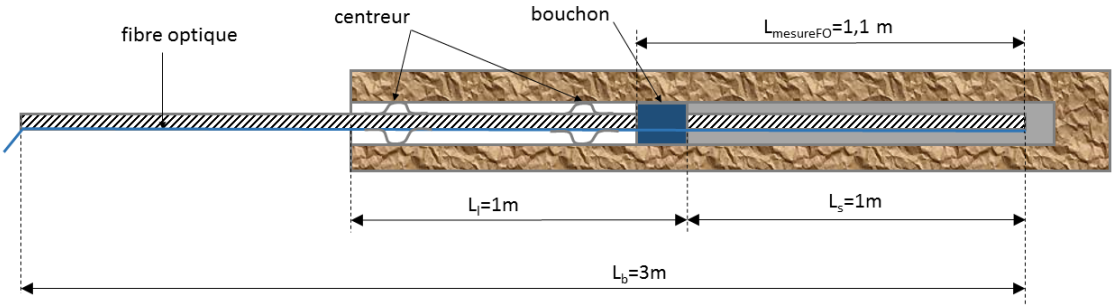

Figure 6.1: Reinforcement's geometry

6.1 Fibre optic

An important aspect of this testing campaigns is the fact that the bolts were equipped with fibre optic instrumentation.
We can observe in the Figure 6.1 that the final 1.1m of the reinforcement are characterized by the presence of the "measuring" fibre. This segment is characterized by the lack of the protecting sheath. In this portion the fibre optic is wrapped with the glue X120. This glue is made with two visco-elastics components that have an important resistance to heat, can harden at ambient temperature and that are designed for the fibre optic applications. This glue is also chosen for its mechanical properties, which are close the the steel ones. This creates a good adherence to the bar and also assures that the behaviour of the glue, which wraps the fibre optic, will be equal of the bolt's once the forces are applied.
The presence of this instrumentation gives us the possibility to monitor the strains in the reinforcement/grout interface. Consequently we can also obtain the forces and the shear stresses that characterize this portion.

The fibre optic was used during the tests to measure the deformations along the steel bar. This measurement technique has already been used in reinforcement bars at the IFSTTAR (Quiertant et al. 2013). It consists into gluing a fibre optic in an engraving realised along the steel bar and it measures to propagation of the light-waves. The light-waves propagation is modified by the deformations of the bar, and this gives us the possibility to calculate the deformations of the rock-bolt.

(a) Bar engraving

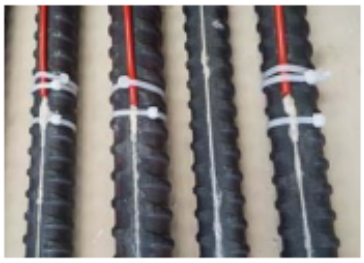

(b) Fibre optic fixing and protection in the head of the grouted part.

(c) Glued fibre optic in the grouted part

Figure 6.2: Fibre optic elements

For the treatment of the fiber optic data the used methodology is the one proposed by Duc An Ho in his PhD thesis. Starting from the strains of the reinforcement bar, we can obtain:

- The axial forces distribution along the reinforcement for each loading step. Considering an elastic behaviour of the steel we can obtain:

$$F_i = E_b A_b \varepsilon_i \tag{6.1}$$

  Where:

  - F_i is the axial force applied on the reinforcement bar calculated in x_i.
  - ε_i are the strain measures by the fibre optic in x_i.
  - E_b is the Young Modulus of the steel.
  - A_b is the section of the reinforcement bar, calculated with the minimum diameter d_b.

- The shear stresses along the interface reinforcement/grout for each step of loading . To obtain these stresses we use the derivation of the forces:

$$\tau^i_{b-g} = \frac{dF^i}{\pi d_b dx^i} \approx \frac{F^{i+1} - F^{i-1}}{\pi d_b (x^{i+1} - x^{i-1})} \tag{6.2}$$

  Where:

  - τ^i_{b-g} is the shear stress calculated in x_i.
  - F^{i+1} and F^{i-1} are the forces in x^{i+1} and x^{i-1}.
    It is important to consider that the oscillations of F create wrongly amplified oscillations of τ^i_{b-g}. To avoid this, the axial force's curves were smoothed before the derivation. For the smoothing it was used a Gaussian filter with a smoothing segment of 24mm, which includes then 4 measurement points.

  Once we have obtained the shear stresses along the interface steel/grout we can fit these results using an exponential equation:

$$\tau_{fit} = ae^{bx} \tag{6.3}$$

(a) Magnetostrictive sensor (b) LVDT sensor

Figure 6.3: Displacement sensors

6.2 Displacement and load measurement

For the measurement of the forces and of the displacements in the head of the anchorage the following instruments were used:

- A magnetostrictive senso (see figure 6.3a) for the displacement measurements, which was considered a better choice rather than the conventional LVDT sensors (see figure 6.3b), for its ease in the measurement of the sinking displacements of the hydraulic jack in the rock.
- A force sensor for the loads.

6.3 Pull-out test

The pull-out test was realized with the following geometry:

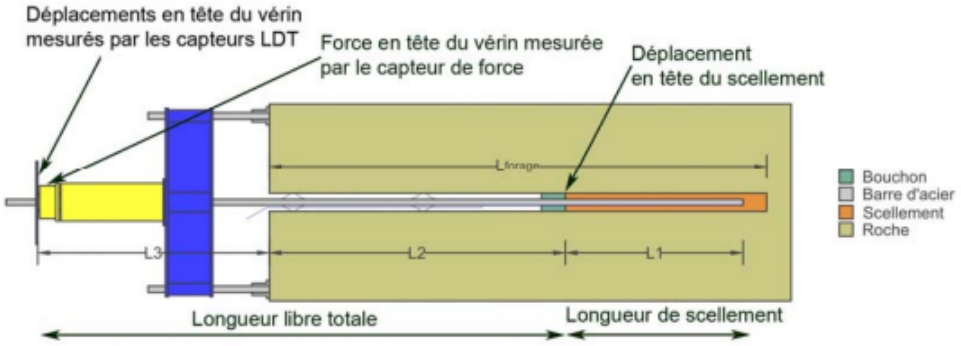

Figure 6.4: Rock bolt and instrumentation geometry (Duc An Ho, 2017)

The set-up of a pull-out test is composed by a hydraulic jack that is attached to the bolt, and an adjustable support frame that is placed under the jack; this frame is used to compensate the unevenness of the rock surface and also to position the jack in axis of the rock-bolt.

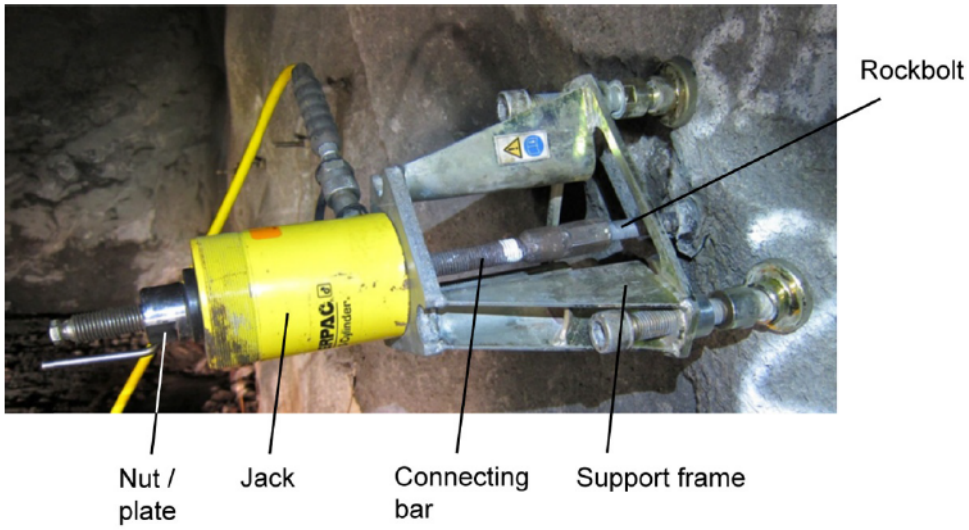

Figure 6.5: Pull test of a rock-bolt on site (Charlie Chunlin Li)

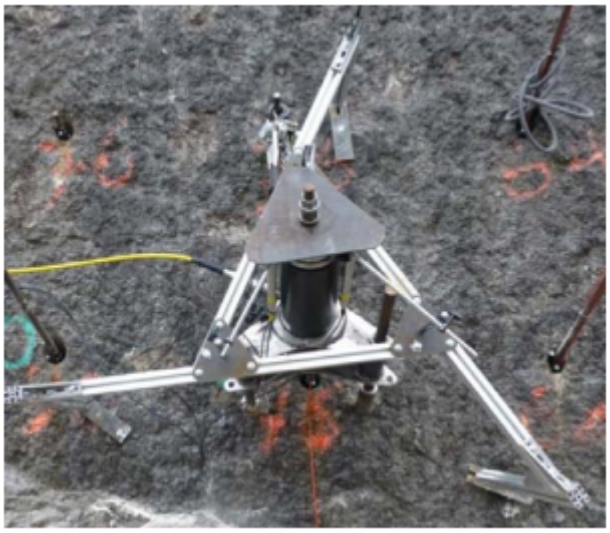

Figure 6.6: Pull-out test setup (Duc An Ho, 2017)

6.4 Materials

As previously introduced the construction of a rock-bolt is a relatively simple task, this is due also to the limited quantity of materials needed. These elements are, in fact, made by two materials:

- The steel bar.
- The grout.

6.4.1 Steel bar

The used bars for these anchorages are the same ones that are used in reinforced concrete. These bars are characterized by an important adherence to the grout, which is assured by the presence of the ribs along the steel.

Some important prescriptions, for the reinforced concrete, are defined regarding the ductility of the bar. It is, in fact, important that the bar can develop meaningful displacements before reaching the failure; this assures energy dissipation in case of a stress concentration. The Eurocode 2 and its national french application norm NF EN 1992-1-1 :2005 define three ductility classes (see table 6.1).

	Ductility class		
	A	B	C
f_{yk} or $f_{0,2k}$ [MPa]	from 400 to 600		
$k = (\frac{f_u}{f_y})_k$	$\geqslant 1.05$	$\geqslant 1.08$	$\geqslant 1.15$ (< 1.35)
ε_{uk} (%)	$\geqslant 2.5$	$\geqslant 5.0$	$\geqslant 7.5$

Table 6.1: Ductility classes defined by NF EN 1992-1-1 :2005.

In this case the used bars were SAS 500/550 (see figure 6.7), which are characterised by an elastic limit of 500 MPa and a failure limit of 550 MPa.

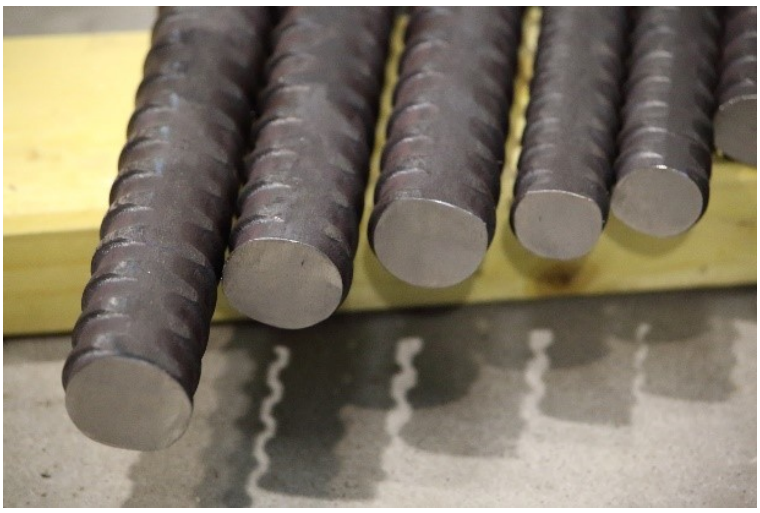

Figure 6.7: Three bars SAS 500/550 with 32 mm diameters (left) and two with 25 mm diameter (right)

6.4.2 Grout

As already introduced an anchorage can be grouted both with resin and cement. In the test campaigns that will be presented the rock-bolts were grouted with the use of a cementitious grout.
This grout is realized with CEM I (42.5 MPa) with a water cement ratio of 0.5 and a density of 1.81.
During the Oisans campaign several samples were made of the grout and after curing for 28 day they were tested. See table 6.2 for results; in this tables we can observe the geometrical characteristics of each sample, the force applied on it and

the resisting tension of the sample.

Sample	1	2	3	4
Height [cm]	8.0	8.0	8.2	8.2
Diameter 1 [cm]	4.1	4.1	4.1	4.1
Diameter 2 [cm]	4.0	4.0	4.0	4.0
Mass [kg]	0.195	0.195	0.200	0.200
Force [kN]	55.0	25.3	47.7	57.8
R_c [MPa]	43.8	20.1	38.0	46.0

Table 6.2: Results from the grout tested samples

7 Data measurements campaign

In this paragraph the results of the testing campaigns will be presented. Several rock-bolts were installed and axial loads were applied according to French Norm XP P94-444 which prescribes loading steps in different cycles (see 7.1).
Another requirement is that the maximum load expected has to be less than 0.9 T_p, which is the elastic limit of the steel reinforcement.

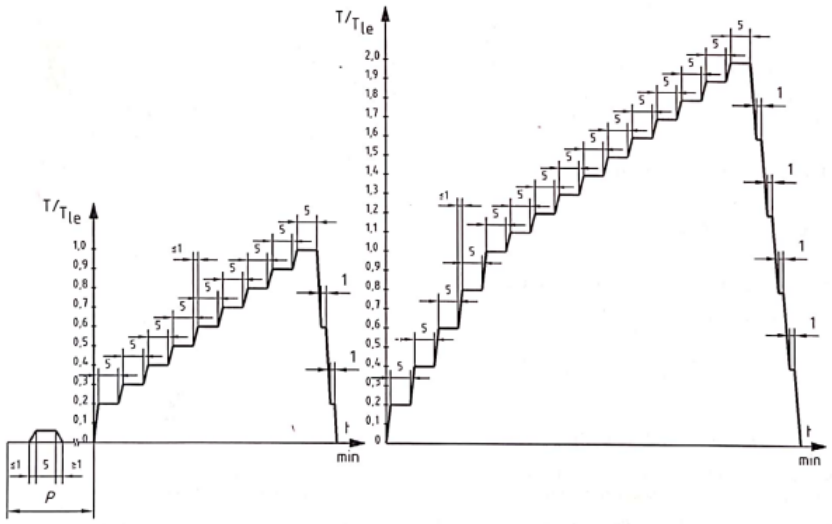

Figure 7.1: Loading cycles proposed by the XP P94-444 norm

$$T_{max} = 2T_{le} \leq 0.9T_p \tag{7.1}$$

Where:

- T is the traction force.
- T_{le} Traction force estimated from the geotechnical data.
- t time, in minutes.
- P preparatory phase of the test.

Since T_p is the elastic limit of the steel bar it can be calculated as following:

$$T_p = \sigma_{yk} A_s$$

Where σ_{yk} is the steel's yielding stress and A_s is the bolt's section.
While T_{le} is defined in the NF P94-242-1 norm as:

$$T_{le} = q_{se} S$$

Where S is the lateral surface of the rock-bolt that is in contact with the rock and q_{se} is the friction shear stress deducted by the geotechnical data.

Although, differently than the prescription of the XP P94-444 norm, in the conducted tests the loading steps did not last 5 minutes; it was considered that shorter steps were adequate.
With this testing method we can analyse different aspects of the behaviour of this element: the presence or of creep deformations during each step, or also the change of performance due to loading and unloading cycles.
The trials were conducted in three different sites:

- Seyssel
- Oisans
- Mongalgan

In each site at least six rock-bolts were made. We can observe in the Figure 7.2 the characterising parameters of the rock-bolts's traversal sections.

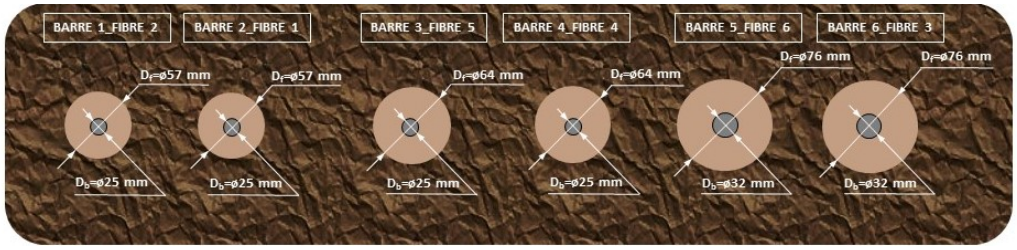

Figure 7.2: Rock-bolts's geometry

The steel reinforcement has a diameter of 25 mm for the holes with 57 and 64 mm diameter and 32 mm for the other ones.

7.1 Seyssel

Seyssel is a small municipality in the Occitanie region (see figure 7.3).

Figure 7.3: Geographical localisation of Seyssel

One of the testing campaigns was realized here in the proximity of the SNCF train station of Seyssel-Corbonod as we can observe in the figure 7.4.

(a) SNCF train station of Seyssel-Corbonod

(b) Rock wall in Seyssel with the installed anchorage and the pull-out device.

Figure 7.4: Seyssel's site

The site is characterized by alluvial materials as we can see in figure 7.5 where this area is defined by the presence of marine limestone from the Miocene period. While the massif used for the rock-bolts installation is characterized by heterogeneous moraine materials that are quite compacted.

We can also observe a photogrammetric model of the used rock wall in figure 7.6:

In Seyssel seven rock-bolts were realized and we can see their characteristics in the table 7.1.

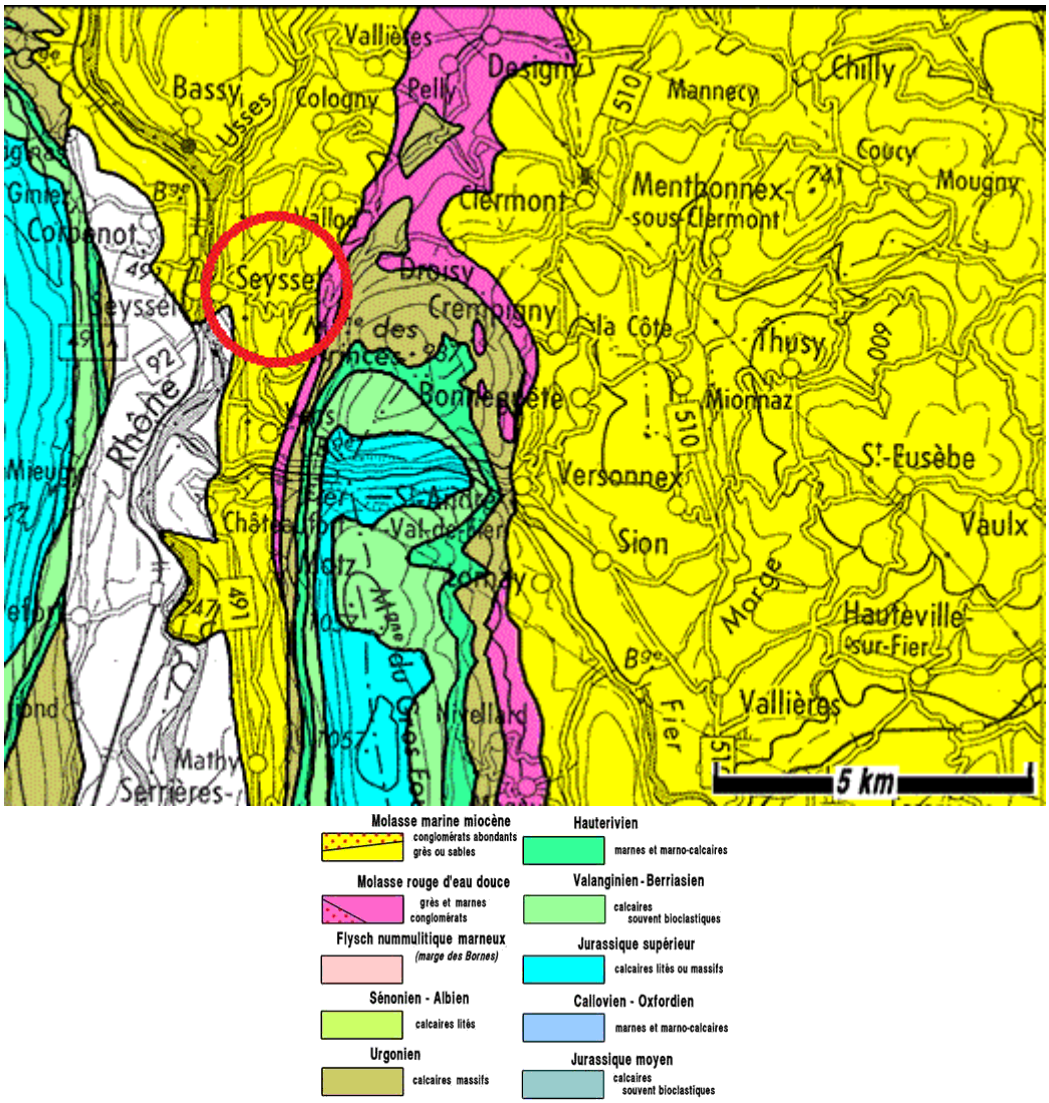

Figure 7.5: Seyssel's geologic map

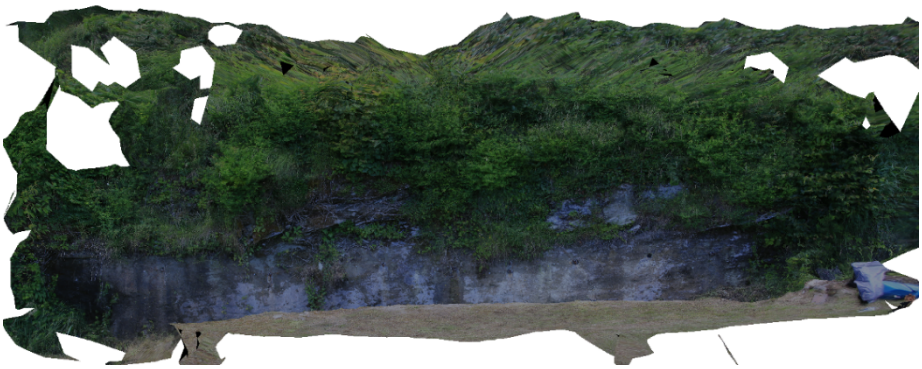

Figure 7.6: Photogrammetric model of the used rock wall in Seyssel

We can observe in the Figures 7.7 and 7.8 the behaviour of these rock-bolts in terms of force-displacements. In figure 7.7 we can observe the load displacement graph of the rock-bolts in Seyssel as measured, which is defined as the gross displacement; while in figure 7.8 the displacements plotted are the resilt of subtraction between

Ancorage	ϕ renforcement [mm]	ϕ hole [mm]
A1	25	57
A2	25	57
A3	25	64
A4	25	64
A5	25	64
A6	32	76
A7	32	76

Table 7.1: Rock-bolts characteristics in Seyssel

the measured displacements and the theoretical ones of the ungrouted bar, which is obtained with an elastic correlation between force and displacement, these are called net displacements.

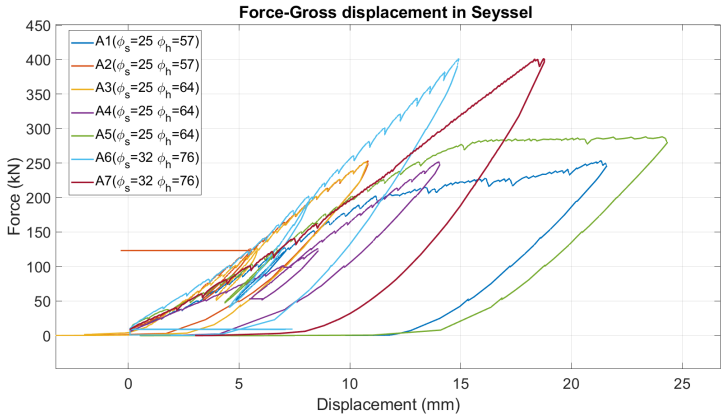

Figure 7.7: Axial force and gross displacement behaviour for the rock-bolts in Seyssel

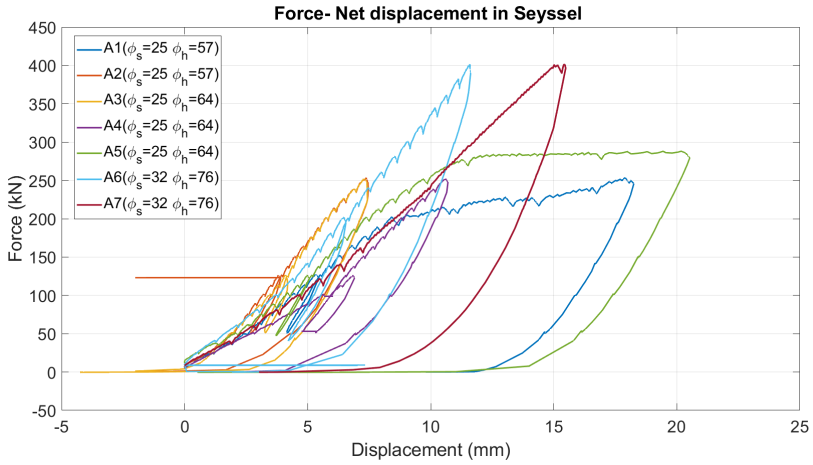

Figure 7.8: Axial force and net displacement behaviour for the rock-bolts in Seyssel

7.1.1 Force-displacement in Seyssel

For a better clarity of the results we can observe some examples of the force displacement in some rock-bolts, we can see for example in figure 7.9 the displacements in the first anchorage at Seyssel, we observe a linear growth in the first segment and then we get into a step, which shows a plasticization of the system. While in figure 7.10 we can observe only the former behaviour, as there is a lack of the plastic step.

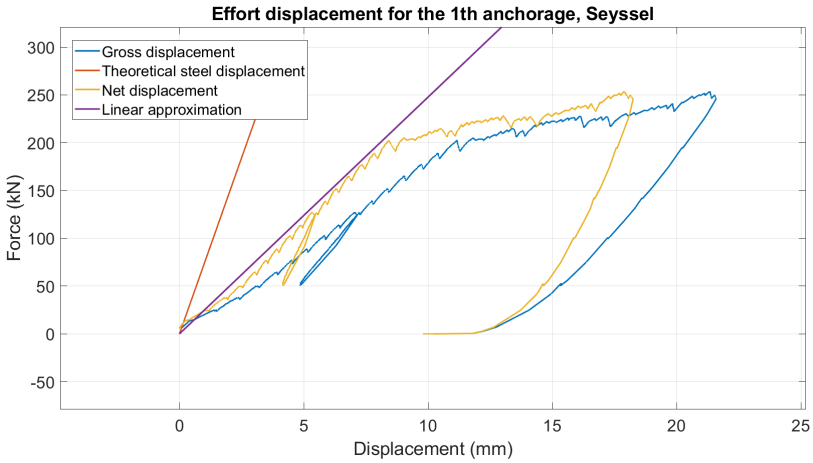

Figure 7.9: Force displacement for the 1^{st} anchorage, Seyssel

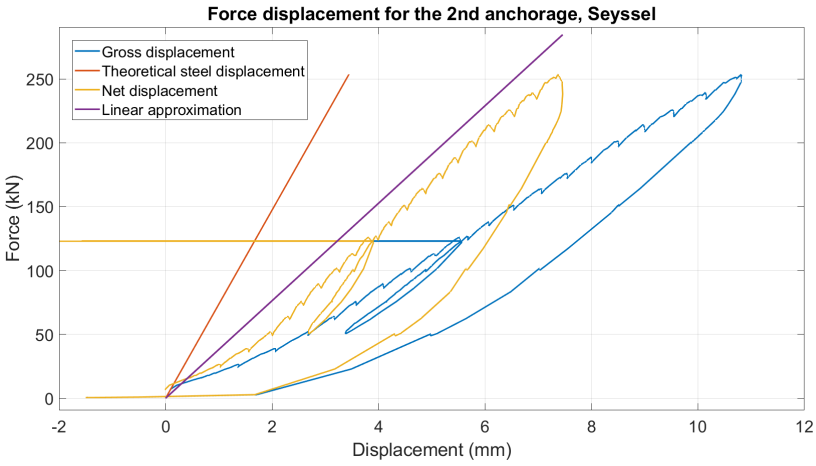

Figure 7.10: Force displacement for the 2^{nd} anchorage, Seyssel

In the figures 7.9 and 7.10 we can observe the gross displacements, which are measured by the sensor in the head of the bolt, the theoretical steel displacements, which are deducted by the loads using the steel's Young Modulus, and the net displacements, which are the result of the subtraction of the previous two. A linear approximation was also made of the net displacements.

7.1.2 Fibre optic results in Seyssel

In this paragraph some fibre optic results, in Seyssel, will be presented; for a better intelligibility, they will not be plotted for all the loading steps but only for some virgin loadings.

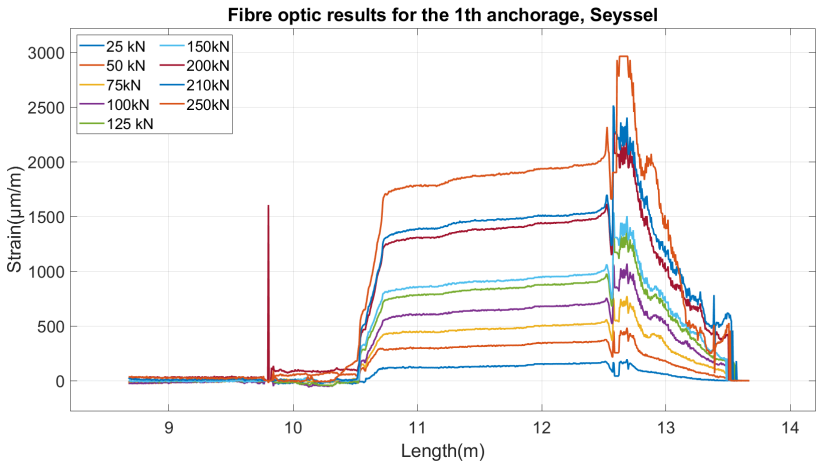

Figure 7.11: Fibre optic results for some virgin loading steps in the 1^{st} anchorage, Seyssel

In the figure 7.11 we can observe the typical result of a fibre optic measurement of the strains. We can describe three zones (see figure 7.12):

- The first zone: the strains are zero here and this happens because the fibre is outside the rock bolt.
- The second zone is characterised by a quasi constant value of the strains. This is explained by the fact that this corresponds to the free length of the steel-bar. These values, though, are hard to interpret as in this segment the fibre optic is surrounded by the protecting sheath; this causes a lack in the certitude of the measurements.
- The third zone is characterized by an exponential decrease of the strains; this corresponds to the grouted segment. In this zone the measurements are very reliable as the used fibre optic has no sheath around it. The core is directly buried in the connecting glue.

To understand the behaviour in the grouted zone we can observe the figure 7.13.

We can observe in figure 7.13 how the exponential behaviour is not perfect, there are several zones were we have a constant or even increasing strain value, this could be explained by the heterogeneity of the site, where each constant step corresponds to a change in the properties of the massif.

The same observations could be made for other rock-bolts. In figure 7.14,for example, we can observe the measured strains in the fourth anchorage in Seyssel.

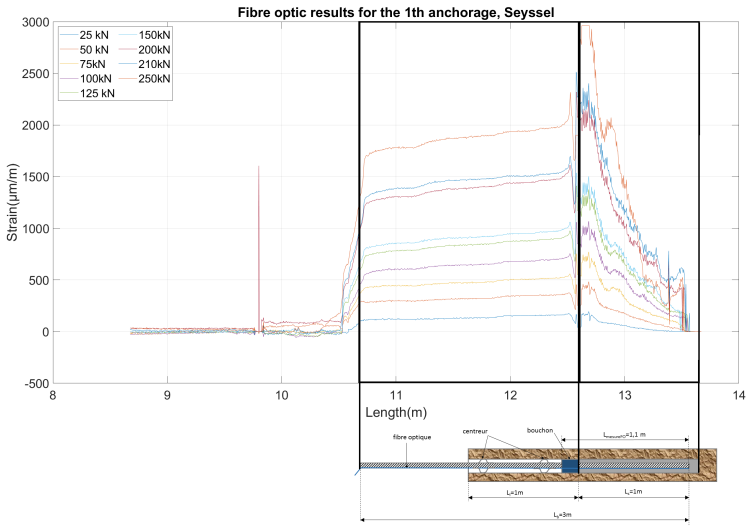

Figure 7.12: Fibre optic results for some virgin loading steps in the 1^{st} anchorage, Seyssel

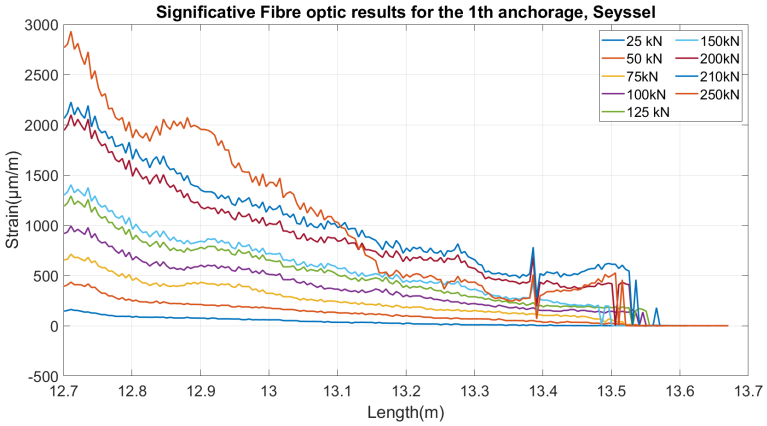

Figure 7.13: Fibre optic results in the grouted segment for some virgin loading steps in the 1^{st} anchorage, Seyssel

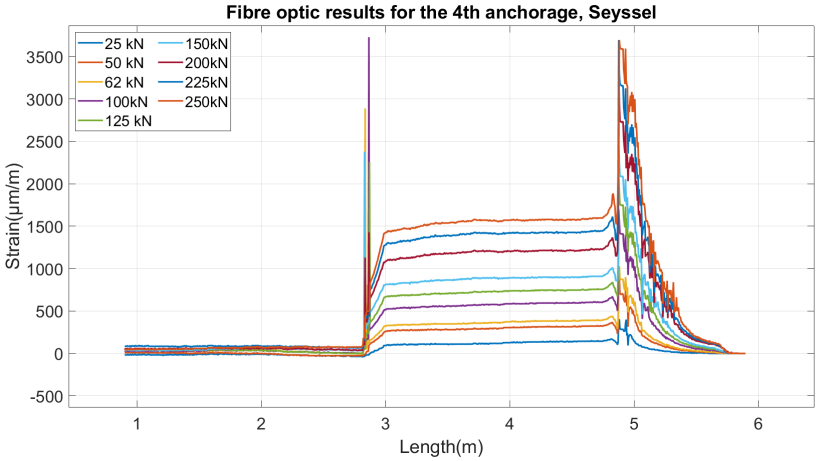

Figure 7.14: Fibre optic results for the virgin loading steps in the 4^{th} anchorage, Seyssel

7.2 Oisans

Bourg-d'Oisans is a municipality in the Auvergne-Rhône-Alpes region in France (see figure 7.16).

(a) 3D view of Oisans's valley.

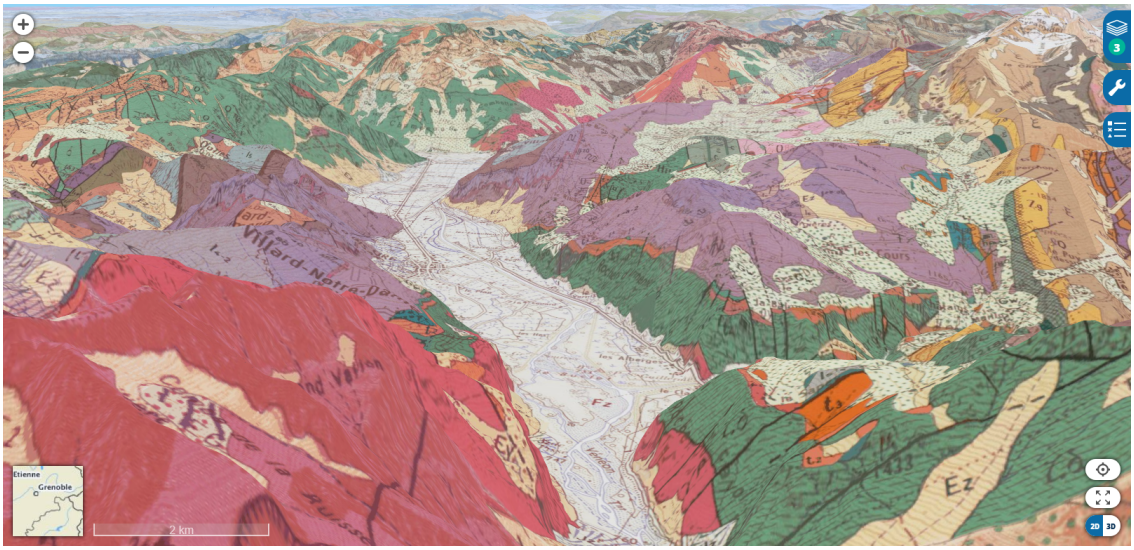

(b) 3D view of the geologic map of Oisans's valley.

Figure 7.15: View of Oisans's valley (géoportail.gouv.fr).

In this municipality, the location where the test were conducted is called "La Garde" in proximity to the la Sarenne waterfall. In figure 7.17 we can observe the concerned rock wall.

This site is characterized by the presence of limestone rock with two principal discontinuities Which can be seen in the photogrammetric model in figure 7.18.
Thanks to the use of the website géoportail.gouv.fr made by the IGN (Institut géographique national) it was possible to have a sight of the 3D view of the valley (see figure).

Figure 7.16: Geographical localisation of Bourg-d'Oisans

Figure 7.17: Rock wall in Bourg-d'Oisans

In Oisans six rock-bolts were realized, but we have only the data of five which have the following characteristics that are reported in the table 7.2.

Ancorage	ϕ renforcement [mm]	ϕ hole [mm]
B2	25	57
B3	25	64
B4	25	64
B5	32	76
B6	32	76

Table 7.2: Rock-bolts characteristics in Oisans

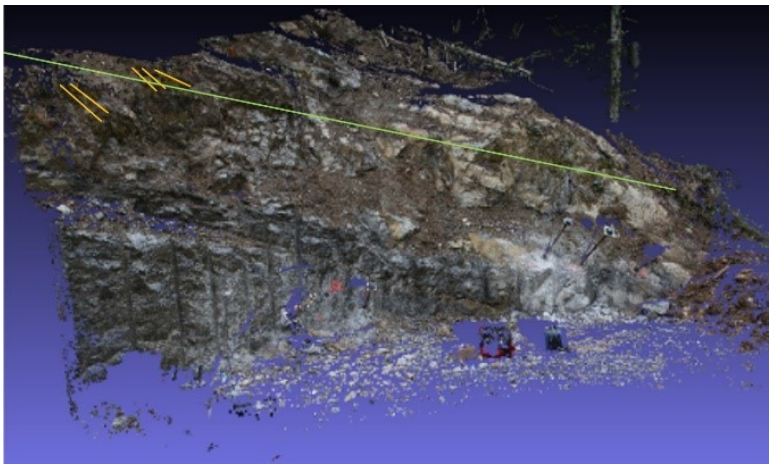

(a) First view of the photogrammetric model in Oisans.

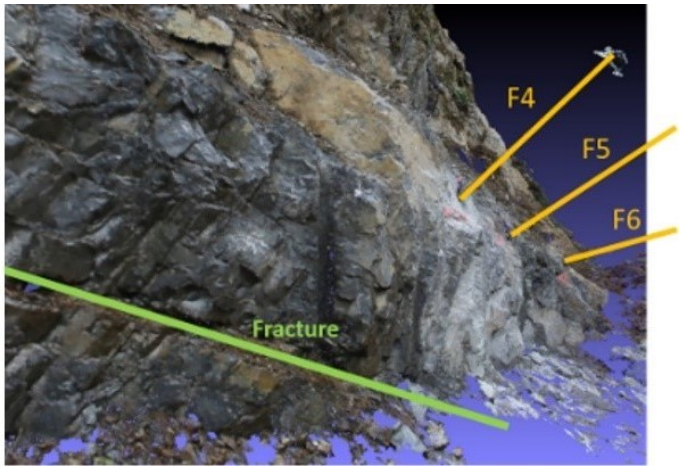

(b) Second view of the photogrammetric model in Oisans.

Figure 7.18: Photogrammetric model of the rock wall in Oisans.

As reported previously for Seyssel we can display the load displacement behaviour of the different anchorages in Oisans. In figure 7.19 we can observe the net displacements caused by the application of the loads, which means that they are the results of the free steel displacements subtracted by the measured displacements.

7.2.1 Force displacement in Oisans

While observing figure 7.19 we can notice that the behaviour of the second (see also figure 7.20) and the fourth anchorage are quite different than the other ones. In fact it is quite evident that the stiffness of these two rock-bolts is lower than the other ones even if the yielding limit of the bar has not been reached. This behaviour could be explained with the presence of some problems in the grouting. It is possible that either the grout quality was inferior in these rock-bolts or that the presence of fractures inside the cavity has drained the liquid grout in some parts of the bolt.

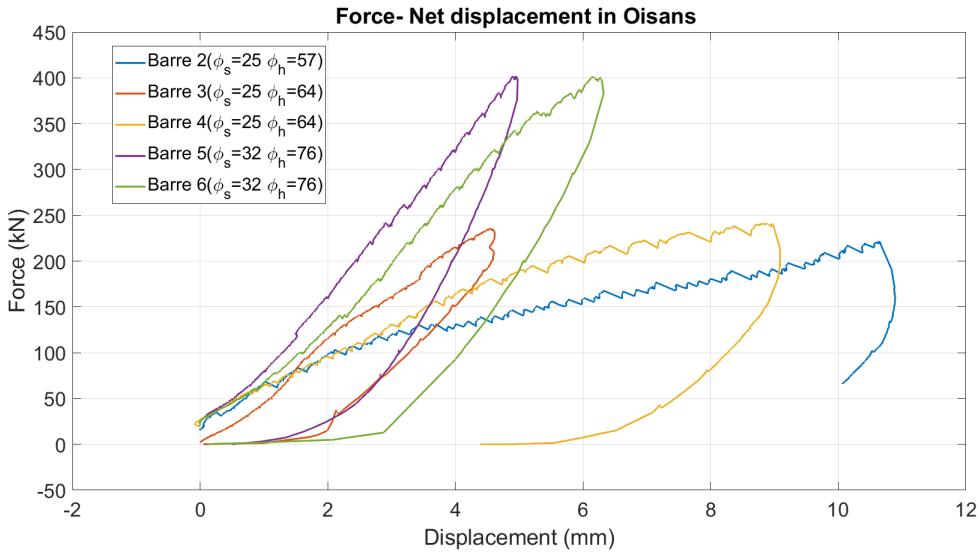

Figure 7.19: Force and net displacement behaviour for the rock-bolts in Oisans

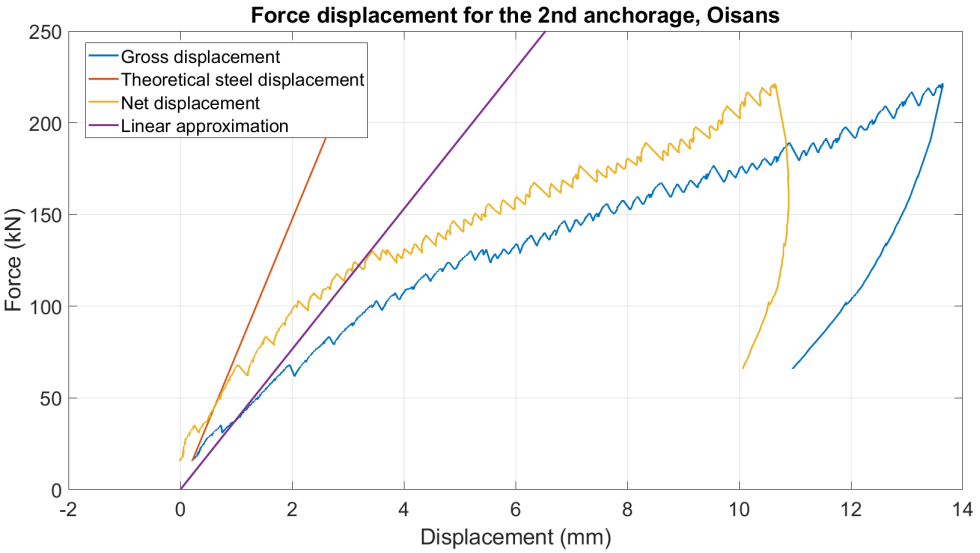

Figure 7.20: Force displacement for the 2^{nd} anchorage, Oisans

The difference in the stiffness of the element is evident by the comparison of the second (see figure 7.20) and the fifth (see figure 7.21) anchorages for example.

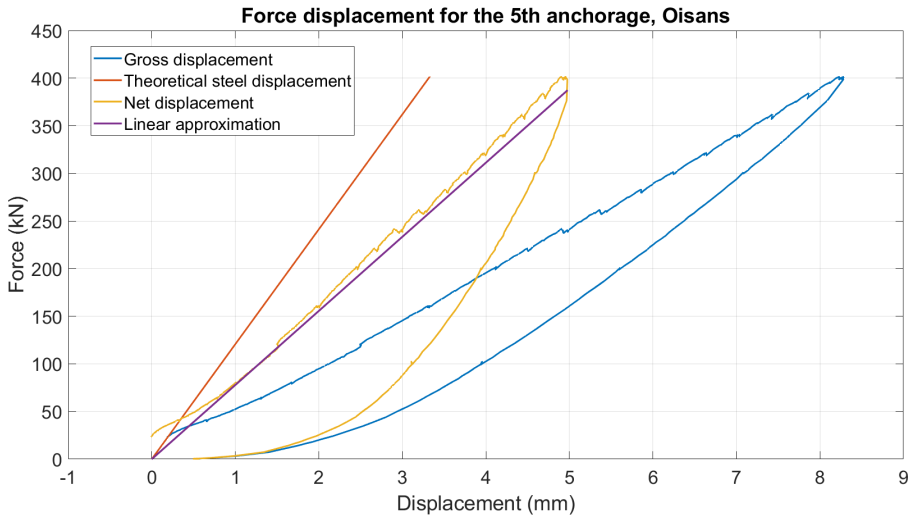

Figure 7.21: Force displacement for the 5^{th} anchorage, Oisans

7.2.2 Fibre optic results in Oisans

As already seen in 7.1.2 the strain results measured with the fibre optic are generally characterized by the presence of three zones, which are visible also in the outputs of this testing campaign as we can observe in the figure 7.22

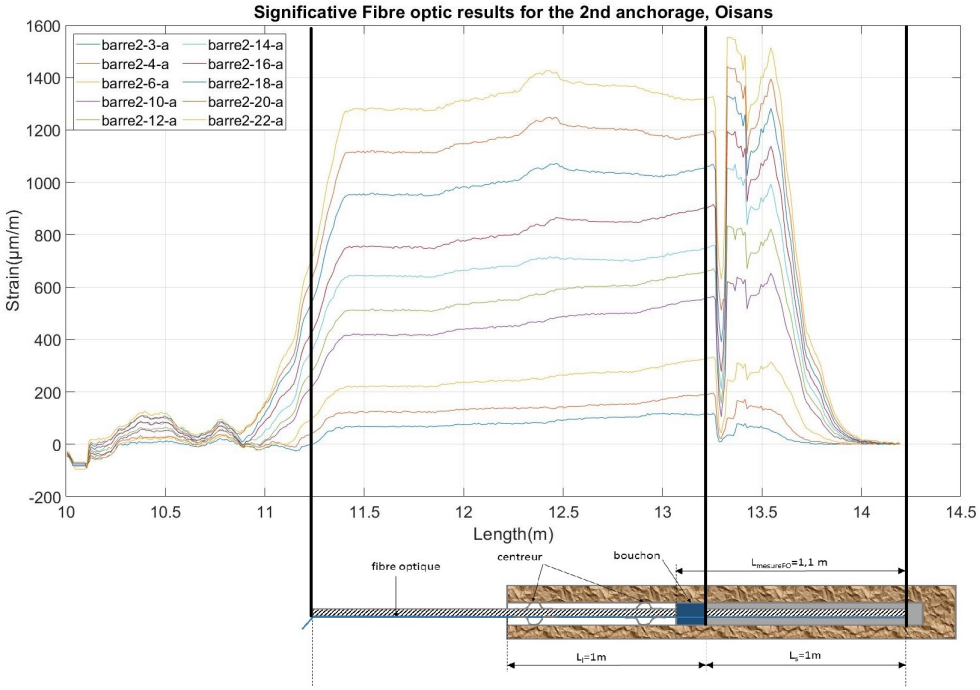

Figure 7.22: Fibre optic results for some virgin loading steps in the 2^{nd} anchorage, Oisans

We can also observe the exponential decrease in the grouted segment in the figure 7.23. We can see that in this case the measured strains are characterized by a smoother behaviour compared to Seyssel (see figure 7.13 for the results in the first rock-bolt), this is connected to the homogeneity of the rock massif in this site. We can confirm this observation looking at the results in the different anchorages from example the ones of the fifth rock-bolt (see figure 7.24).

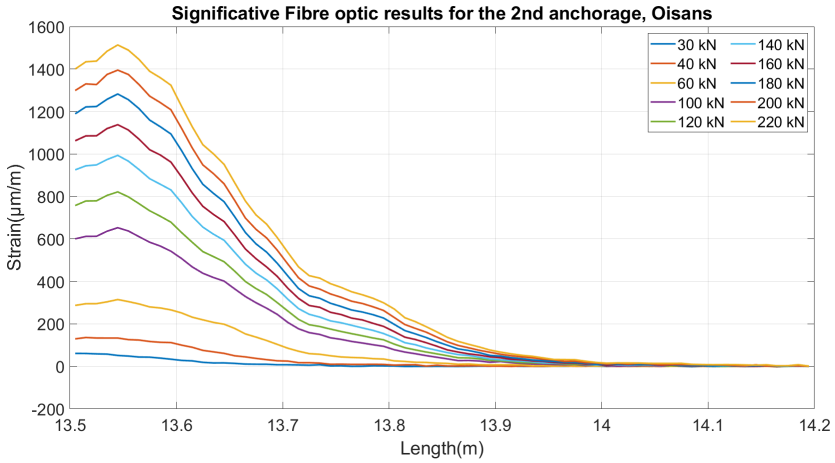

Figure 7.23: Fibre optic results in the grouted segment for some virgin loading steps in the 2^{nd} anchorage, Oisans

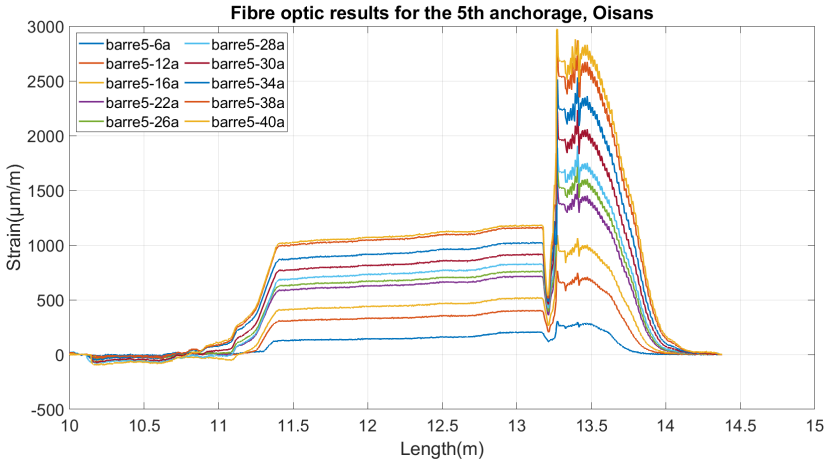

Figure 7.24: Fibre optic results for some virgin loading steps in the 5^{th} anchorage, Oisans

7.3 Mongalgan

Mongalgan is a locality in the municipality of Moûtiers in the Auvergne-Rhône-Alpes region in France (see figure 7.25).

Figure 7.25: Geographical localisation of Moûtiers

For a better understanding of this locality we can observe its 3D model obtained from geoportail.gouv.fr in figure 7.26.

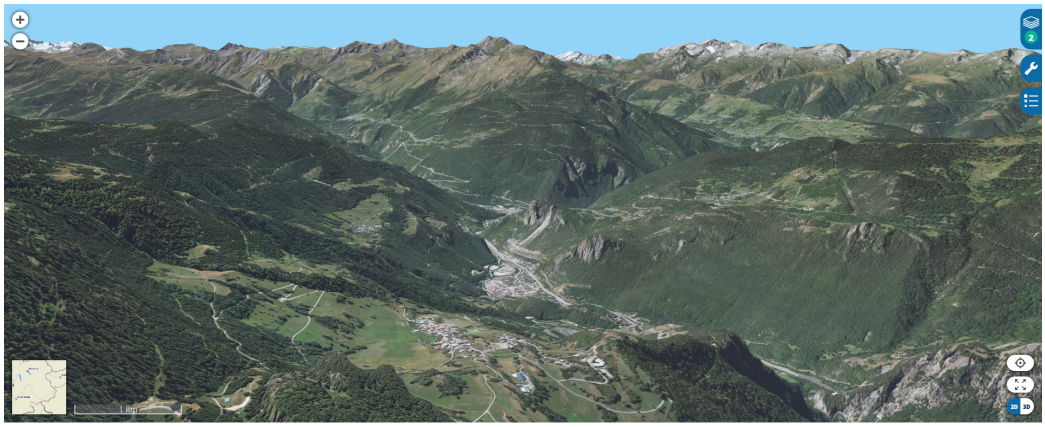

Figure 7.26: 3D view of Mongalgan

We can also observe in figure 7.27 the geological map of this site.
The tested location is characterized by fractured limestone, we can observe in figure 7.28 the rock wall where the anchorages were realized.

In the photogrammetric model (see figure 7.29) we can observe the position of the different anchorages.

In Mongalgan six rock-bolts were realized, but we have only the data of four, which characteristics can be seen in table 7.3.

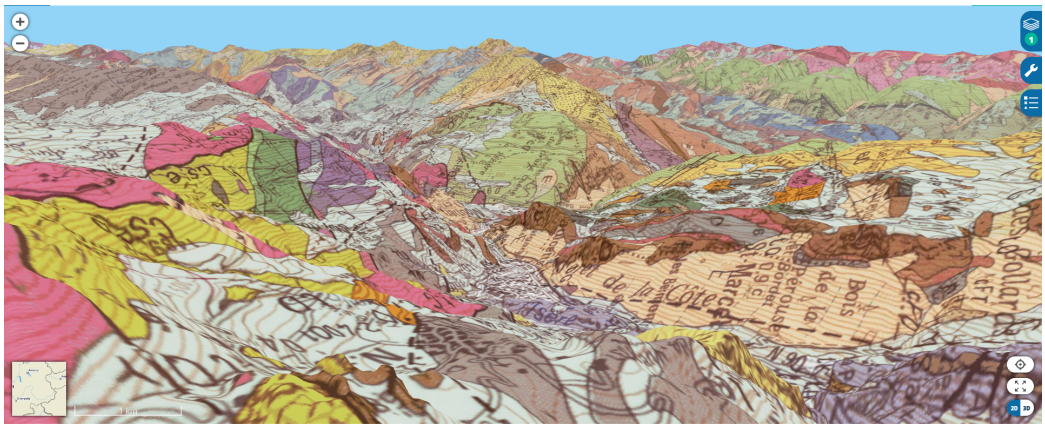

Figure 7.27: 3D view of Mongalgan

Figure 7.28: Tested rock wall in Mongalgan

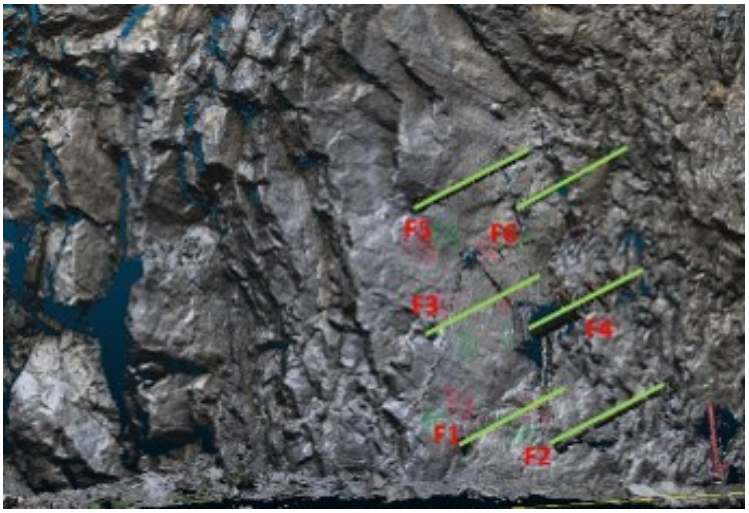

Figure 7.29: Photogrammetric model of the rock wall in Mongalgan

As reported for the previous site we can observe in figure 7.30 the behaviour of these rock-bolts in terms of force-displacements, where the the plotted displacements are

Ancorage	ϕ renforcement [mm]	ϕ hole [mm]
F2	32	76
F4	25	64
F5	25	64
F6	32	76

Table 7.3: Rock-bolts characteristics in Mongalgan

the net ones.

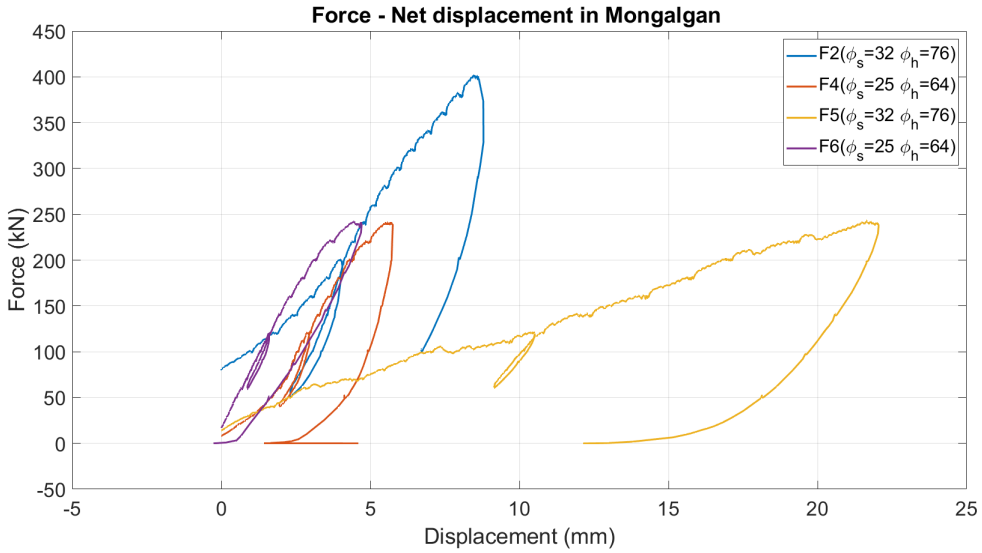

Figure 7.30: Force and net displacement behaviour for the rock-bolts in Mongalgan

7.3.1 Force displacement in Mongalgan

While observing the results in the figure 7.30, we can see that the fifth anchorage is characterized by a peculiar behaviour, in fact the stiffness of this element is significantly inferior to the others. This is very similar to what was observed for Bourg-d'Oisans in 7.2.1.

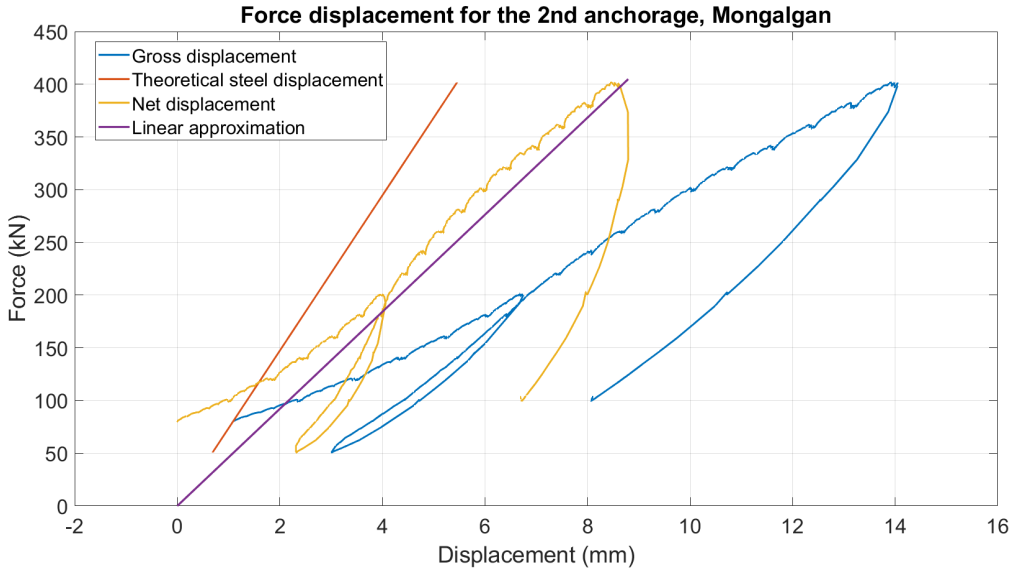

Figure 7.31: Force displacement for the 2^{nd} anchorage, Mongalgan

This can be observed also by the comparison of figures 7.31 and 7.32. And it could be explained by the presence of problems in the grout. A possible explanation could be connected to the presence of fractures. It is possible that the liquid grout was drained by the fractures and this caused the absence of cement on some parts, decreasing the resistance of the whole element.

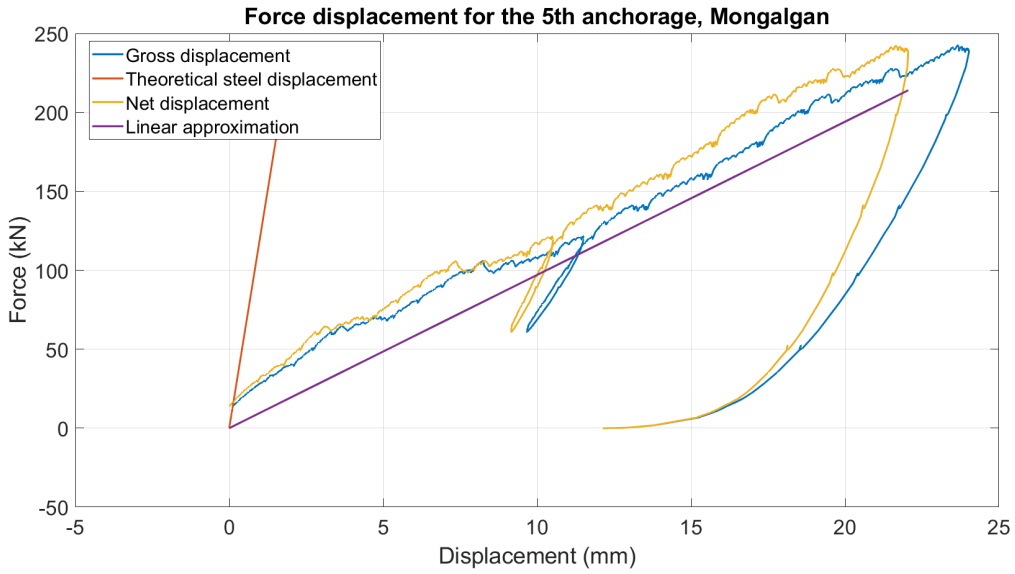

Figure 7.32: Force displacement for the 5^{th} anchorage, Mongalgan

7.3.2 Fibre optic results in Mongalgan

As already presented in 7.1.2 also in this case we can observe the same behaviour of the strains (see figure 7.33).

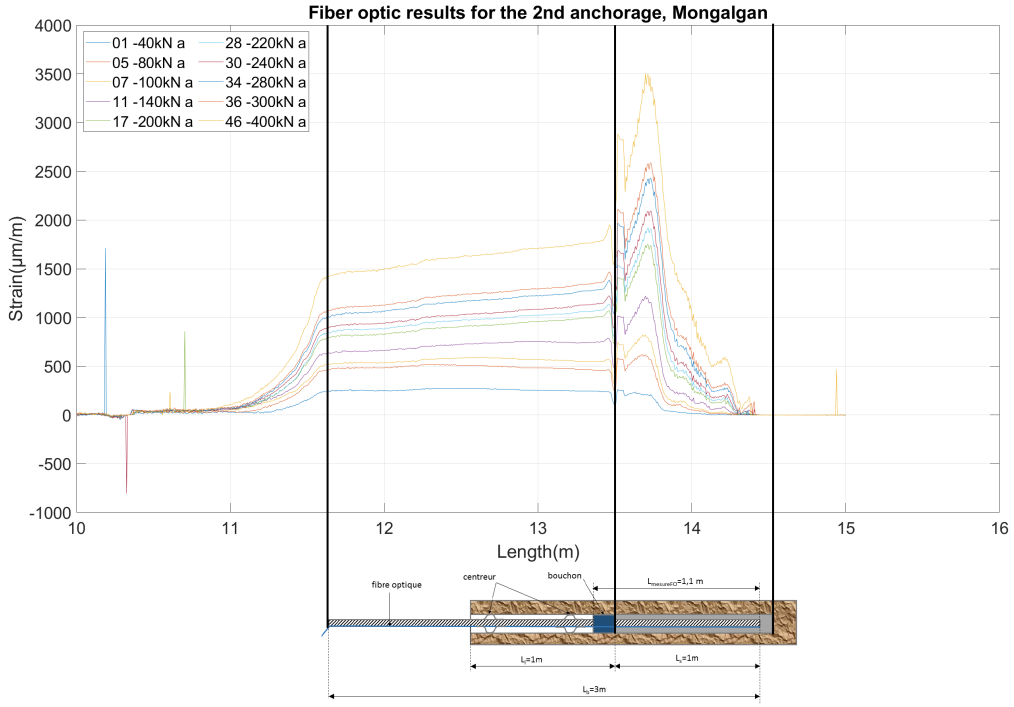

Figure 7.33: Fibre optic results for the virgin loading steps in the 2^{nd} anchorage, Mongalgan

We can observe the same zones observed in the previous sites. In this case the grouted segment is characterised by several steps in the exponential decrease which can be explained by the presence of fractures in the rock massif; this can be observed in figures 7.34, 7.35 and 7.36

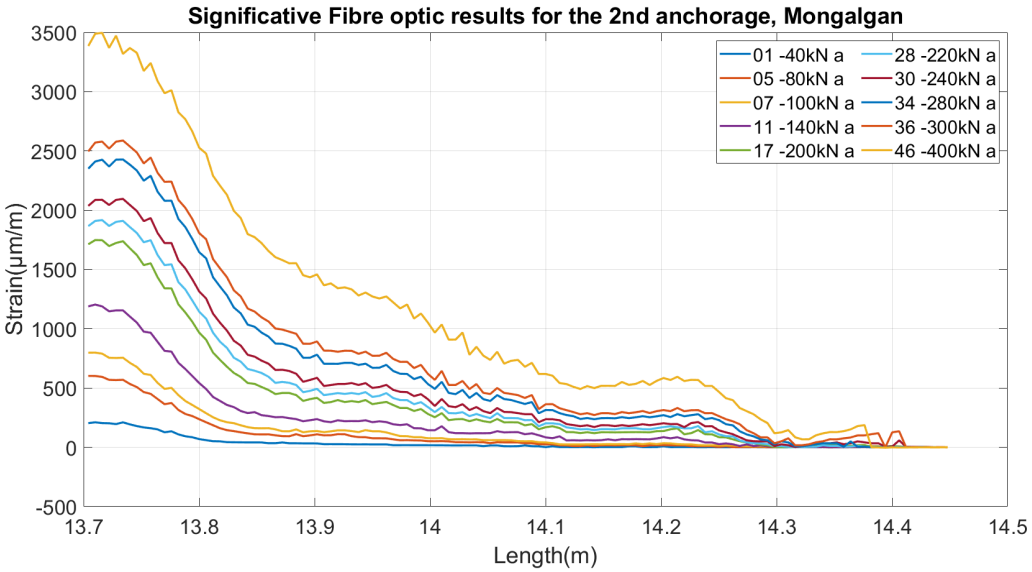

Figure 7.34: Fibre optic results in the grouted segment for some virgin loading steps in the 2^{nd} anchorage, Mongalgan

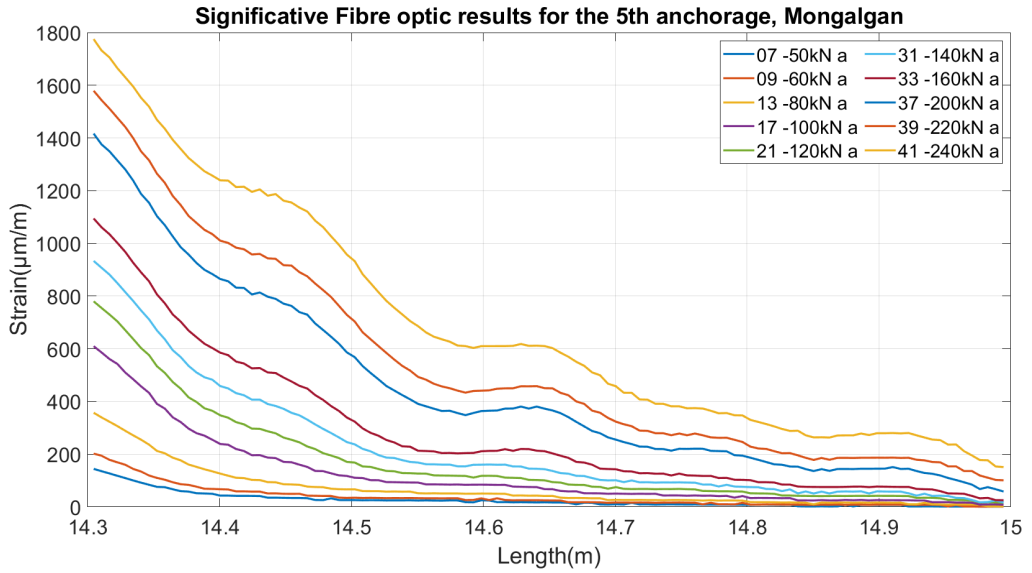

Figure 7.35: Fibre optic results in the grouted segment for some virgin loading steps in the 5^{th} anchorage, Mongalgan

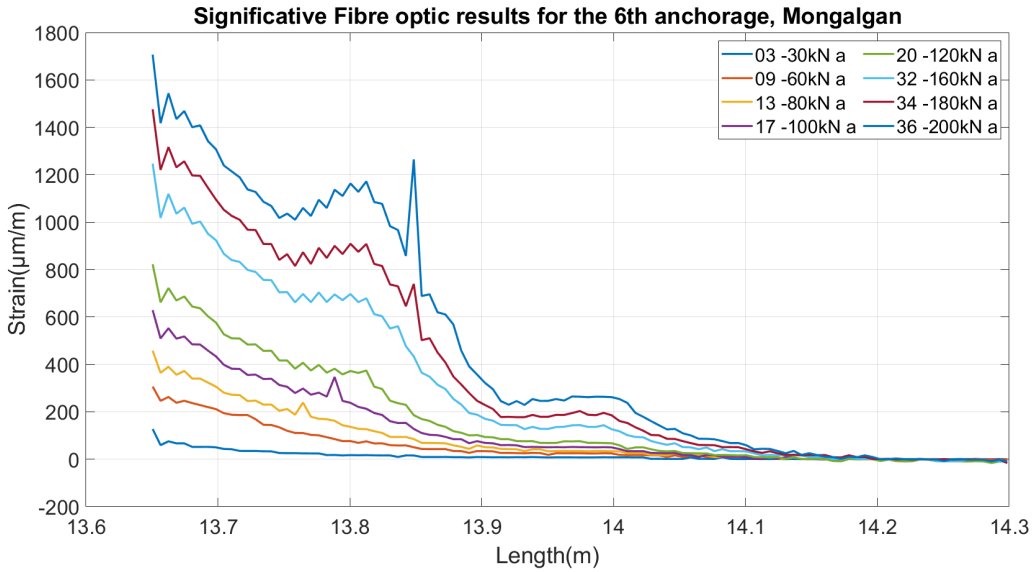

Figure 7.36: Fibre optic results in the grouted segment for some virgin loading steps in the 6^{th} anchorage, Mongalgan

7.4 Comparison between the three sites

The comparison between the results introduced in the previous paragraphs could be used to improve our understanding of the three sites and the behaviour of the anchorages in each one of them. To do this we will use the force displacement graphs and compare them for the different elements and sites.
In figure 7.37 we can observe the behaviour of the rock-bolts with a steel bar diameter of 25mm.

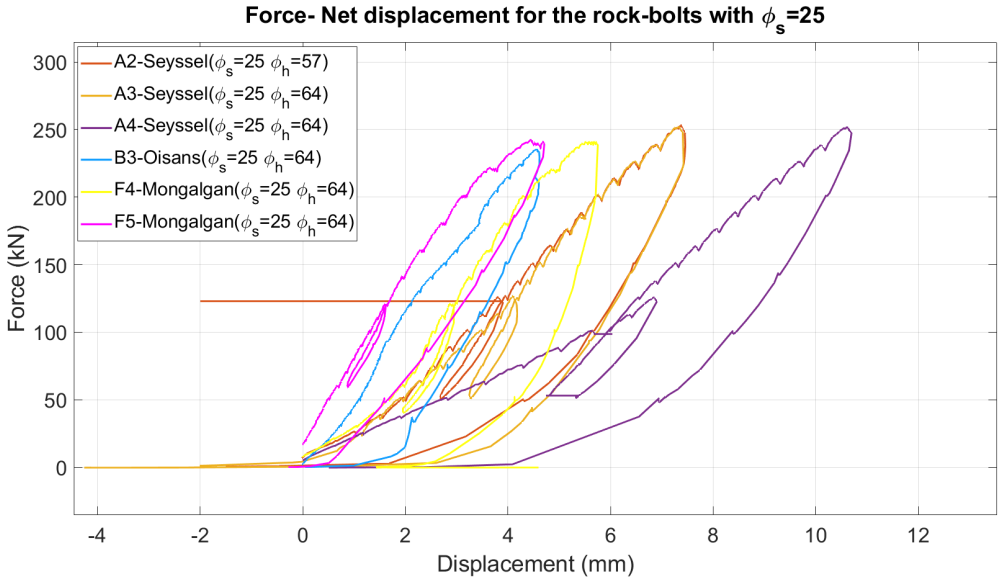

Figure 7.37: Force displacement behaviour for the rock-bolts with a steel bar diameter ϕ_s=25mm

While observing figure 7.37 we can see how the behaviour of the second and third anchorages in Seysell are very close, even if the borehole diameters of these two rock-bolts are different. The former, in fact, if characterized by a borehole diameter of 57mm, while in the latter it corresponds to 64mm. In the same site the fourth anchorage has the same geometrical characteristics of the third one, but it shows a different behaviour.
From these anchorages we can deduct that the borehole diameter is either: a parameter that is inversely proportional to the stiffness of the element (the forth anchorage is the less rigid one); or a parameter that does not influence much the behaviour of the rock-bolt, this could be justified by the perfect correspondence between the second and the third element in Seyssel. In this last case the lack of stiffness of the forth anchorage could be explained assuming a strong variability in the mechanical properties of the rock, we can suspect that this anchorage crosses a weaker portion of rock; the rock massif, in fact, is not a perfectly homogeneous medium, which makes also this explanation plausible. With the data provided then we can not decide which one of the two assumptions is the correct one.
It would be quite interesting to understand this phenomenon; this could be done by performing other tests and seeing how the rigidity of the analysed elements is affected by changing the borehole diameter. In this study this was not possible because the other elements that have a borehole diameter of 64 mm showed a

strange behaviour; they developed important displacements and a very low stiffness and this is the reason why they were not taken into account; their behaviour was considered corrupted by other sources, probably problems in the grouting.

We can observe in figure 7.38 the force displacement comparison for the anchorages with a steel bar diameter of 32 mm.

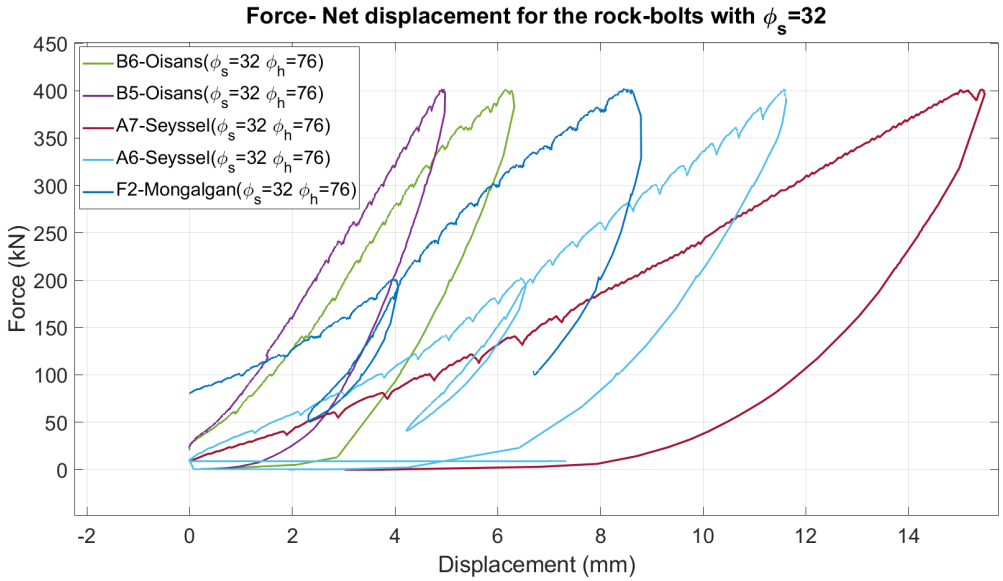

Figure 7.38: Force displacement behaviour for the rock-bolts with a steel bar diameter ϕ_s=32mm

In the figures 7.37 and 7.38 we can deduct some informations regarding the three sites. Oisans is, generally speaking, the one were the rock-bolts have developed a bigger stiffness; although Mongalgan's anchorages show a rigidity that is generally close, sometimes even higher.
Between the elements with a 25mm steel bar diameter, in fact, the most rigid one is F5 in Mongalgan, followed by B3 in Oisans, the lower stiffness in the other anchorages in Mongalgan could be explained by the fact that this site is characterized by several fractures in the rock massif. F5 then could be characterized by an important stiffness because, maybe, it crosses an area of the rock were these fractures are less important.
The fractured state of the rock massif, in Mongalgan, can then be a reason for the variability of the stiffnesses in this site's rock-bolts, as the non-fractured state of Oisans's rock could be the reason why its anchorages are generally the most rigid ones.
In other hand Seyssel has been proven by both figures 7.37 and 7.38 the site with the least rigid elements, this could be explained by the presence of a softer rock there, which does not apply the same confinement to the rock-bolt as in the other two sites.

For a better understanding of the stiffness of each anchorage, the developed displacements for each anchorage will be presented in the tables 7.4 and 7.5. This

	Displacements [mm]	
Anchorage	at 150 kN	at 250 kN
A2-Seyssel	4.457	7.39
A3-Seyssel	4.678	7.39
A4-Seyssel	7.297	10.61
B3-Oisans	2.809	4.538
F4-Mongalgan	3.415	5.718
F5-Mongalgan	2.092	4.443

Table 7.4: Developed displacements by the rock-bolts with a steel bar diameter ϕ_s=25mm

	Displacements [mm]	
Anchorage	at 250 kN	at 400 kN
A6-Seyssel	7.701	11.59
A7-Seyssel	10.17	15.45
B5-Seyssel	3.06	4.943
B6-Oisans	3.661	6.158
F2-Mongalgan	4.909	8.617

Table 7.5: Developed displacements by the rock-bolts with a steel bar diameter ϕ_s=32mm

can give us a practical understanding of the stiffness in these elements.
In the table 7.4 the displacements of the rock-bolts with a steel bar diameter of 25mm are presented; while in the table 7.5 we can get the same information about the anchorages with a 32mm steel bar diameter.

8 Data Interpretation

8.1 Residual resistance

One of the questions addressed during the analysis of the presented data is regarding the residual resistance of the rock-bolts; in fact these elements are not subjected to a constant load during their use. During the lifetime of an anchorage, in fact, it will be subjected to different loading and unloading cycles and it is interesting to see if these cycles can influence the behaviour and the resistance of the system.
To evaluate to difference of behaviour, at the end of a cycle, the strains, the forces and the stresses along the steel-grout interface were plotted for different steps.

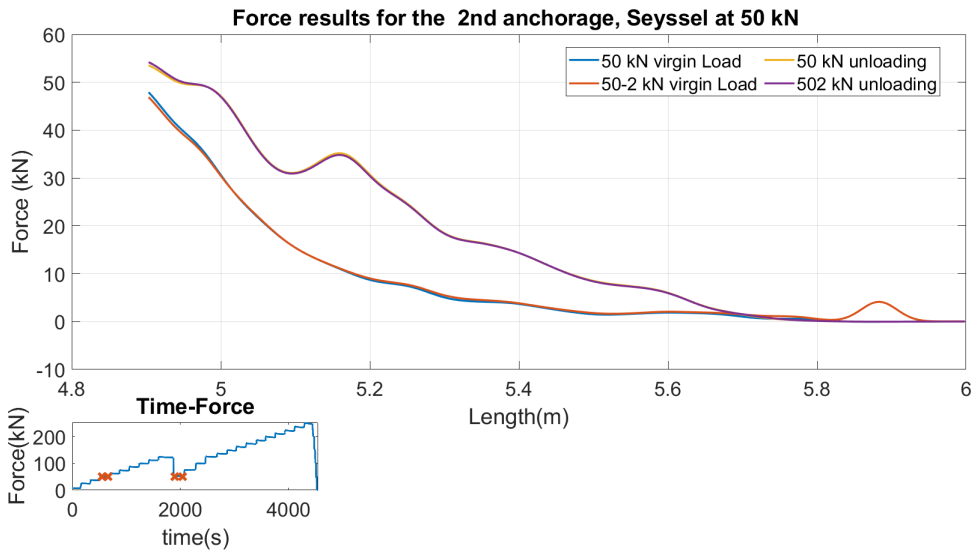

Figure 8.1: Force results for the 2^{nd} anchorage, Seyssel at 50kN

As we can observe in the figures at the end of a loading cycle, we have some residual forces. These forces depend from the maximum load applied in the first cycle. This means that not all the strains get to zero after removing a load, we have some residual ones. This is also a confirmation of what has been observed in the force displacements figures, where the behaviour of the unloading and reloading curve is different from the one in the virgin loading curve. Somehow having a previous loading cycle changes the stiffness of the system at least for the forces that are lower than the maximum load applied.

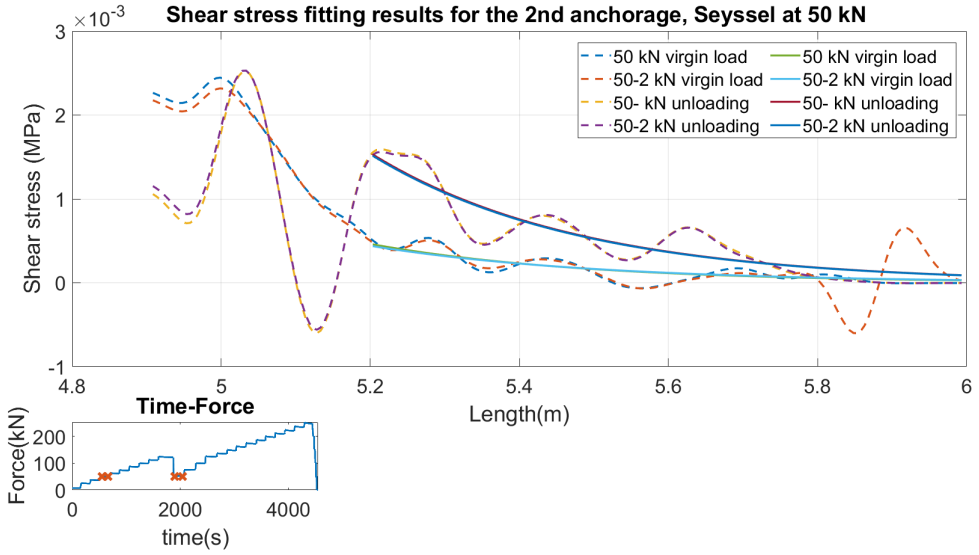

Figure 8.2: Shear stress fitting results for the 2^{nd} anchorage, Seyssel at 50kN

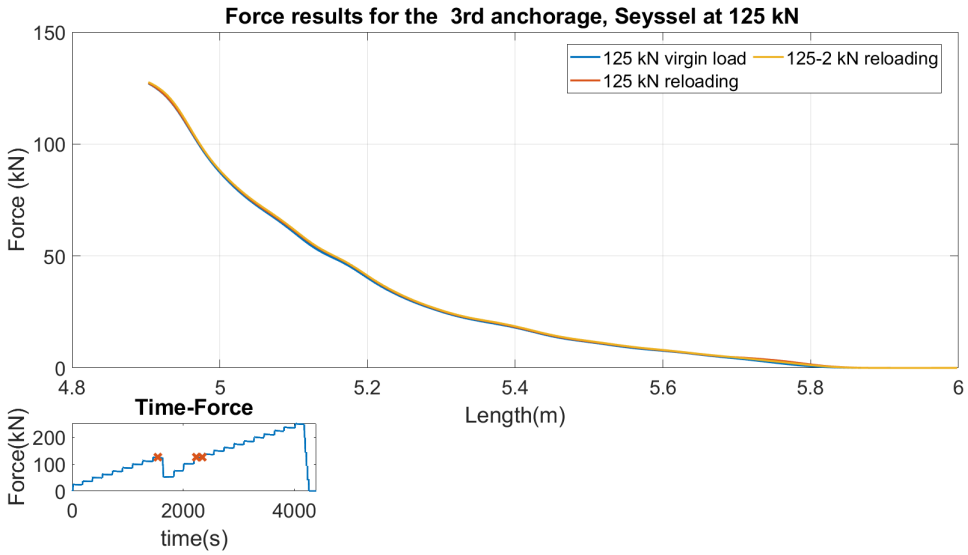

Figure 8.3: Force results for the 3^{rd} anchorage, Seyssel at 125kN

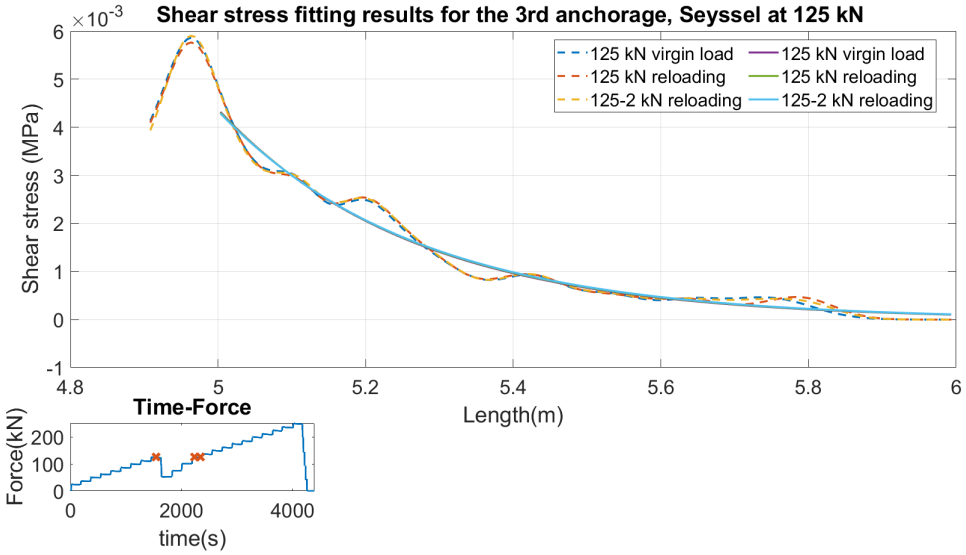

Figure 8.4: Shear stress fitting results for the 3^{rd} anchorage, Seyssel at 125kN

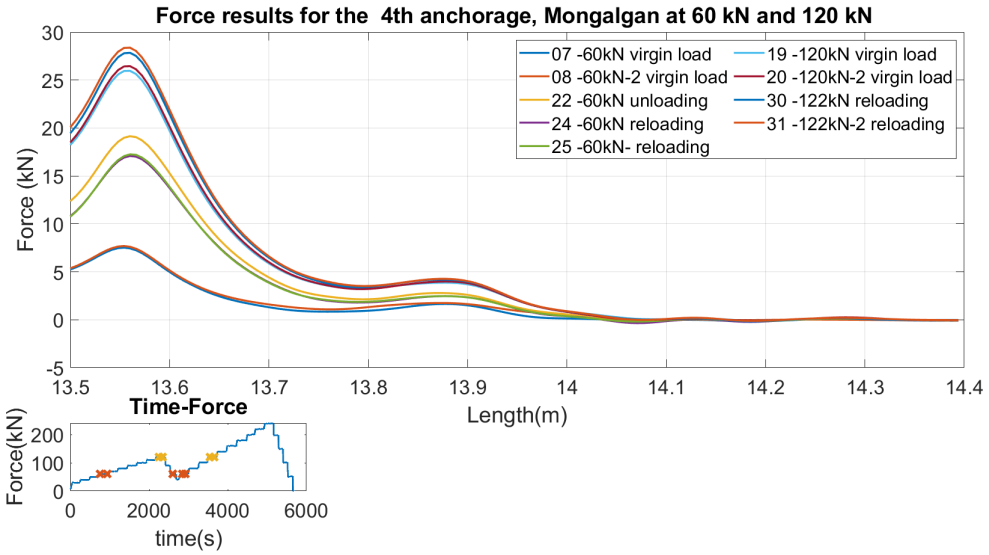

Figure 8.5: Force results for the 4^{th} anchorage, Mongalgan at 60 kN and 120 kN

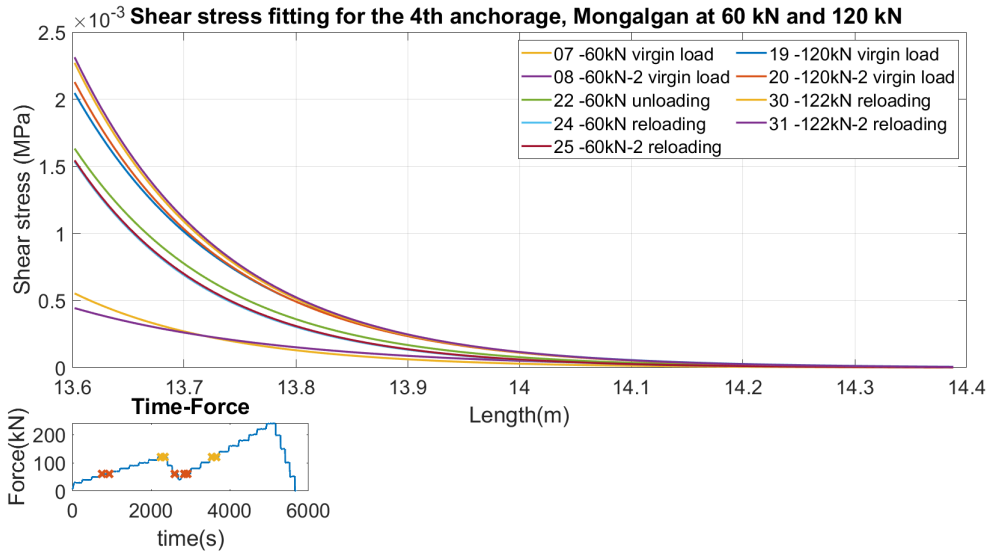

Figure 8.6: Shear stress fitting results for the 4^{th} anchorage, Mongalgan at 60 kN and 120 kN

8.2 Creep

Another interesting topic observed during the analysis of the collected data is the absence of creep deformations, in fact for each loading step, which lasts approximatively three minutes, two measurements were made. One measurement at the beginning and one at the end of the step. And we can not observe any specific difference between the two.

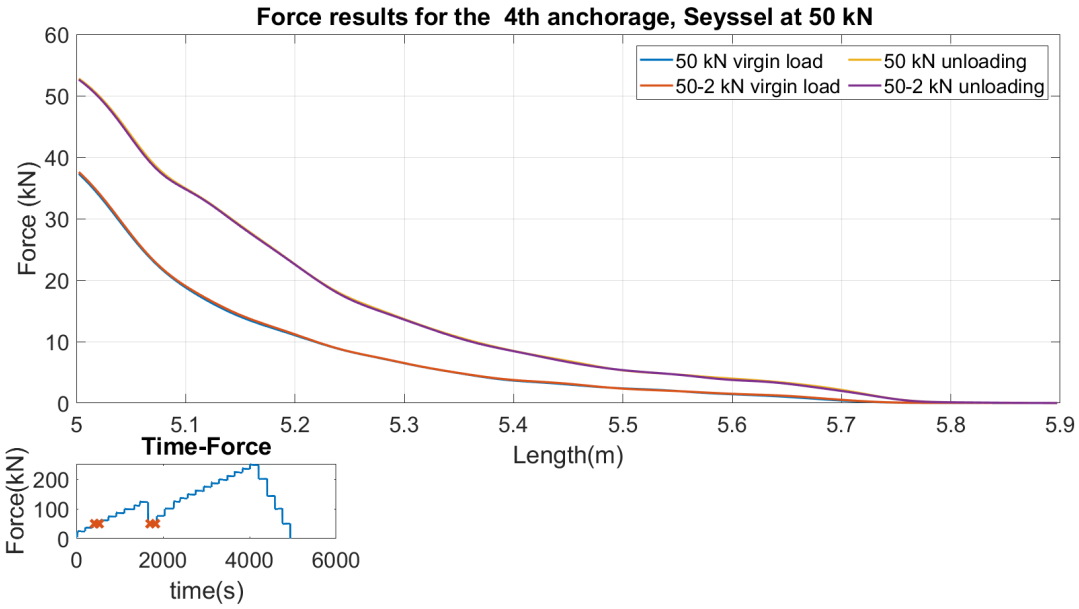

Figure 8.7: Force results for the 4^{th} anchorage, Seyssel at 50kN

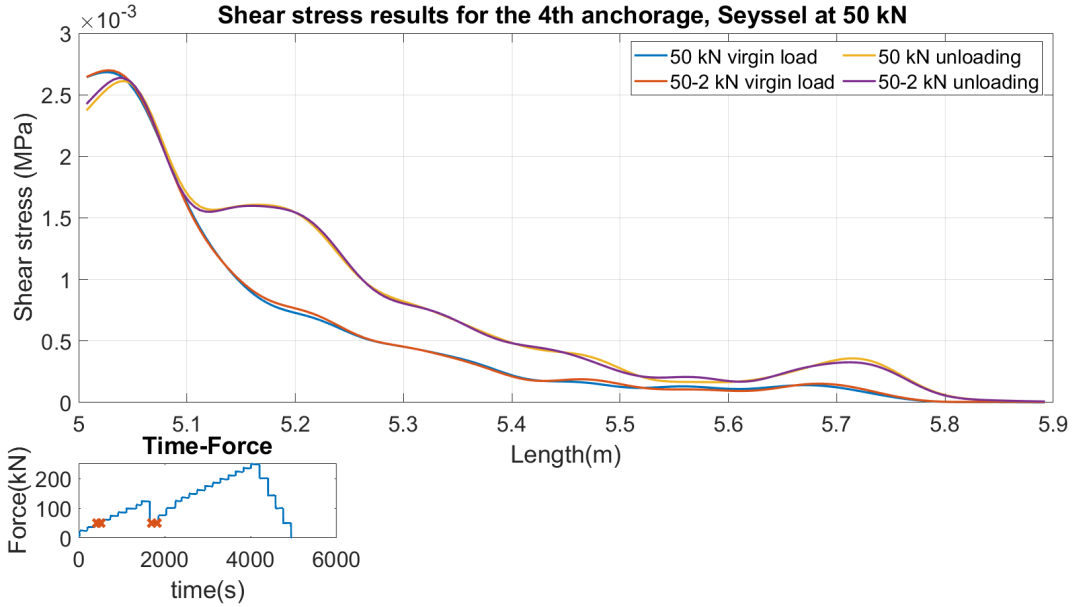

Figure 8.8: Shear stress fitting results for the 4^{th} anchorage, Seyssel at 50kN

It might be important to observe that the absence of creep deformation might be connected to the extent of the loading, it is possible that if we apply the load for more than three minutes (the used duration), some creep deformations could become visible.

8.3 Fibre optic measurements in the non-grouted steel

During the data analysis another question concerned the possibility of using the fibre optic measurements in the non-grouted segment. The fibre in this part is covered by the sheath so the measurements are not as precise as in the grouted part, but the hope of this analysis was to find a correlation between these measurements and the steels characteristics (for example the Young Modulus). This could have been very useful for the analysis of the behaviour of these elements because it would give us the possibility to work with the real attributes of the bar and not the nominal ones. This analysis was performed comparing the applied forces and the corresponding forces to the measured strains (using equation 6.1). The idea behind this comparison was the following: if we find that the slope coefficient obtained by the linear approximation is generally constant in all the rock-bolts, this would mean that the fibre measures only a portion of the strains in this segment. This information could be then used to compute the mechanical characteristics of the steel bar.
The obtained results show a good correlation between the compared entities, we have R^2 values that are very close to 1; but the slope coefficient, as we can see in the figures, is different for each anchorage, this shows that we do not always measure a constant portion of the strains in this segment, but the percentage of the measured strains varies for each element.

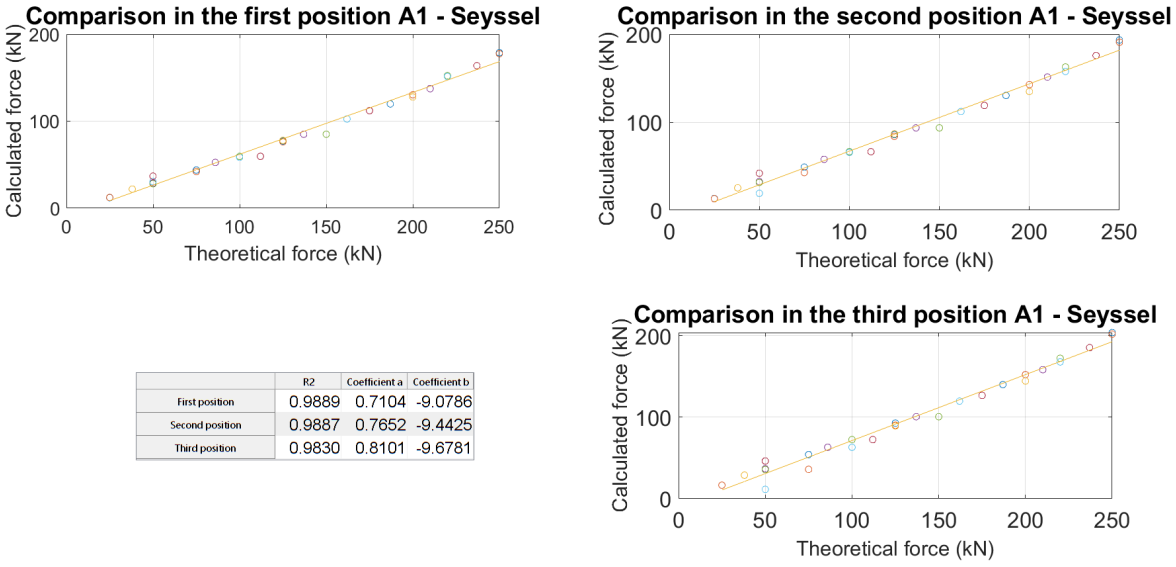

	R2	Coefficient a	Coefficient b
First position	0.9889	0.7104	-9.0786
Second position	0.9887	0.7652	-9.4425
Third position	0.9830	0.8101	-9.6781

Figure 8.9: Comparison between calculated force and theoretical force in the 1^{st} anchorage, Seyssel

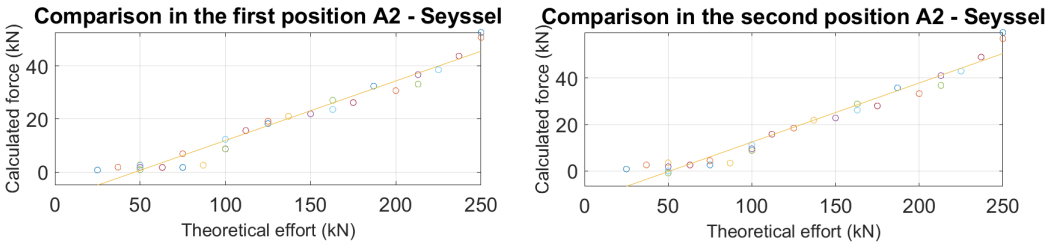

	R2	Coefficient a	Coefficient b
First position	0.9632	0.2247	-10.57...
Second position	0.9610	0.2543	-12.97...
Third position	0.9593	0.3290	-16.81...

Figure 8.10: Comparison between calculated force and theoretical force in the 2^{nd} anchorage, Seyssel

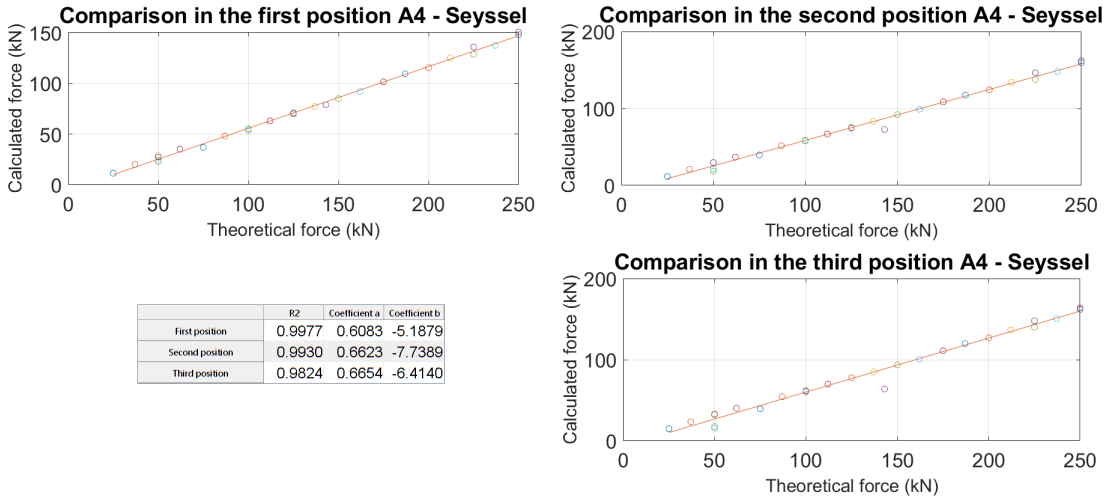

	R2	Coefficient a	Coefficient b
First position	0.9977	0.6083	-5.1879
Second position	0.9930	0.6623	-7.7389
Third position	0.9824	0.6654	-6.4140

Figure 8.11: Comparison between calculated force and theoretical force in the 4^{th} anchorage, Seyssel

8.4 Deduced displacement from the FO

A final analysis that was conducted concerns the possibility of determining the displacements in the head of the anchorage from the fibre optic as an integral of the measured strains. Two kinds of integrals were made in the former only the strains in the grouted segment were considered while in the latter all the strains along the bar were used. To both these integrals the theoretical displacement of the free length was added to obtain the gross displacement.

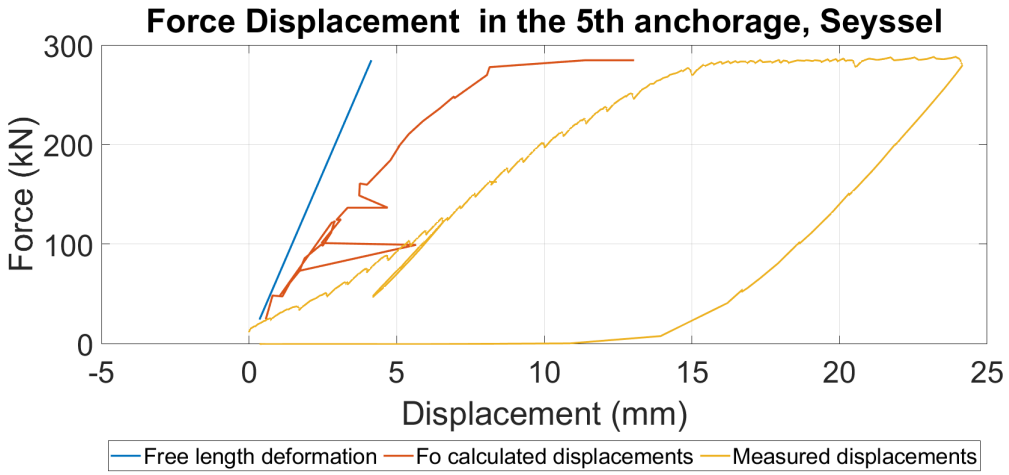

Figure 8.12: Force displacement curves comparison between measured and calculated with the use of the integral along the whole steel bar, 5^{th} anchorage, Seyssel

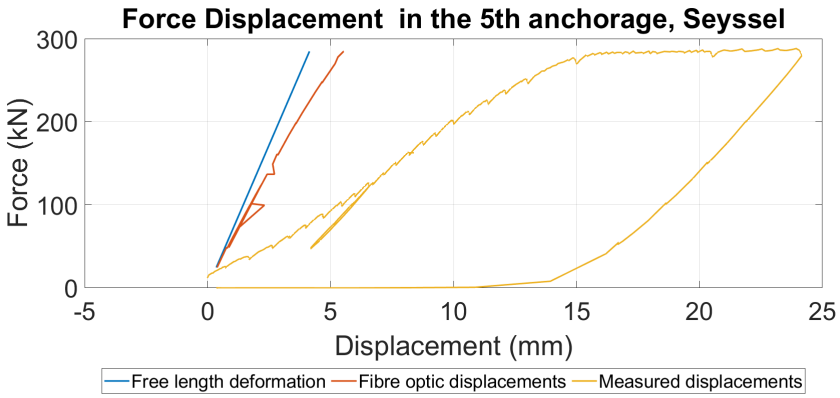

Figure 8.13: Force displacement curves comparison between measured and calculated with the use of the integral along the grouted segment of the steel bar, 5^{th} anchorage, Seyssel

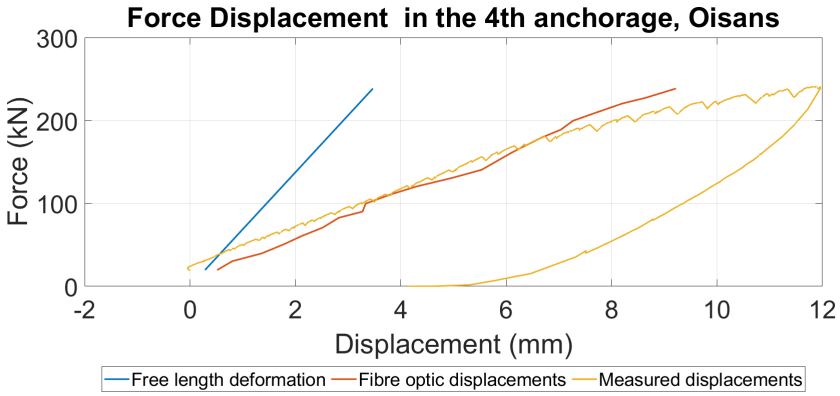

Figure 8.14: Force displacement curves comparison between measured and calculated with the use of the integral along the whole steel bar, 4^{th} anchorage, Oisans

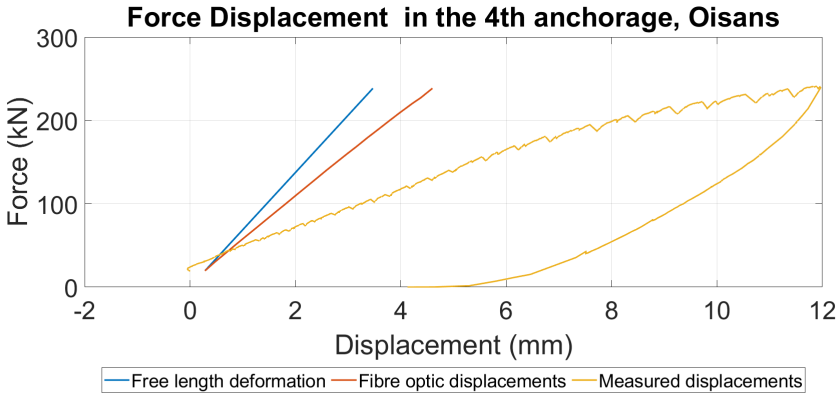

Figure 8.15: Force displacement curves comparison between measured and calculated with the use of the integral along the grouted segment of the steel bar, 4^{th} anchorage, Oisans

We can observe that, generally speaking, the use of the integral along the whole length of the steel bar gives us a better approximation of the real displacement, even if there is not always a perfect correspondence between the two.

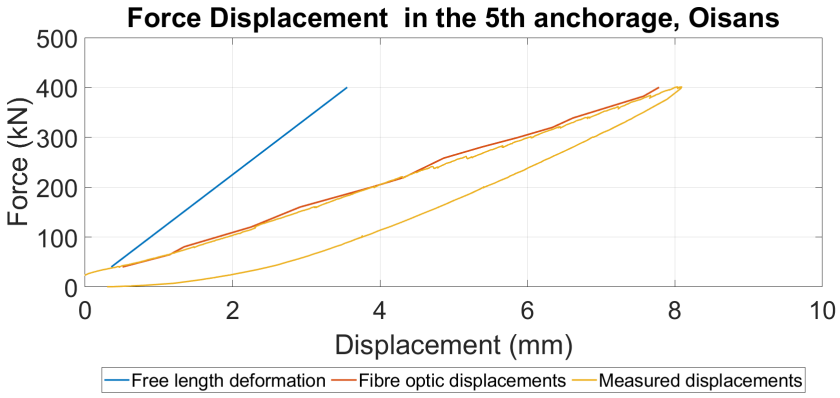

Figure 8.16: Force displacement curves comparison between measured and calculated with the use of the integral along the whole steel bar, 5^{th} anchorage, Oisans

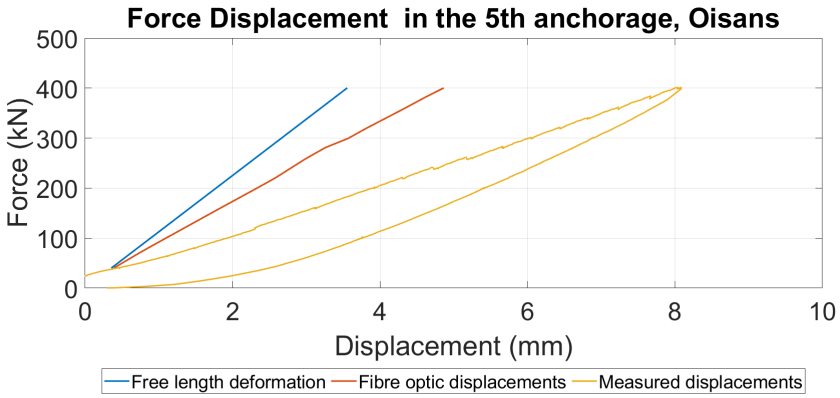

Figure 8.17: Force displacement curves comparison between measured and calculated with the use of the integral along the grouted segment of the steel bar, 5^{th} anchorage, Oisans

8.5 Analysis of the results

From the previous results we can conclude that the behaviour of the analysed elements during an axial loading is comparable to the one of a pre-consolidated soil. We can observe this both in the force displacement curves, which are very similar to the ones obtained from an oedometre test, and from the measurements of the fibre optic where we can observe that there is a residual strain at the end of each loading cycle which disappears only once reached the "pre-consolidation load". This shows how the unloading and reloading curve does not have the same behaviour of the virgin loading.

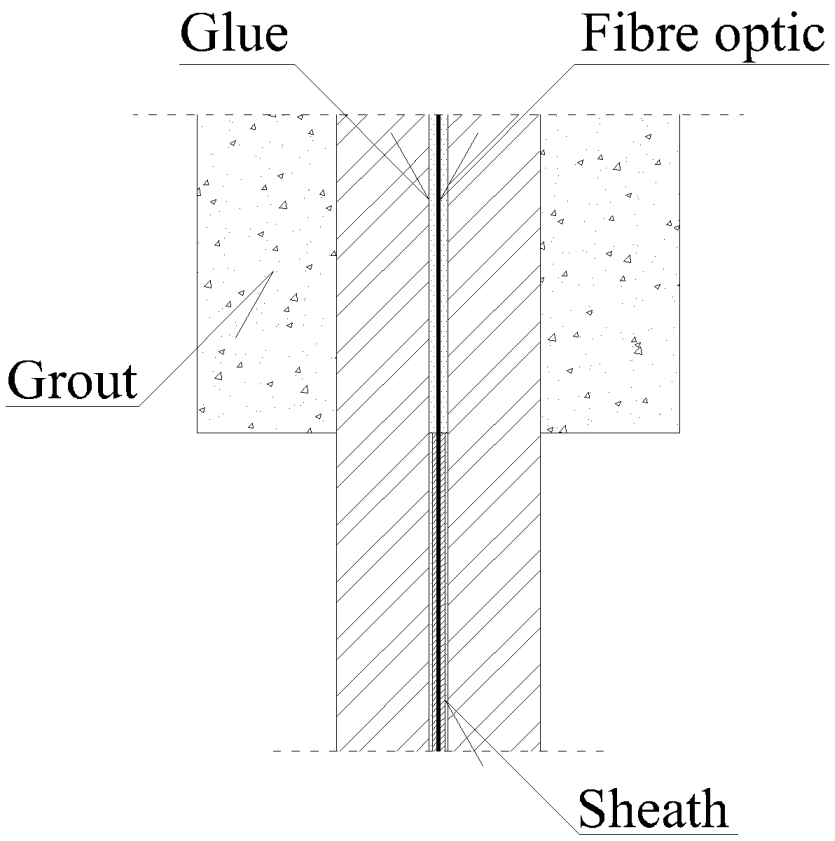

Figure 8.18: Scheme of the interface between the two different types of fibre optic

Another interesting aspect is the measurement made by the fibre optic in the non-grouted segment; during the analysis of the data we tried to interpret these measurements and see if there any useful information that could be taken from them, but as we can see the calculated forces from the measured strains do not have a precise connection with the theoretical forces applied, the relationship between the results has an ample margin of variability. If we observe the slope of the linear fit we can see it change from 0.3 to 0.9 for the different rock-bolts, which implies that this measurement is hardly connected to the forces applied on the free segment of the steel bar, they are probably more linked to some strains in the grouted part which end up being averaged by the fibre optic here, which could slide inside the

sheath.

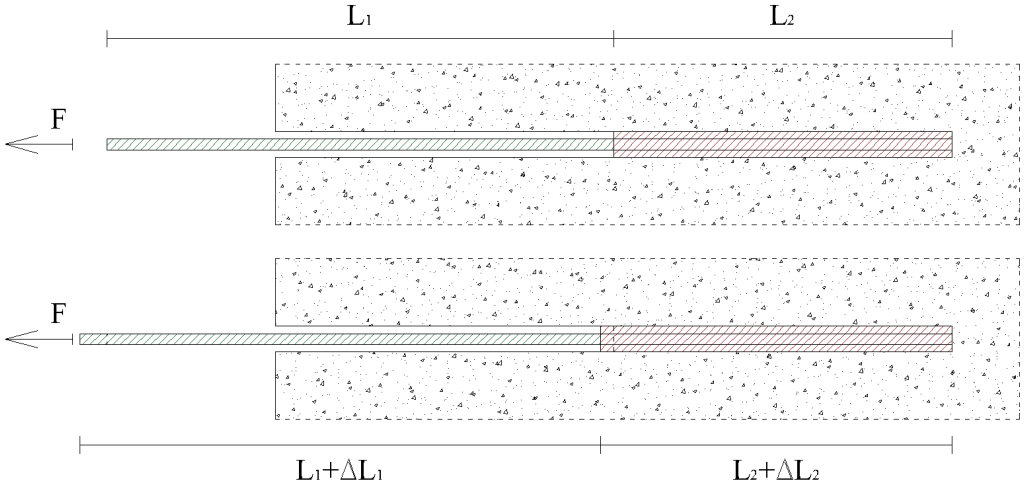

Figure 8.19: Axial deformation of the rock-bolts

This proves also that the approach used to calculate the displacements from the fibre optic is a good one, in fact, if the fibre slides in the sheath then the displacements in the free steel are not considered, we have to add them, then, for a correct measurement. Considering the integral of the measured strains along the whole bar and not only on the grouted part is also justified by the previous interpretation made about the measurements of the strains in the free segment.

Although, the displacements deducted with the fibre optic are not extremely precise. This can be due to different aspects; first of all it could be connected to how with the fibre optic we can observe and monitor only the strains in the steel grout interface, if some strains occur in the rock grout surface then these can not be observed.
Another cause of the imperfect deduction of the displacements could be connected to a translation of the system, these displacements are measured in the head of the bar, but are very hard to identify with the use of the fibre optic which can measure only the strains. This aspect can be considered as a possible limit of the fibre optic monitoring, which is completely blind to eventual translations.

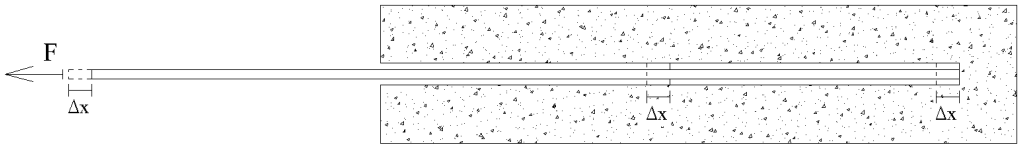

Figure 8.20: Translation of the anchorage

Other interesting observations that could be seen in the fibre optic data are connected to the characteristics of the rocks, for example in Mongalgan we can see

several times that we have some stages in the decreasing part. This is connected to morphology of the site which is characterised by several fractures.
Deducting the site characteristics from a rock-bolt's test, could be very useful but it is not an easy task. In fact the noise in the measurements could be caused by different sources, like the presence of a fracture but also a problem in the grout or in steel. Unless we already know then that a fracture is present in a certain depth it is hard to justify the behaviour of the strains. A solution to this problem could be the use of non-destructive geophysical tests to understand the state of the rock massif after the installation of the anchorages.

We can also observe how the deducted forces from the fibre optic in some cases do not correspond in the head of the grouted segment to the measured force by the load cell. This can be explained either with the plasticization of the a part of the rock-bolt, either with the fact that the used Young Modulus in the force computation, which is the one indicated by the constructor, is not the real one of the bar.

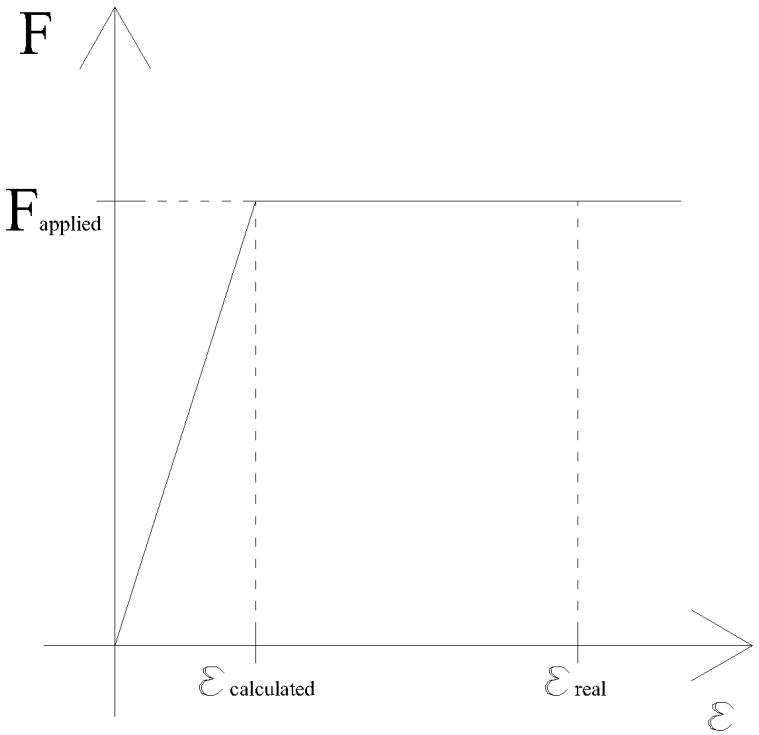

Figure 8.21: Example of plastic behaviour

Another interesting observation is the correspondence between the theoretical results expected (Li and Stillborg, 1999) (see figure 8.22), and the measured results in the fibre optic (see figure 8.23); we can see that the two behaviours are close.

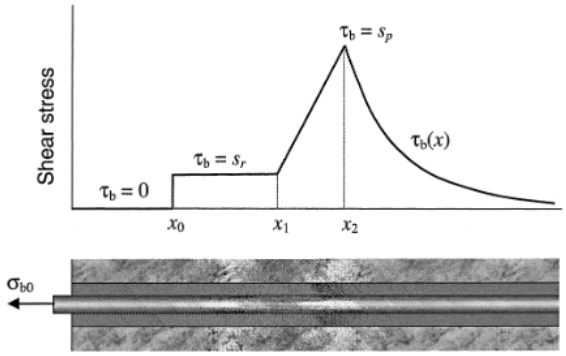

Figure 8.22: Distribution of shear stress along a fully grouted rock bolt subjected to an axial load. (Li and Stillborg 1999)

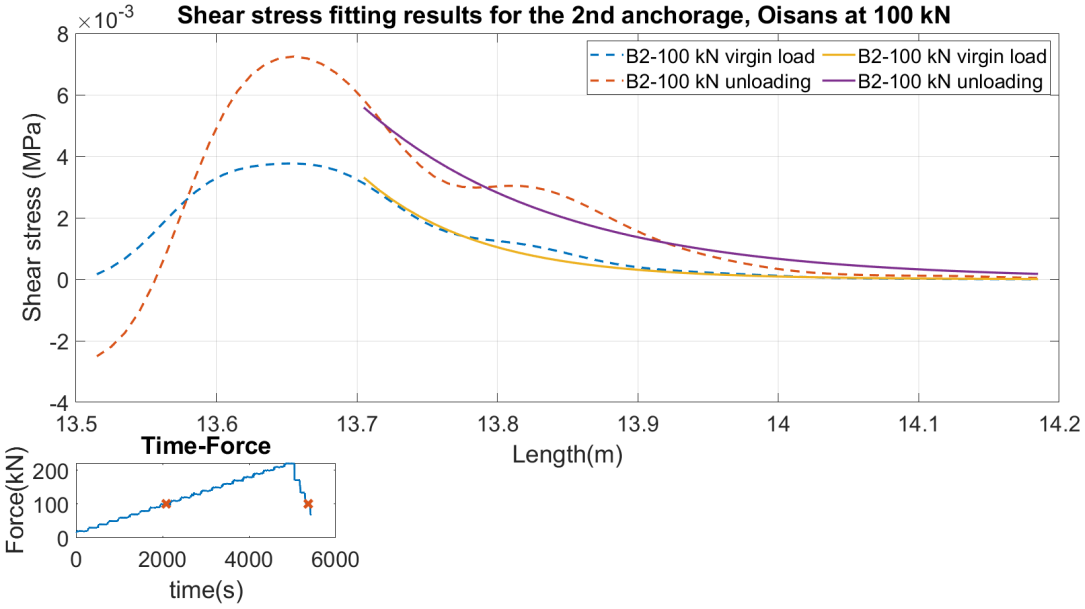

Figure 8.23: Shear stress fitting results for the 2^{nd} anchorage in Oisans at 100kN

9 Numerical modelling

To study the behaviour of the rock-bolts two numerical models were developed:

- An axisymmetric model developed with the use of Abaqus.
- A FEM program, called ANCHOR, developed by Jean-Pierre Rajot, the director of the RRo laboratory. This program studies the behaviour of grouted bars in soil or rock masses.

9.1 Axisymmetric model

The geometry used in this model considered a bar with a 32mm diameter and a borehole with a diameter of 76mm. The conducted analysis considered an elastic behaviour of the materials.
An important aspect of this axisymmetric model is the fact that the ribs geometry, in reality, is different than the one represented (see figure 9.1). In fact, if we represent the ribs in axisymmetry, what we are actually representing is circular area around the bar, while in reality this area surrounds the bar only partially.

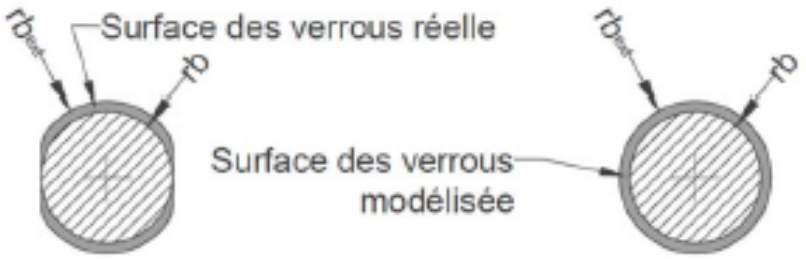

dnom	B16	B20	B25	B28	B32
dmin	15,8	20	24,2	27	30,8
hr	1,1	1,5	1,8	2	2,5
fs	1,28	1,294	1,292	1,292	1,31

Figure 9.1: Real and modelled section of the bolt (Duc An Ho, 2017)

It is important then to remember that: if the model is used to compute the resisting force, we have to decrease the result using a coefficient which is given by the ratio between the real and the modelled section (see figure 9.1). In this case, we are not interested into computing the resisting force, but more interested to the strains caused by the application of a load. This is the reason why it was decided instead of decreasing the loads to increase the strains using the same ratio. This is possible because we are considering a linear correlation between loads and strains.

We can observe in figure 9.2 the loading program used during the modelling.

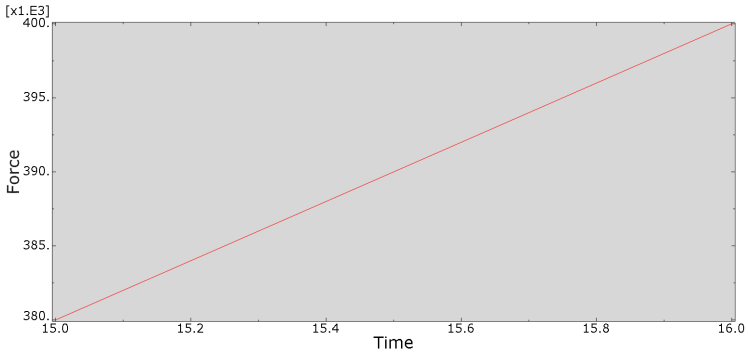

Figure 9.2: Loading program on Abaqus

We can also see the geometry of the model and also the results obtained for the displacements for a load of 400kN in figure 9.3.

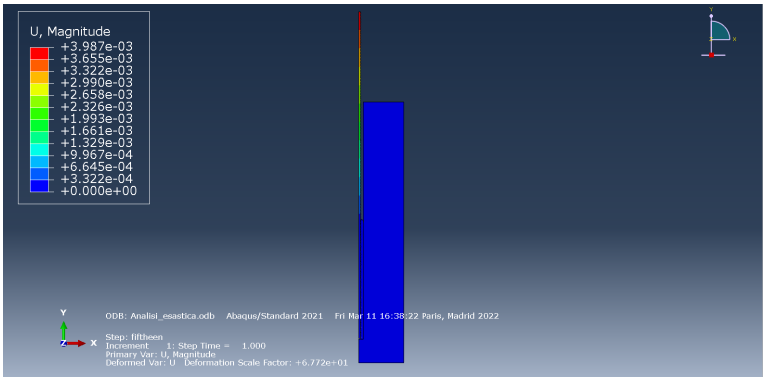

Figure 9.3: Displacements in Abaqus for 400kN

In figure 9.4 where we can see a zoom on the ribs.

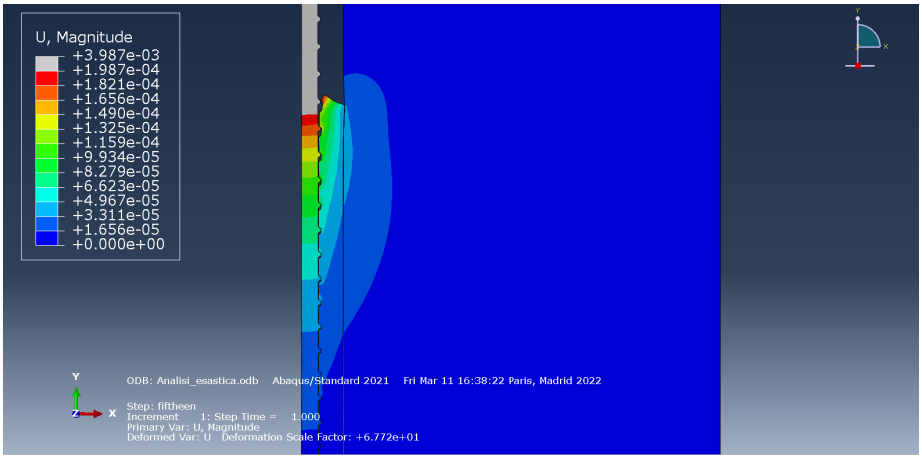

Figure 9.4: Displacements in Abaqus for 400kN with a zoom on the steel ribs

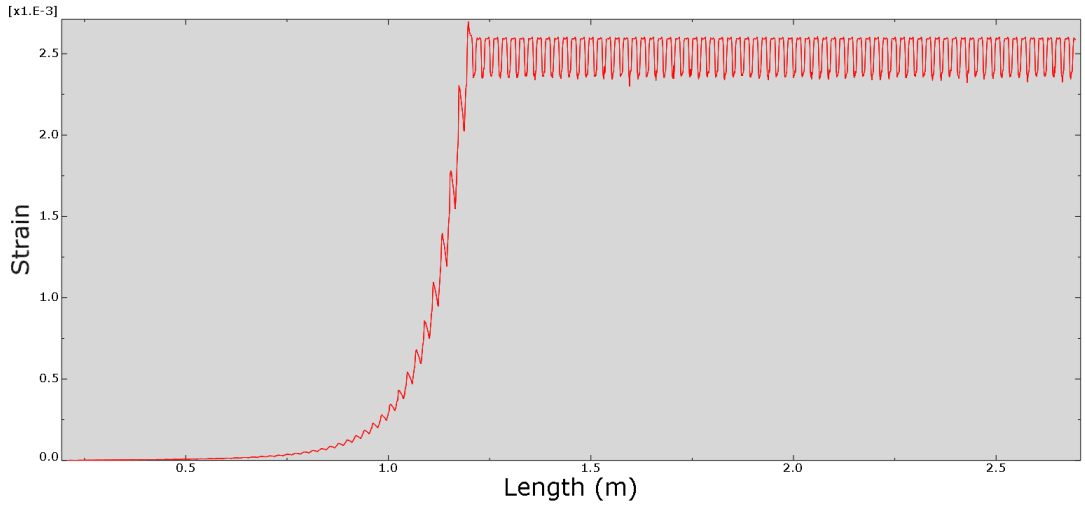

Figure 9.5: Strains calculated with Abaqus at 400kN in the steel grout interface

We can also plot for the interface between the grout and the steel the calculated strains (see figure 9.5). We can observe that the behaviour is exactly the one expected: we have a constant behaviour in the the free length and then an exponential decrease in the grouted part. We can observe that there is an influence of the ribs presence on the strain behaviour. For example, in the free segment of the bar the force is constant, the changes that we see in the strain values are just caused by the changes in the bar's section.

In table 9.1 we can observe the characteristics of the different materials used in the modelling. Another important parameter that was used is the friction coefficient in the steel grout surface, which was considered 0.4.

Material	Density (ρ [$\frac{kg}{m^3}$])	Young Modulus (E [GPa])	Poisson's ratio (ν [-])
Grout	2000	16	0.26
Steel	7850	210	0.25
Rock	2700	30	0.26

Table 9.1: Values of the parameters used for the different materials in the Abaqus Model

9.2 ANCHOR model

This program was developed by Jean-Pierre Rajot, director of the RRo laboratory, and it was used to have a better understanding of the anchorage behaviour. In this program the performance of the rock-bolt is dependent by the rigidity of the whole system, it is then important to understand how this parameter changes to comprehend how the rock-bolt reacts when it is subjected to a force.
In a first moment the fibre optic results were compared to the analytical solution

of the differential equation that describes the pull out of an anchorage with a constant stiffness along its grouting. The displacements of the grouted segment can be expressed as:

$$u(x) = \lambda e^{\frac{x}{l_0}} + \mu e^{\frac{x}{l_0}}$$

where

$$\lambda = \frac{F\frac{l_0}{EA}}{1 - e^{-2\frac{l_g}{l_0}}}$$

and

$$\mu = \lambda e^{-2\frac{l_g}{l_0}}$$

- l_0 is the axial transfer length calculated as:

$$l_0 = \sqrt{\frac{EA}{kP}}$$

- F is the axial force.
- E is Young Modulus of the steel bar.
- A is the bar section.
- l_g is the grouted segment length.
- k is the stiffness of the anchorage.
- P is the perimeter of the borehole.

Once obtained the displacements we can also obtain the strains as their derivative.

Step [kN]	K_{opt} $[\frac{GPa}{m}]$	ε [-]
100	12.7	14.4
140	11.0	10.1
220	8	8.1
360	5.5	10.6

Table 9.2: Optimum stiffness value and its corresponding error from the analytical solution for the compared steps.

We compare ANCHOR's results with the ones measured with the fibre optic in the sixth anchorage on Seyssel at several loading steps, and for each step we tried to find the optimum stiffness that best fits the FO strains, by minimising the error. We can observe the results at 100 kN in figure 9.6 and at 220 kN in figure 9.7. While in table 9.2 we can have a resume of all the compared steps.

The error is calculated as follows:

$$\varepsilon(x) = \frac{log_{10}(strains_{analytic}(x)) - log_{10}(strains_{FO}(x))}{log_{10}(strains_{FO}(x))}$$

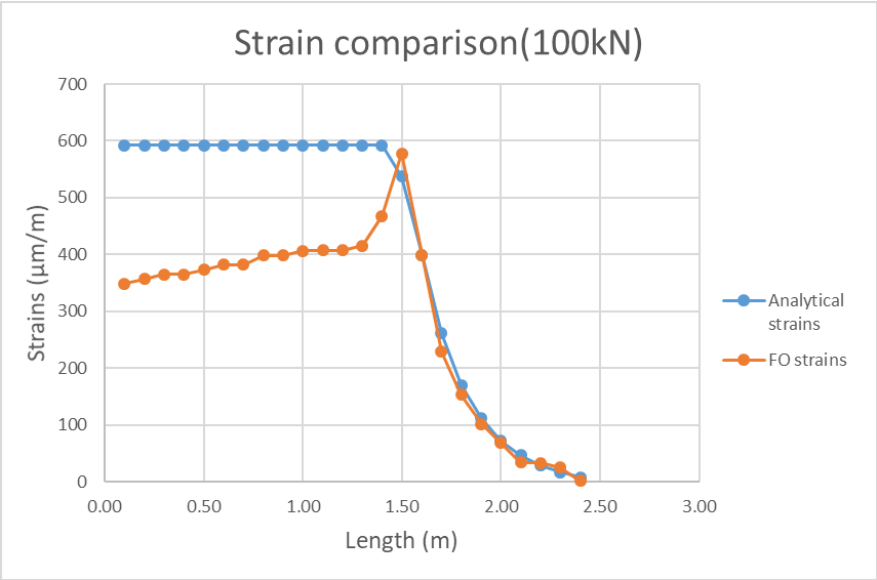

Figure 9.6: Strains comparison between the analytical solution and the FO results at 100kN.

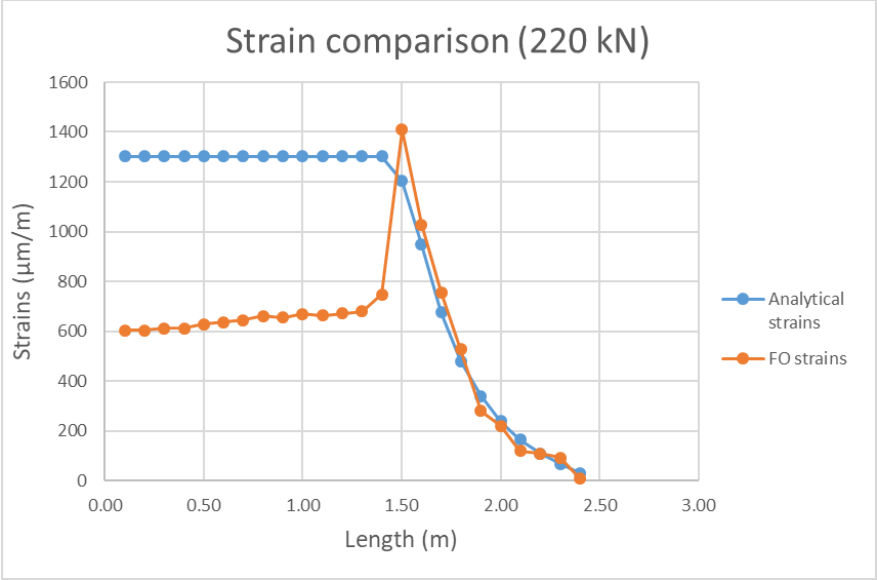

Figure 9.7: Strains comparison between the analytical solution and the FO results at 220kN.

We can plot the trend of the stiffness with the increase of applied load in figure 9.8.

We can see that in the analysed steps the stiffness decreases with the increase of the applied force. This behaviour, thought, cannot be confirmed by the force displacement graphs were even if we can see a decrease in the stiffness of the system on most of the graph, we can also observe to opposite effect for the smaller forces. This can be explained with eventual damaging of the rock during the realization of the borehole, creating fractures in the head of the anchorage, and as this is the segment that reacts first to the forces. This could explain a different behaviour in the the first steps, but this information has to be verified during future campaign

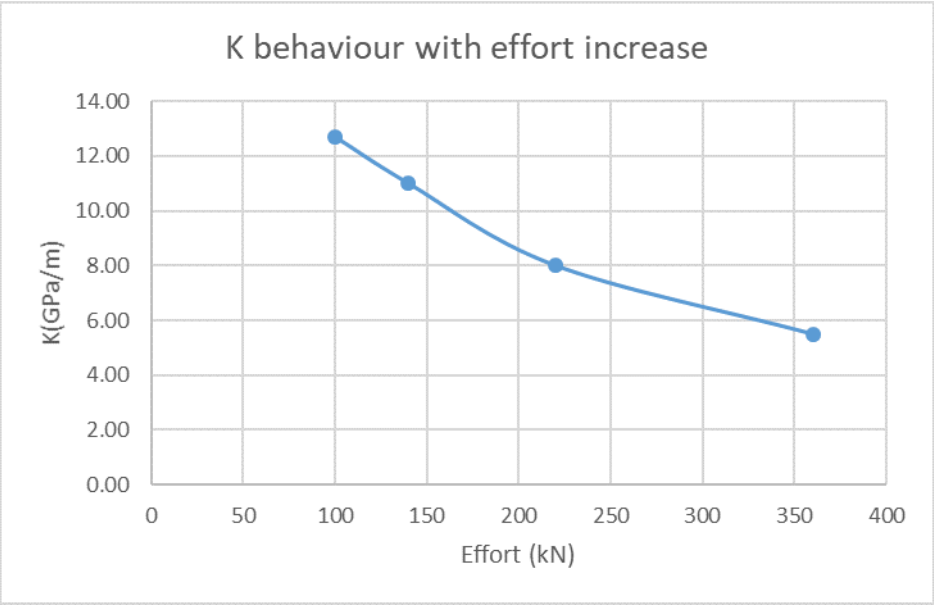

Figure 9.8: Stiffness trend for different forces.

test by checking the state of the rock after the realization of the borehole and before grouting the bar.

Another important aspect to keep in mind is the following: the value of the stiffness was calibrated with the use of the FO measurements on the grouted segment; in fact several stiffness values were tried until it was found the one that assures the lower error possible, this stiffness value is defined the optimum stiffness. This is why the displacement are quite different from the ones measured by the sensor in the head of the bar. This has already been observed in 8.4 where it was shown how the displacements obtained from the integral of the grouted segment are characterized by an important difference in comparison to the measured ones. This can also be observed in figure 9.9.

Figure 9.9: Comparison between the displacements measured in the head of the bar and the ones deducted from the FO and from the analytical solution.

This result was perfectly predictable as the calibration of the stiffness has been made on the FO.

Once we have compared the fibre optic strains with the ones from the analytical solution, and calibrated the values of the optimum stiffness, which was the one with the lower distance between the two strains, the second step was to use the FEM program ANCHOR and analyse if its results are comparable with the FO ones, as the ones of the analytical solution. In table 9.3 we can see:

- The loading steps considered.
- The value of the optimum stiffness obtained with a sensitivity analysis.
- The distance between the two strain curves defined as an error.

Step [kN]	K_{opt} $[\frac{GPa}{m}]$	ε [-]
100	12.7	15.2
140	11.0	7.8
220	8	7.4
360	5.5	7.8

Table 9.3: Optimum stiffness value and its corresponding error from ANCHOR for the compared steps.

We observe that the differences between the measured and the calculated strains are quite important; but the most important errors are concentrated in the final points of the anchorage. This could be connected to the boundary conditions applied. Since in any case the strain values measured in these points are extremely modest we can exclude them for the error assessment and we can obtain the results in table 9.4.

Step [kN]	ε [-]
100	9.0
140	6.3
220	5.7
360	3.9

Table 9.4: Error from ANCHOR for the compared load steps.

We can observe the results of the comparison between the fibre optic measured strains and the ones calculate with the use of ANCHOR at 140 kN in figure 9.10 and at 360 kN in figure 9.11.

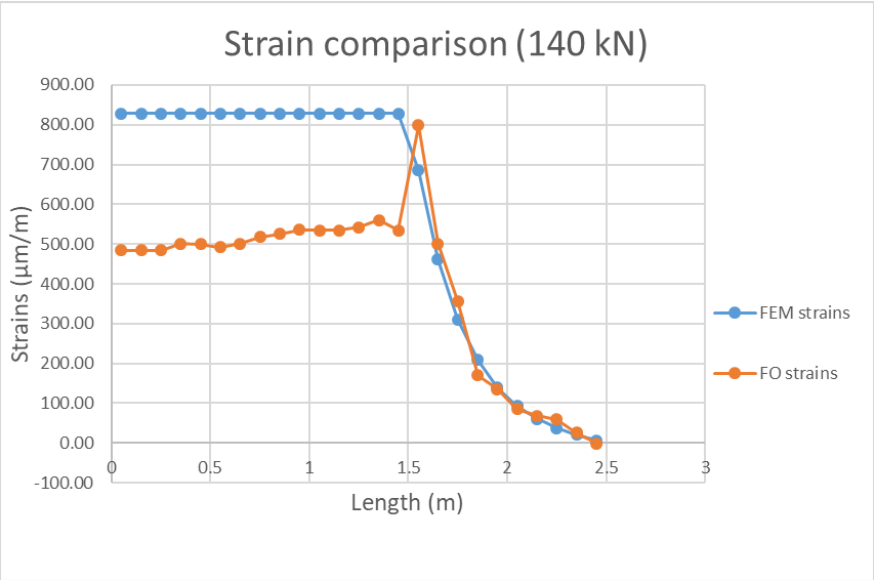

Figure 9.10: Strains comparison between ANCHOR's solution and the FO results at 140kN.

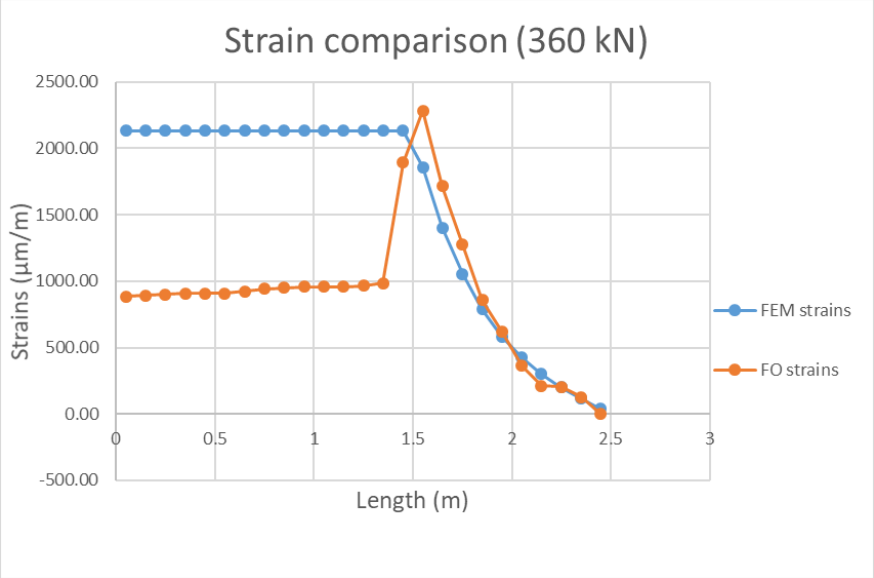

Figure 9.11: Strains comparison between ANCHOR's solution and the FO results at 360kN.

In a final analysis it was also attempted to study the behaviour of the rock-bolt using ANCHOR and simulating different parts with different stiffnesses along the grouting and several fractures. This analysis was proposed ones it was observed the decreasing trend of the stiffness with the increase of the load. The objective of this analysis is to verify if this global phenomenon observed, is seen also in the local portion of the rock-bolt. Along the element, in fact, the distribution of the forces is not constant as we have seen during this thesis, it might be possible then that also the stiffness of the anchorage is not constant either, it could be changing along the element according to the applied load in that portion of the bolt.

Segment	Coordinates [m]	K $[\frac{GPa}{m}]$
1^{st} segment	1.50 - 1.55	2.5
1^{st} fracture	1.55 - 1.60	0.0
2^{nd} segment	1.60 - 1.85	8.0
2^{nd} fracture	1.85 - 1.90	0.0
3^{rd} segment	1.90 - 2.05	16.0
3^{rd} fracture	2.05 - 2.15	0.0
4^{th} segment	2.15 - 2.50	17.5

Table 9.5: Characteristics of the ANCHOR test with several segments.

We can observe in table 9.5 the parts in which the grout was divided, we can see that the optimum stiffness value used is increasing with the depth of the rock-bolt, while the fractures are simulated by segments with absent stiffness.

And in figure 9.12 we can observe the strains of this test at 360 kN.

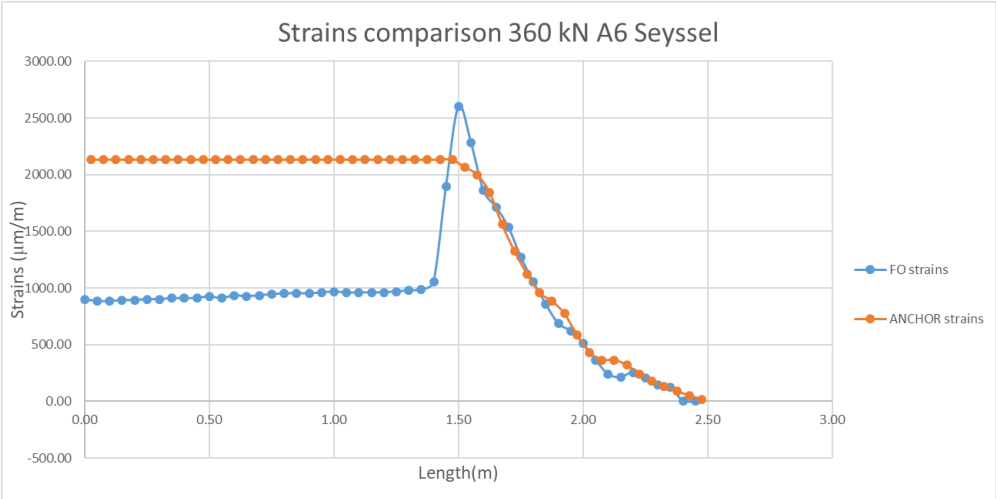

Figure 9.12: Strains comparison between ANCHOR's solution with multiple stifnesses and the FO results at 360kN.

The error obtained with the use of different stiffness values along the rockbolt, excluding the last point, equals 3.05.

10 Conclusions

In conclusion, with this thesis, some aspects of the behaviour of rock-bolts subjected to axial loads have been presented. After an overview of the different rock-bolts and the most relevant aspects in literature, the results of the testing campaigns were introduced.

In the results that were presented it was possible to observe several aspects of the behaviour of these elements. For example while analysing the measurements from the fibre optic we were able to see their coherence with the predicted ones in literature. The strains and the shear stresses obtained, for example, have the same trend of the ones expected by Stillborg and Li. And the differences from the literature's models could be explained by heterogeneity of the medium that we work with in situ. For example the behaviour of the strains in the grouted segment was characterized by an exponential decrease in all the rock-bolts, the only exceptions from this general behaviour was due to presence of heterogeneities in the rock massif or to the presence fractures.

During this work it has also been confirmed, several times, that the behaviour of the rock-bolt is strongly dependent from the state of the surrounding rock; as previously introduced, in fact, fractured and non-fractured rocks show different behaviours (see Oisans and Mongalgan).

The numerical models also acted as an ulterior validation of the obtained results, showing a coherence between the expected results and the ones obtained. An important aspect in the numerical analysis was also the possibility to use the software ANCHOR. This software, in fact, made possible a better understanding of the rock-bolts and the working mechanisms of these elements when subjected to loading conditions analysed in this thesis.

Although, there are also some important aspects that would need to be improved, for example, understanding properly the reasons behind the differences between the displacements deducted from the fibre optic and the ones measure by the sensor. It is, in fact, important to understand properly which are the causes of these differences, because, even if some possible explanations were given during this thesis, it is still possible that other explanations are required for a perfect picture of the mechanisms behind the behaviour of these elements.
To be able to do this it might be needed to use some geophysical tests to understand properly the state of the rock massif, and, for a proper interpretation of the fibre optic data, it might be necessary to use the measuring fibre optic on the whole length of the bar and not only in the grouted segment. This latter point, in fact, will give us the possibility to compute the real mechanical parameters of the steel to use them in the data interpretation, this would free us from the use of the parameters suggested by the manufacturer, giving us more sophisticated results.

Another interesting aspect that should be studied properly, is a numerical modelling that takes into account the damage of the grout and of the surrounding rock. In this work, in fact, the realised models were all elastic ones. Although this could be a

good approach to get a general idea of the behaviour of the rock-bolts, it introduces a number of very strong simplifications in the model. For a proper understanding it should be necessary to see how the application of a load on the anchorage changes the mechanical parameters of the grout and of the rock, and also to understand if these changes are partially or not reversible.

11 Annexes Seyssel

The results for each rock-bolt in Seyssel will be presented in this chapter.

11.0.1 A1 - Seyssel

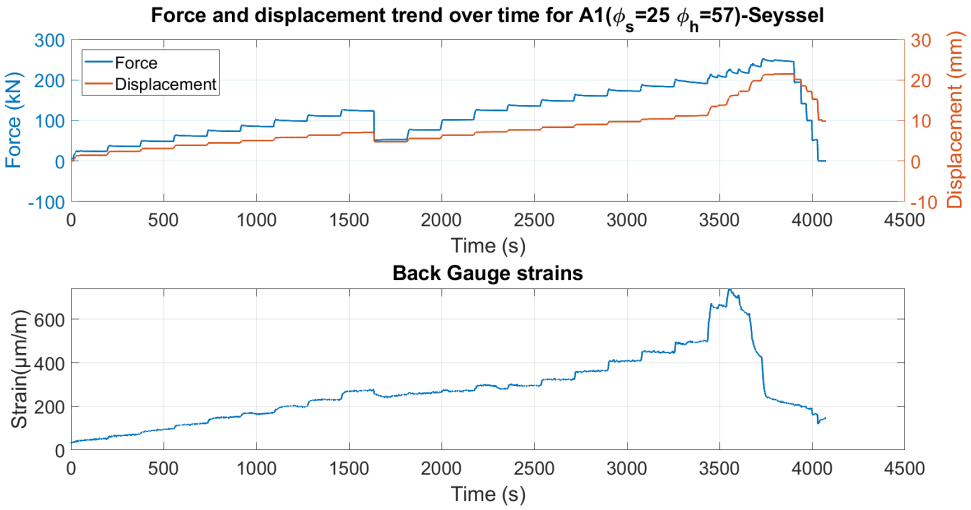

Figure 11.1: Force, displacement and Gauge strains trend over time for A1-Seyssel

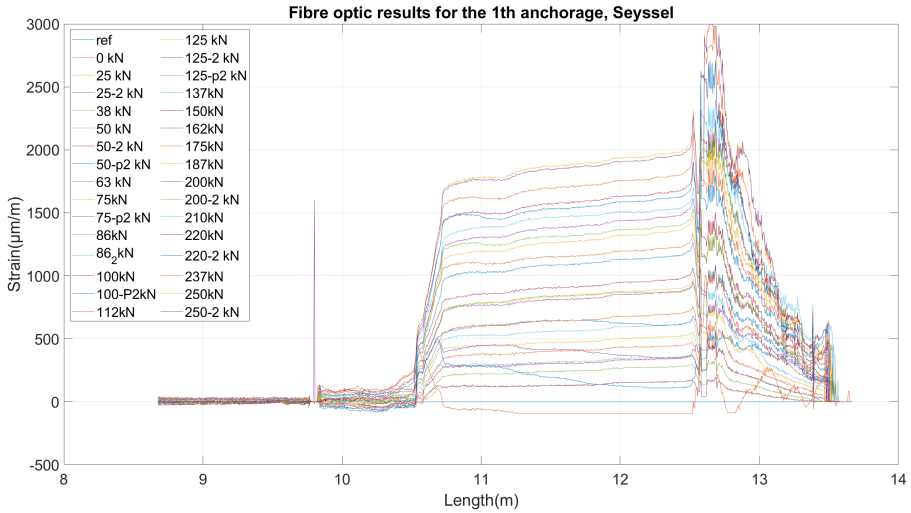

Figure 11.2: Fibre optic results for the 1^{st} anchorage, Seyssel

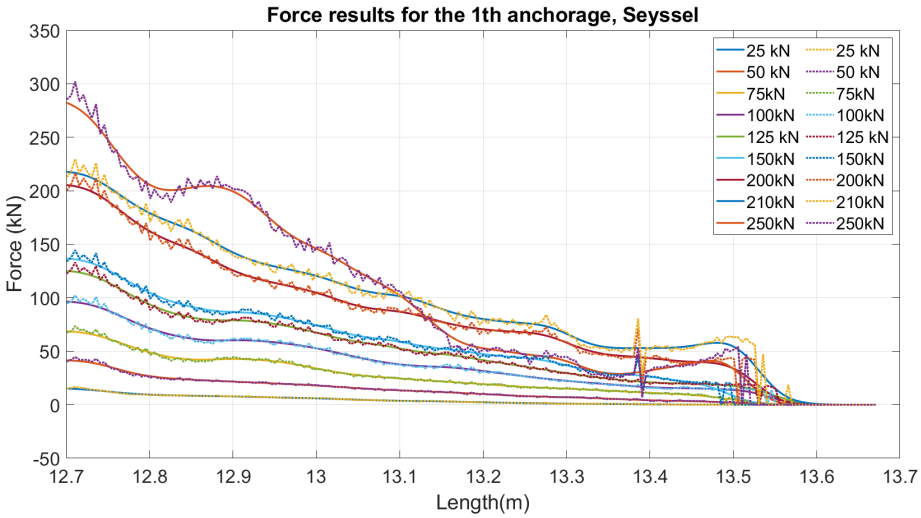

Figure 11.3: Force results for the virgin loading steps in the 1^{st} anchorage, Seyssel

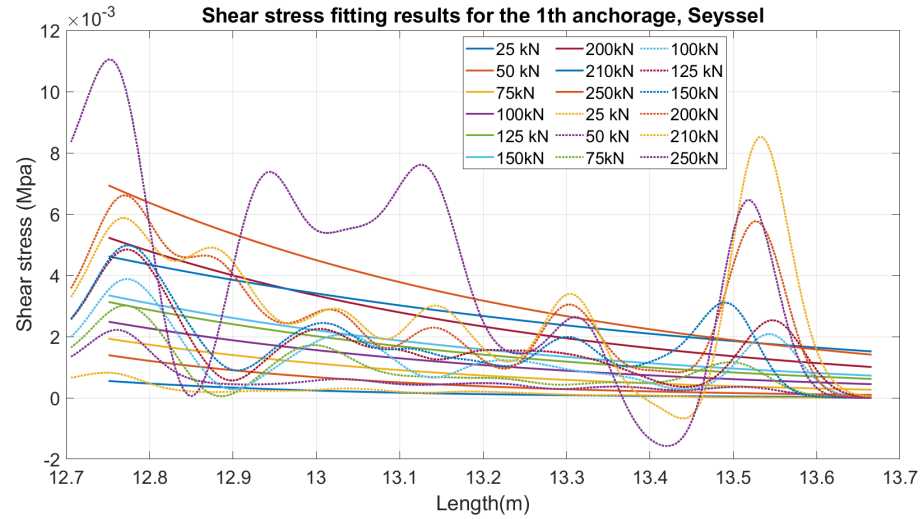

Figure 11.4: Shear stress results for the virgin loading steps in the 1^{st} anchorage, Seyssel

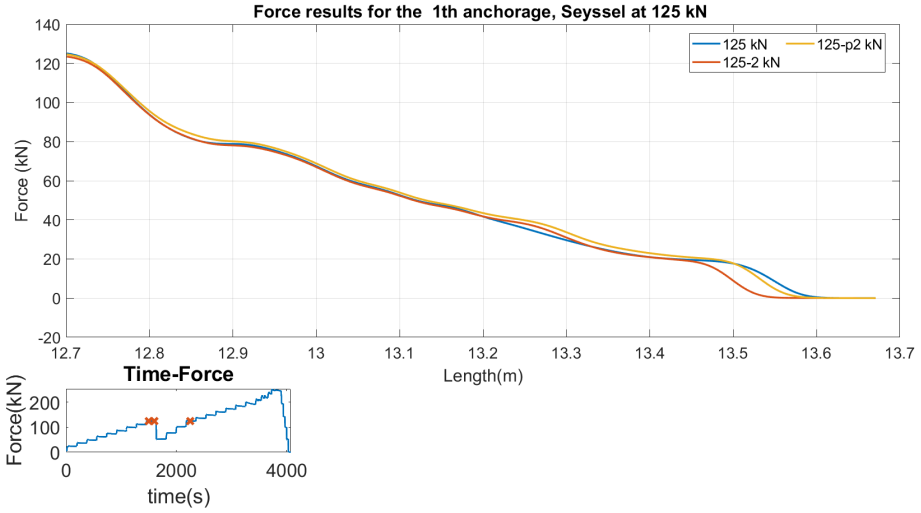

Figure 11.5: Force results for the 1^{st} anchorage, Seyssel at 125kN

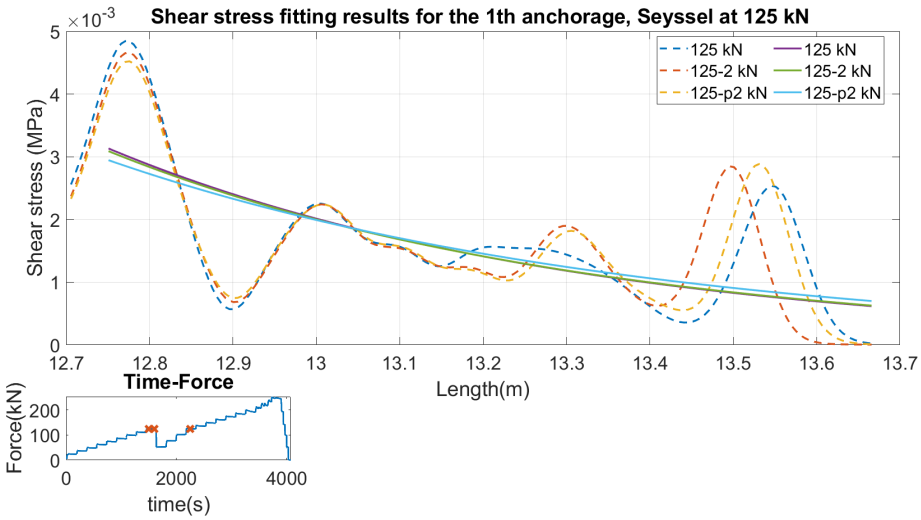

Figure 11.6: Shear stress fitting results for the 1^{st} anchorage, Seyssel at 125kN

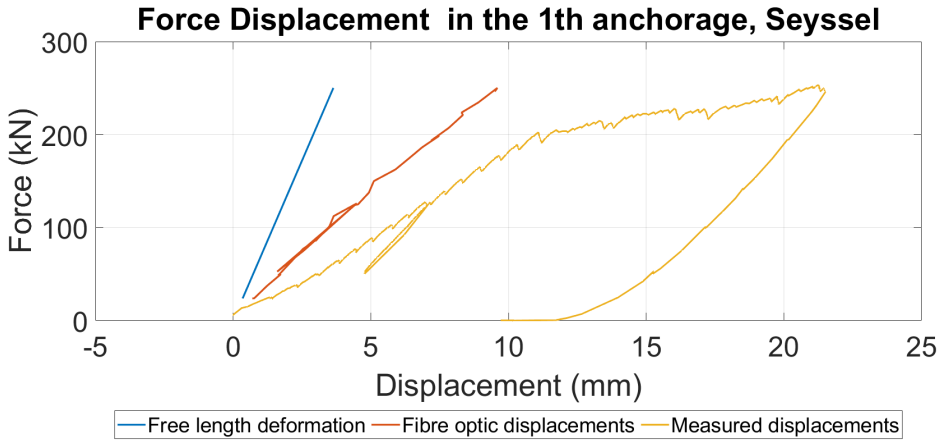

Figure 11.7: Force displacement curves comparison between measured and calculated with the use of the integral along the whole steel bar, 1^{st} anchorage, Seyssel

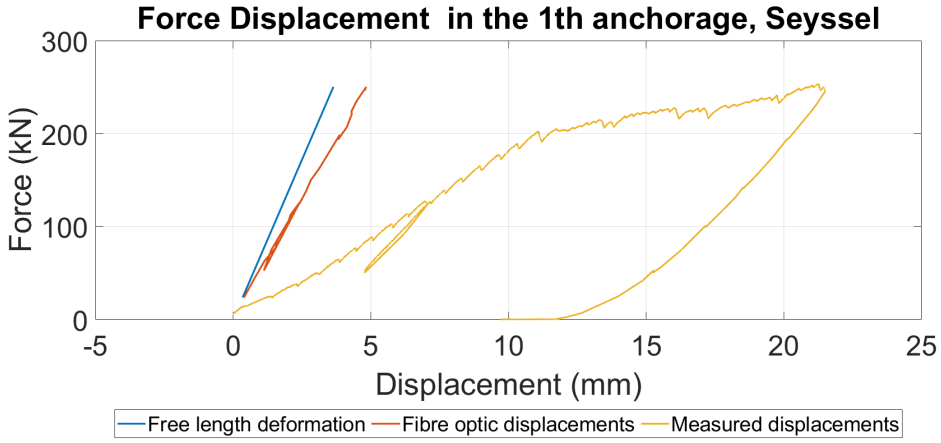

Figure 11.8: Force displacement curves comparison between measured and calculated with the use of the integral along the grouted segment of the steel bar, 1^{st} anchorage, Seyssel

11.0.2 A2 - Seyssel

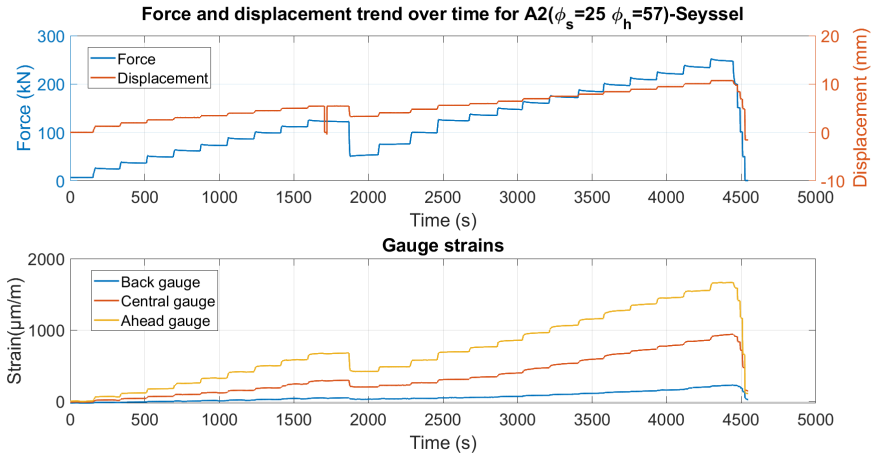

Figure 11.9: Force displacement and Gauge strains trend over time for A2-Seyssel

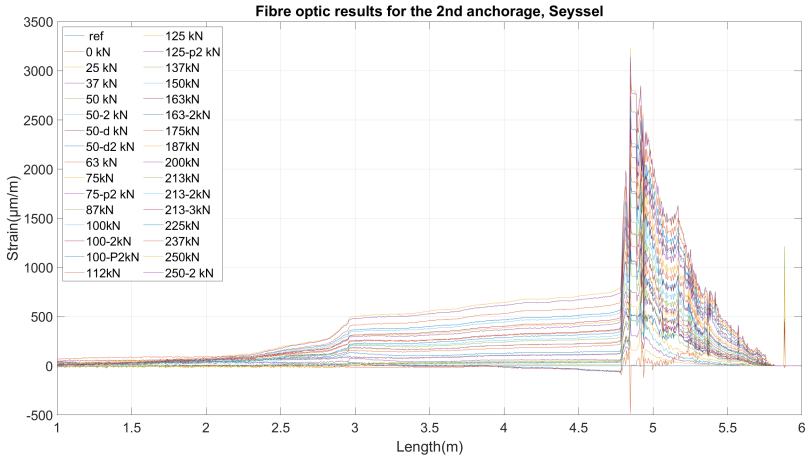

Figure 11.10: Fibre optic results for the 2^{nd} anchorage, Seyssel

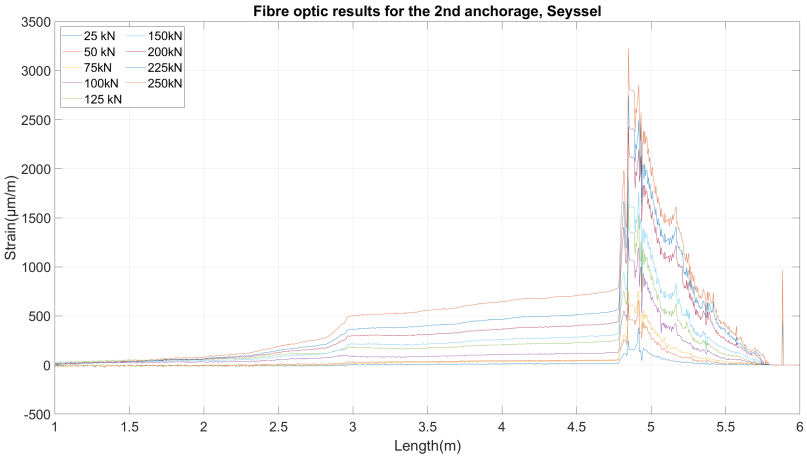

Figure 11.11: Fibre optic results for some virgin loading steps in the 2^{nd} anchorage, Seyssel

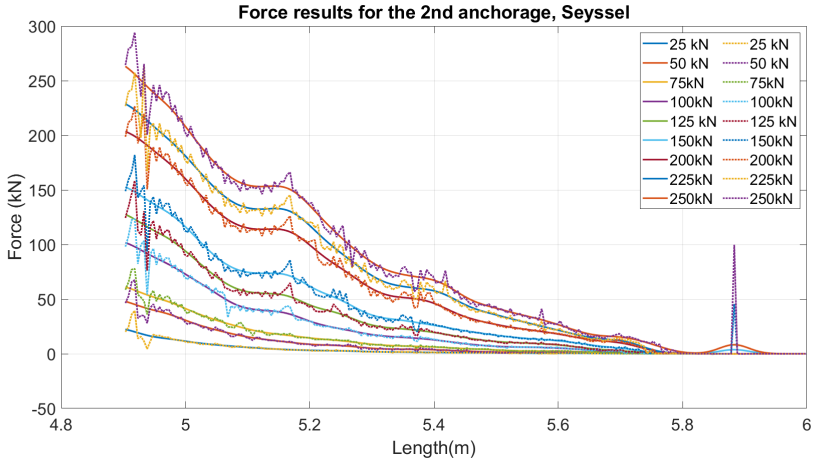

Figure 11.12: Force results for the virgin loading steps in the 2^{nd} anchorage, Seyssel

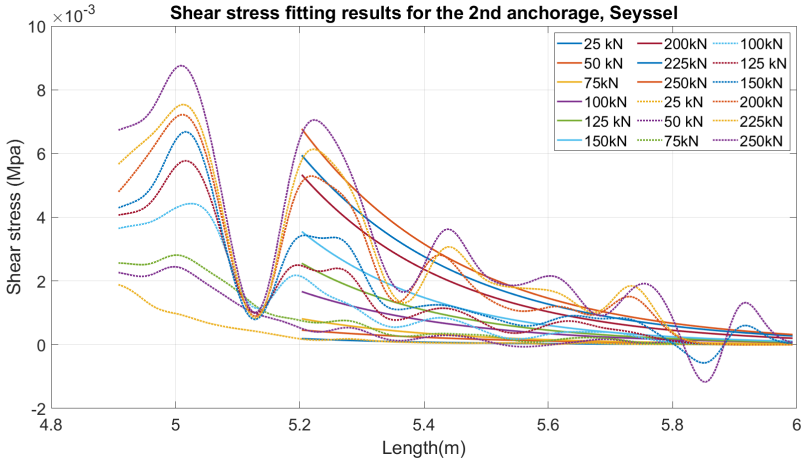

Figure 11.13: Shear stress results for the virgin loading steps in the 2^{nd} anchorage, Seyssel

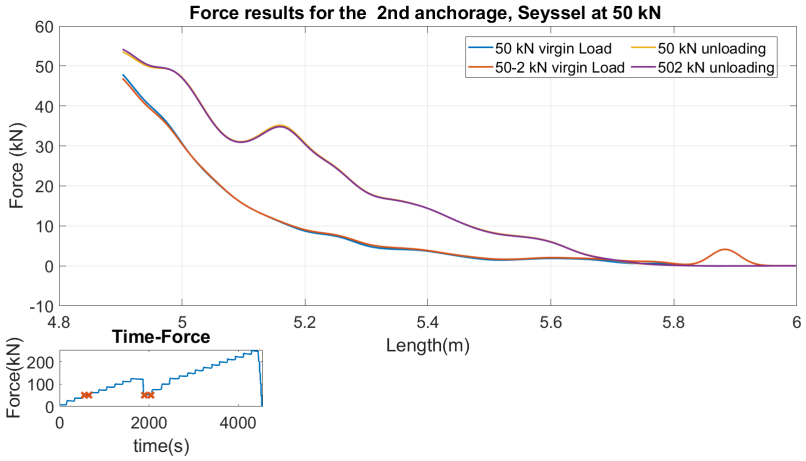

Figure 11.14: Force results for the 2^{nd} anchorage, Seyssel at 50kN

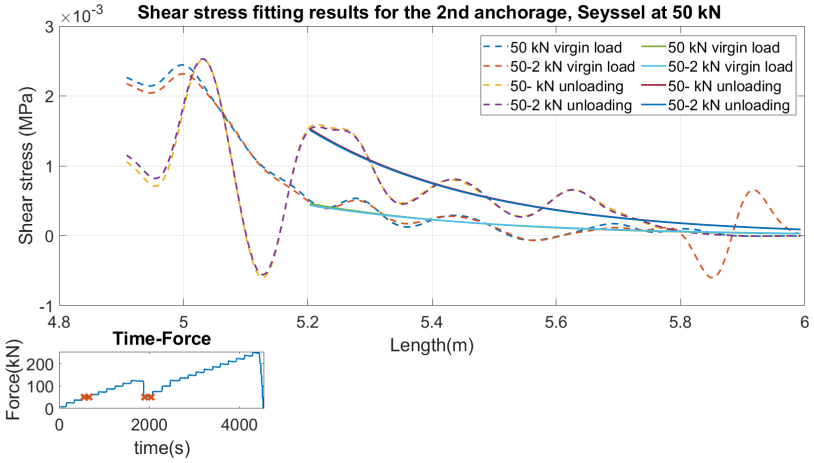

Figure 11.15: Shear stress fitting results for the 2^{nd} anchorage, Seyssel at 50kN

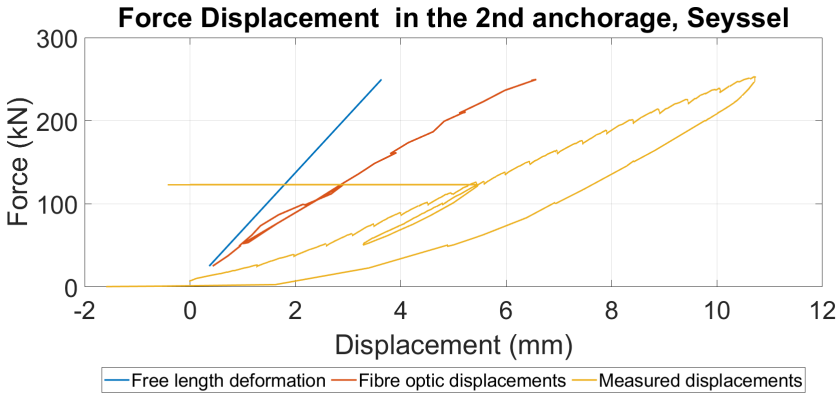

Figure 11.16: Force displacement curves comparison between measured and calculated with the use of the integral along the whole steel bar, 2^{nd} anchorage, Seyssel

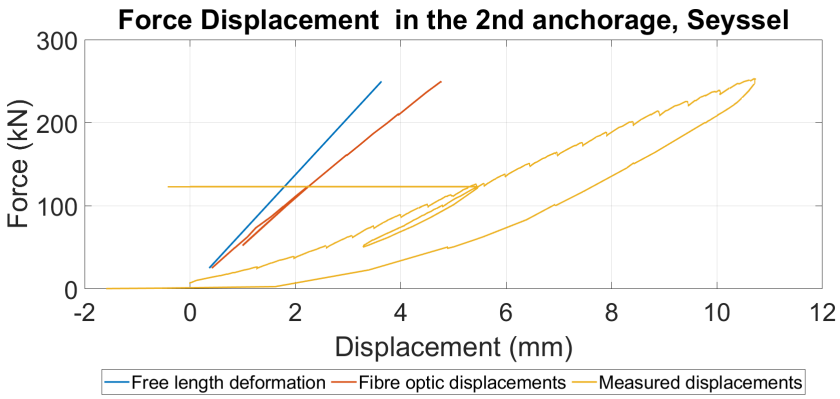

Figure 11.17: Force displacement curves comparison between measured and calculated with the use of the integral along the grouted segment of the steel bar, 2^{nd} anchorage, Seyssel

11.0.3 A3 - Seyssel

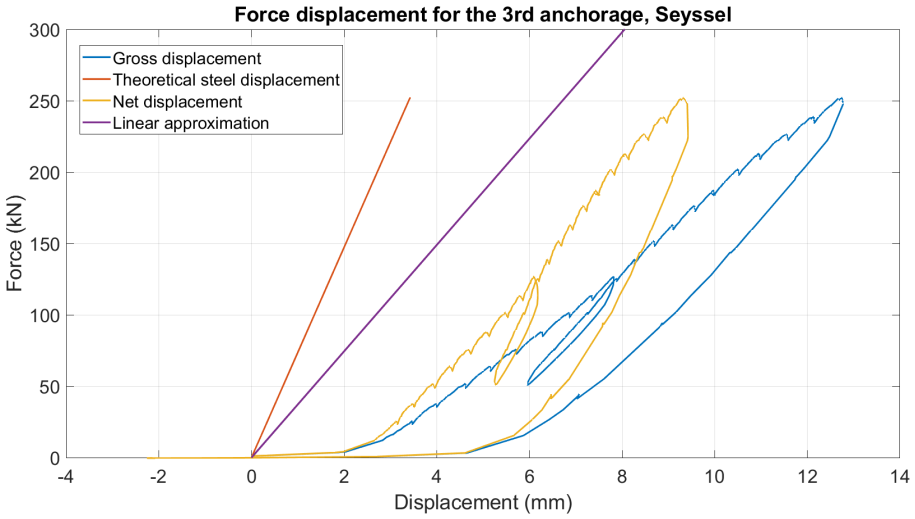

Figure 11.18: Force displacement for the 3^{rd} anchorage, Seyssel

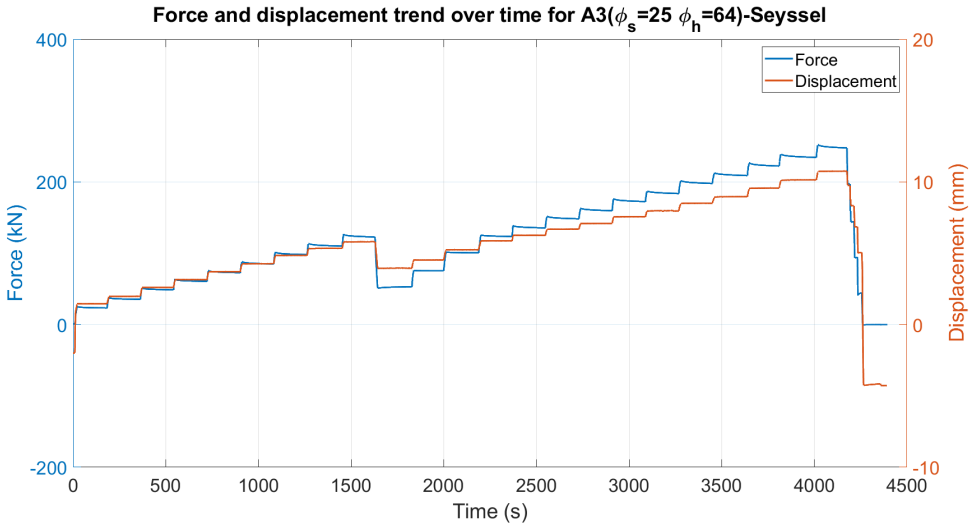

Figure 11.19: Force and displacement trend over time for A3-Seyssel

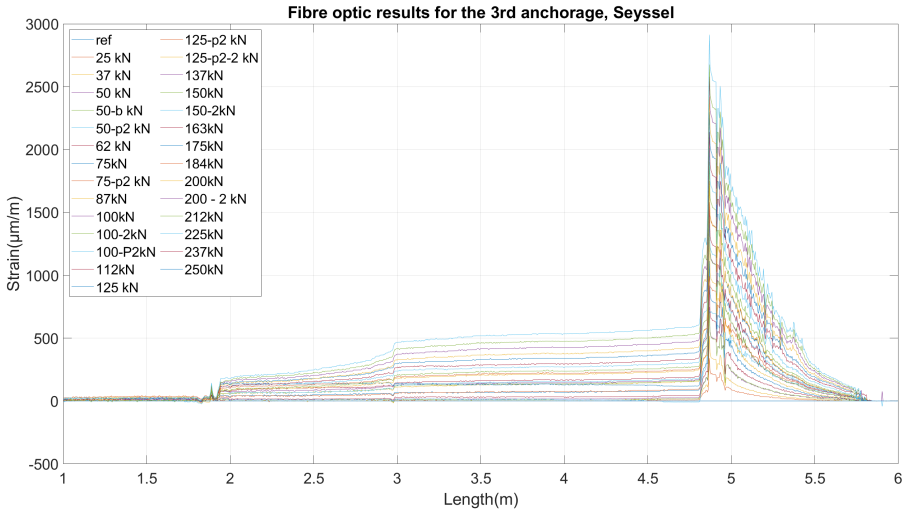

Figure 11.20: Fibre optic results for the 3^{rd} anchorage, Seyssel

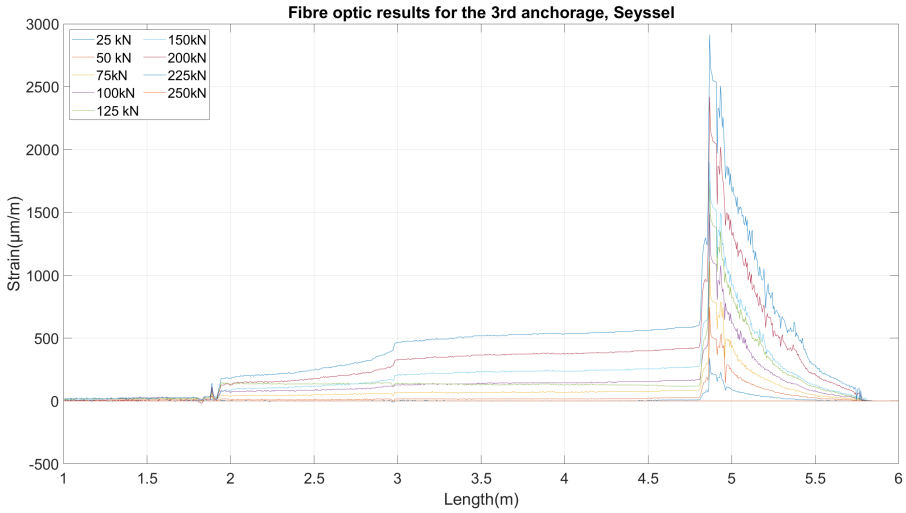

Figure 11.21: Fibre optic results for some virgin loading steps in the 3^{rd} anchorage, Seyssel

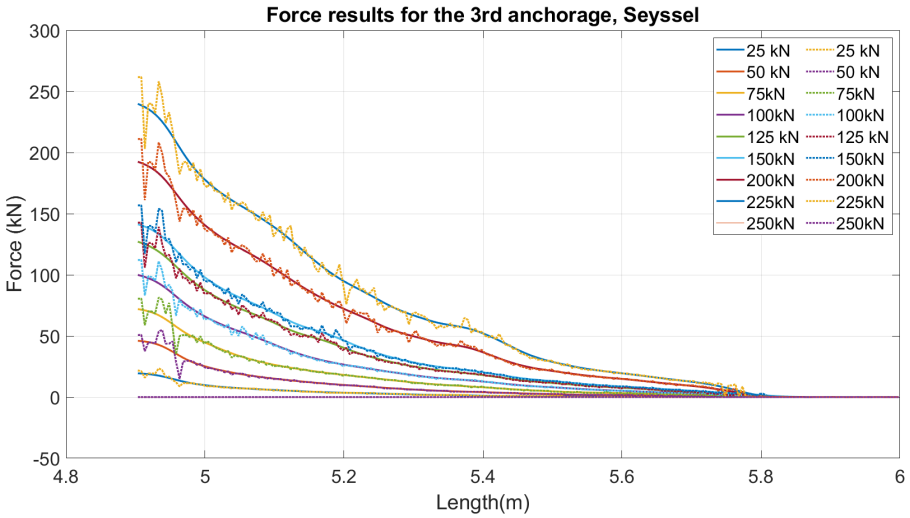

Figure 11.22: Force results for the virgin loading steps in the 3^{rd} anchorage, Seyssel

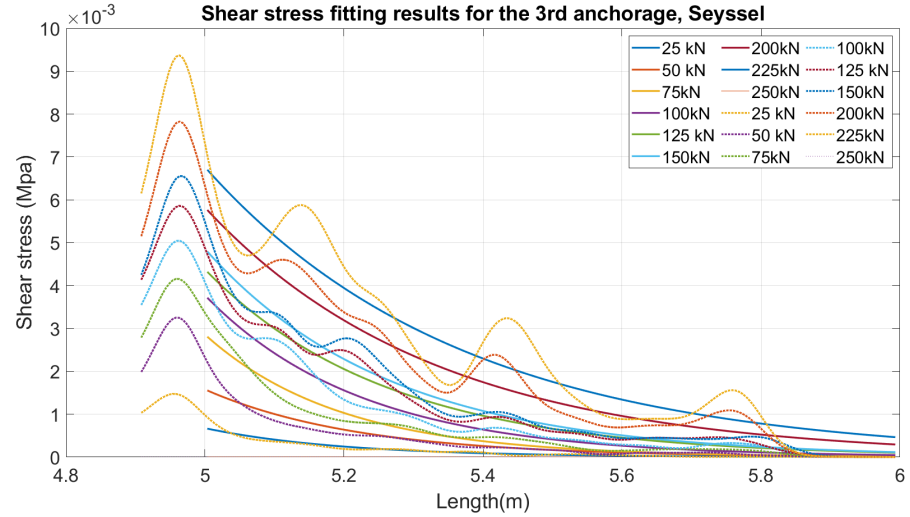

Figure 11.23: Shear stress results for the virgin loading steps in the 3^{rd} anchorage, Seyssel

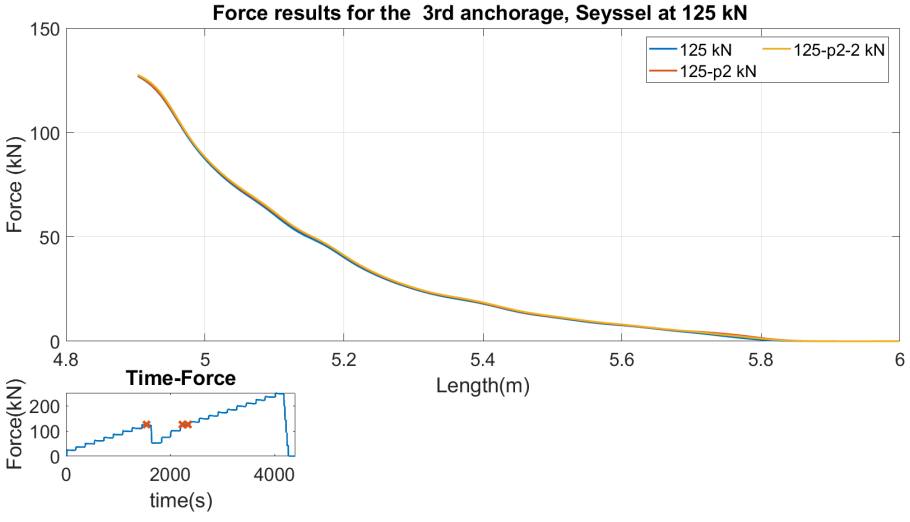

Figure 11.24: Force results for the 3^{rd} anchorage, Seyssel at 125kN

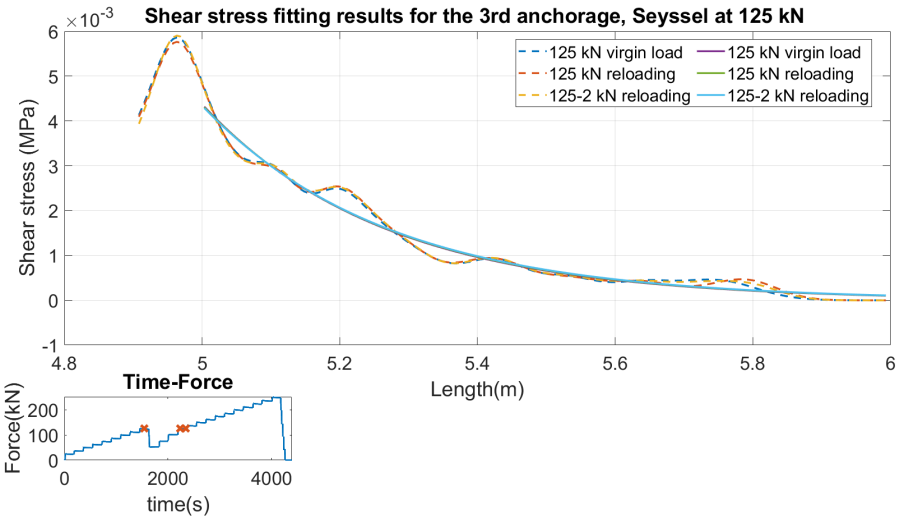

Figure 11.25: Shear stress fitting results for the 3^{rd} anchorage, Seyssel at 125kN

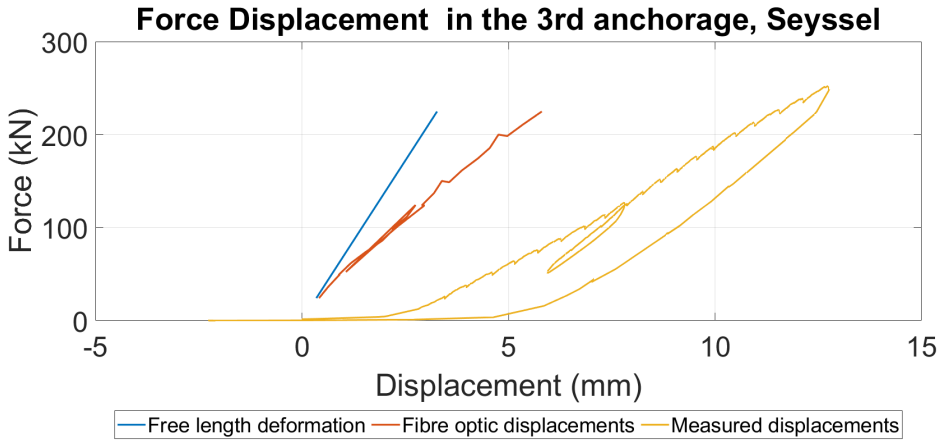

Figure 11.26: Force displacement curves comparison between measured and calculated with the use of the integral along the whole steel bar, 3^{rd} anchorage, Seyssel

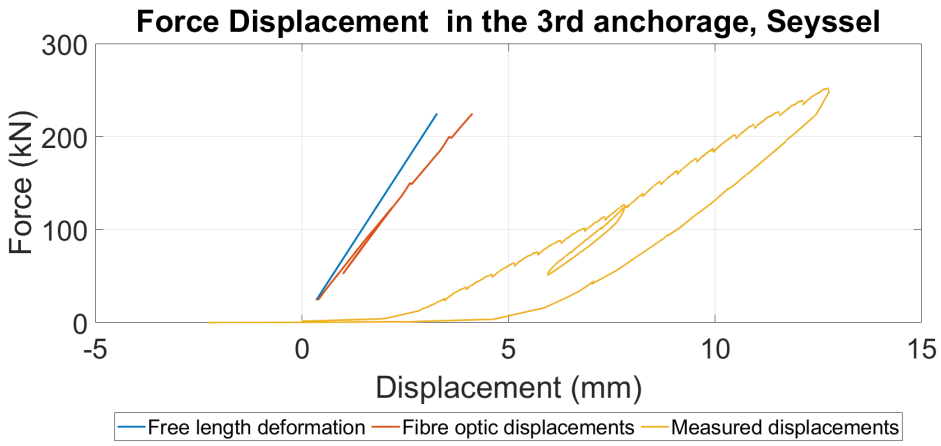

Figure 11.27: Force displacement curves comparison between measured and calculated with the use of the integral along the grouted segment of the steel bar, 3^{rd} anchorage, Seyssel

11.0.4 A4 - Seyssel

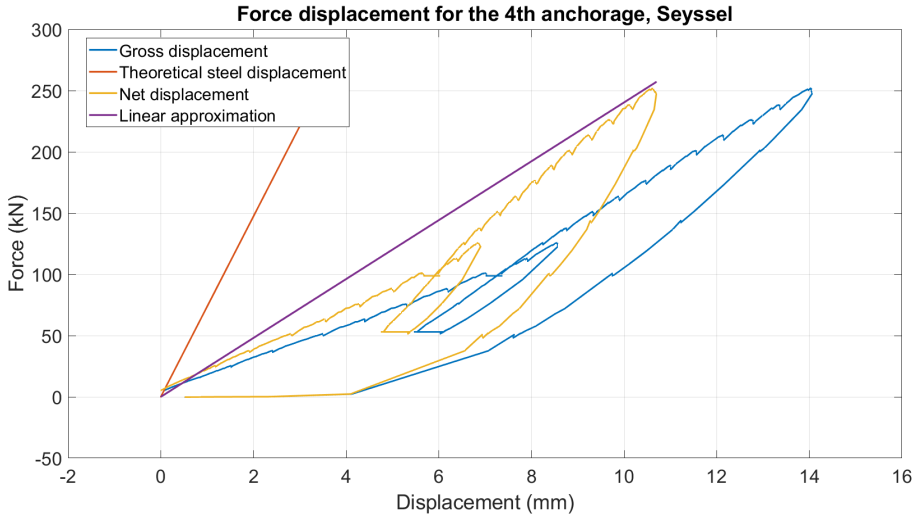

Figure 11.28: Force, displacement for the 4^{th} anchorage, Seyssel

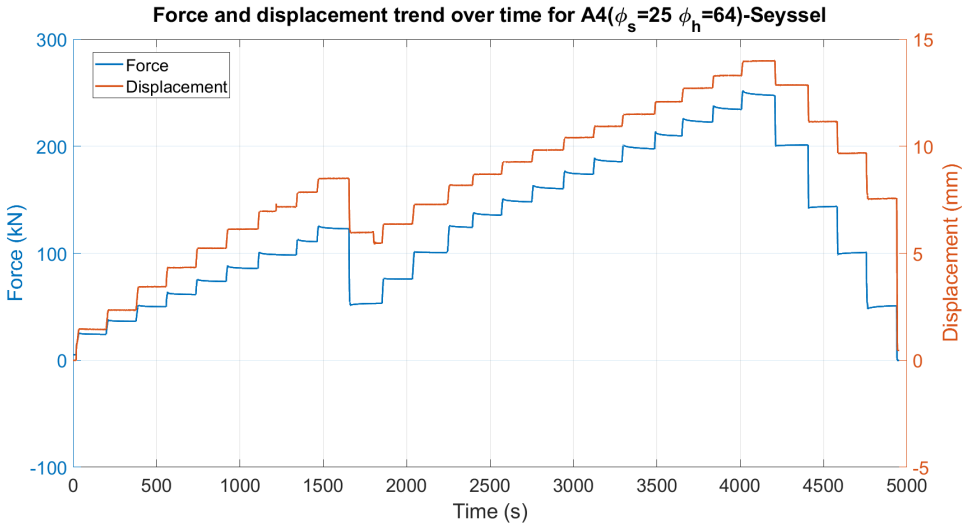

Figure 11.29: Force and displacement trend over time for A4-Seyssel

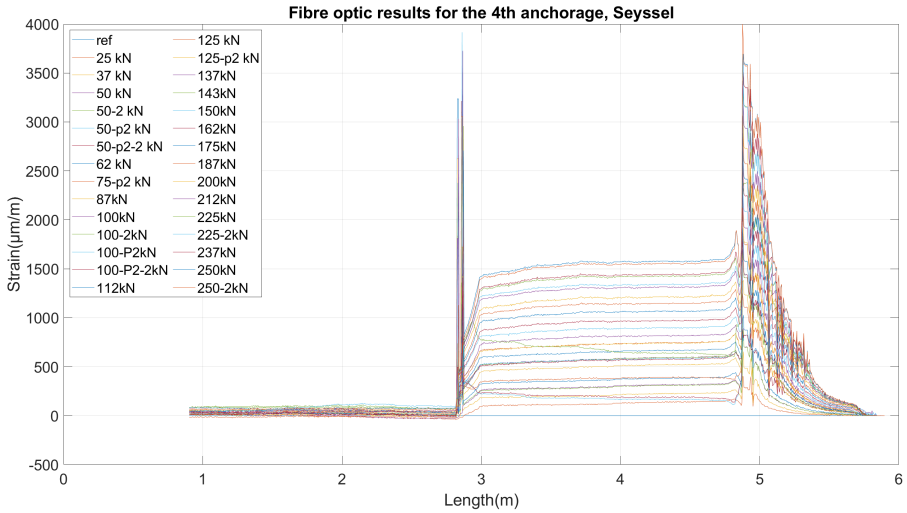

Figure 11.30: Fibre optic results for the 4^{th} anchorage, Seyssel

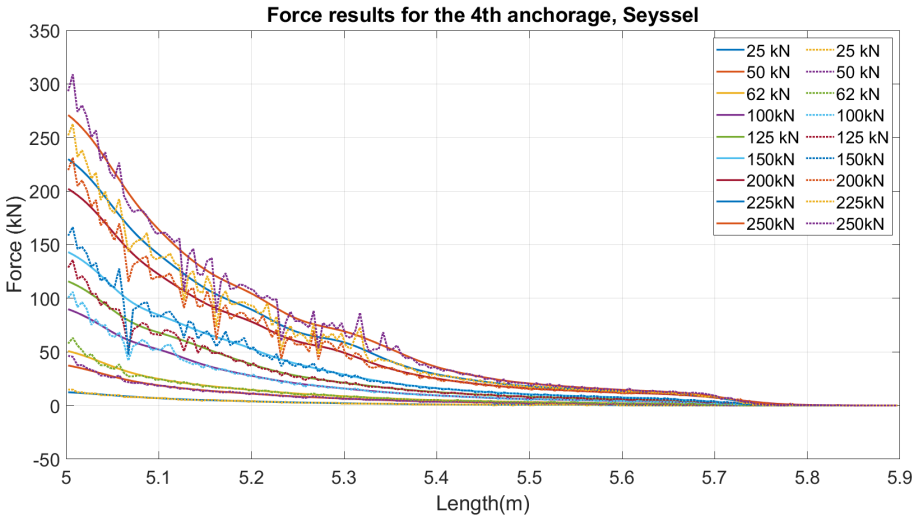

Figure 11.31: Force results for the virgin loading steps in the 4^{th} anchorage, Seyssel

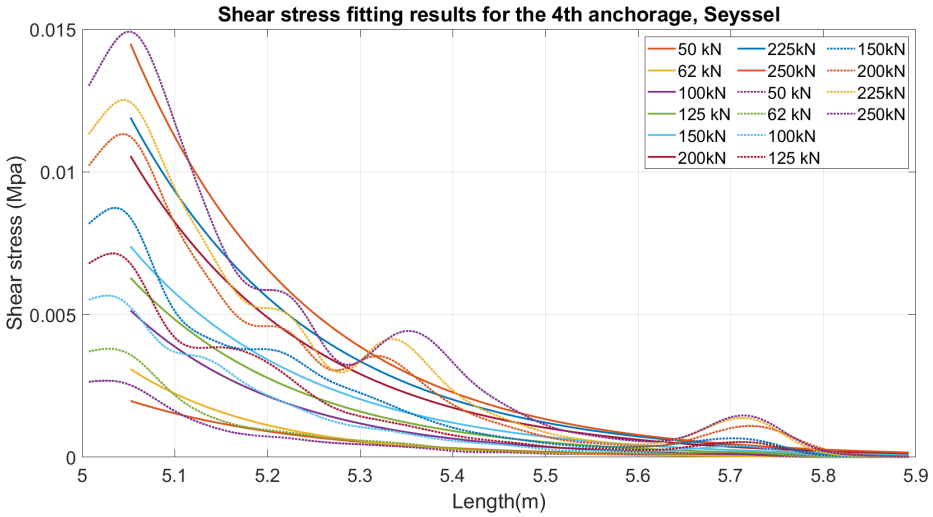

Figure 11.32: Shear stress results for the virgin loading steps in the 4^{th} anchorage, Seyssel

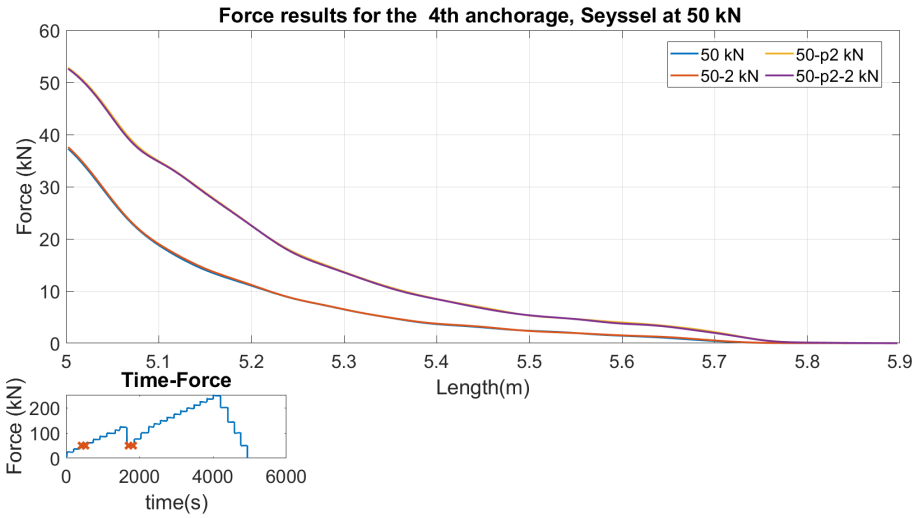

Figure 11.33: Force results for the 4^{th} anchorage, Seyssel at 50kN

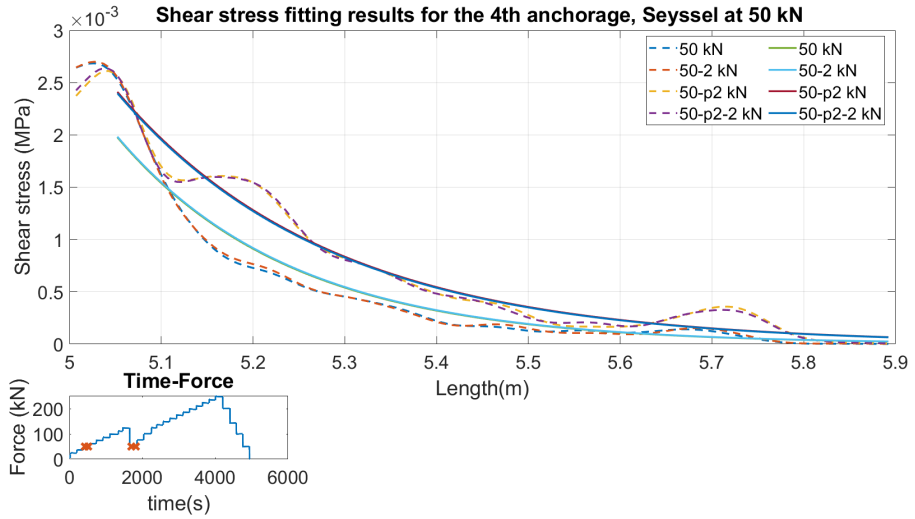

Figure 11.34: Shear stress fitting results for the 4^{th} anchorage, Seyssel at 50kN

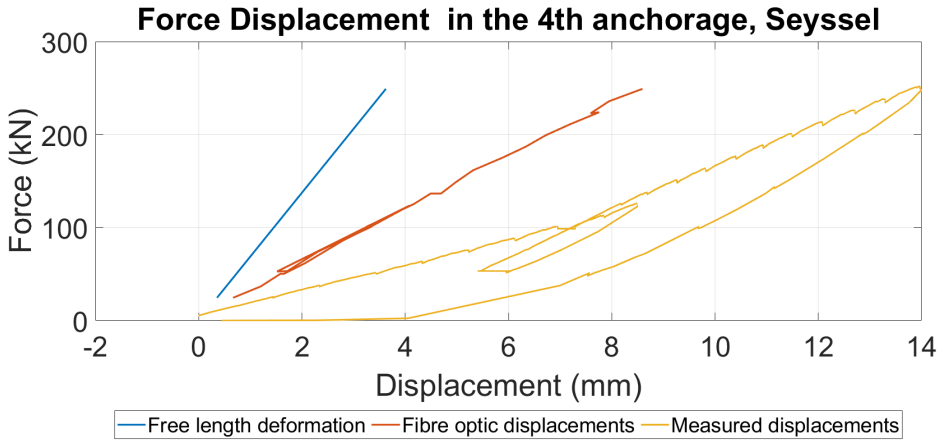

Figure 11.35: Force displacement curves comparison between measured and calculated with the use of the integral along the whole steel bar, 4^{th} anchorage, Seyssel

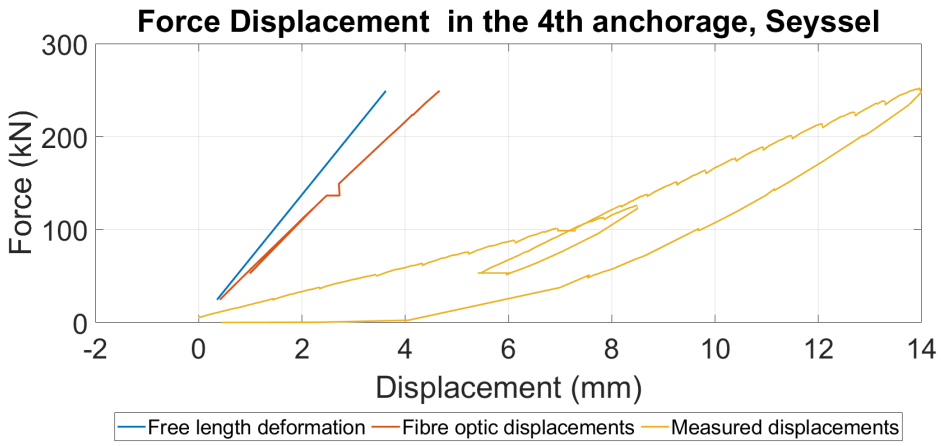

Figure 11.36: Force displacement curves comparison between measured and calculated with the use of the integral along the grouted segment of the steel bar, 4^{th} anchorage, Seyssel

11.0.5 A5 - Seyssel

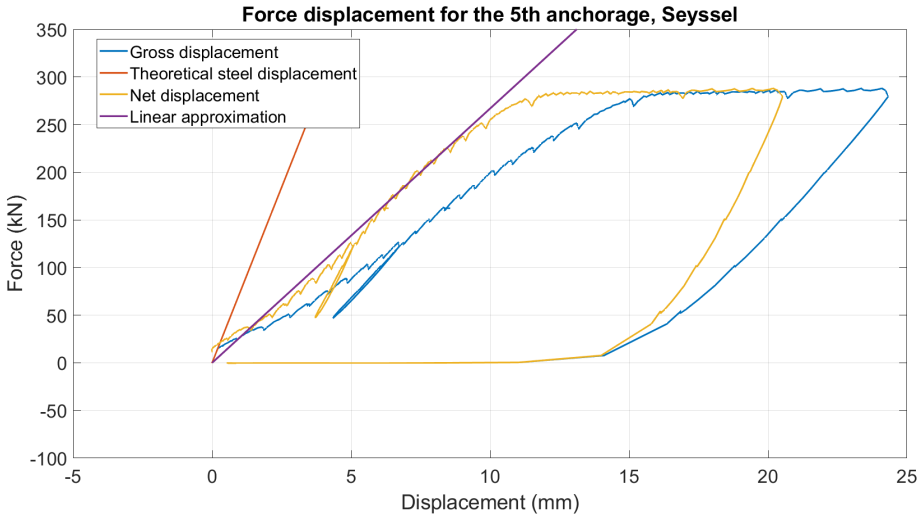

Figure 11.37: Force, displacement for the 5^{th} anchorage, Seyssel

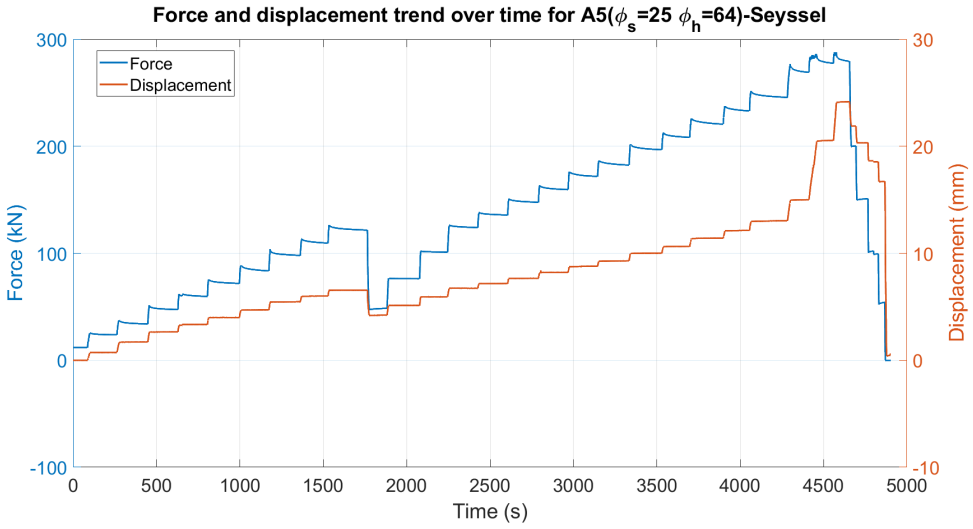

Figure 11.38: Force and displacement trend over time for A5-Seyssel

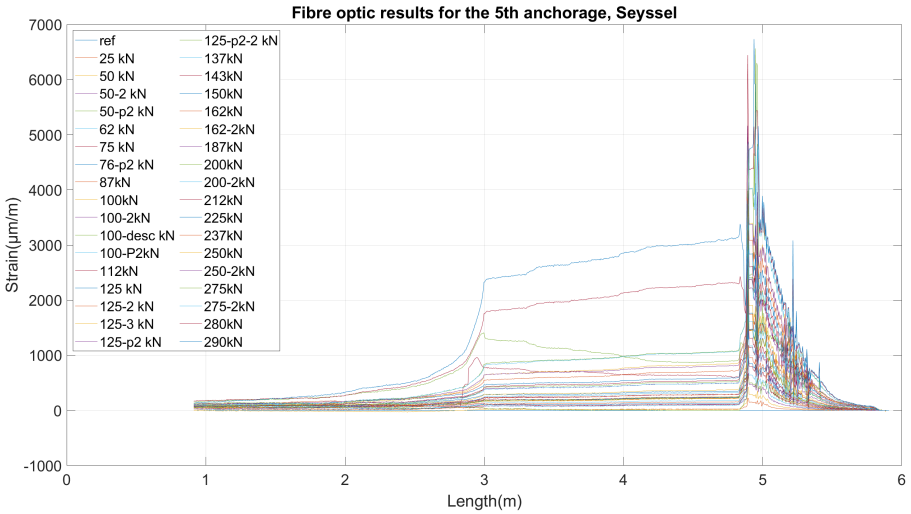

Figure 11.39: Fibre optic results for the 5^{th} anchorage, Seyssel

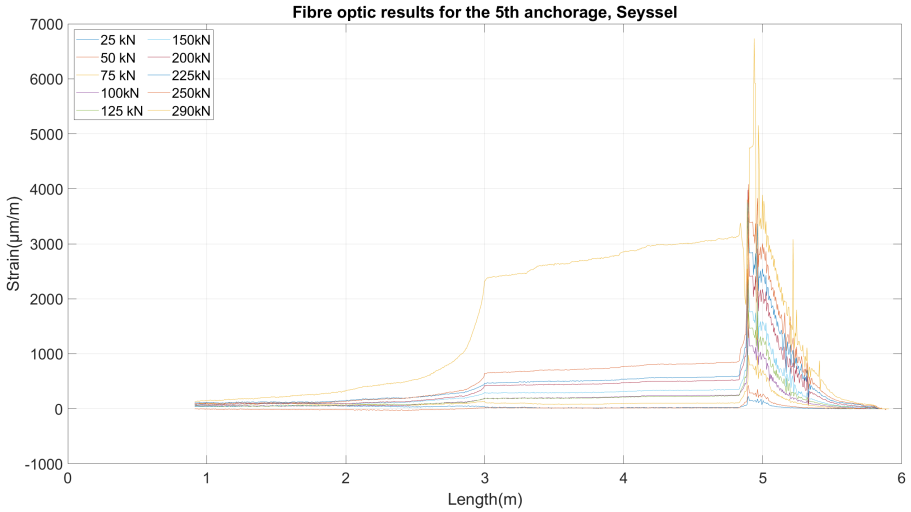

Figure 11.40: Fibre optic results for some virgin loading steps in the 5^{th} anchorage, Seyssel

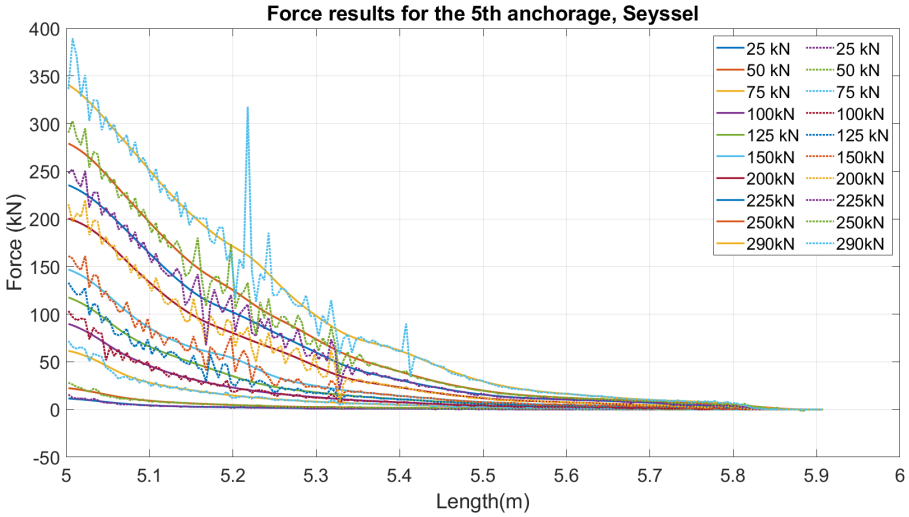

Figure 11.41: Force results for the virgin loading steps in the 5^{th} anchorage, Seyssel

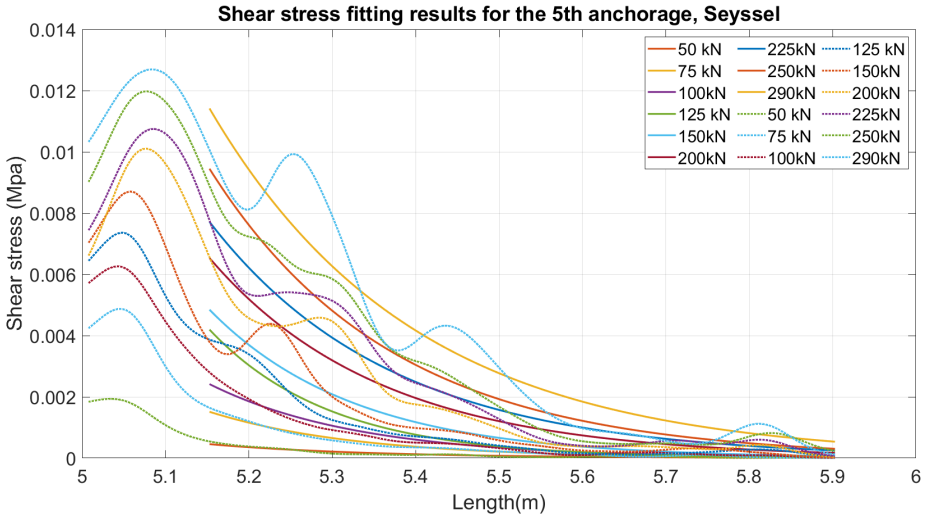

Figure 11.42: Shear stress results for the virgin loading steps in the 5^{th} anchorage, Seyssel

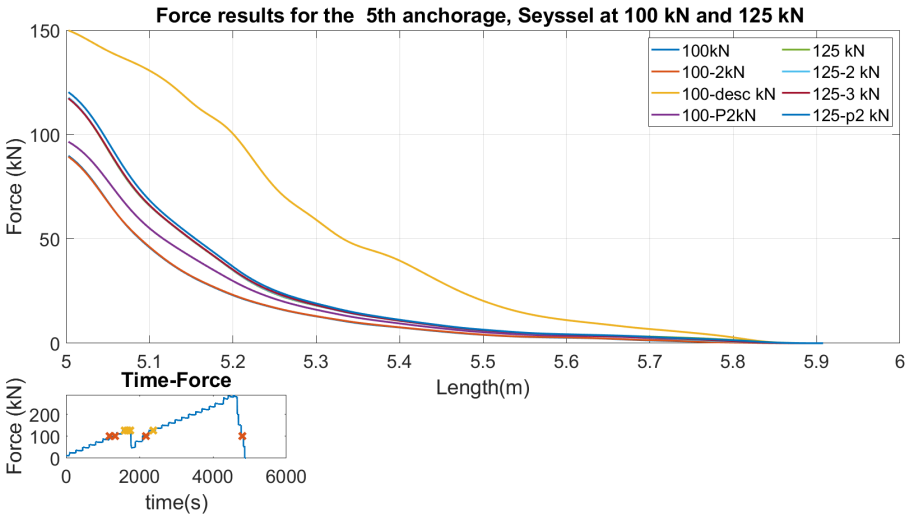

Figure 11.43: Force results for the 5^{th} anchorage, Seyssel at 100kN and 125 kN

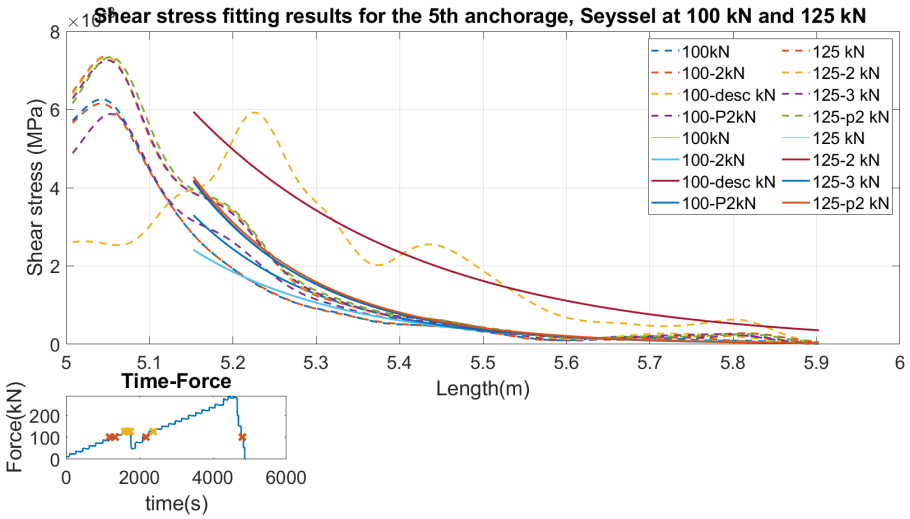

Figure 11.44: Shear stress fitting results for the 5^{th} anchorage, Seyssel at 100kN and 125 kN

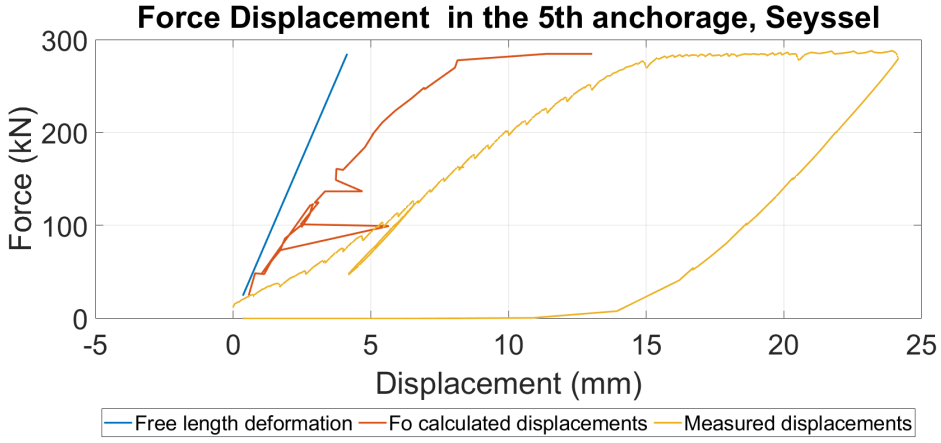

Figure 11.45: Force displacement curves comparison between measured and calculated with the use of the integral along the whole steel bar, 5^{th} anchorage, Seyssel

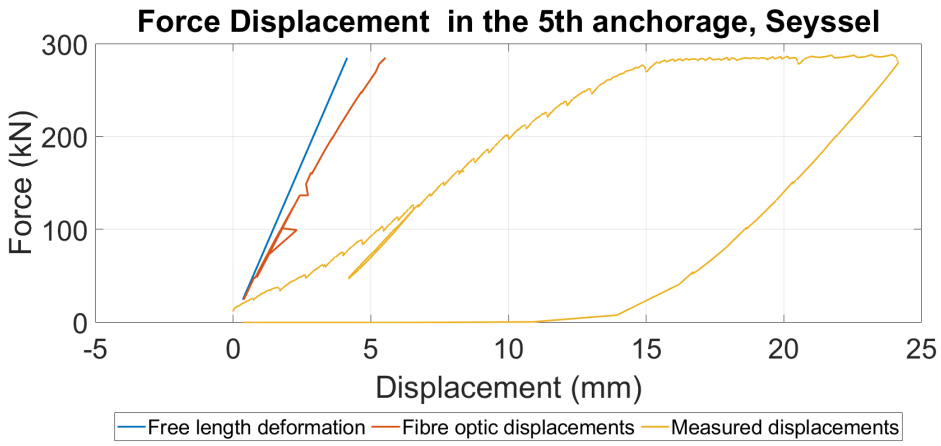

Figure 11.46: Force displacement curves comparison between measured and calculated with the use of the integral along the grouted segment of the steel bar, 5^{th} anchorage, Seyssel

11.0.6 A6 - Seyssel

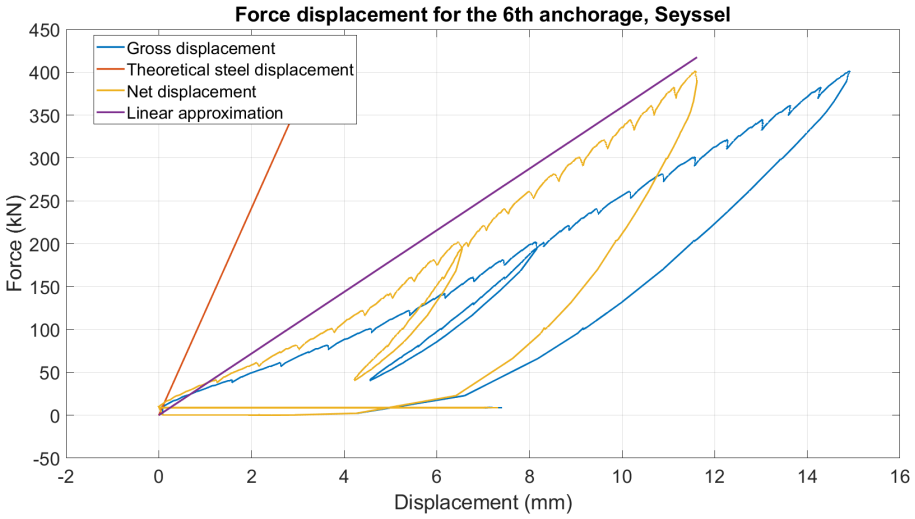

Figure 11.47: Force displacement for the 6^{th} anchorage, Seyssel

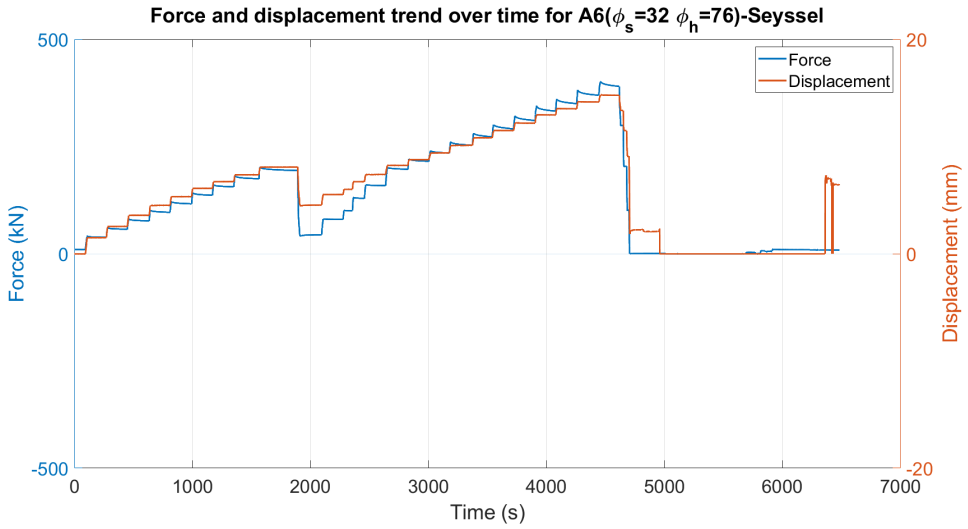

Figure 11.48: Force and displacement trend over time for A6-Seyssel

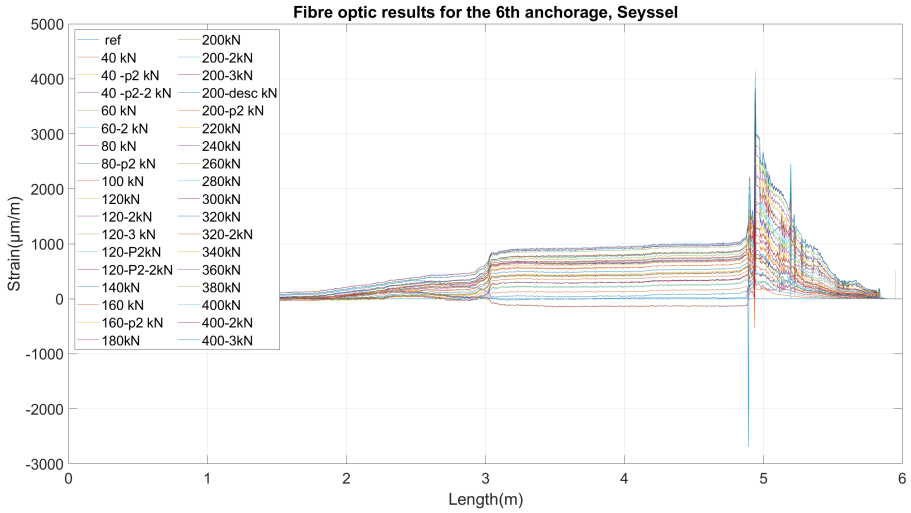

Figure 11.49: Fibre optic results for the 6^{th} anchorage, Seyssel

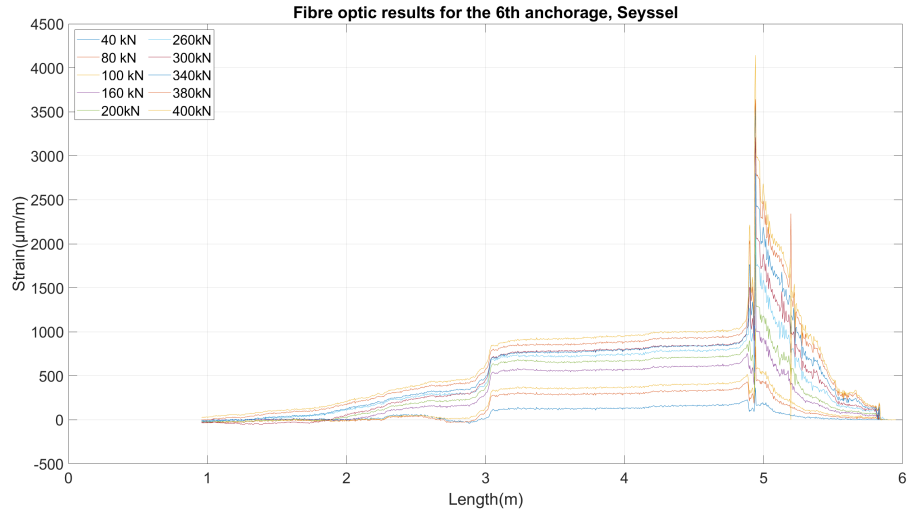

Figure 11.50: Fibre optic results for some virgin loading steps in the 6^{th} anchorage, Seyssel

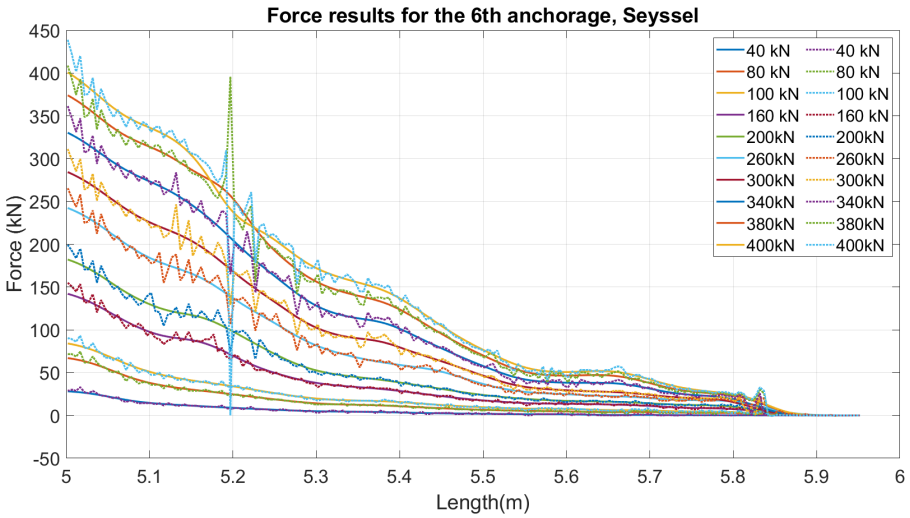

Figure 11.51: Force results for the virgin loading steps in the 6^{th} anchorage, Seyssel

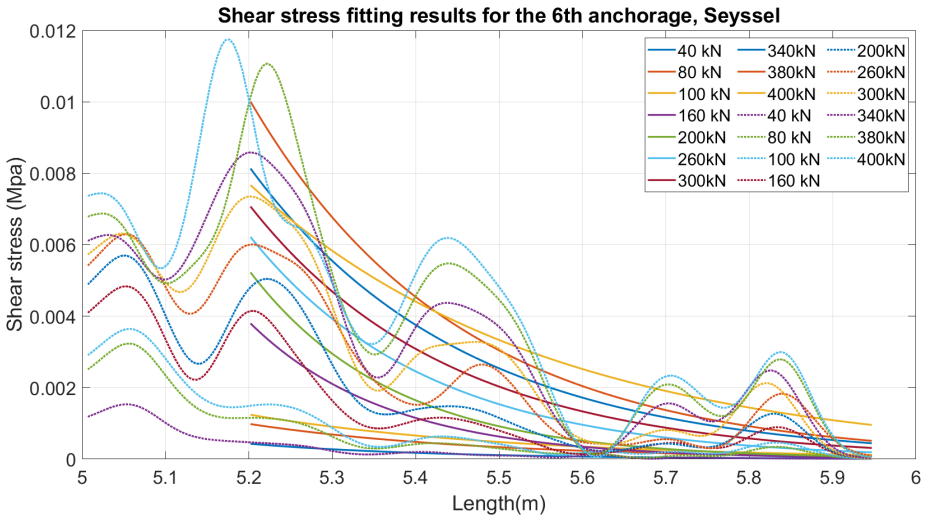

Figure 11.52: Shear stress results for the virgin loading steps in the 6^{th} anchorage, Seyssel

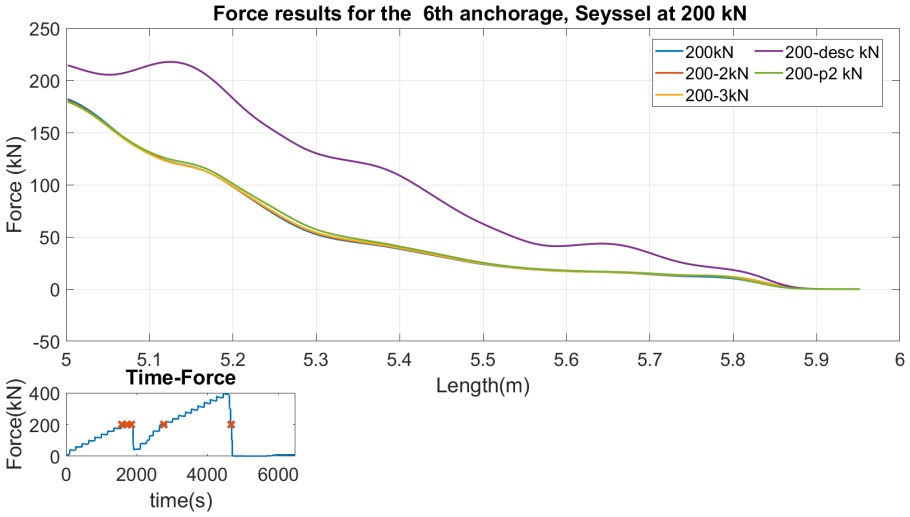

Figure 11.53: Force results for the 6^{th} anchorage, Seyssel at 200kN

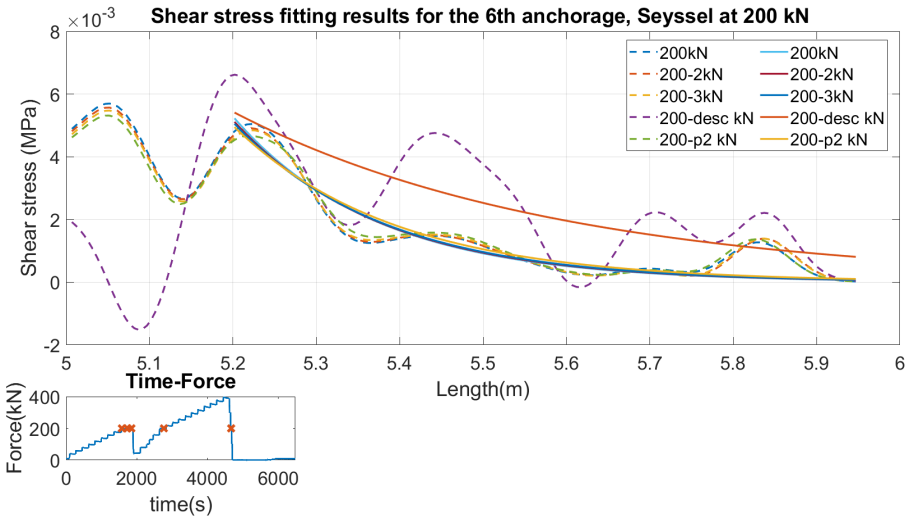

Figure 11.54: Shear stress fitting results for the 6^{th} anchorage, Seyssel at 200kN

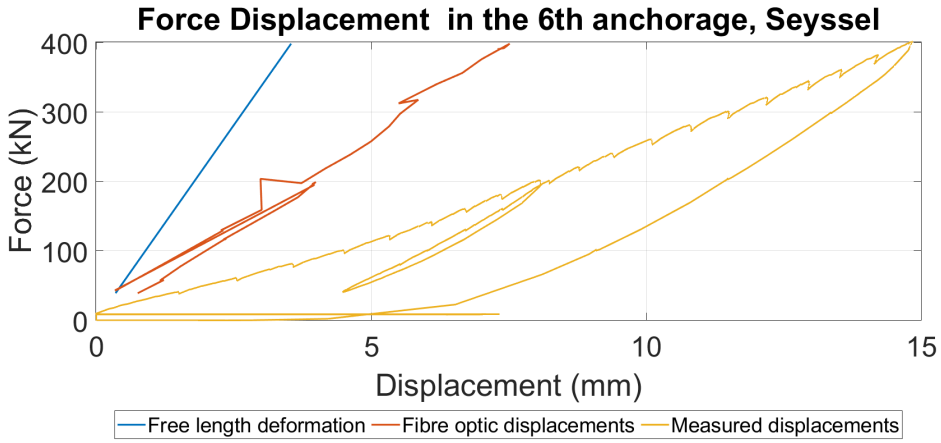

Figure 11.55: Force displacement curves comparison between measured and calculated with the use of the integral along the whole steel bar, 6^{th} anchorage, Seyssel

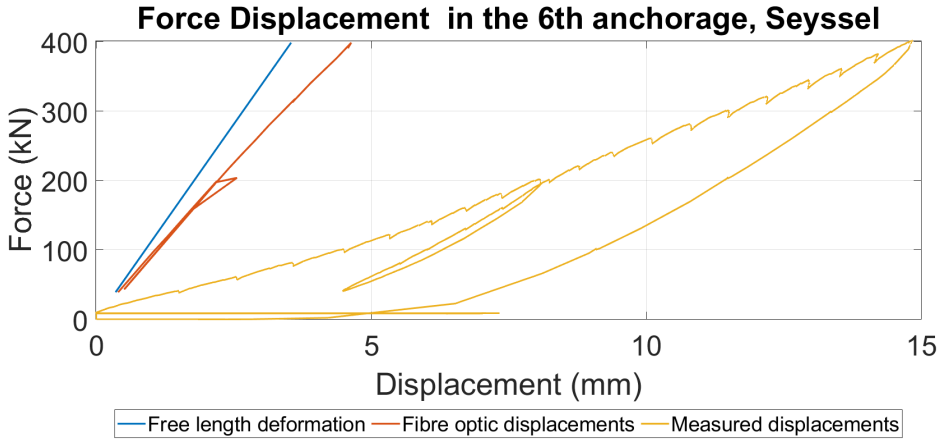

Figure 11.56: Force displacement curves comparison between measured and calculated with the use of the integral along the grouted segment of the steel bar, 6^{th} anchorage, Seyssel

11.0.7 A7 - Seyssel

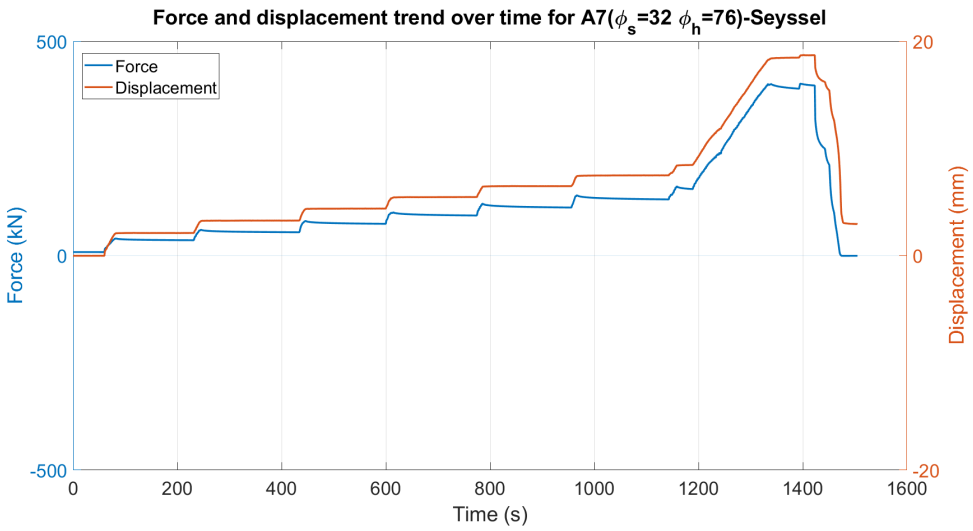

Figure 11.57: Force and displacement trend over time for A7-Seyssel

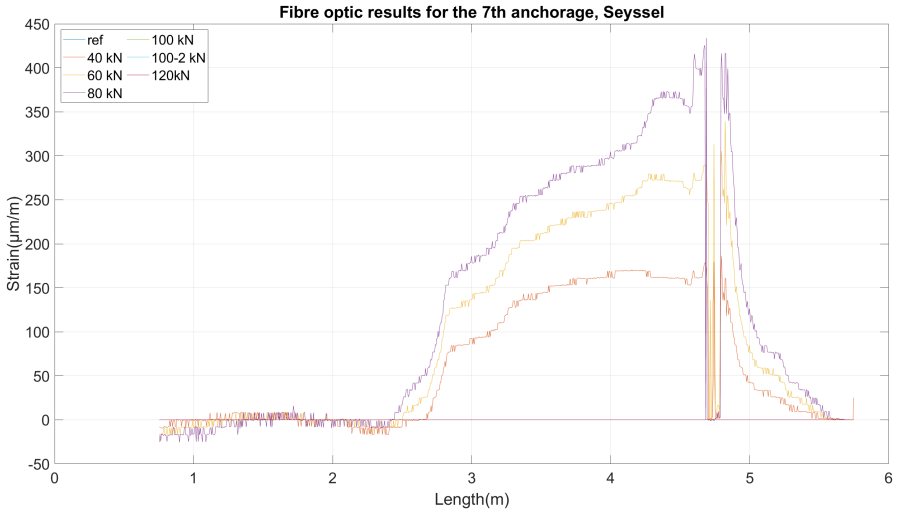

Figure 11.58: Fibre optic results for the 7^{th} anchorage, Seyssel

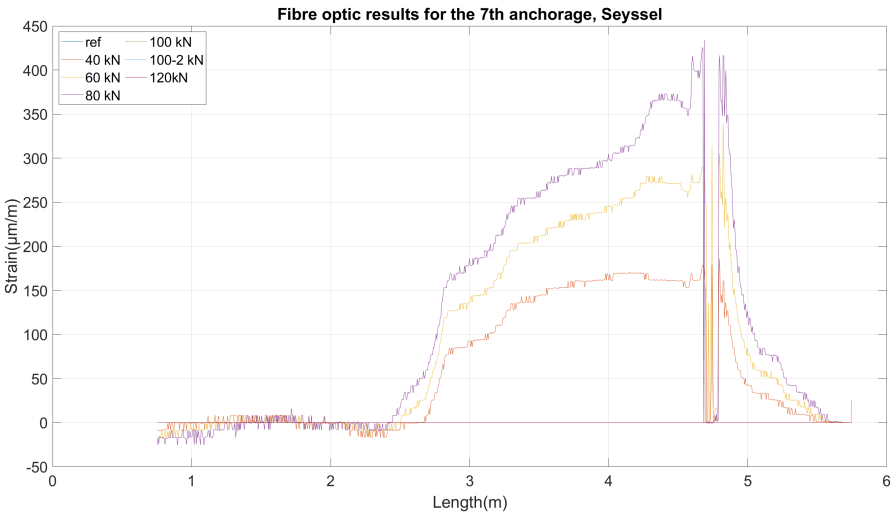

Figure 11.59: Fibre optic results for the 7^{th} anchorage, Seyssel

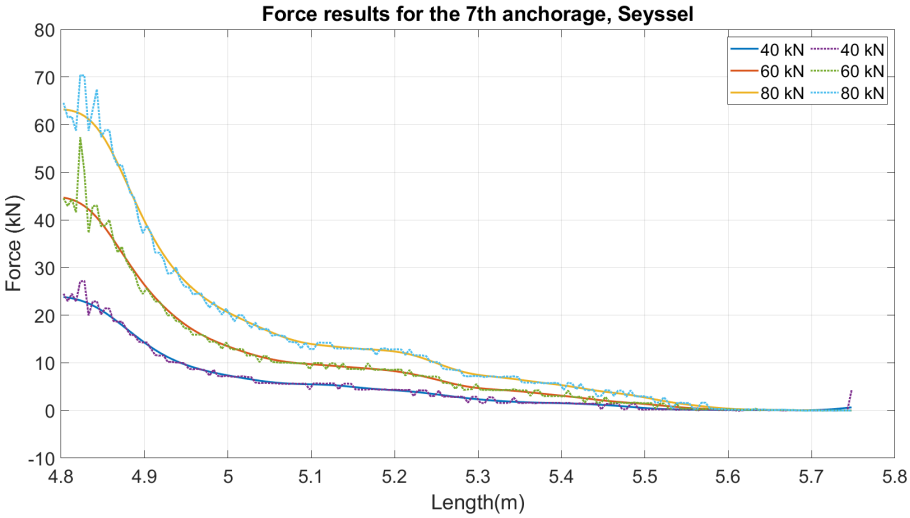

Figure 11.60: Force results in the 7^{th} anchorage, Seyssel

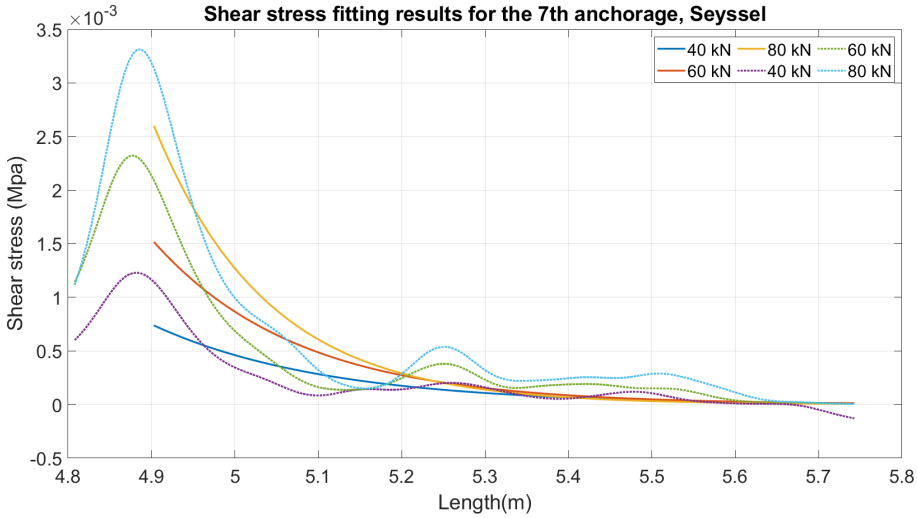

Figure 11.61: Shear stress results for the 7^{th} anchorage, Seyssel

12 Annexes Oisans

The results for each rock-bolt in Oisans will be presented in this chapter.

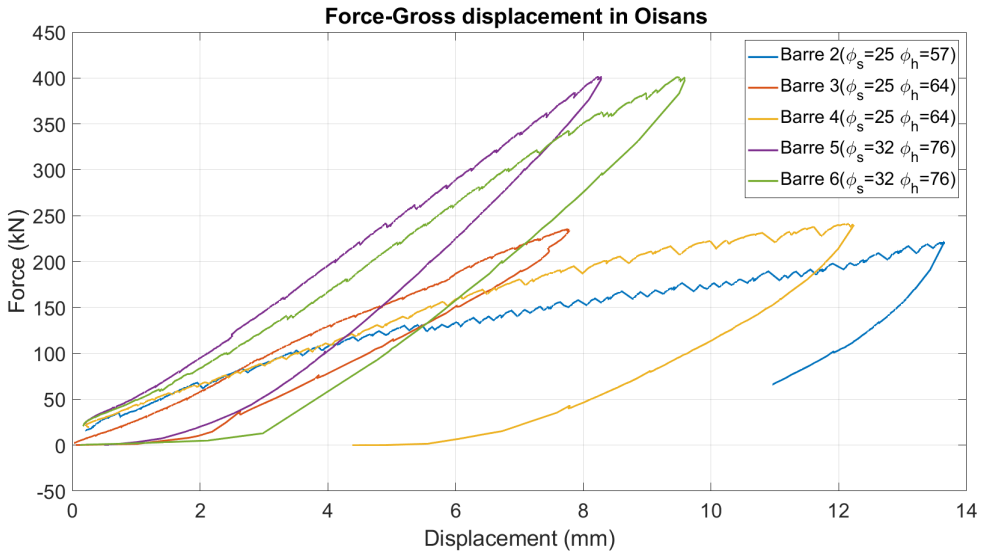

Figure 12.1: Force and gross displacement behaviour for the rock-bolts in Oisans

12.0.1 B2 - Oisans

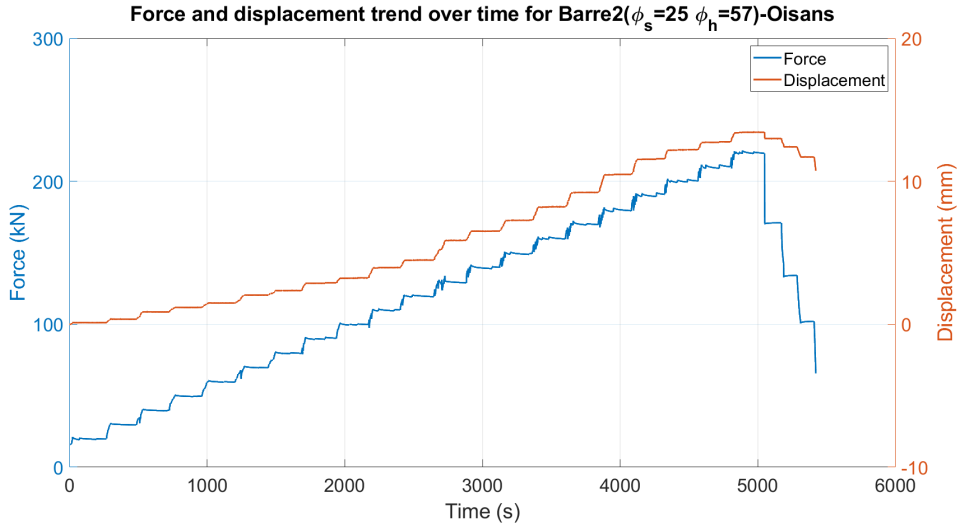

Figure 12.2: Force and displacement trend over time for Barre2-Oisans

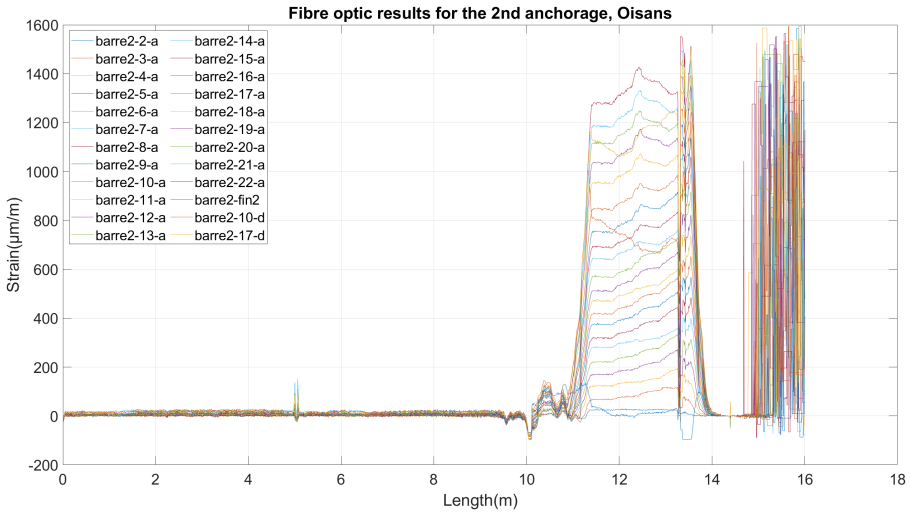

Figure 12.3: Fibre optic results for the 2^{nd} anchorage, Oisans

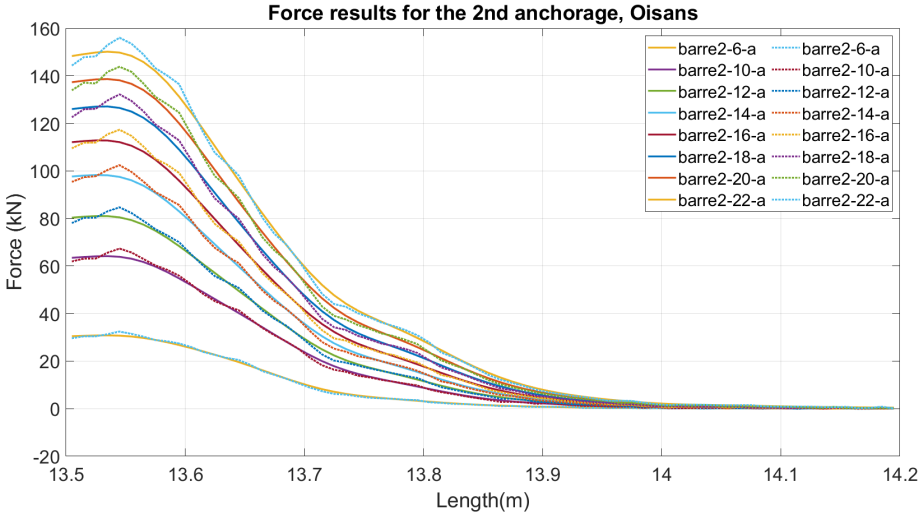

Figure 12.4: Force results for the virgin loading steps in the 2^{nd} anchorage, Oisans

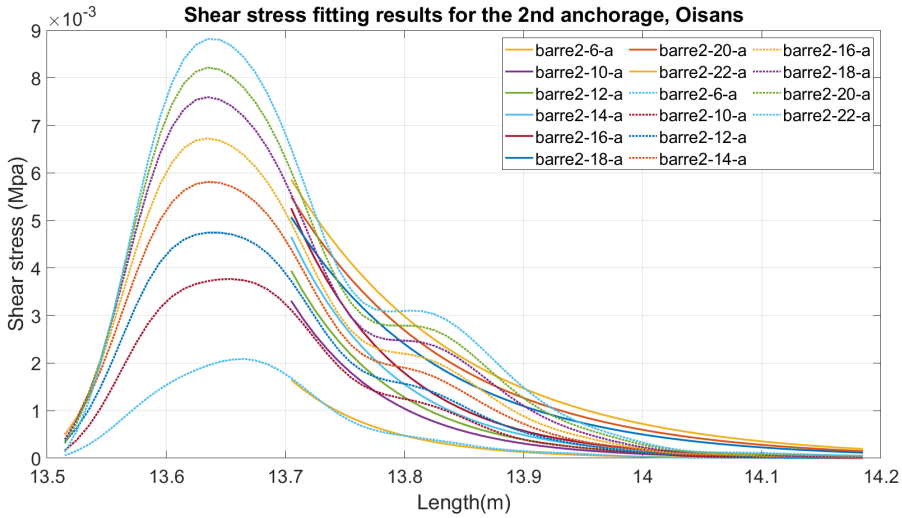

Figure 12.5: Shear stress results for the virgin loading steps in the 2^{nd} anchorage, Oisans

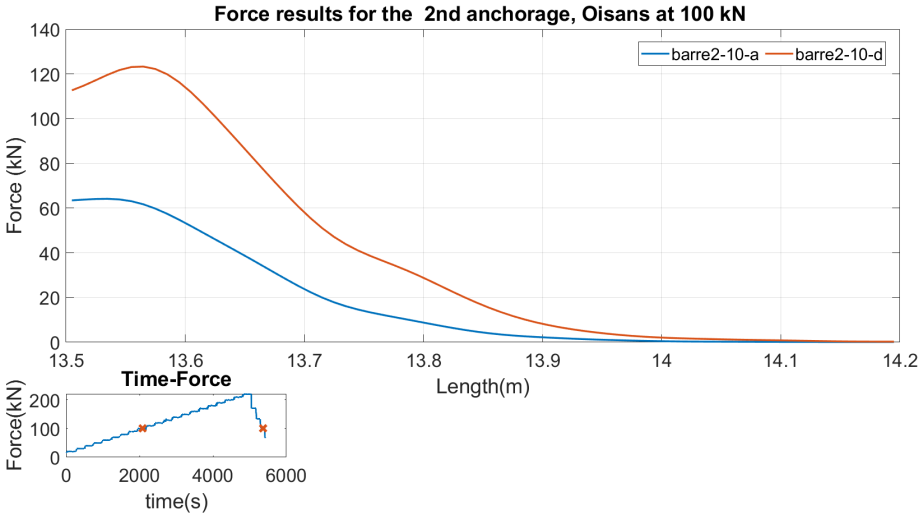

Figure 12.6: Force results for the 2^{nd} anchorage, Oisans at 100kN

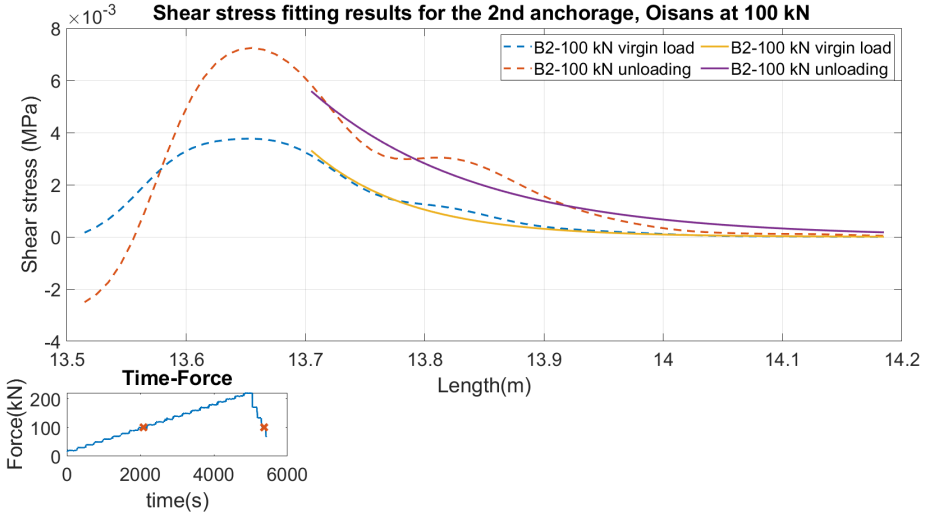

Figure 12.7: Shear stress fitting results for the 2^{nd} anchorage, Seyssel at 100kN

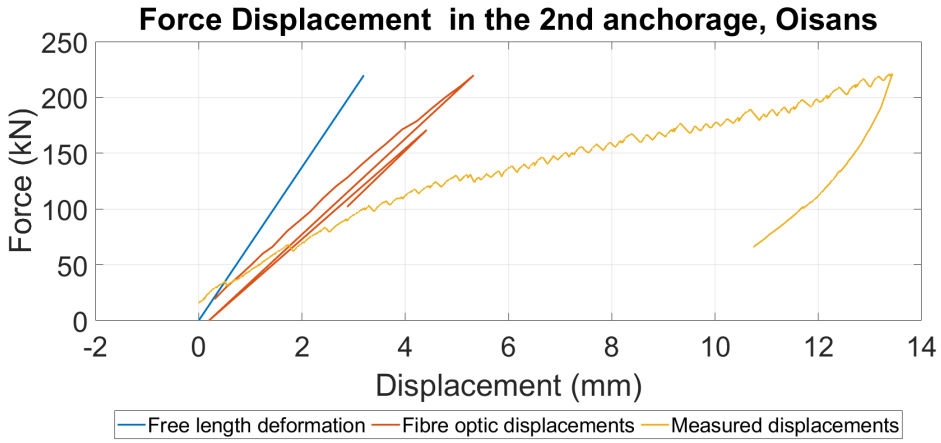

Figure 12.8: Force displacement curves comparison between measured and calculated with the use of the integral along the whole steel bar, 2^{nd} anchorage, Oisans

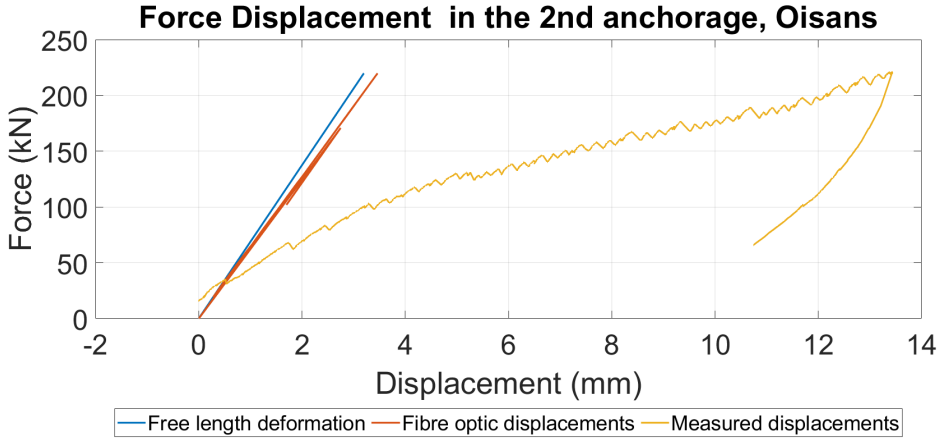

Figure 12.9: Force displacement curves comparison between measured and calculated with the use of the integral along the grouted segment of the steel bar, 2^{nd} anchorage, Oisans

12.0.2 B3 - Oisans

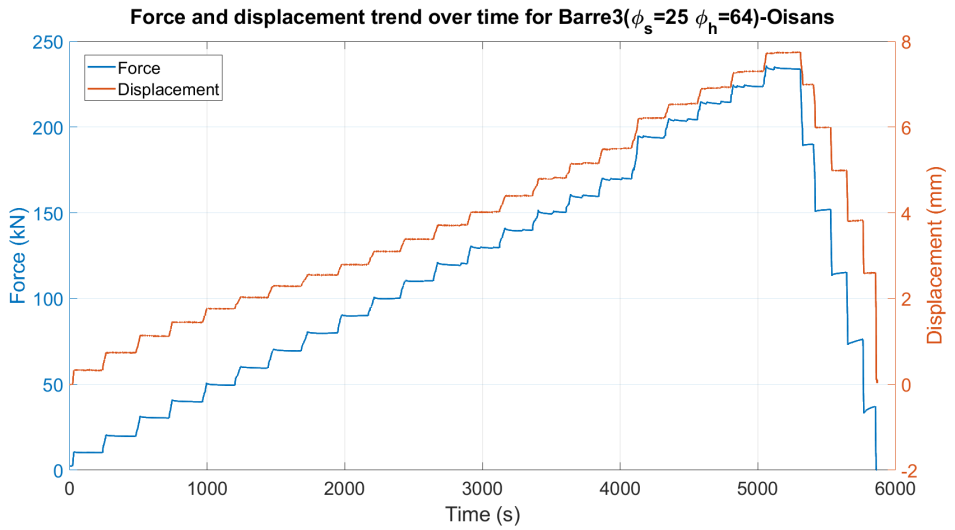

Figure 12.10: Force and displacement trend over time for Barre3-Oisans

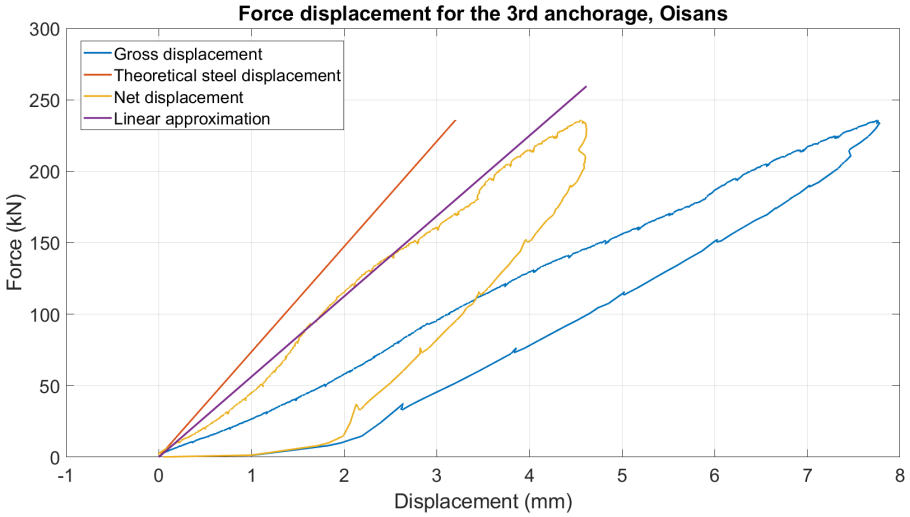

Figure 12.11: Force displacement for the 3^{rd} anchorage, Oisans

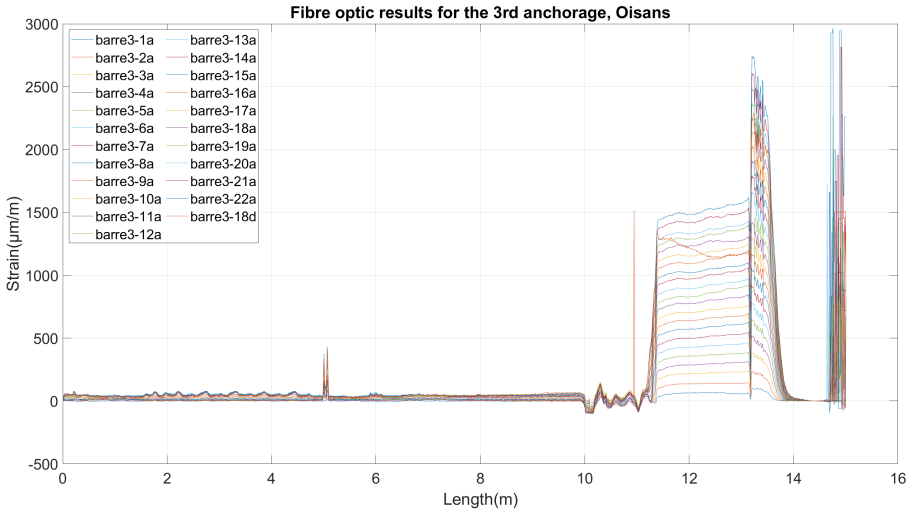

Figure 12.12: Fibre optic results for the 3^{rd} anchorage, Oisans

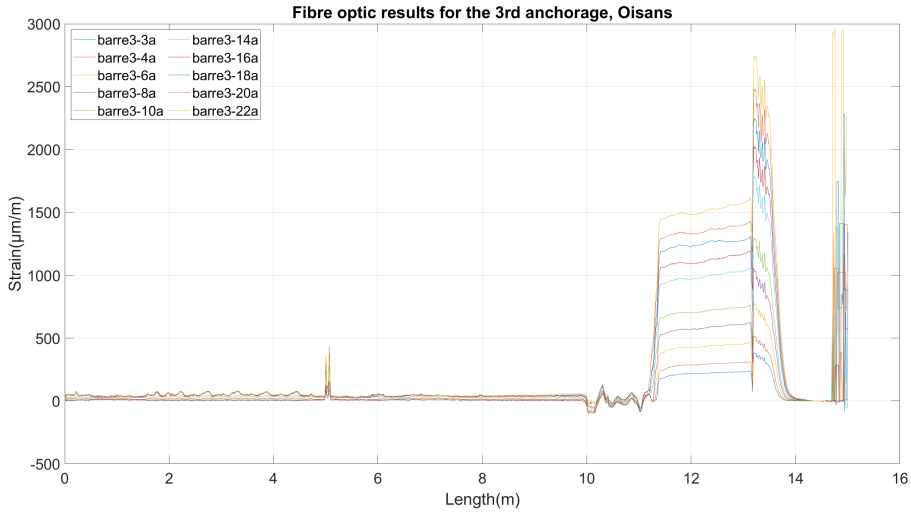

Figure 12.13: Fibre optic results for some virgin loading steps in the 3^{rd} anchorage, Oisans

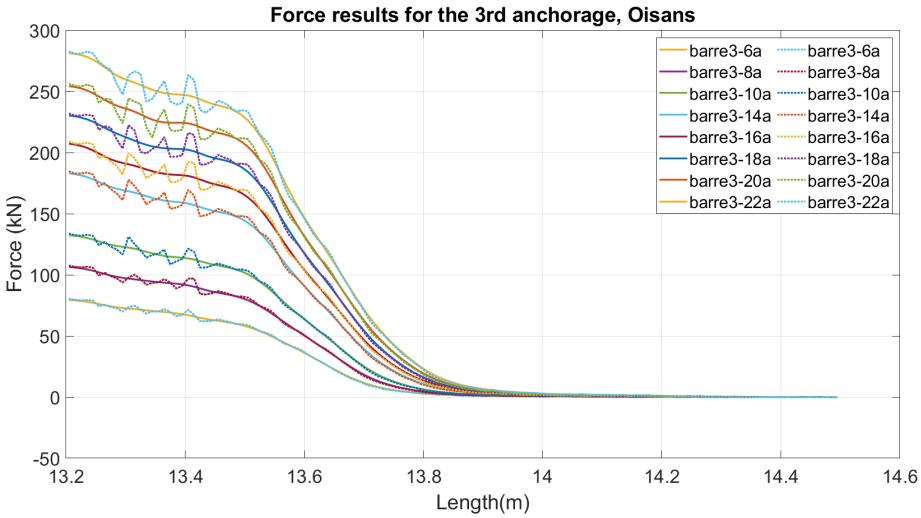

Figure 12.14: Force results for the virgin loading steps in the 3^{rd} anchorage, Oisans

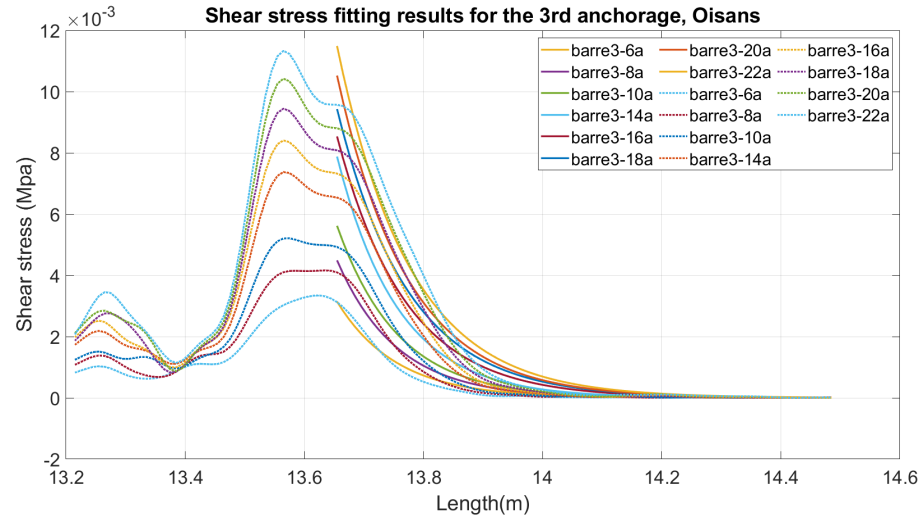

Figure 12.15: Shear stress results for the virgin loading steps in the 3^{rd} anchorage, Oisans

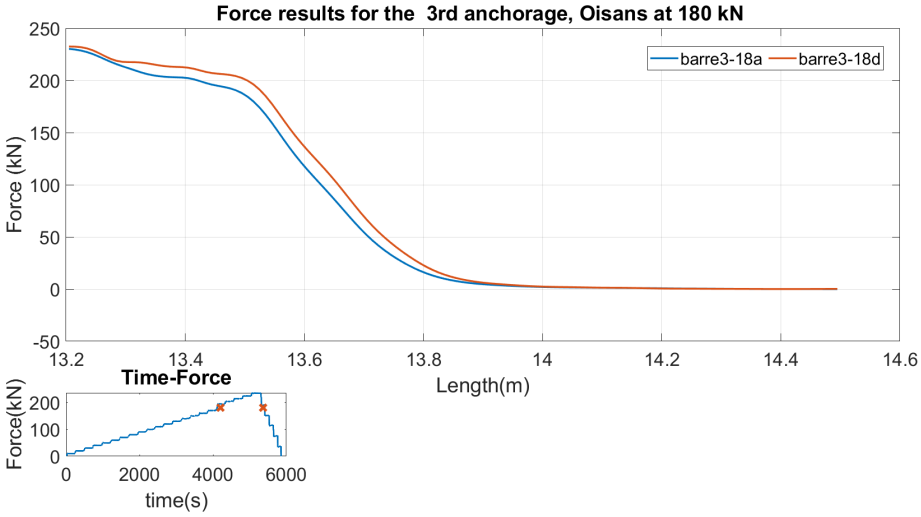

Figure 12.16: Force results for the 3^{rd} anchorage, Oisans at 180kN

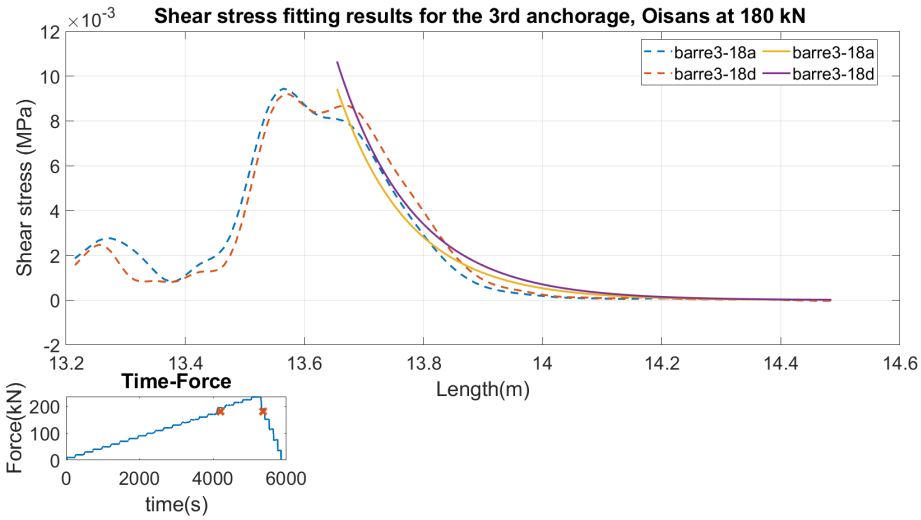

Figure 12.17: Shear stress fitting results for the 3^{rd} anchorage, Seyssel at 180kN

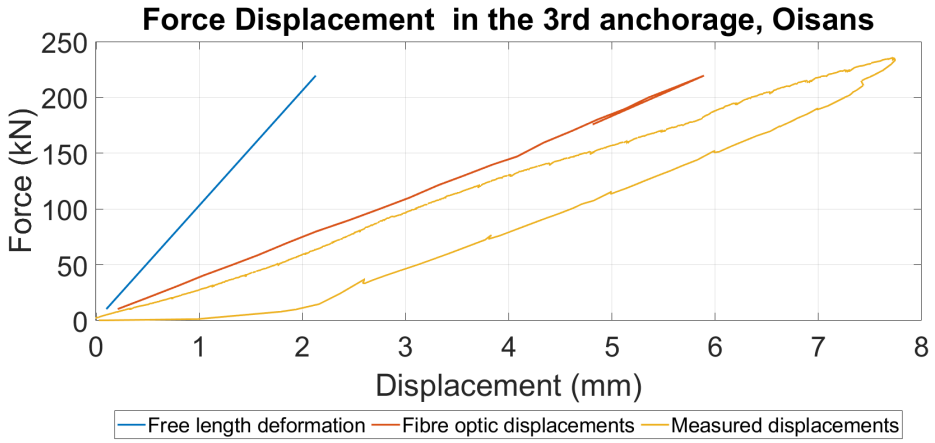

Figure 12.18: Force displacement curves comparison between measured and calculated with the use of the integral along the whole steel bar, 3^{rd} anchorage, Oisans

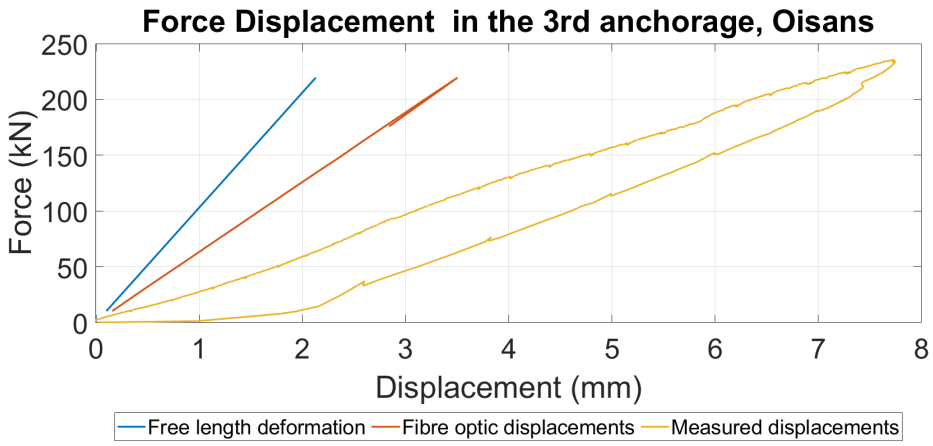

Figure 12.19: Force displacement curves comparison between measured and calculated with the use of the integral along the grouted segment of the steel bar, 3^{rd} anchorage, Oisans

12.0.3 B4 - Oisans

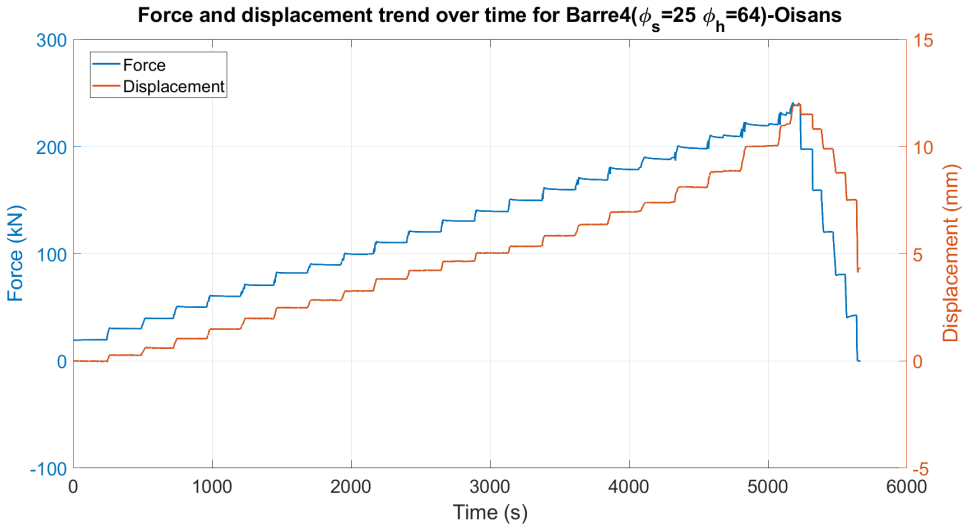

Figure 12.20: Force and displacement trend over time for Barre4-Oisans

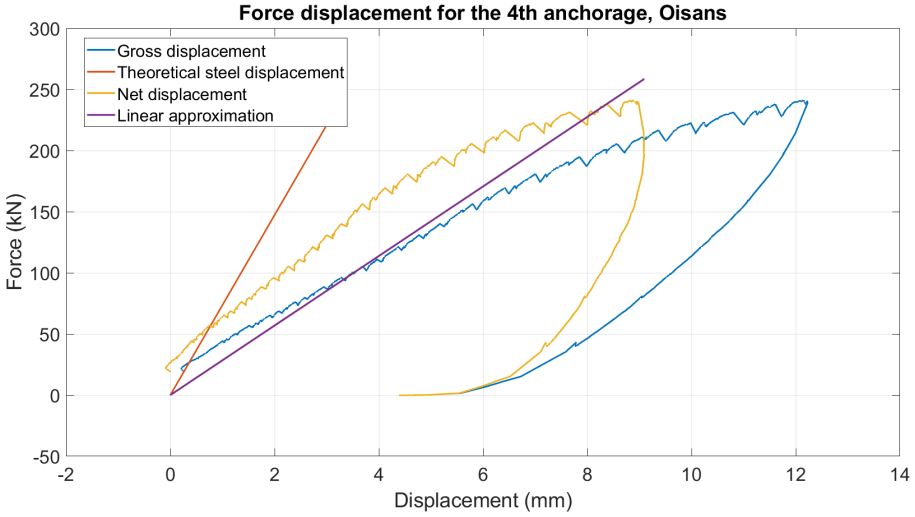

Figure 12.21: Force displacement for the 4^{th} anchorage, Oisans

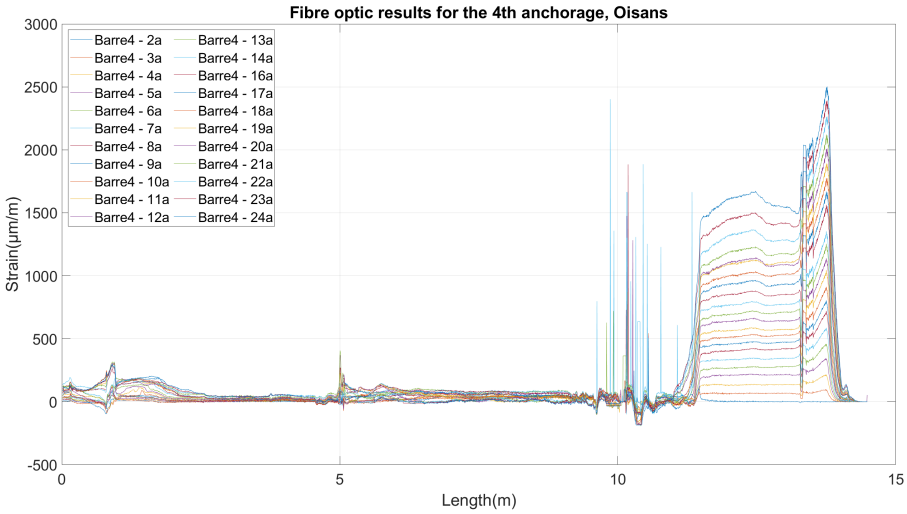

Figure 12.22: Fibre optic results for the 4^{th} anchorage, Oisans

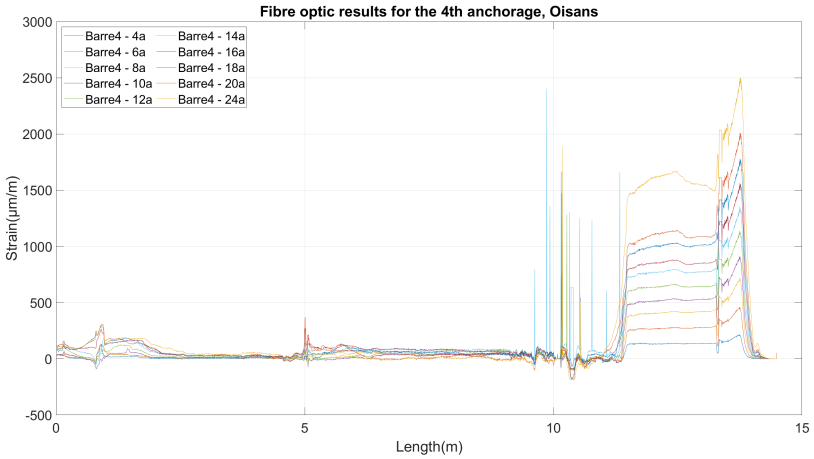

Figure 12.23: Fibre optic results for some virgin loading steps in the 4^{th} anchorage, Oisans

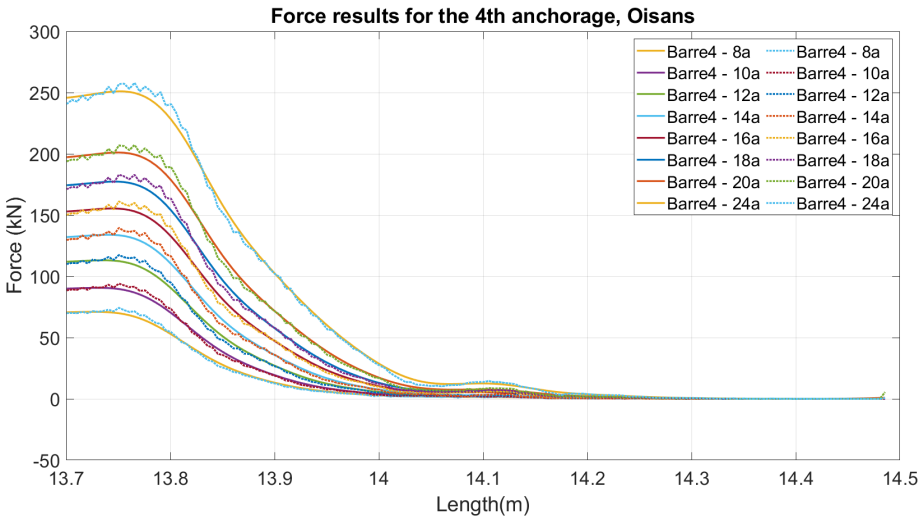

Figure 12.24: Force results for the virgin loading steps in the 4^{th} anchorage, Oisans

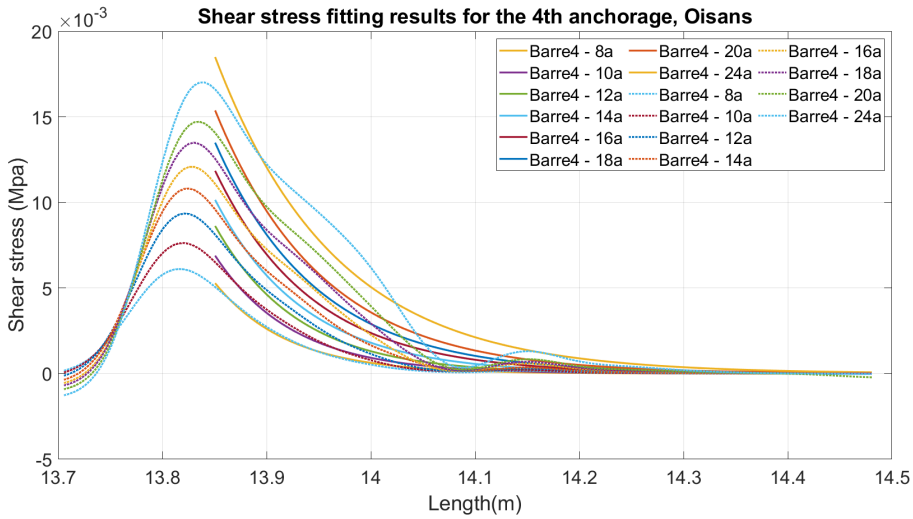

Figure 12.25: Shear stress results for the virgin loading steps in the 4^{th} anchorage, Oisans

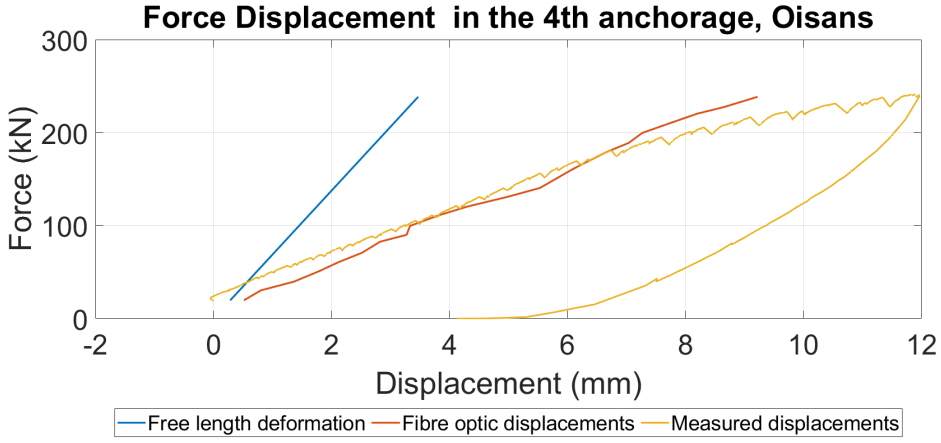

Figure 12.26: Force displacement curves comparison between measured and calculated with the use of the integral along the whole steel bar, 4^{th} anchorage, Oisans

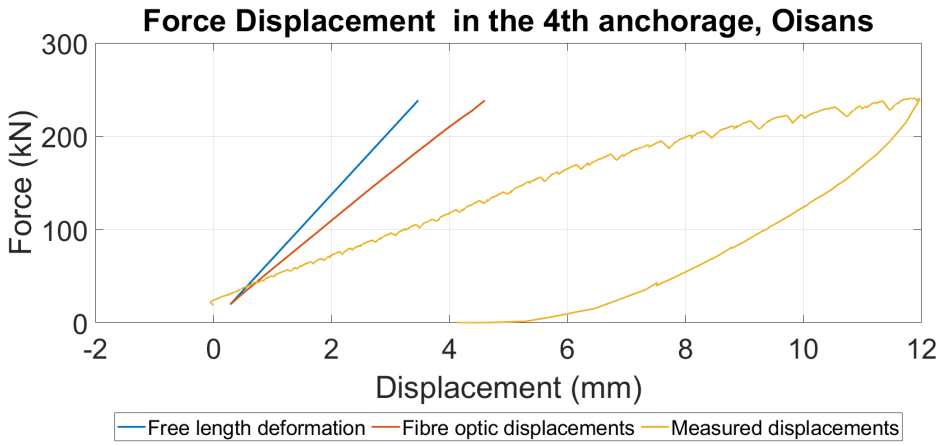

Figure 12.27: Force displacement curves comparison between measured and calculated with the use of the integral along the grouted segment of the steel bar, 4^{th} anchorage, Oisans

12.0.4 B5 - Oisans

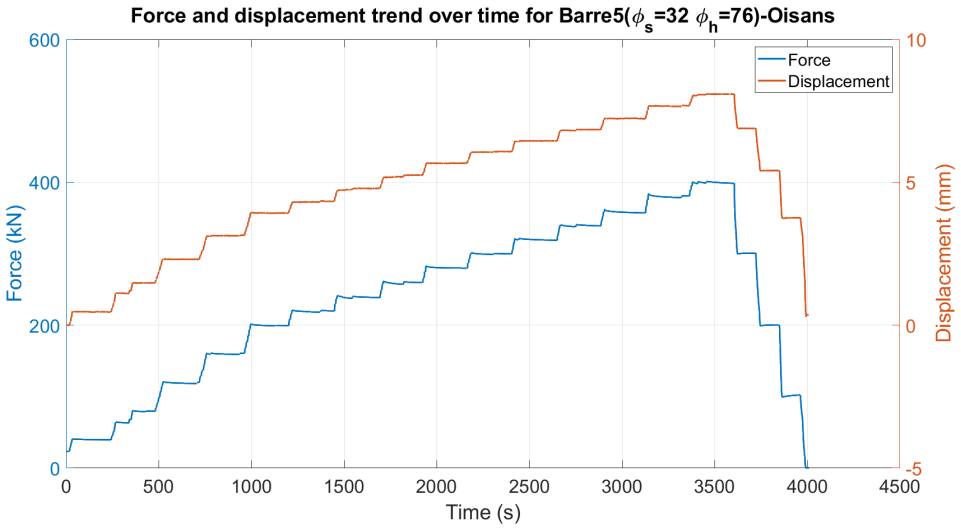

Figure 12.28: Force and displacement trend over time for Barre5-Oisans

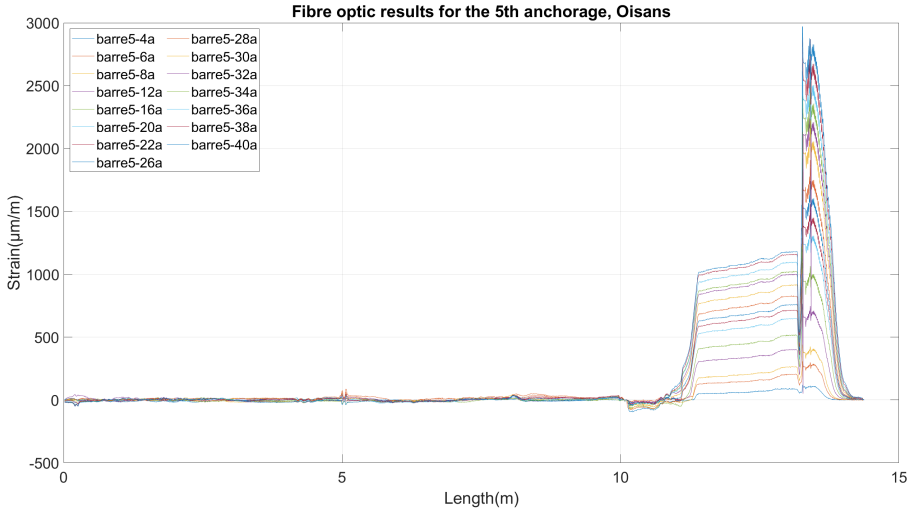

Figure 12.29: Fibre optic results for the 5^{th} anchorage, Oisans

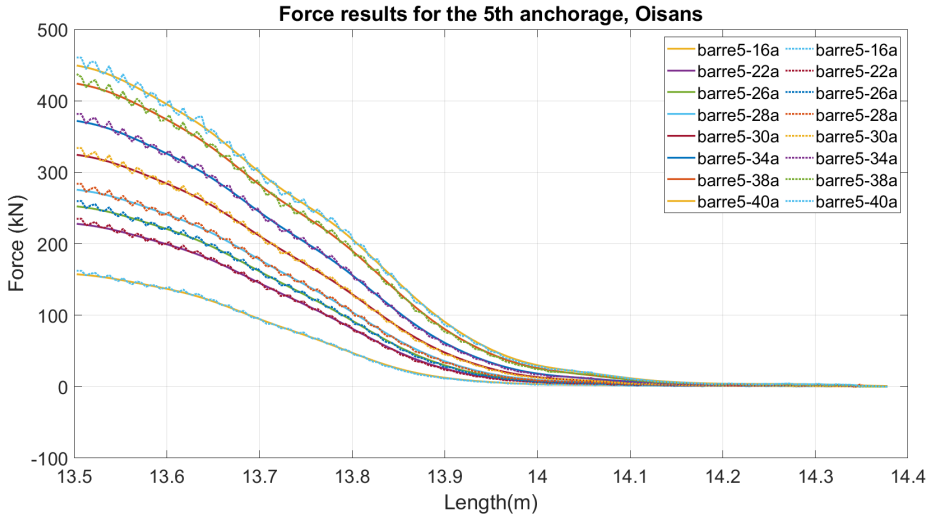

Figure 12.30: Force results for the virgin loading steps in the 5^{th} anchorage, Oisans

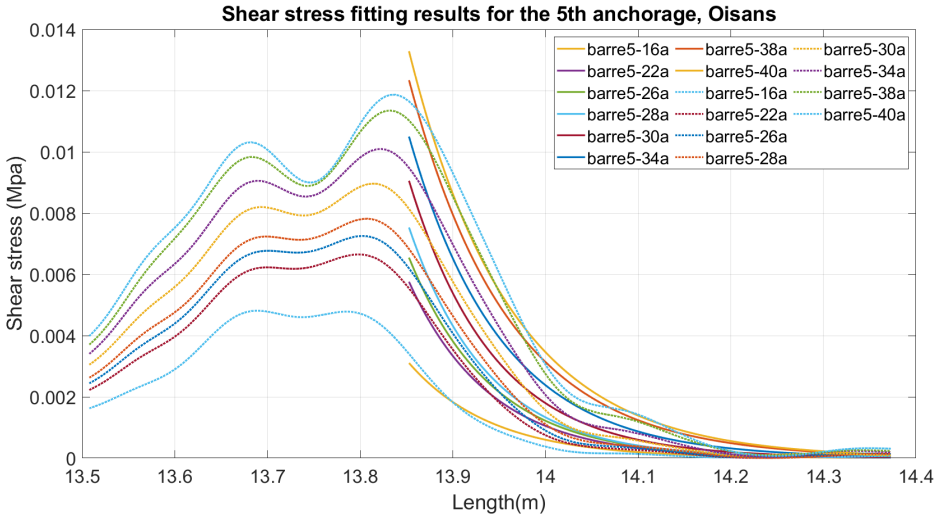

Figure 12.31: Shear stress results for the virgin loading steps in the 5^{th} anchorage, Oisans

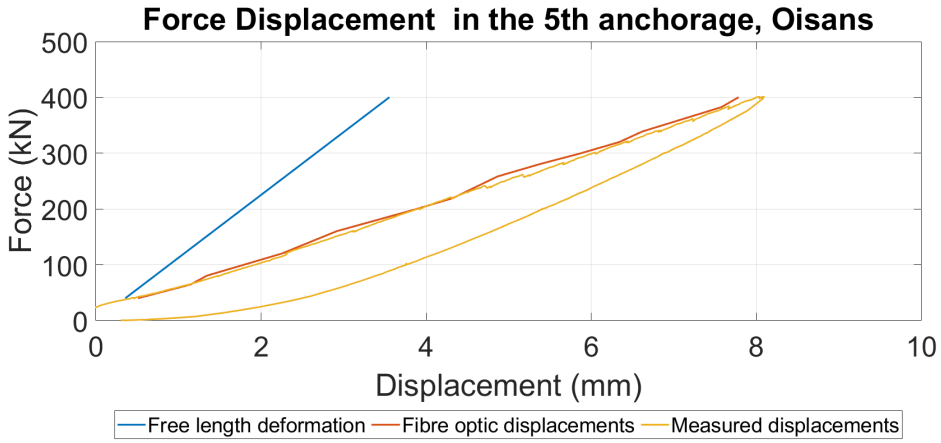

Figure 12.32: Force displacement curves comparison between measured and calculated with the use of the integral along the whole steel bar, 5^{th} anchorage, Oisans

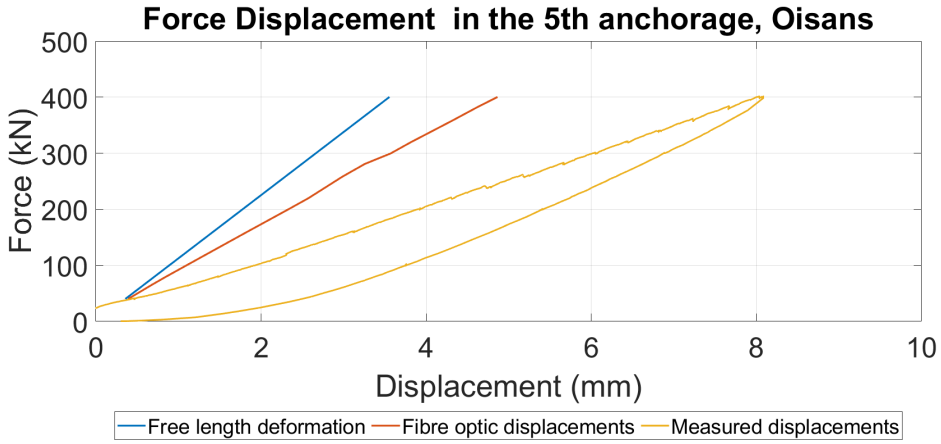

Figure 12.33: Force displacement curves comparison between measured and calculated with the use of the integral along the grouted segment of the steel bar, 5^{th} anchorage, Oisans

12.0.5 B6 - Oisans

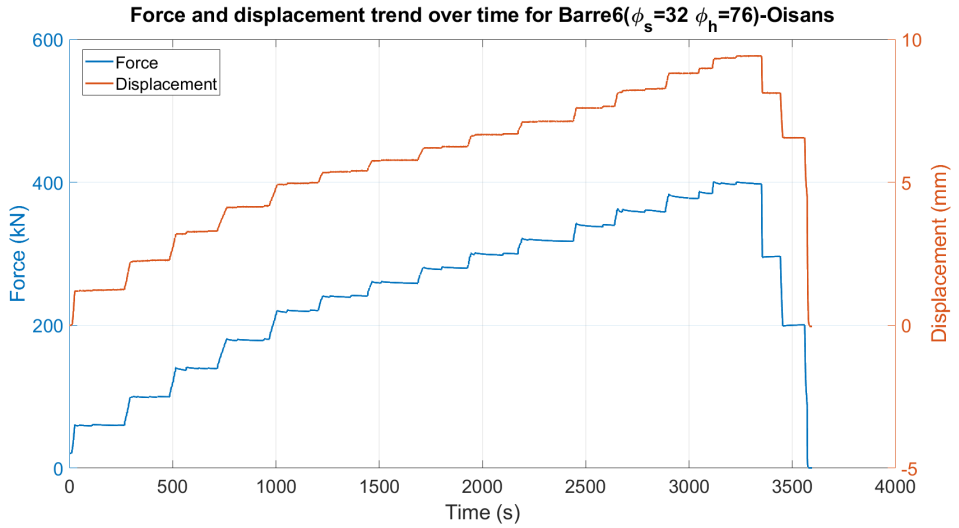

Figure 12.34: Force and displacement trend over time for Barre6-Oisans

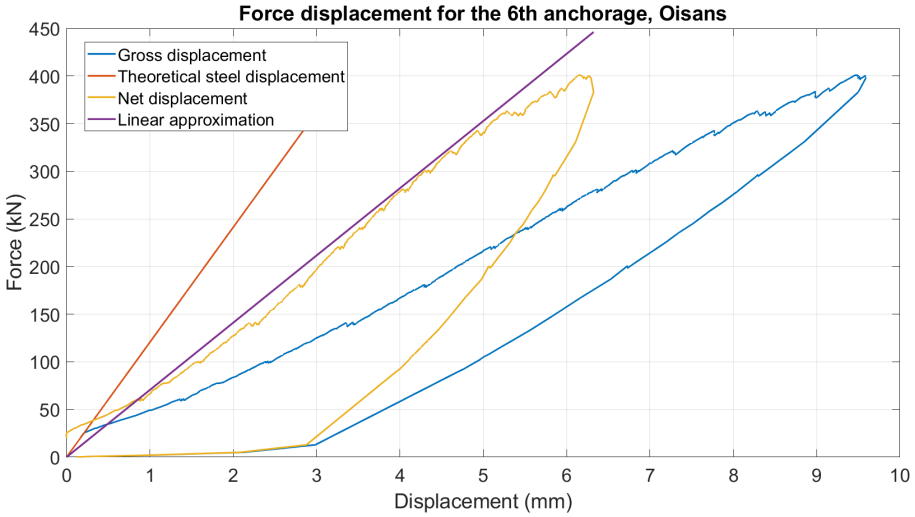

Figure 12.35: Force displacement for the 6^{th} anchorage, Oisans

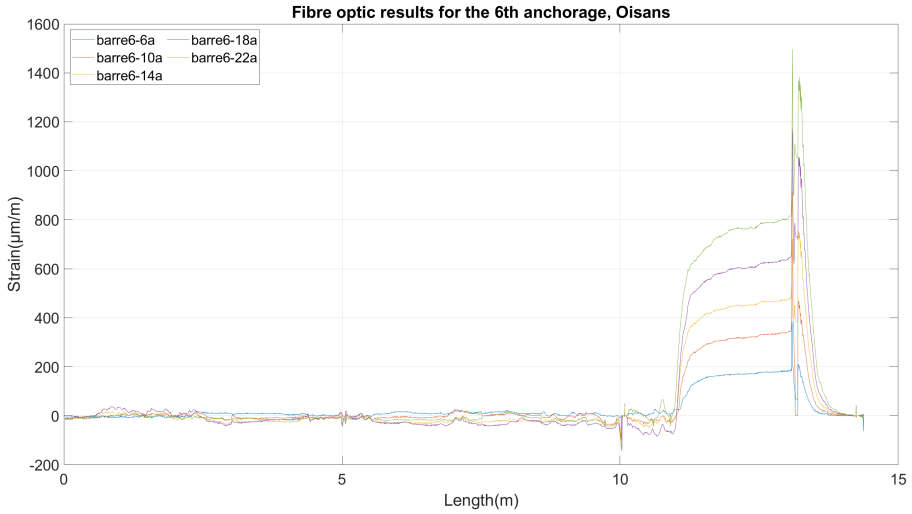

Figure 12.36: Fibre optic results for the 6^{th} anchorage, Oisans

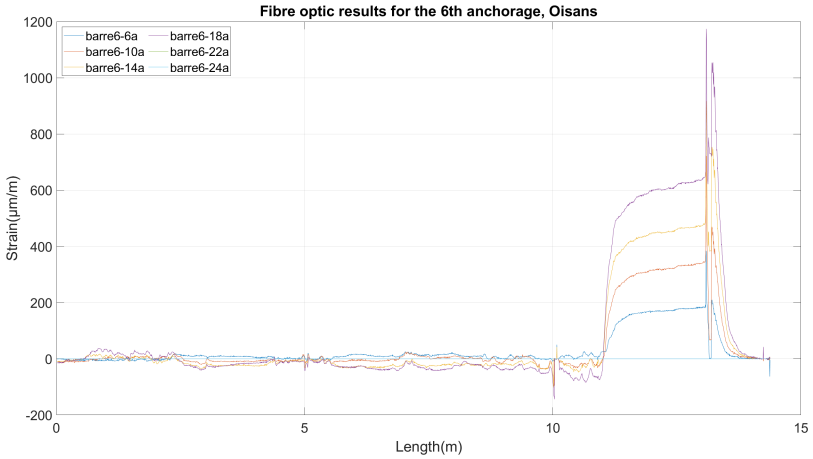

Figure 12.37: Fibre optic results for some virgin loading steps in the 6^{th} anchorage, Oisans

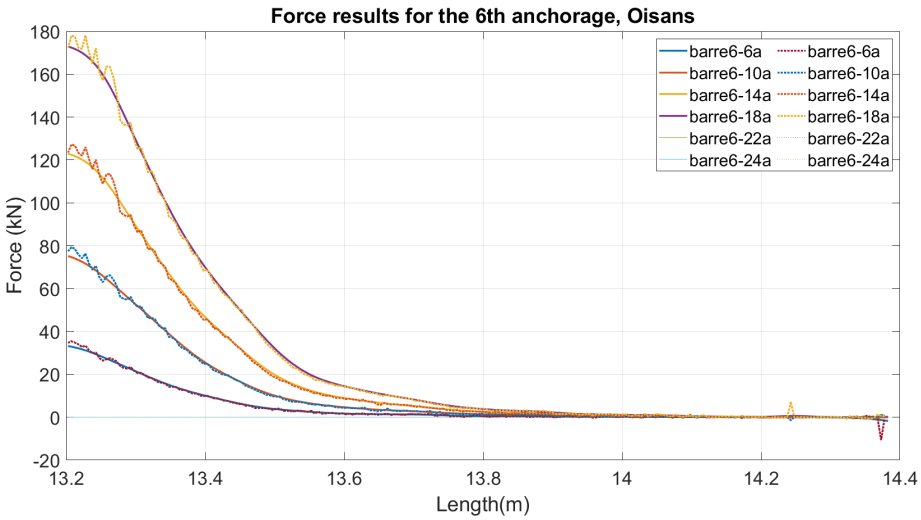

Figure 12.38: Force results for the virgin loading steps in the 6^{th} anchorage, Oisans

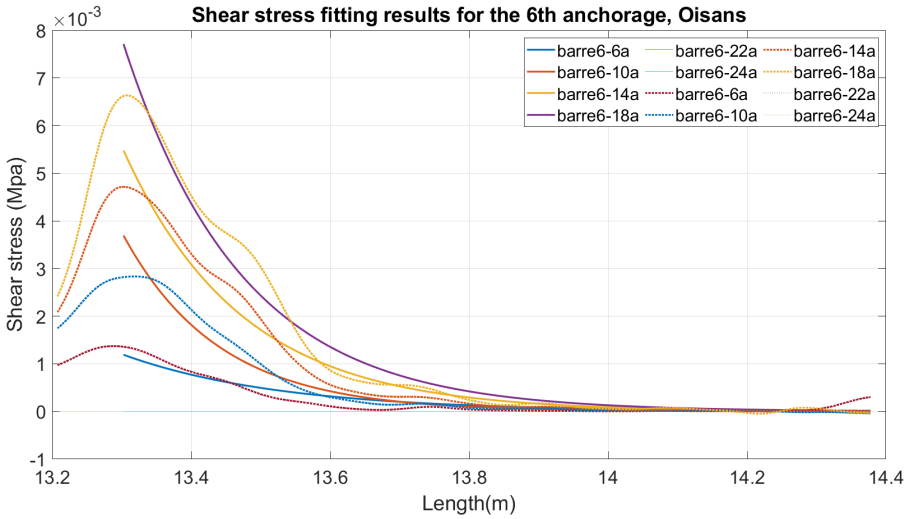

Figure 12.39: Shear stress results for the virgin loading steps in the 6^{th} anchorage, Oisans

13 Annexes Mongalgan

The results for each rock-bolt in Mongalgan will be presented in this chapter.

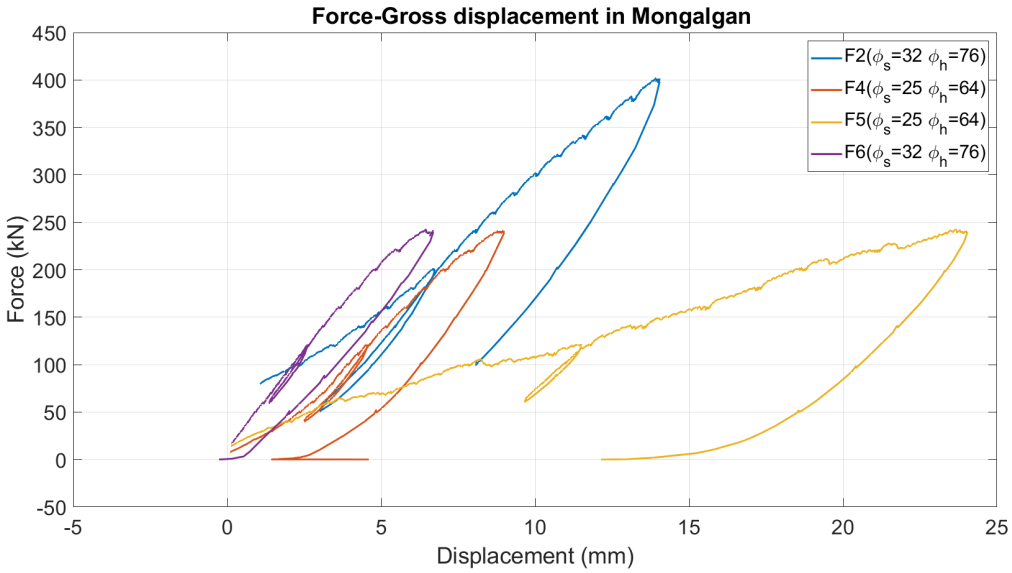

Figure 13.1: Force and gross displacement behaviour for the rock-bolts in Mongalgan

13.0.1 F2 - Mongalgan

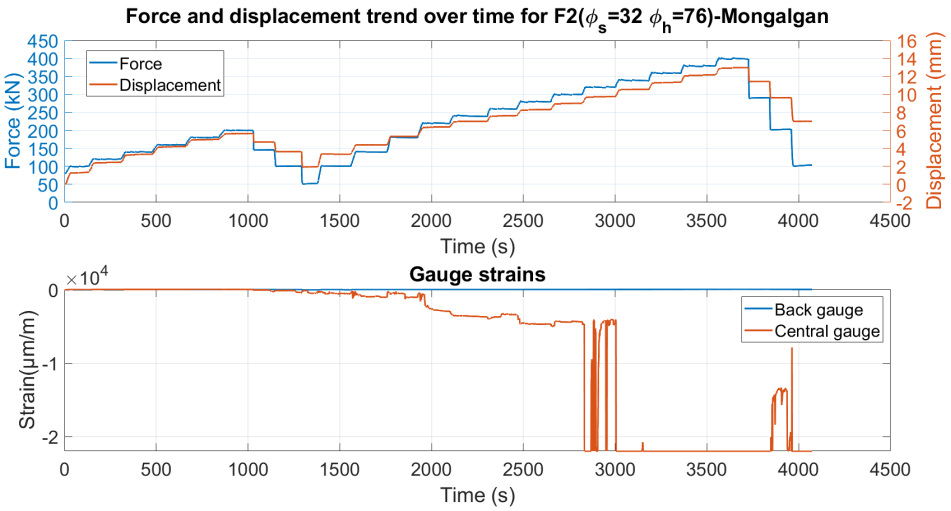

Figure 13.2: Force and displacement trend over time for F2-Mongalgan

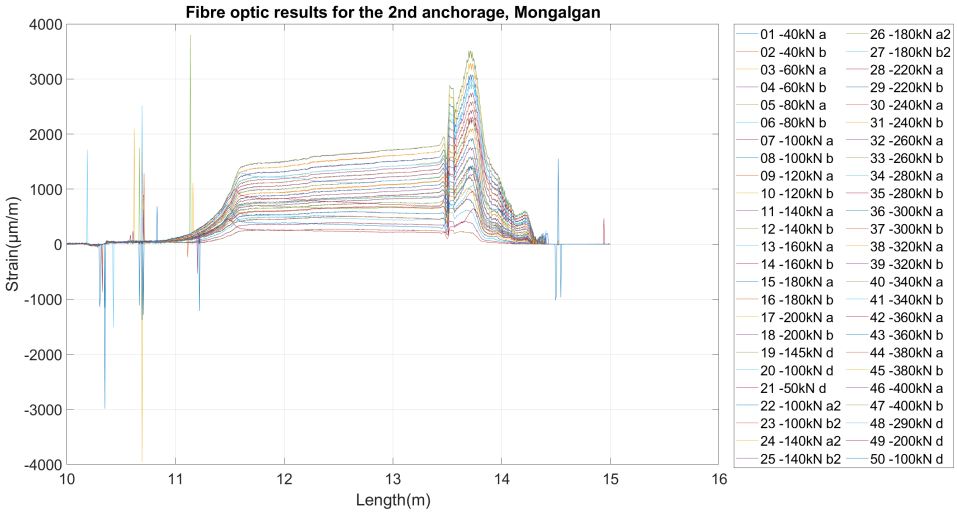

Figure 13.3: Fibre optic results for the 2^{nd} anchorage, Mongalgan

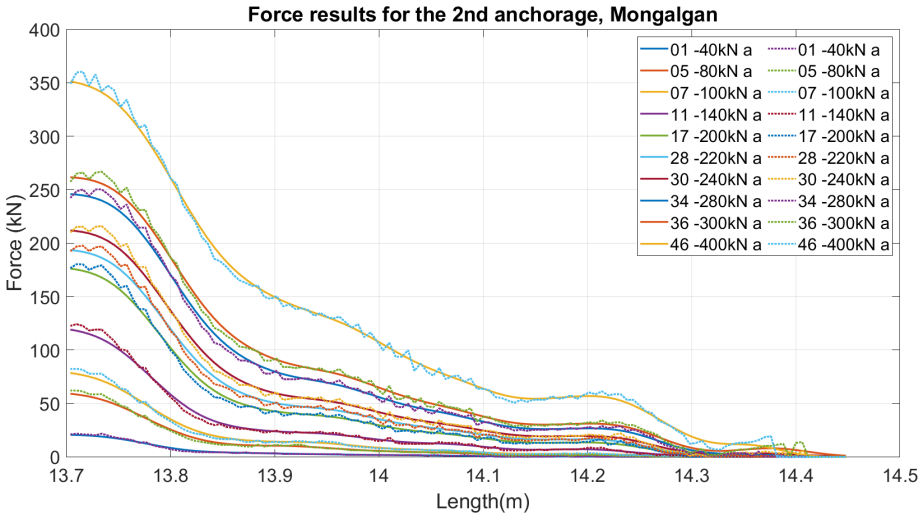

Figure 13.4: Force results for the virgin loading steps in the 2^{nd} anchorage, Mongalgan

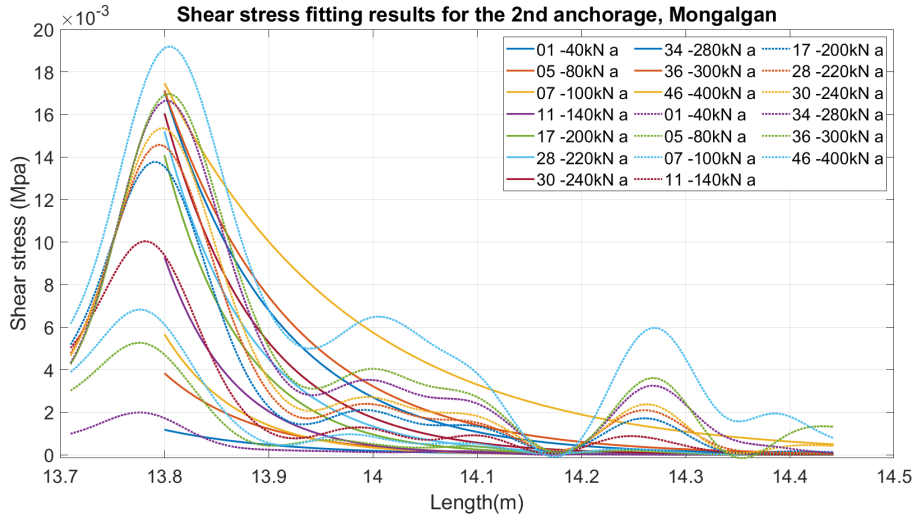

Figure 13.5: Shear stress results for the virgin loading steps in the 2^{nd} anchorage, Mongalgan

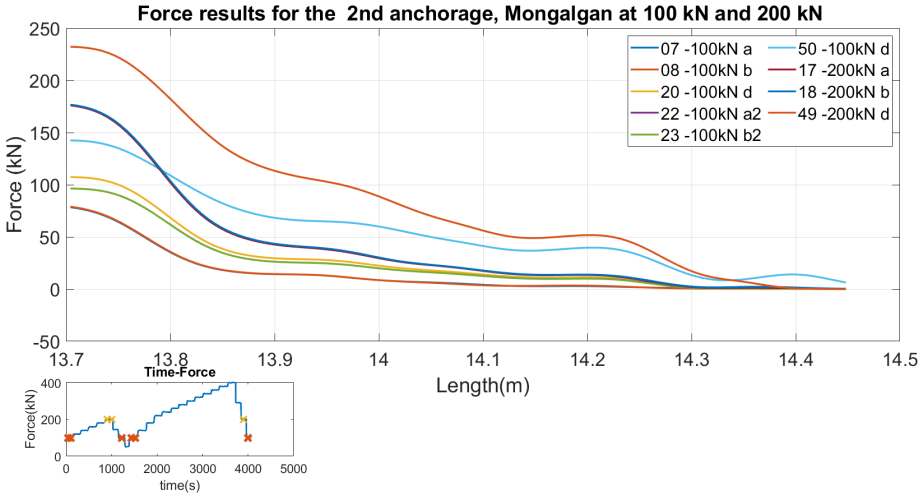

Figure 13.6: Force results for the 2^{nd} anchorage, Mongalgan at 100 kN and 200 kN

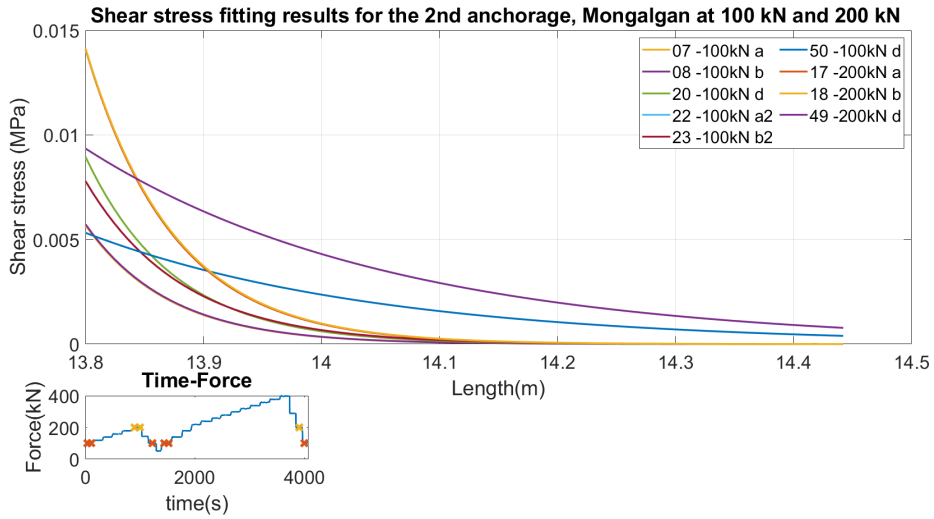

Figure 13.7: Shear stress fitting results for the 2^{nd} anchorage, Mongalgan at 100 kN and 200 kN

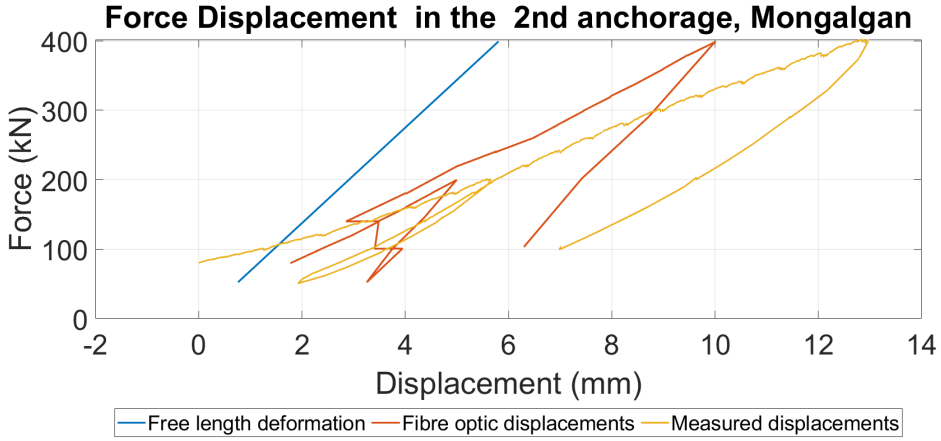

Figure 13.8: Force displacement curves comparison between measured and calculated with the use of the integral along the whole steel bar, 2^{nd} anchorage, Mongalgan

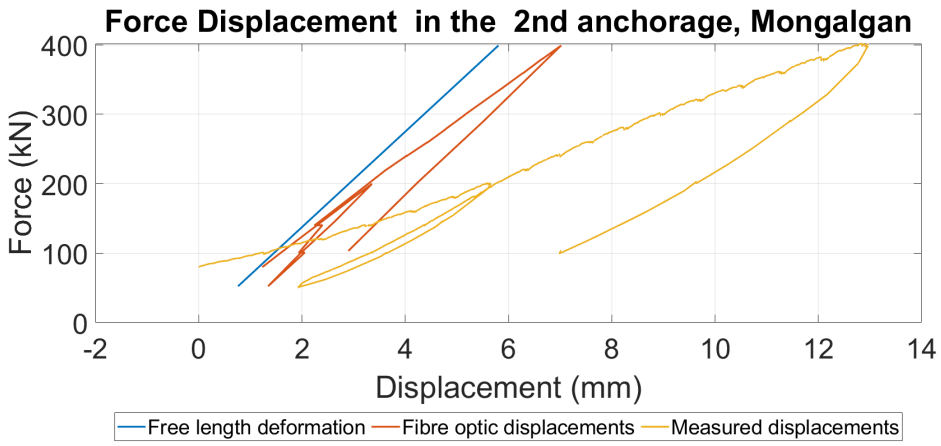

Figure 13.9: Force displacement curves comparison between measured and calculated with the use of the integral along the grouted segment of the steel bar, 2^{nd} anchorage, Mongalgan

13.0.2 F4 - Mongalgan

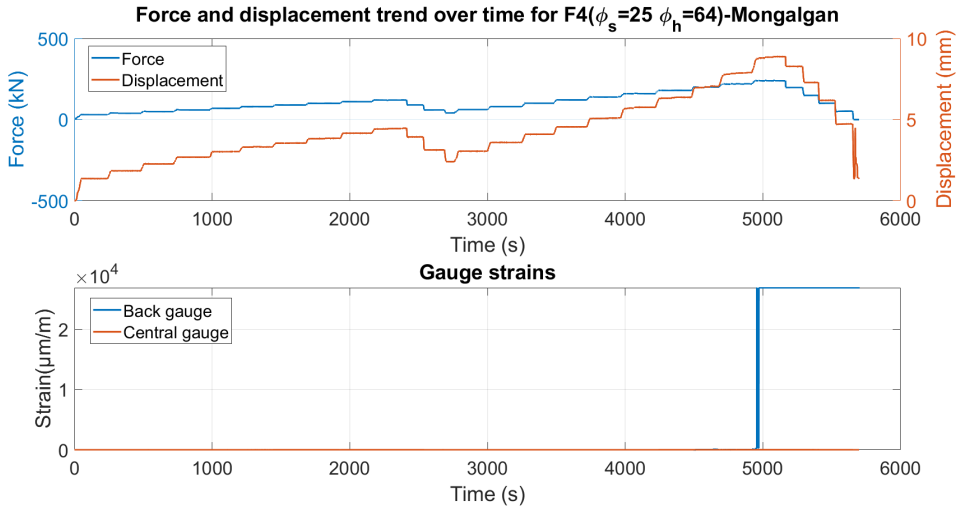

Figure 13.10: Force and displacement trend over time for F4-Mongalgan

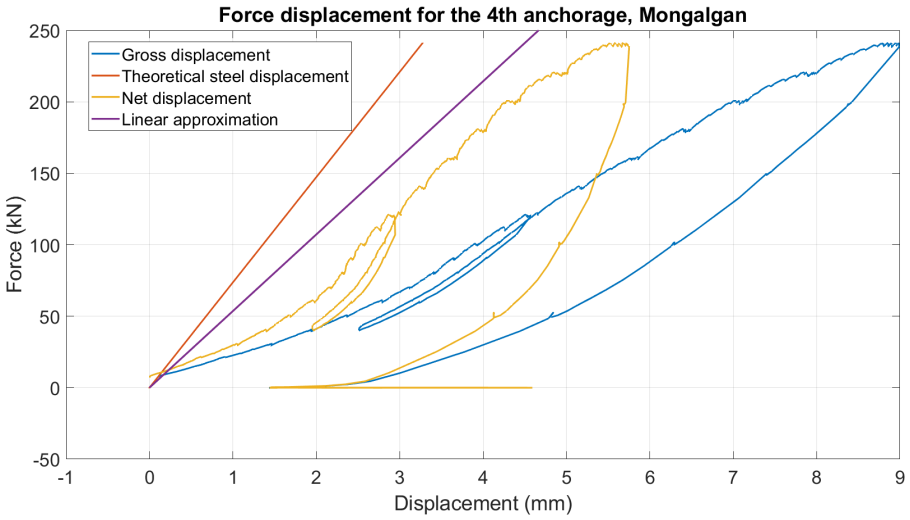

Figure 13.11: Force displacement for the 4^{th} anchorage, Mongalgan

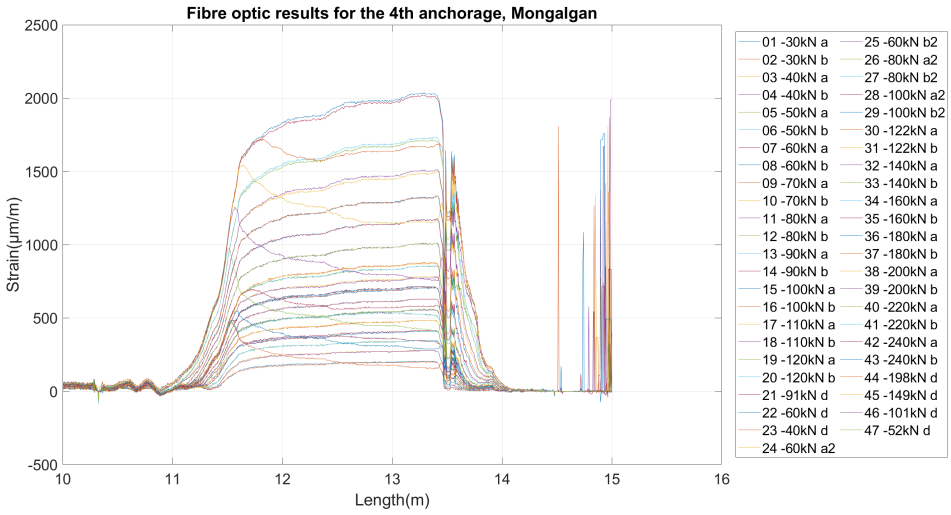

Figure 13.12: Fibre optic results for the 4^{th} anchorage, Mongalgan

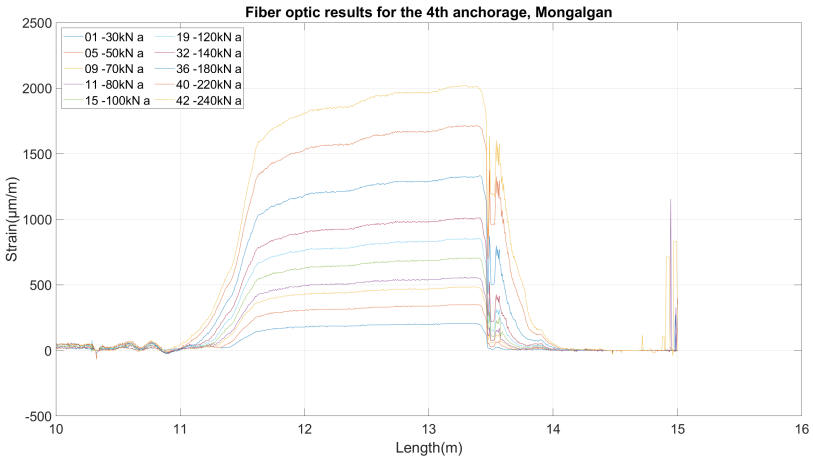

Figure 13.13: Fibre optic results for the virgin loading steps in the 4^{th} anchorage, Mongalgan

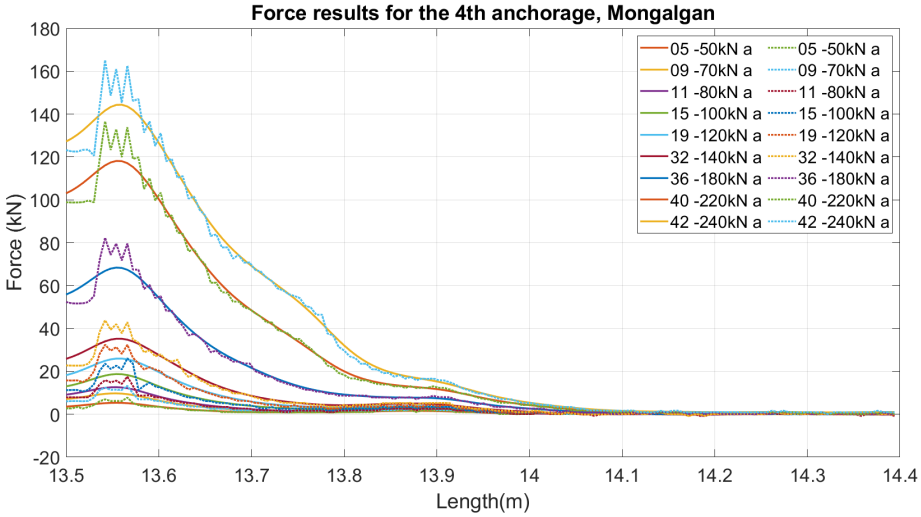

Figure 13.14: Force results for the virgin loading steps in the 4^{th} anchorage, Mongalgan

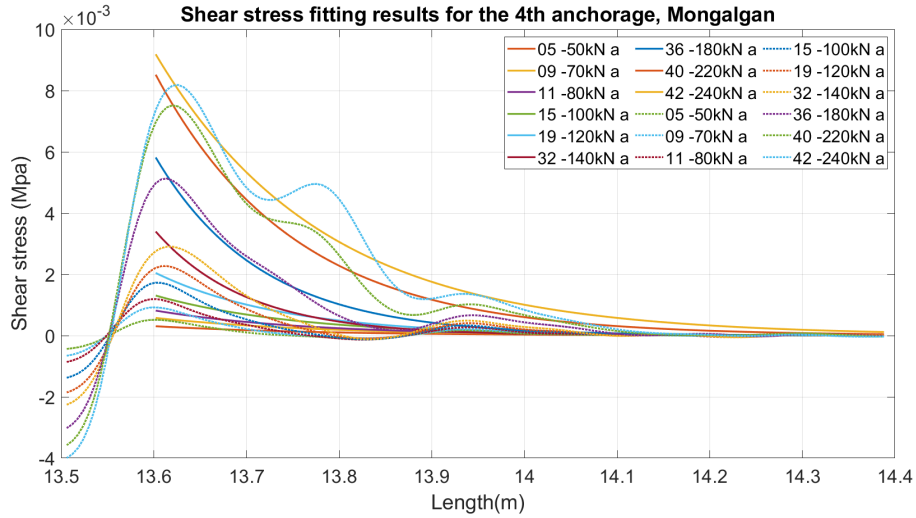

Figure 13.15: Shear stress results for the virgin loading steps in the 4^{th} anchorage, Mongalgan

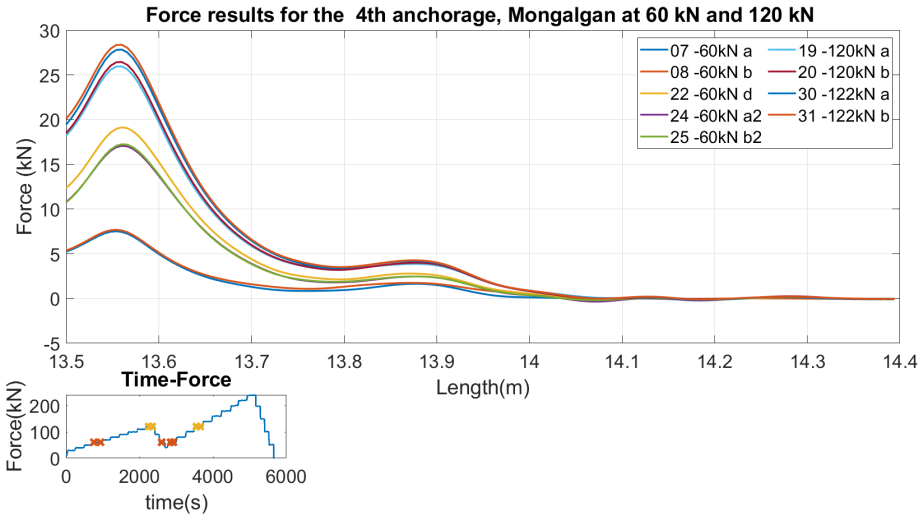

Figure 13.16: Force results for the 4^{th} anchorage, Mongalgan at 60 kN and 120 kN

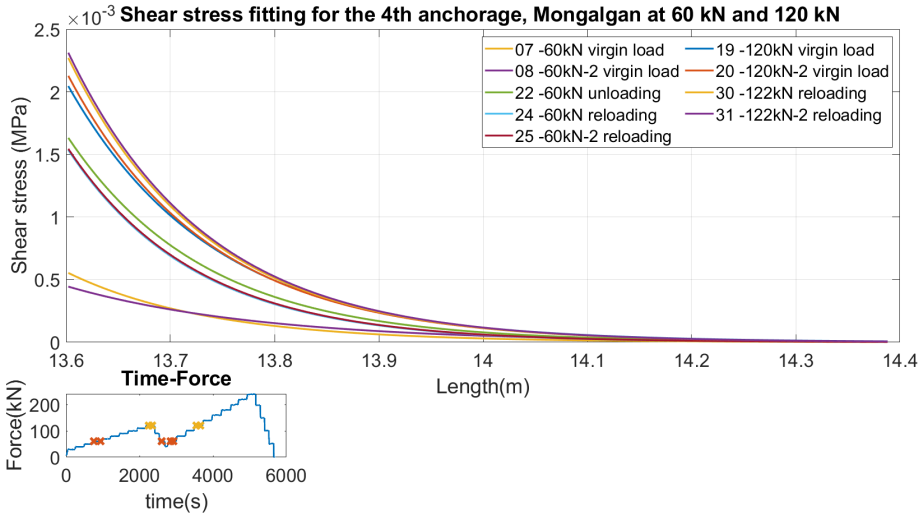

Figure 13.17: Shear stress fitting results for the 4^{th} anchorage, Mongalgan at 60 kN and 120 kN

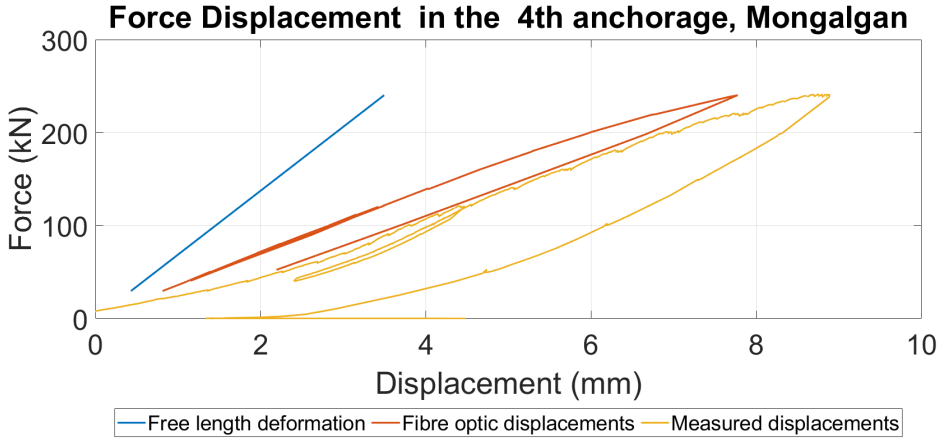

Figure 13.18: Force displacement curves comparison between measured and calculated with the use of the integral along the whole steel bar, 4^{th} anchorage, Mongalgan

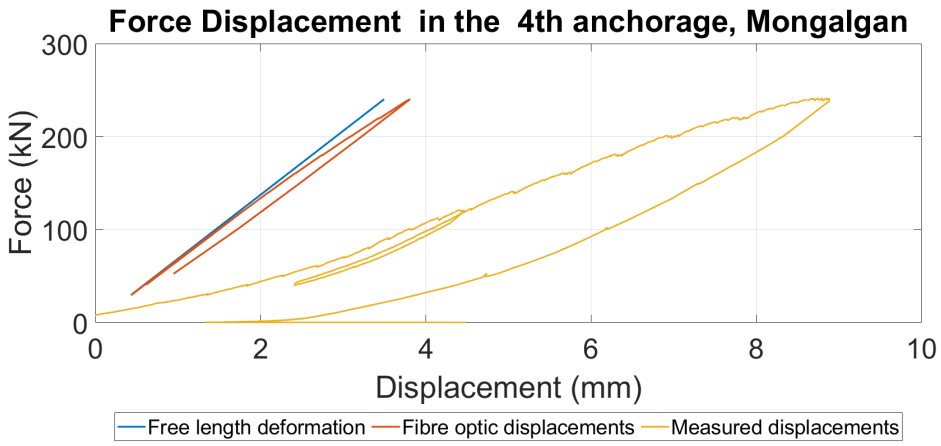

Figure 13.19: Force displacement curves comparison between measured and calculated with the use of the integral along the grouted segment of the steel bar, 4^{th} anchorage, Mongalgan

13.0.3 F5 - Mongalgan

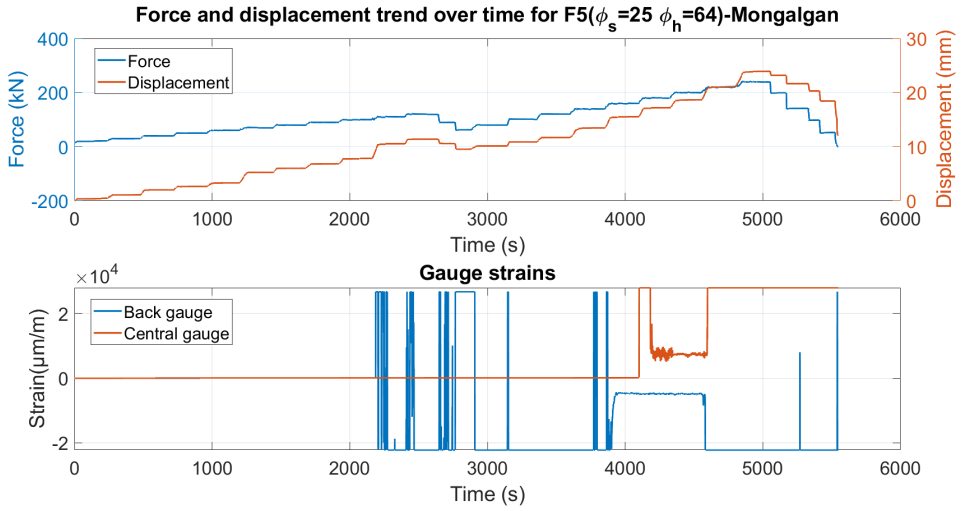

Figure 13.20: Force and displacement trend over time for F5-Mongalgan

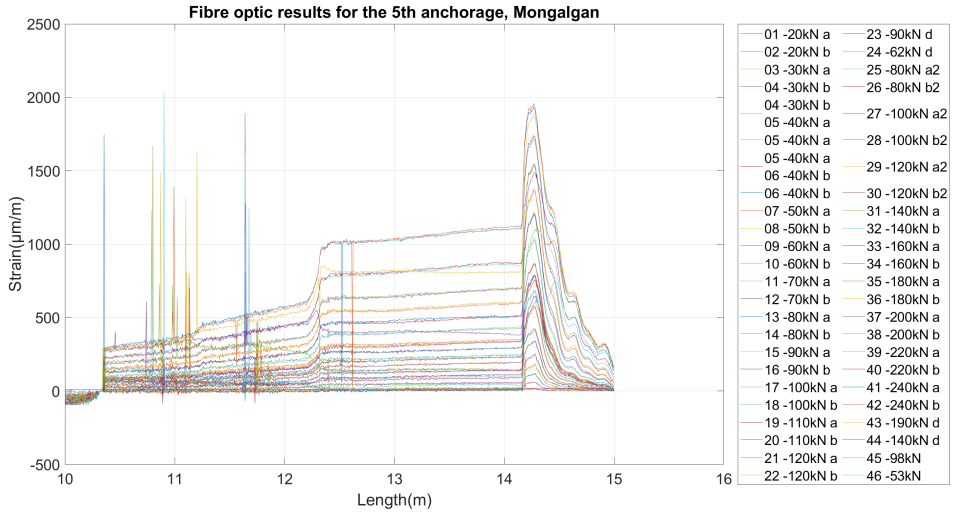

Figure 13.21: Fibre optic results for the 5^{th} anchorage, Mongalgan

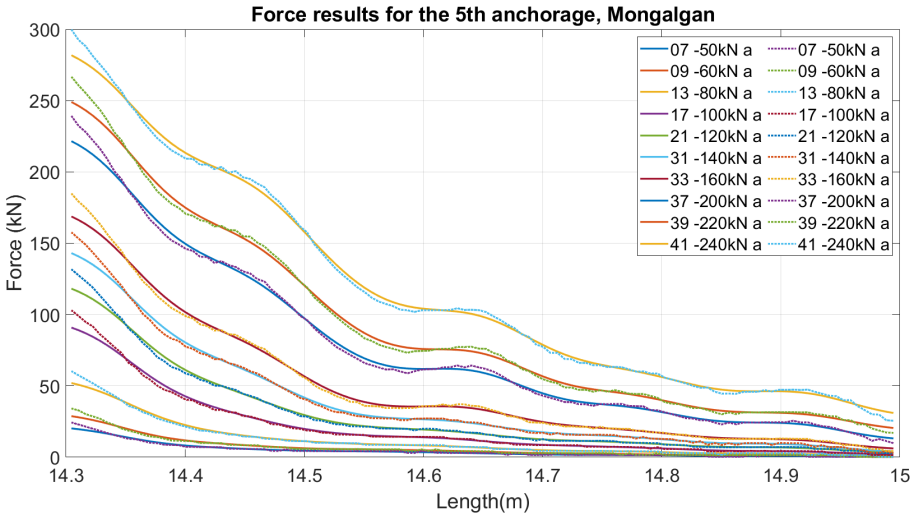

Figure 13.22: Force results for the virgin loading steps in the 5^{th} anchorage, Mongalgan

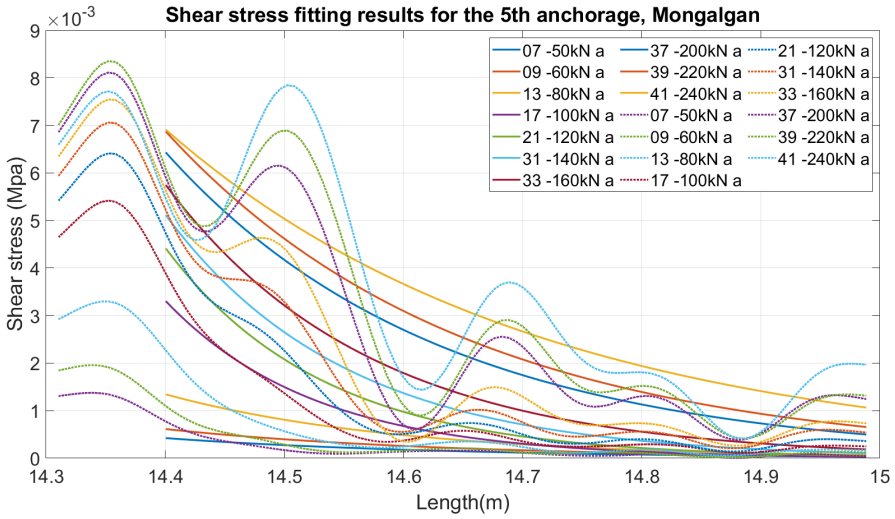

Figure 13.23: Shear stress results for the virgin loading steps in the 5^{th} anchorage, Mongalgan

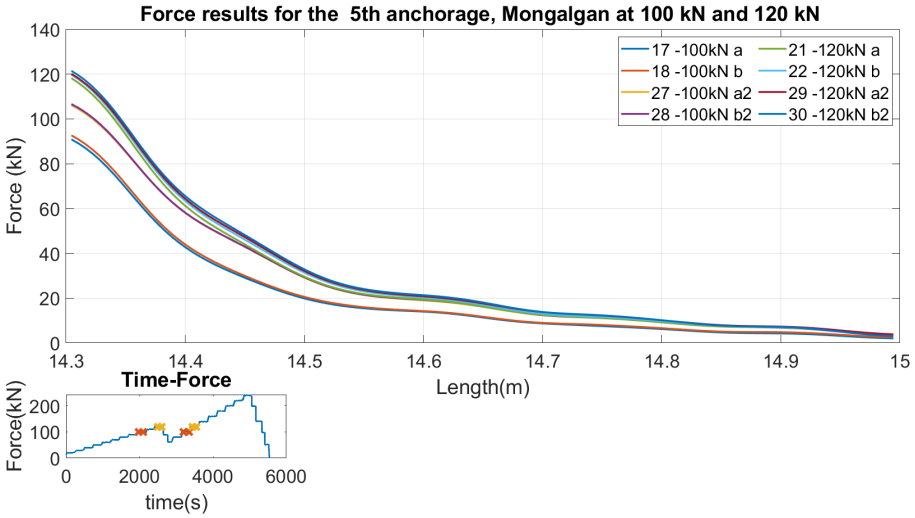

Figure 13.24: Force results for the 5^{th} anchorage, Mongalgan at 100 kN and 120 kN

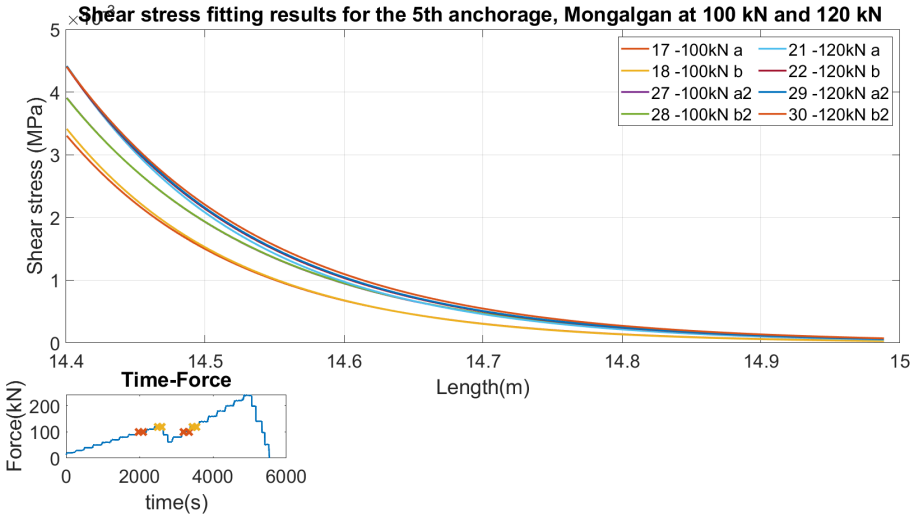

Figure 13.25: Shear stress fitting results for the 5^{th} anchorage, Mongalgan at 100 kN and 120 kN

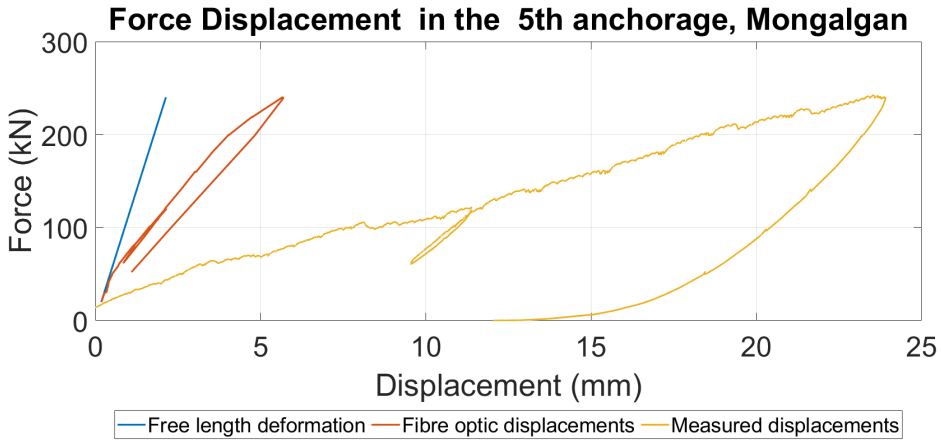

Figure 13.26: Force displacement curves comparison between measured and calculated with the use of the integral along the whole steel bar, 5^{th} anchorage, Mongalgan

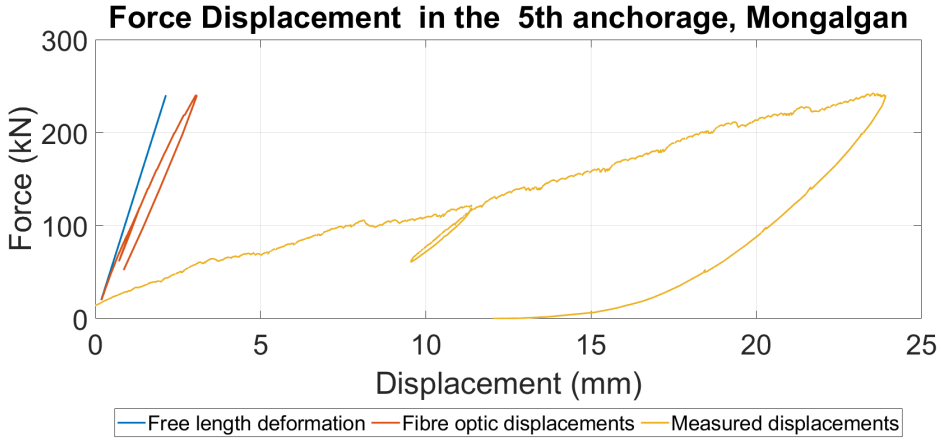

Figure 13.27: Force displacement curves comparison between measured and calculated with the use of the integral along the grouted segment of the steel bar, 5^{th} anchorage, Mongalgan

13.0.4 F6 - Mongalgan

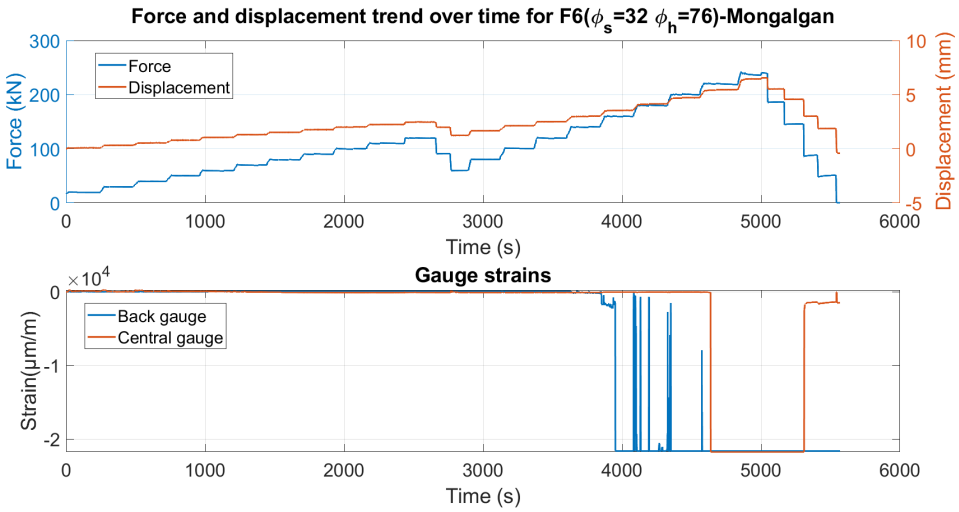

Figure 13.28: Force and displacement trend over time for F6-Mongalgan

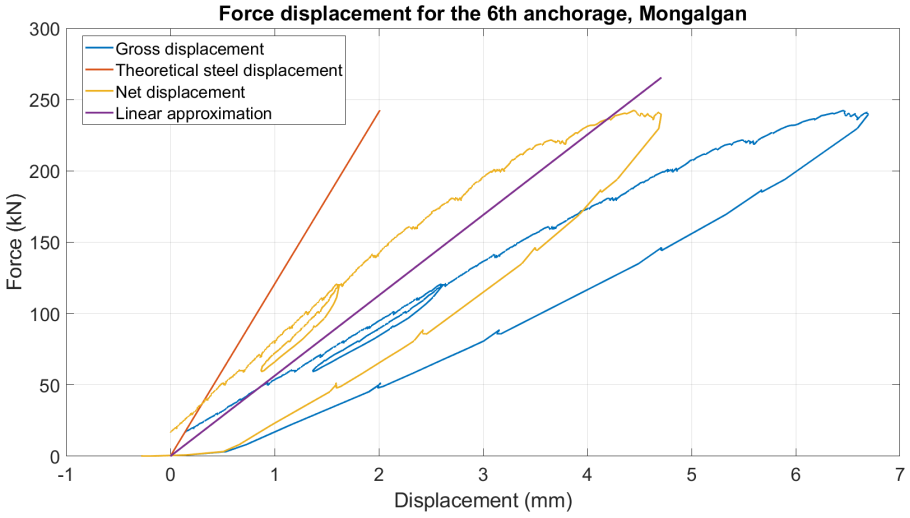

Figure 13.29: Force displacement for the 6^{th} anchorage, Mongalgan

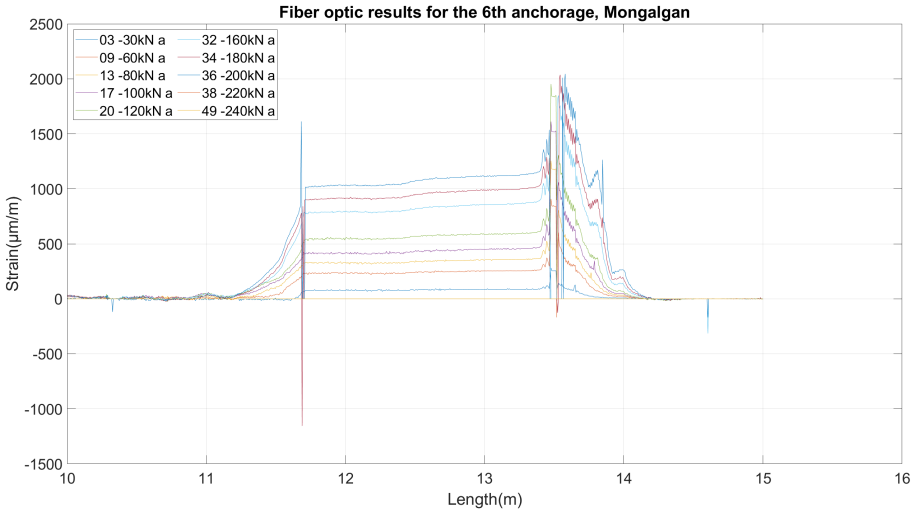

Figure 13.30: Fibre optic results for the virgin loading steps in the 6^{th} anchorage, Mongalgan

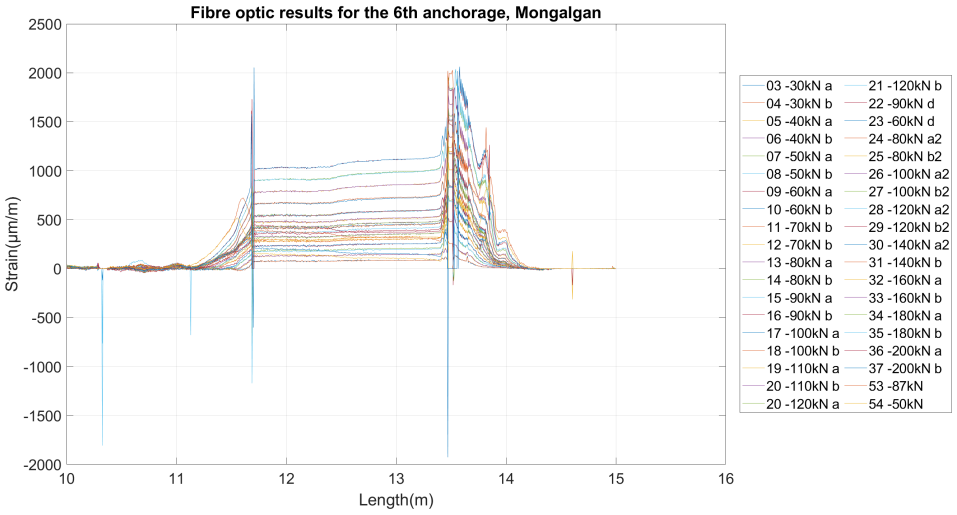

Figure 13.31: Fibre optic results for the 6^{th} anchorage, Mongalgan

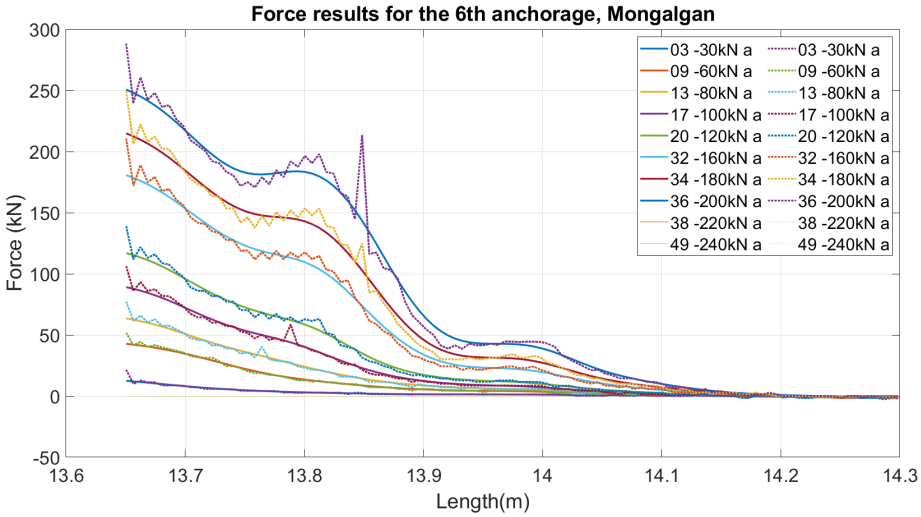

Figure 13.32: Force results for the virgin loading steps in the 6^{th} anchorage, Mongalgan

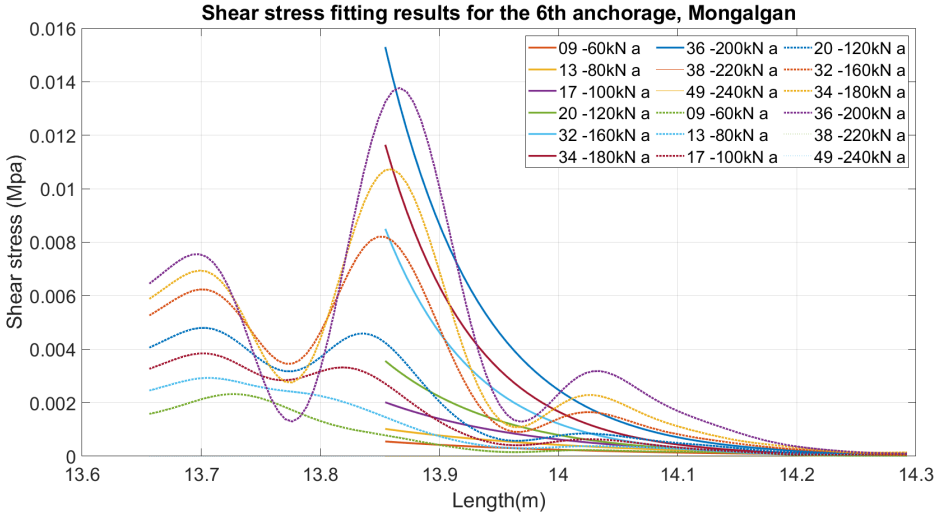

Figure 13.33: Shear stress results for the virgin loading steps in the 6^{th} anchorage, Mongalgan

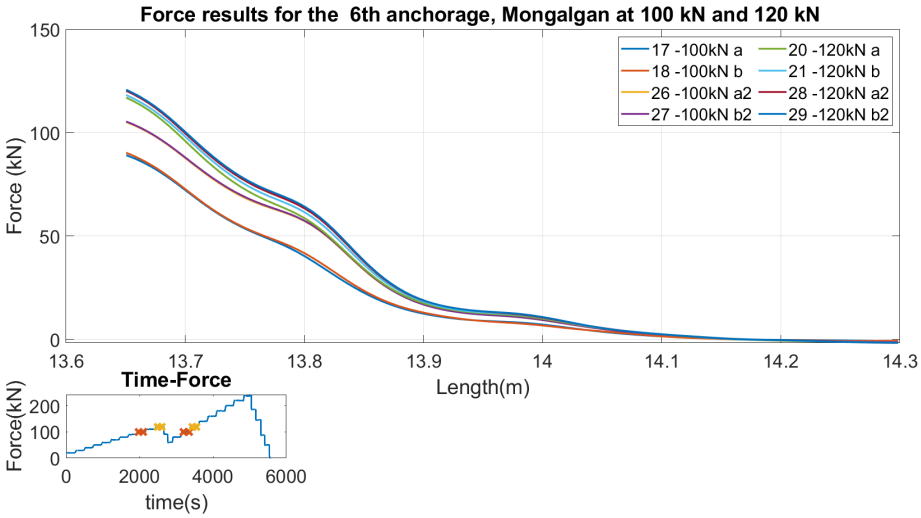

Figure 13.34: Force results for the 6^{th} anchorage, Mongalgan at 100 kN and 120 kN

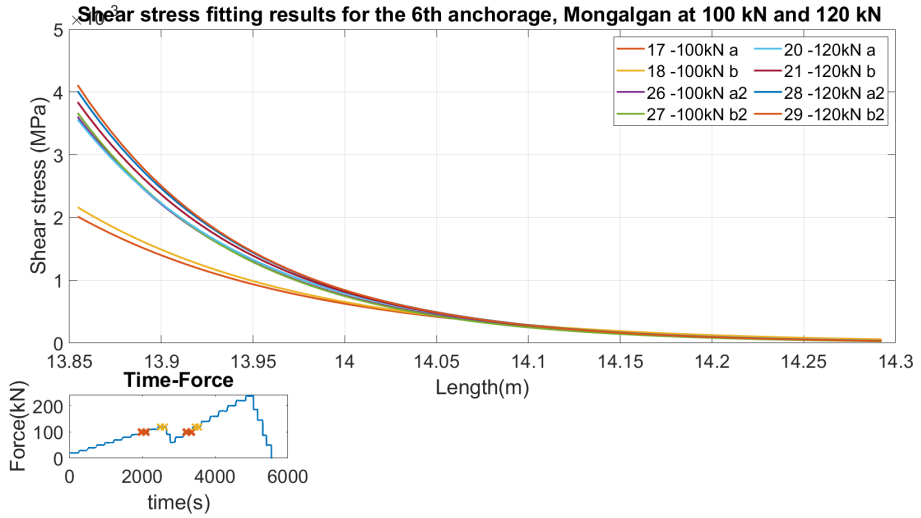

Figure 13.35: Shear stress fitting results for the 6^{th} anchorage, Mongalgan at 100 kN and 120 kN

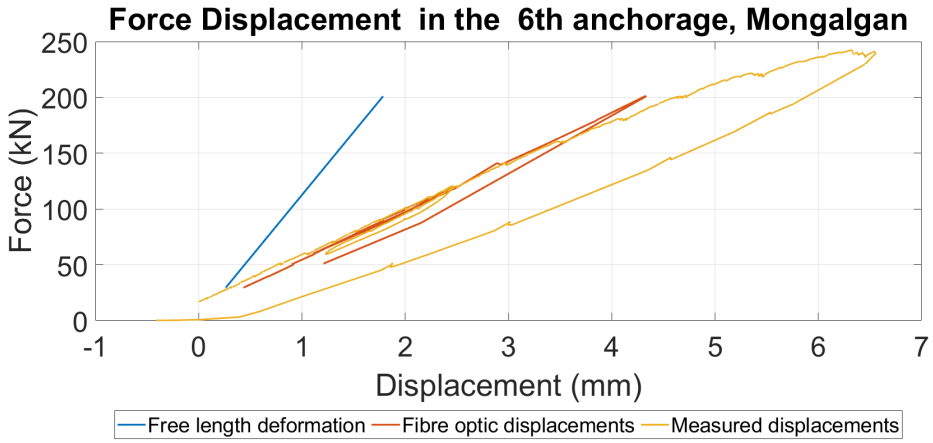

Figure 13.36: Force displacement curves comparison between measured and calculated with the use of the integral along the whole steel bar, 6^{th} anchorage, Mongalgan

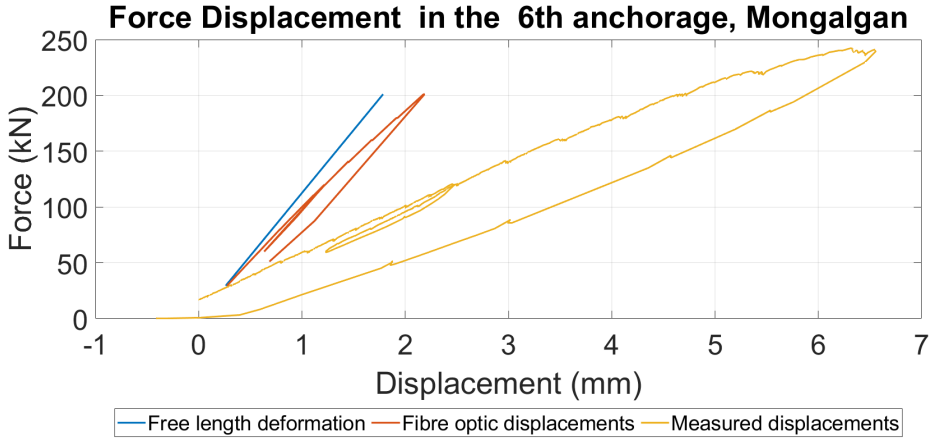

Figure 13.37: Force displacement curves comparison between measured and calculated with the use of the integral along the grouted segment of the steel bar, 6^{th} anchorage, Mongalgan

14 Annexes codes

Here some examples of the matlab codes used for the data analysis will be introduced. For example the one used for the second anchorage in Mongalgan:

```
clc
clear all
Directorypath = uigetdir();
ds=25;%mm
A=(ds^2/4)*pi;%mm^2
E=210; %GPa
% significative data start at 13.7 m
% significative data start at 14.45 m
%interp=13.8
freeL=1.4; %m
ancor='2nd anchorage, Mongalgan';
cwd=pwd;
cd('Excel')
%% Setup the Import Options
%FIBER OPTIC RESULTS IMPORTING
opts = spreadsheetImportOptions("NumVariables", 59);

% Specify sheet and range
opts.Sheet = "Barre 2";
opts.DataRange = "A4:BG837";

% Specify column names and types
opts.VariableNames = ["VarName1", "avant0", "avant1", "avant2",
                      "ref", "reference0", "reference1", "kNA",
                       "kNB", "kNA_1", "kNB_1", "kNA_2", "kNB_2",
                        "kNA_3", "kNB_3", "kNA_4","kNB_4", "kNA_5"
                        , "kNB_5", "kNA_6", "kNB_6", "kNA_7",
                        "kNB_7", "kNA_8", "kNB_8", "kND", "kND_1"
                        , "kND_2", "kNA2", "kNB2", "kNA2_1",
                        "kNB2_1", "kNA2_2", "kNB2_2","kNA_9",
                        "kNB_9", "kNA_10", "kNB_10", "kNA_11",
                        "kNB_11", "kNA_12", "kNB_12", "kNA_13",
                        "kNB_13","kNA_14", "kNB_14", "kNA_15",
                        "kNB_15", "kNA_16", "kNB_16", "kNA_17",
                        "kNB_17", "kNA_18", "kNB_18","kND_3",
                        "kND_4", "kND_5", "fin", "VarName59"];
opts.VariableTypes = ["double", "double", "double", "double",
                      "double", "double","double", "double",
                       "double", "double", "double", "double",
                       "double", "double", "double", "double"
                       , "double", "double","double", "double"
                       , "double", "double", "double", "double"
```

```
                          , "double", "double", "double", "double"
                          , "double", "double" , "double", "double"
                          , "double", "double", "double", "double",
                           "double", "double", "double", "double",
                            "double", "double","double", "double",
                             "double", "double","double","double",
                             "double", "double", "double", "double",
                              "double", "double","double", "double",
                                "double", "double", "double"];

% Import the data
MatFO = readtable("F2_fo.xlsx", opts, "UseExcel", false);
MatFO = table2array(MatFO);

%% Setup the Import Options
% IMPORTING THE ARRAY FOR THE LEGEND
opts = spreadsheetImportOptions("NumVariables", 59);

% Specify sheet and range
opts.Sheet = "Barre 2";
opts.DataRange = "A3:BG3";

% Specify column names and types
opts.VariableNames = ["VarName1", "avant0", "avant1", "avant2",
                      "ref", "reference0", "reference1", "kNA",
                       "kNB", "kNA_1", "kNB_1", "kNA_2", "kNB_2",
                        "kNA_3", "kNB_3", "kNA_4", "kNB_4", "kNA_5",
                         "kNB_5", "kNA_6", "kNB_6", "kNA_7", "kNB_7",
                          "kNA_8", "kNB_8", "kND", "kND_1", "kND_2",
                           "kNA2", "kNB2", "kNA2_1", "kNB2_1", "kNA2_2"
                           , "kNB2_2", "kNA_9", "kNB_9", "kNA_10",
                           "kNB_10", "kNA_11", "kNB_11", "kNA_12",
                           "kNB_12", "kNA_13", "kNB_13", "kNA_14",
                           "kNB_14", "kNA_15", "kNB_15", "kNA_16",
                           "kNB_16", "kNA_17", "kNB_17", "kNA_18",
                           "kNB_18", "kND_3", "kND_4", "kND_5",
                           "fin", "VarName59"];
opts.VariableTypes = ["string", "string", "string", "string",
                      "string", "string", "string", "string",
                      "string", "string", "string", "string",
                      "string", "string", "string", "string",
                      "string", "string", "string", "string",
                      "string", "string", "string", "string",
                      "string", "string", "string", "string",
                      "string", "string", "string", "string",
                      "string", "string", "string", "string",
                      "string", "string", "string", "string",
```

```
                        "string", "string", "string", "string",
                        "string", "string", "string", "string",
                        "string", "string", "string", "string",
                        "string", "string", "string"];

% Specify variable properties
opts = setvaropts(opts, ["VarName1", "avant0", "avant1", "avant2",
                         "ref", "reference0", "reference1", "kNA",
                         "kNB", "kNA_1", "kNB_1", "kNA_2", "kNB_2",
                         "kNA_3", "kNB_3", "kNA_4", "kNB_4", "kNA_5",
                         "kNB_5", "kNA_6", "kNB_6", "kNA_7", "kNB_7",
                         "kNA_8", "kNB_8", "kND", "kND_1", "kND_2",
                         "kNA2", "kNB2", "kNA2_1", "kNB2_1", "kNA2_2",
                         "kNB2_2", "kNA_9", "kNB_9", "kNA_10", "kNB_10",
                         "kNA_11", "kNB_11", "kNA_12", "kNB_12", "kNA_13",
                         "kNB_13", "kNA_14", "kNB_14", "kNA_15", "kNB_15",
                         "kNA_16", "kNB_16", "kNA_17", "kNB_17", "kNA_18",
                         "kNB_18", "kND_3", "kND_4", "kND_5", "fin",
                         "VarName59"], "WhitespaceRule", "preserve");
opts = setvaropts(opts, ["VarName1", "avant0", "avant1", "avant2", "ref",
                        "reference0", "reference1", "kNA", "kNB", "kNA_1",
                        "kNB_1", "kNA_2", "kNB_2", "kNA_3", "kNB_3",
                        "kNA_4", "kNB_4", "kNA_5", "kNB_5", "kNA_6",
                        "kNB_6", "kNA_7", "kNB_7", "kNA_8", "kNB_8",
                        "kND", "kND_1", "kND_2", "kNA2", "kNB2",
                        "kNA2_1", "kNB2_1", "kNA2_2", "kNB2_2",
                        "kNA_9", "kNB_9", "kNA_10", "kNB_10",
                        "kNA_11", "kNB_11", "kNA_12", "kNB_12",
                        "kNA_13", "kNB_13", "kNA_14", "kNB_14",
                        "kNA_15", "kNB_15", "kNA_16", "kNB_16",
                        "kNA_17", "kNB_17", "kNA_18", "kNB_18",
                        "kND_3", "kND_4", "kND_5", "fin",
                        "VarName59"], "EmptyFieldRule", "auto");

% Import the data
lgarray = readmatrix("F2_fo.xlsx", opts, "UseExcel", false);


%% Set up the Import Options and import the data
opts = spreadsheetImportOptions("NumVariables", 1);

% Specify sheet and range
opts.Sheet = "Feuil1";
opts.DataRange = "E5:E4078";

% Specify column names and types
opts.VariableNames = "effortkN";
opts.VariableTypes = "double";
```

```
% Import the data
eff = readtable("F2 - bis.xlsx", opts, "UseExcel", false);
eff = table2array(eff);


%% Setup the Import Options
opts = spreadsheetImportOptions("NumVariables", 1);

% Specify sheet and range
opts.Sheet = "Feuil1";
opts.DataRange = "J5:J4078";

% Specify column names and types
opts.VariableNames = "elongenf";
opts.VariableTypes = "double";

% Import the data
disp = readtable("F2 - bis.xlsx", opts, "UseExcel", false);
disp = table2array(disp);

%% Use of the class
cd(cwd)

dati=DATA(A,E,MatFO,freeL,lgarray,eff,disp,ancor,ds,Directorypath);
[F,T,a_and_b]=dati.stresses();
%[real_disp]=dati.real_displacement();


%% Point extraction

position(1)=11.6;
position(2)=12.3;
position(3)=13;
entries=zeros(3,1);
position_array=MatFO(:,1);
for i=1:3
    distance=position_array-position(i);
    abs_distance=abs(distance);
    closest=min(abs_distance);
    closest_entry=find(abs_distance==closest);
    entries(i)=closest_entry;
    position(i)=position_array(closest_entry);
end

Theoretical_force=[40,40,60,60,80,80,100 ,100,
                   120,120,140,140,160,
                   160,180,180,200,200,
```

```
                    145,100,50,100,100,
                    140,140,180,180,220,
                    220,240,240,260,260 ,
                    280 ,280 ,300 ,300 ,320
                    ,320,340,340 ,360 ,360 ,
                    380 ,380 ,400 ,400,290,
                    200,100];

strains_position_1=MatFO(entries(1),:);
strains_position_2=MatFO(entries(2),:);
strains_position_3=MatFO(entries(3),:);
n=length(strains_position_1);
calculated_force_1=(strains_position_1(2:n)/1000000)*A*E;
calculated_force_2=(strains_position_2(2:n)/1000000)*A*E;
calculated_force_3=(strains_position_3(2:n)/1000000)*A*E;
larray=lgarray(2:n);
nn=length(larray);
larray(nn+1)=('Linear interpolation');
coefficient_1=polyfit(Theoretical_force,calculated_force_1,1);
inter_forces_1=polyval(coefficient_1,Theoretical_force);
R_square_1=1-((sum((calculated_force_1-inter_forces_1).^2))/(sum(
           (calculated_force_1-mean(calculated_force_1)).^2)));
coefficient_2=polyfit(Theoretical_force,calculated_force_2,1);
inter_forces_2=polyval(coefficient_2,Theoretical_force);
R_square_2=1-((sum((calculated_force_2-inter_forces_2).^2))/(sum(
           (calculated_force_2-mean(calculated_force_2)).^2)));
coefficient_3=polyfit(Theoretical_force,calculated_force_3,1);
inter_forces_3=polyval(coefficient_3,Theoretical_force);
R_square_3=1-((sum((calculated_force_3-inter_forces_3).^2))/(sum(
           (calculated_force_3-mean(calculated_force_3)).^2)));

f7=figure(7);
f7.WindowState = 'maximized';

plot(Theoretical_force(1),calculated_force_1(1),'o')
hold on
for i=2:(n-1)
    plot(Theoretical_force(i),calculated_force_1(i),'o')
end
title(['Comparison between calculated effort and theorical effort
      in the first position F2 - Mongalgan'])
xlabel('Theoretical effort (kN)')
ylabel('Calculated effort (kN)')
plot(Theoretical_force,inter_forces_1)
legend(larray,'Location','southeast','NumColumns',2)
grid on
set(gca,'Fontsize',20)
whereToStore=fullfile(Directorypath,['Comparison between calculated
```

```
             effort and theorical effort in the first position F2 -
             Mongalgan.fig']);
saveas(gcf, whereToStore);
hold off

f8=figure(8);
f8.WindowState = 'maximized';

plot(Theoretical_force(1),calculated_force_2(1),'o')
hold on
for i=2:(n-1)
    plot(Theoretical_force(i),calculated_force_2(i),'o')
end
title(['Comparison between calculated effort and theorical effort
     in the second position F2 - Mongalgan'])
xlabel('Theoretical effort (kN)')
ylabel('Calculated effort (kN)')
plot(Theoretical_force,inter_forces_2)
legend(larray,'Location','southeast','NumColumns',2)
grid on
set(gca,'Fontsize',20)
whereToStore=fullfile(Directorypath,['Comparison between calculated
             effort and theorical effort in the second position F2 -
             Mongalgan.fig']);
saveas(gcf, whereToStore);
hold off


f9=figure(9);
f9.WindowState = 'maximized';

plot(Theoretical_force(1),calculated_force_3(1),'o')
hold on
for i=2:(n-1)
    plot(Theoretical_force(i),calculated_force_3(i),'o')
end
title(['Comparison between calculated effort and theorical effort
      in the third position F2 - Mongalgan'])
xlabel('Theoretical effort (kN)')
ylabel('Calculated effort (kN)')
plot(Theoretical_force,inter_forces_3)
legend(larray,'Location','southeast','NumColumns',2)
grid on
set(gca,'Fontsize',20)
whereToStore=fullfile(Directorypath,['Comparison between calculated
             effort and theorical effort in the third position F2 -
             Mongalgan.fig']);
saveas(gcf, whereToStore);
```

```
hold off

Positions=["First position";"Second position"; "Third position"];
R2=[R_square_1;R_square_2;R_square_3];
coefficient_a=[coefficient_1(1);coefficient_2(1);coefficient_3(1)];
coefficient_b=[coefficient_1(2);coefficient_2(2);coefficient_3(2)];
tab=table(Positions,R2,coefficient_a,coefficient_b);
data=[R2,coefficient_a,coefficient_b];
f10=figure(10);
f10.WindowState = 'maximized';

cnames = {'R2','Coefficient a','Coefficient b'};
rnames = {'First position','Second position','Third position'};
t = uitable(f10,'Data',data,...
            'ColumnName',cnames,...
            'RowName',rnames,...
            'ColumnWidth',{80});
t.FontSize=15;
subplot(4,3,11),plot(3)
pos = get(subplot(4,3,11),'position');
delete(subplot(4,3,11))
set(t,'units','normalized')
set(t,'position',pos)
subplot(4,1,1),plot(Theoretical_force(1),calculated_force_1(1),'o')
hold on
for i=2:(n-1)
    plot(Theoretical_force(i),calculated_force_1(i),'o')
end
title(['Comparison between calculated effort and theorical effort
     in the first position F2 - Mongalgan'])
xlabel('Theoretical effort (kN)')
ylabel('Calculated effort (kN)')
plot(Theoretical_force,inter_forces_1)
grid on
set(gca,'Fontsize',20)
%legend(larray,'Location','northwest')
subplot(4,1,2),plot(Theoretical_force(1),calculated_force_2(1),'o')
hold on
for i=2:(n-1)
    plot(Theoretical_force(i),calculated_force_2(i),'o')
end
title(['Comparison between calculated effort and theorical effort in
     the second position F2 - Mongalgan'])
xlabel('Theoretical effort (kN)')
ylabel('Calculated effort (kN)')
plot(Theoretical_force,inter_forces_2)
grid on
set(gca,'Fontsize',20)
```

```
subplot(4,1,3),plot(Theoretical_force(1),calculated_force_3(1),'o')
hold on
for i=2:(n-1)
    plot(Theoretical_force(i),calculated_force_3(i),'o')
end
title(['Comparison between calculated effort and theorical effort
     in the third position F2 - Mongalgan'])
xlabel('Theoretical effort (kN)')
ylabel('Calculated effort (kN)')
plot(Theoretical_force,inter_forces_3)
grid on
set(gca,'Fontsize',20)
whereToStore=fullfile(Directorypath,['Comparison between calculated
             effort and theorical effort in F2 - Mongalgan.fig']);
saveas(gcf, whereToStore);
hold off

%% Interpolation of a and d staps with different lines

%d_entries=[19,20,21,48,49,50,51];
d_entries=[19,20,21,48,49];
n_d=length(d_entries);
Theoretical_force_d=Theoretical_force(d_entries);
calculated_force_1_d=calculated_force_1(d_entries);
calculated_force_2_d=calculated_force_2(d_entries);
calculated_force_3_d=calculated_force_3(d_entries);

larray_d=lgarray(d_entries);
larray_d(n_d+1)=('Linear interpolation of d steps');
coefficient_1_d=polyfit(Theoretical_force_d,calculated_force_1_d,1);
inter_forces_1_d=polyval(coefficient_1_d,Theoretical_force_d);
R_square_1_d=1-((sum((calculated_force_1_d-inter_forces_1_d).^2))/(sum(
            (calculated_force_1_d-mean(calculated_force_1_d)).^2)));
coefficient_2_d=polyfit(Theoretical_force_d,calculated_force_2_d,1);
inter_forces_2_d=polyval(coefficient_2_d,Theoretical_force_d);
R_square_2_d=1-((sum((calculated_force_2_d-inter_forces_2_d).^2))/(sum(
            (calculated_force_2_d-mean(calculated_force_2_d)).^2)));
coefficient_3_d=polyfit(Theoretical_force_d,calculated_force_3_d,1);
inter_forces_3_d=polyval(coefficient_3_d,Theoretical_force_d);
R_square_3_d=1-((sum((calculated_force_3_d-inter_forces_3_d).^2))/(sum(
            (calculated_force_3_d-mean(calculated_force_3_d)).^2)));

Theoretical_force_a=Theoretical_force;
calculated_force_1_a=calculated_force_1;
calculated_force_2_a=calculated_force_2;
calculated_force_3_a=calculated_force_3;
larray(nn+1)=('Linear interpolation (a-b)');
larray(nn+2)=('Linear interpolation (d)');
```

```
Theoretical_force_a(d_entries)=[];
calculated_force_1_a(d_entries)=[];
calculated_force_2_a(d_entries)=[];
calculated_force_3_a(d_entries)=[];


coefficient_1_a=polyfit(Theoretical_force_a,calculated_force_1_a,1);
inter_forces_1_a=polyval(coefficient_1_a,Theoretical_force_a);
R_square_1_a=1-((sum((calculated_force_1_a-inter_forces_1_a).^2))/(sum(
            (calculated_force_1_a-mean(calculated_force_1_a)).^2)));
coefficient_2_a=polyfit(Theoretical_force_a,calculated_force_2_a,1);
inter_forces_2_a=polyval(coefficient_2_a,Theoretical_force_a);
R_square_2_a=1-((sum((calculated_force_2_a-inter_forces_2_a).^2))/(sum(
            (calculated_force_2_a-mean(calculated_force_2_a)).^2)));
coefficient_3_a=polyfit(Theoretical_force_a,calculated_force_3_a,1);
inter_forces_3_a=polyval(coefficient_3_a,Theoretical_force_a);
R_square_3_a=1-((sum((calculated_force_3_a-inter_forces_3_a).^2))/(sum(
             (calculated_force_3_a-mean(calculated_force_3_a)).^2)));



R2_1=[R_square_1_a;R_square_1_d];
coefficient_a_1=[coefficient_1_a(1);coefficient_1_d(1)];
coefficient_b_1=[coefficient_1_a(2);coefficient_1_d(2)];
data_1=[R2_1,coefficient_a_1,coefficient_b_1];


f11=figure(11);
f11.WindowState = 'maximized';

cnames = {'R2','Coeff. a','Coeff. b'};
rnames = {'a and b','d'};
t1 = uitable(f11,'Data',data_1,...
            'ColumnName',cnames,...
            'RowName',rnames,...
            'ColumnWidth',{73});

subplot(8,4,28),plot(3)
pos1 = get(subplot(8,4,28),'position');
delete(subplot(8,4,28))
set(t1,'units','normalized')
set(t1,'position',pos1)
subplot(1,1,1),plot(Theoretical_force(1),calculated_force_1(1),'o')
hold on
for i=2:(n-1)
    plot(Theoretical_force(i),calculated_force_1(i),'o')
end
title(['Comparison between calculated effort and theorical effort
```

```
     in the first position of the' ancor])
xlabel('Theoretical effort (kN)')
ylabel('Calculated effort (kN)')
plot(Theoretical_force_a,inter_forces_1_a)
plot(Theoretical_force_d,inter_forces_1_d)
legend(larray,'Location','northeastoutside','NumColumns',2)
grid on
set(gca,'Fontsize',20)
whereToStore=fullfile(Directorypath,['Comparison between calculated
            effort and theorical effort in the first position of
            the ' ancor '.fig']);
saveas(gcf, whereToStore);
hold off



R2_2=[R_square_2_a;R_square_2_d];
coefficient_a_2=[coefficient_2_a(1);coefficient_2_d(1)];
coefficient_b_2=[coefficient_2_a(2);coefficient_2_d(2)];
data_2=[R2_2,coefficient_a_2,coefficient_b_2];


f12=figure(12);
f12.WindowState = 'maximized';

cnames = {'R2','Coeff. a','Coeff. b'};
rnames = {'a and b','d'};
t2 = uitable(f12,'Data',data_2,...
            'ColumnName',cnames,...
            'RowName',rnames,...
            'ColumnWidth',{73});

subplot(8,4,28),plot(3)
pos2 = get(subplot(8,4,28),'position');
delete(subplot(8,4,28))
set(t2,'units','normalized')
set(t2,'position',pos2)
subplot(1,1,1),plot(Theoretical_force(1),calculated_force_2(1),'o')
hold on
for i=2:(n-1)
    plot(Theoretical_force(i),calculated_force_2(i),'o')
end
title(['Comparison between calculated effort and theorical effort
     in the first position of the' ancor])
xlabel('Theoretical effort (kN)')
ylabel('Calculated effort (kN)')
plot(Theoretical_force_a,inter_forces_2_a)
```

```
plot(Theoretical_force_d,inter_forces_2_d)
legend(larray,'Location','northeastoutside','NumColumns',2)
grid on
set(gca,'Fontsize',20)
whereToStore=fullfile(Directorypath,['Comparison between calculated
             effort and theorical effort in the second position of
             the ' ancor '.fig']);
saveas(gcf, whereToStore);
hold off



R2_3=[R_square_3_a;R_square_3_d];
coefficient_a_3=[coefficient_3_a(1);coefficient_3_d(1)];
coefficient_b_3=[coefficient_3_a(2);coefficient_3_d(2)];
data_3=[R2_3,coefficient_a_3,coefficient_b_3];


f13=figure(13);
f13.WindowState = 'maximized';

cnames = {'R2','Coeff. a','Coeff. b'};
rnames = {'a and b','d'};
t3 = uitable(f13,'Data',data_3,...
             'ColumnName',cnames,...
             'RowName',rnames,...
             'ColumnWidth',{73});

subplot(8,4,28),plot(3)
pos3 = get(subplot(8,4,28),'position');
delete(subplot(8,4,28))
set(t3,'units','normalized')
set(t3,'position',pos3)
subplot(1,1,1),plot(Theoretical_force(1),calculated_force_3(1),'o')
hold on
for i=2:(n-1)
    plot(Theoretical_force(i),calculated_force_3(i),'o')
end
title(['Comparison between calculated effort and theorical effort
     in the first position of the' ancor])
xlabel('Theoretical effort (kN)')
ylabel('Calculated effort (kN)')
plot(Theoretical_force_a,inter_forces_3_a)
plot(Theoretical_force_d,inter_forces_3_d)
legend(larray,'Location','northeastoutside','NumColumns',2)
grid on
set(gca,'Fontsize',20)
whereToStore=fullfile(Directorypath,['Comparison between calculated
```

```
            effort and theorical effort in the second position of
            the ' ancor '.fig']);
saveas(gcf, whereToStore);
hold off
%% Creep

considered_effort=100;      %kN
considered_effort_string='100';

opts = spreadsheetImportOptions("NumVariables", 1);

% Specify sheet and range
opts.Sheet = "Feuil1";
opts.DataRange = "A5:A4078";

% Specify column names and types
opts.VariableNames = "Times";
opts.VariableTypes = "double";
cwd=pwd;
cd('Excel')
% Import the data
time_eff = readtable("F2 - bis.xlsx", opts, "UseExcel", false);
time_eff = table2array(time_eff);
cd(cwd)
wanted_entries=[8  ,9,21,23,24,51];
wanter_time=[40,110,1220,1440,1520,4000];
n1=length(wanted_entries);
wanted_effort=ones(n1,1)*considered_effort;
strains(:,1)=MatFO(:,1);
for i=1:n1
    strains(:,(i+1))=MatFO(:,wanted_entries(i));
end


for i=1:n1
    wanted_forces(:,(i))=F(:,wanted_entries(i)-1);
end


wanted_stresses(:,1)=T(:,1);
for i=1:n1
    wanted_stresses(:,(i+1))=T(:,wanted_entries(i));
end

wanted_T_fit(:,1)=T_fit(:,1);
for i=1:n1
    wanted_T_fit(:,(i+1))=T_fit(:,wanted_entries(i));
end
```

```
wanted_legend=lgarray(wanted_entries);
data_a_and_b=a_and_b(:,wanted_entries-1);

f14=figure(14);
f14.WindowState = 'maximized';
rnames = {'a','b'};
t = uitable(f14,'Data',data_a_and_b,...
            'ColumnName',wanted_legend,...
            'RowName',rnames,...
            'ColumnWidth',{62});
subplot(4,3,12),plot(3)
pos = get(subplot(10,3,30),'position');
delete(subplot(4,3,12))
set(t,'units','normalized')
set(t,'position',pos)
subplot(4,1,[1,2,3]),plot(strains(:,1),strains(:,2))
hold on
for i=3:(n1+1)
    plot(strains(:,1),strains(:,i))
end
title(['Fiber optic results for the ' ancor ' at
     ' considered_effort_string ' kN ']);
xlabel('Length(m)')
ylabel('Strain(μm/m)')
legend(wanted_legend,'Location','northwest','NumColumns',2)
grid on
set(gca,'Fontsize',20)
subplot(4,3,10),plot(time_eff,eff)
hold on
plot(wanter_time,wanted_effort,'x')
title(['Time-Effort'])
xlabel('time(s)')
ylabel('Effort(kN)')
set(gca,'Fontsize',20)
whereToStore=fullfile(Directorypath,['Fiber optic results for
            the ' ancor ' at ' considered_effort_string 'kN.fig']);
saveas(gcf, whereToStore);
hold off


f15=figure(15)
f15.WindowState = 'maximized';
rnames = {'a','b'};
t = uitable(f15,'Data',data_a_and_b,...
            'ColumnName',wanted_legend,...
            'RowName',rnames,...
            'ColumnWidth',{62});
```

```
subplot(4,3,12),plot(3)
pos = get(subplot(10,3,30),'position');
delete(subplot(4,3,12))
set(t,'units','normalized')
set(t,'position',pos)
subplot(4,1,[1,2,3]),plot(l,wanted_forces(:,1))
hold on
for i=2:(n1)
    plot(l,wanted_forces(:,i))
end
title(['Force results for the  ' ancor ' at
     ' considered_effort_string ' kN '])
xlabel('Length(m)')
ylabel('Force (kN)')
legend(wanted_legend,'Location','northeast','NumColumns',2)
grid on
set(gca,'Fontsize',20)
subplot(4,3,10),plot(time_eff,eff)
hold on
plot(wanter_time,wanted_effort,'x')
title(['Time-Effort'])
xlabel('time(s)')
ylabel('Effort(kN)')
set(gca,'Fontsize',20)
whereToStore=fullfile(Directorypath,['Force results for the  ' ancor ' at
            '  considered_effort_string 'kN.fig']);
saveas(gcf, whereToStore);
hold off


f16=figure(16)
f16.WindowState = 'maximized';
rnames = {'a','b'};
t = uitable(f16,'Data',data_a_and_b,...
            'ColumnName',wanted_legend,...
            'RowName',rnames,...
            'ColumnWidth',{62});
subplot(4,3,12),plot(3)
pos = get(subplot(10,3,30),'position');
delete(subplot(4,3,12))
set(t,'units','normalized')
set(t,'position',pos)
subplot(4,1,[1,2,3]),plot(wanted_stresses(:,1),wanted_stresses(:,2))
hold on
for i=3:(n1+1)
    plot(wanted_stresses(:,1),wanted_stresses(:,i))
end
title(['Fiber optic results for the ' ancor ' at
```

```
     ' considered_effort_string ' kN '])
xlabel('Length(m)')
ylabel('Shear stress (MPa)')
legend(wanted_legend,'Location','northeast','NumColumns',2)
grid on
set(gca,'Fontsize',20)
subplot(4,3,10),plot(time_eff,eff)
hold on
plot(wanter_time,wanted_effort,'x')
title(['Time-Effort'])
xlabel('time(s)')
ylabel('Effort(kN)')
set(gca,'Fontsize',20)
whereToStore=fullfile(Directorypath,['Fiber optic results for the
            ' ancor ' at ' considered_effort_string 'kN.fig']);
saveas(gcf, whereToStore);
hold off

wanted_legend1=[wanted_legend,wanted_legend],


f17=figure(17)
f17.WindowState = 'maximized';

subplot(4,1,[1,2,3]),plot(wanted_stresses(:,1),wanted_stresses(:,2),'--')
hold on
for i=3:(n1+1)
    plot(wanted_stresses(:,1),wanted_stresses(:,i),'--')
end
plot(wanted_T_fit(:,1),wanted_T_fit(:,2))
for i=3:(n1+1)
    plot(wanted_T_fit(:,1),wanted_T_fit(:,i))
end
title(['Shear stress fitting results for the ' ancor ' at
     ' considered_effort_string ' kN '])
xlabel('Length(m)')
ylabel('Shear stress (MPa)')
legend(wanted_legend1,'Location','northeast','NumColumns',2)
grid on
set(gca,'Fontsize',20)
subplot(4,3,10),plot(time_eff,eff)
hold on
plot(wanter_time,wanted_effort,'x')
title(['Time-Effort'])
xlabel('time(s)')
ylabel('Effort(kN)')
set(gca,'Fontsize',20)
whereToStore=fullfile(Directorypath,['Shear stress fitting results
```

```
            for the ' ancor ' at ' considered_effort_string 'kN.fig']);
saveas(gcf, whereToStore);
hold off

%% Creep

considered_effort2=200;      %kN
considered_effort_string2='200';



wanted_entries2=[18,19,50];
wanter_time2=[900, 1000 , 3900 ];
n2=length(wanted_entries2);
wanted_effort2=ones(n2,1)*considered_effort2;
strains2(:,1)=MatFO(:,1);
for i=1:n2
    strains2(:,(i+1))=MatFO(:,wanted_entries2(i));
end


for i=1:n2
    wanted_forces2(:,(i))=F(:,wanted_entries2(i)-1);
end


wanted_stresses2(:,1)=T(:,1);
for i=1:n2
    wanted_stresses2(:,(i+1))=T(:,wanted_entries2(i));
end

wanted_T_fit2(:,1)=T_fit(:,1);
for i=1:n2
    wanted_T_fit2(:,(i+1))=T_fit(:,wanted_entries2(i));
end

wanted_legend2=lgarray(wanted_entries2);
data_a_and_b2=a_and_b(:,wanted_entries2-1);

f18=figure(18);
f18.WindowState = 'maximized';
rnames = {'a','b'};
t = uitable(f18,'Data',data_a_and_b2,...
            'ColumnName',wanted_legend2,...
            'RowName',rnames,...
            'ColumnWidth',{125});
subplot(4,3,12),plot(3)
pos = get(subplot(10,3,30),'position');
```

```
delete(subplot(4,3,12))
set(t,'units','normalized')
set(t,'position',pos)
subplot(4,1,[1,2,3]),plot(strains2(:,1),strains2(:,2))
hold on
for i=3:(n2+1)
    plot(strains2(:,1),strains2(:,i))
end
title(['Fiber optic results for the ' ancor ' at
     ' considered_effort_string2 ' kN '])
xlabel('Length(m)')
ylabel('Strain(μm/m)')
legend(wanted_legend2,'Location','northwest','NumColumns',2)
grid on
set(gca,'Fontsize',20)
subplot(4,3,10),plot(time_eff,eff)
hold on
plot(wanter_time2,wanted_effort2,'x')
title(['Time-Effort'])
xlabel('time(s)')
ylabel('Effort(kN)')
set(gca,'Fontsize',20)
whereToStore=fullfile(Directorypath,['Fiber optic results for the
            ' ancor ' at ' considered_effort_string2 'kN.fig']);
saveas(gcf, whereToStore);
hold off


f19=figure(19);
f19.WindowState = 'maximized';
rnames = {'a','b'};
t = uitable(f19,'Data',data_a_and_b2,...
            'ColumnName',wanted_legend2,...
            'RowName',rnames,...
            'ColumnWidth',{125});
subplot(4,3,12),plot(3)
pos = get(subplot(10,3,30),'position');
delete(subplot(4,3,12))
set(t,'units','normalized')
set(t,'position',pos)
subplot(4,1,[1,2,3]),plot(l,wanted_forces2(:,1))
hold on
for i=2:(n2)
    plot(l,wanted_forces2(:,i))
end
title(['Force results for the  ' ancor ' at
     ' considered_effort_string2 ' kN '])
xlabel('Length(m)')
```

```
ylabel('Force (kN)')
legend(wanted_legend2,'Location','northwest','NumColumns',2)
grid on
set(gca,'Fontsize',20)
subplot(4,3,10),plot(time_eff,eff)
hold on
plot(wanter_time2,wanted_effort2,'x')
title(['Time-Effort'])
xlabel('time(s)')
ylabel('Effort(kN)')
set(gca,'Fontsize',20)
whereToStore=fullfile(Directorypath,['Force results for the  ' ancor ' at
            '  considered_effort_string2 'kN.fig']);
saveas(gcf, whereToStore);
hold off


f20=figure(20);
f20.WindowState = 'maximized';
rnames = {'a','b'};
t = uitable(f20,'Data',data_a_and_b2,...
            'ColumnName',wanted_legend2,...
            'RowName',rnames,...
            'ColumnWidth',{125});
subplot(4,3,12),plot(3)
pos = get(subplot(10,3,30),'position');
delete(subplot(4,3,12))
set(t,'units','normalized')
set(t,'position',pos)
subplot(4,1,[1,2,3]),plot(wanted_stresses2(:,1),wanted_stresses2(:,2))
hold on
for i=3:(n2+1)
    plot(wanted_stresses2(:,1),wanted_stresses2(:,i))
end
title(['Fiber optic results for the ' ancor ' at
     ' considered_effort_string2 ' kN ']) 
xlabel('Length(m)')
ylabel('Shear stress (MPa)')
legend(wanted_legend2,'Location','northwest','NumColumns',2)
grid on
set(gca,'Fontsize',20)
subplot(4,3,10),plot(time_eff,eff)
hold on
plot(wanter_time2,wanted_effort2,'x')
title(['Time-Effort'])
xlabel('time(s)')
ylabel('Effort(kN)')
set(gca,'Fontsize',20)
```

```
whereToStore=fullfile(Directorypath,['Fiber optic results for the
             ' ancor ' at ' considered_effort_string2 'kN.fig']);
saveas(gcf, whereToStore);
hold off

wanted_legend3=[wanted_legend2,wanted_legend2];
f21=figure(21);
f21.WindowState = 'maximized';

set(t,'units','normalized')
set(t,'position',pos)
subplot(4,1,[1,2,3]),plot(wanted_stresses2(:,1),wanted_stresses2(:,2),'--')
hold on
for i=3:(n2+1)
    plot(wanted_stresses2(:,1),wanted_stresses2(:,i),'--')
end
plot(wanted_T_fit2(:,1),wanted_T_fit2(:,2))
for i=3:(n2+1)
    plot(wanted_T_fit2(:,1),wanted_T_fit2(:,i))
end
title(['Shear stress fitting results for the ' ancor ' at
     ' considered_effort_string2 ' kN ']);
xlabel('Length(m)')
ylabel('Shear stress (MPa)')
legend(wanted_legend3,'Location','northwest','NumColumns',2)
grid on
set(gca,'Fontsize',20)
subplot(4,3,10),plot(time_eff,eff)
hold on
plot(wanter_time2,wanted_effort2,'x')
title(['Time-Effort'])
xlabel('time(s)')
ylabel('Effort(kN)')
set(gca,'Fontsize',20)
whereToStore=fullfile(Directorypath,['Shear stress fitting results for the
' ancor ' at ' considered_effort_string2 'kN.fig']);
saveas(gcf, whereToStore);
hold off

%% Comparison
strains3=[strains,strains2(:,2:n2+1)];
n3=n2+n1;
data_a_and_b3=[data_a_and_b,data_a_and_b2];
wanted_legend3=[wanted_legend,wanted_legend2];
f22=figure(22);
f22.WindowState = 'maximized';
rnames = {'a','b'};
t = uitable(f22,'Data',data_a_and_b3,...
```

```
            'ColumnName',wanted_legend3,...
            'RowName',rnames,...
            'ColumnWidth',{41});
subplot(4,3,12),plot(3)
pos = get(subplot(10,3,30),'position');
delete(subplot(4,3,12))
set(t,'units','normalized')
set(t,'position',pos)
subplot(4,1,[1,2,3]),plot(strains3(:,1),strains3(:,2))
hold on
for i=3:(n3+1)
    plot(strains3(:,1),strains3(:,i))
end
title(['Fiber optic results for the ' ancor ' at
       ' considered_effort_string ' kN and
       ' considered_effort_string2 ' kN '])
xlabel('Length(m)')
ylabel('Strain(μm/m)')
legend(wanted_legend3,'Location','northwest','NumColumns',2)
grid on
set(gca,'Fontsize',20)
subplot(4,3,10),plot(time_eff,eff)
hold on
plot(wanter_time,wanted_effort,'x')
plot(wanter_time2,wanted_effort2,'x')
title(['Time-Effort'])
xlabel('time(s)')
ylabel('Effort(kN)')
set(gca,'Fontsize',20)
whereToStore=fullfile(Directorypath,['Fiber optic results for the
            ' ancor ' at ' considered_effort_string ' kN and
            ' considered_effort_string2 ' kN .fig']);
saveas(gcf, whereToStore);
hold off

wanted_forces3=[wanted_forces,wanted_forces2];

f23=figure(23);
f23.WindowState = 'maximized';
rnames = {'a','b'};
t = uitable(f23,'Data',data_a_and_b3,...
            'ColumnName',wanted_legend3,...
            'RowName',rnames,...
            'ColumnWidth',{41});
subplot(4,3,12),plot(3)
pos = get(subplot(10,3,30),'position');
delete(subplot(4,3,12))
set(t,'units','normalized')
```

```
set(t,'position',pos)
subplot(4,1,[1,2,3]),plot(l,wanted_forces3(:,1))
hold on
for i=2:(n3)
    plot(l,wanted_forces3(:,i))
end
title(['Force results for the  ' ancor ' at ' considered_effort_string '
     kN and ' considered_effort_string2 ' kN '])
xlabel('Length(m)')
ylabel('Force (kN)')
legend(wanted_legend3,'Location','northeast','NumColumns',2)
grid on
set(gca,'Fontsize',20)
subplot(4,3,10),plot(time_eff,eff)
hold on
plot(wanter_time,wanted_effort,'x')
plot(wanter_time2,wanted_effort2,'x')
title(['Time-Effort'])
xlabel('time(s)')
ylabel('Effort(kN)')
set(gca,'Fontsize',13)
whereToStore=fullfile(Directorypath,['Force results for the  ' ancor '
            at '  considered_effort_string ' kN and
            ' considered_effort_string2 ' kN.fig']);
saveas(gcf, whereToStore);
hold off

wanted_stresses3=[wanted_stresses,wanted_stresses2(:,2:n2+1)];

f24=figure(24);
f24.WindowState = 'maximized';
rnames = {'a','b'};
t = uitable(f24,'Data',data_a_and_b3,...
            'ColumnName',wanted_legend3,...
            'RowName',rnames,...
            'ColumnWidth',{41});
subplot(4,3,12),plot(3)
pos = get(subplot(10,3,30),'position');
delete(subplot(4,3,12))
set(t,'units','normalized')
set(t,'position',pos)
subplot(4,1,[1,2,3]),plot(wanted_stresses3(:,1),wanted_stresses3(:,2))
hold on
for i=3:(n3+1)
    plot(wanted_stresses3(:,1),wanted_stresses3(:,i))
end
title(['Fiber optic results for the ' ancor ' at
     ' considered_effort_string ' kN and '
```

```
      considered_effort_string2 ' kN '])
xlabel('Length(m)')
ylabel('Shear stress (MPa)')
legend(wanted_legend3,'Location','northeast','NumColumns',2)
grid on
set(gca,'Fontsize',20)
subplot(4,3,10),plot(time_eff,eff)
hold on
plot(wanter_time,wanted_effort,'x')
plot(wanter_time2,wanted_effort2,'x')
title(['Time-Effort'])
xlabel('time(s)')
ylabel('Effort(kN)')
set(gca,'Fontsize',20)
whereToStore=fullfile(Directorypath,['Fiber optic results for the
            ' ancor ' at ' considered_effort_string ' kN and
            ' considered_effort_string2 ' kN.fig']);
saveas(gcf, whereToStore);
hold off

wanted_legend4=[wanted_legend3,wanted_legend3];
wanted_T_fit3=[wanted_T_fit,wanted_T_fit2(:,2:n2+1)];

f25=figure(25);
f25.WindowState = 'maximized';

subplot(4,1,[1,2,3]),plot(wanted_stresses3(:,1),wanted_stresses3(:,2),'--')
hold on
for i=3:(n3+1)
    plot(wanted_stresses3(:,1),wanted_stresses3(:,i),'--')
end
plot(wanted_T_fit3(:,1),wanted_T_fit3(:,2))
for i=3:(n3+1)
    plot(wanted_T_fit3(:,1),wanted_T_fit3(:,i))
end
title(['Shear stress fitting results for the ' ancor ' at
     ' considered_effort_string ' kN and '
     considered_effort_string2 ' kN '])
xlabel('Length(m)')
ylabel('Shear stress (MPa)')
legend(wanted_legend4,'Location','northeast','NumColumns',2)
grid on
set(gca,'Fontsize',20)
subplot(4,3,10),plot(time_eff,eff)
hold on
plot(wanter_time,wanted_effort,'x')
plot(wanter_time2,wanted_effort2,'x')
title(['Time-Effort'])
```

```
xlabel('time(s)')
ylabel('Effort(kN)')
set(gca,'Fontsize',20)
whereToStore=fullfile(Directorypath,['Shear stress fitting results
            for the ' ancor ' at ' considered_effort_string ' kN
            and ' considered_effort_string2 ' kN.fig']);
saveas(gcf, whereToStore);
hold off
```

Where the function DATA used is the following:

```
classdef DATA <handle

    %-------------------------------------------------------------------------

    properties
        Area;            %Area of the rockbolt (in mm^2)
        Es;              %Young Modulus of the steel (in GPa)
        Matrice_FO=[];   %Matrix with fiber optic data for the ancorage
        Lengthfree;      %Free length of steel (in m)
        legendarray=[];  %it's a string array for plotting the graphic's
                         legend
        effort=[];       % an array with the efforts
        displacement=[]; % an array with displacement ( we will use
                         élongation-enfoncement)
        ancorage;        %it's a string with the number of the ancorage
                         and the location
        diameter;        %steel bar diameter (in mm)
        Directorypath;   %the folder where the plots will be saved
    end

    %-------------------------------------------------------------------------

    methods
        %---------------------------COSTRUTTORE-----------------------------
        function this=DATA(A,E,MatFO,freeL,lgarray,eff,disp,ancor,ds,
                        Directorypath)
            this.Area=A;
            this.Es=E;
            this.Matrice_FO=MatFO;
            this.Lengthfree=freeL;
            this.legendarray=lgarray;
            this.effort=eff;
            this.displacement=disp;
            this.ancorage=ancor;
            this.diameter=ds;
            this.Directorypath=Directorypath;
```

```
end
%-------------------------------------------------------------------

%-------------------Selection of fiber optic data------------------

function [M]=datacleaning(this)
    length_vector=this.Matrice_FO(:,1);
    nmat=size(this.Matrice_FO);

    f1=figure(1);
    f1.WindowState = 'maximized';
    plot(length_vector,this.Matrice_FO(:,2))
    hold on
    for i=3:nmat(2)
        c=this.Matrice_FO(:,i);
        plot(length_vector,c)
    end
    title(['Fibre optic results for the ' this.ancorage])
    %title('Fiber optic results')
    xlabel('Length(m)')
    ylabel('Strain(µm/m)')
    legend(this.legendarray(2:nmat(2)),'Location','northwest'
          ,'NumColumns',2)
    grid on
    set(gca,'Fontsize',20)
    if this.Directorypath~=0
        whereToStore=fullfile(this.Directorypath,['Fiber optic
                    results for the ' this.ancorage '.fig']);
        saveas(gcf, whereToStore);
    end



    hold off




    prompt="Where does the significative data of the
           Fiber Optic start?";
    significative_L1=input(prompt);
    data_OK1=length_vector>significative_L1;
    prompt="Where does the significative data of the
           Fiber Optic end?";
    significative_L2=input(prompt);
    data_OK2=length_vector<significative_L2;
    data_OK_first=data_OK1+data_OK2;
    data_OK=data_OK_first>1;
```

```
    data_OK_entries=find(data_OK);
    M=this.Matrice_FO(data_OK_entries,:);


    f2=figure(2);
    f2.WindowState = 'maximized';
    plot(M(:,1),M(:,2))
    hold on
    for i=3:nmat(2)
        c=M(:,i);
        plot(M(:,1),c)
    end
    title(['Significative Fibre optic results for the
         ' this.ancorage])
    %title('Significative Fiber optic results')
    xlabel('Length(m)')
    ylabel('Strain(µm/m)')
    legend(this.legendarray(2:nmat(2)),'Location','northeast'
          ,'NumColumns',2)
    grid on
    set(gca,'Fontsize',20)
    whereToStore=fullfile(this.Directorypath,['Significative
                Fiber optic results for the ' this.ancorage
                '.fig']);
    saveas(gcf, whereToStore);
    hold off
end


%-----------------------------------------------------------------
%-----------------------Tangential stresses-----------------------

function [F,T,a_and_b]=stresses(this)
    Mat=this.datacleaning;
    l=Mat(:,1);
    m=size(Mat);
    T=zeros(m(1)-2,m(2));
    T(:,1)=Mat(2:(m(1)-1),1);
    n=m(2);
    Mat1=Mat(:,2:n);
    F=this.Es*this.Area*Mat1*10^(-6);  %µstrains so we moltiply
                                        for E-6
    FF=F;                              % for non smoothed force
    n1=size(F);
    T1=T;
    for i=1:n1(2)
        forza=F(:,i);
        forza=ksr(l,forza,0.024,n1(1));
```

```
    vettoreforza=forza.f;
    F(:,i)=vettoreforza;
end
for i=1:n1(2)
    c=F(:,i);
    tt=zeros(n1(1)-2,1);
    numero=length(tt);
    for j=1:(n1(1)-2)
        tt(j)=(c(j+2)-c(j))/(pi*this.diameter*
              ((l(j+2)-l(j))*1000));
    end
    T1(:,i+1)=-tt;
    regressionett=ksr(T(:,1),tt,0.024,numero);
    tt=regressionett.f;
    for ii=1:n1(1)-2
        tt(ii)=-(tt(ii));
    end
    T(:,i+1)=tt;
end
r=isnan(T);
ffff=find(r);
T(ffff)=0;
lunghezze_t=T(:,1);
vettore_legenda(1:(n-1))=this.legendarray(2:n);
vettore_legenda(n:((2*n)-2))=this.legendarray(2:n);



f3=figure(3);
f3.WindowState = 'maximized';
plot(l,F(:,1))
hold on
for i=2:n1(2)
    plot(l,F(:,i))
end
plot(l,FF(:,1),':')
for i=2:n1(2)
    plot(l,FF(:,i),':')
end
title(['Force results for the ' this.ancorage])
xlabel('Length(m)')
ylabel('Force (kN)')
legend(vettore_legenda,'Location','northeast','NumColumns',2)
grid on
set(gca,'Fontsize',20)
whereToStore=fullfile(this.Directorypath,['Force results
             for the ' this.ancorage '.fig']);
saveas(gcf, whereToStore);
```

```
hold off

f4=figure(4);
f4.WindowState = 'maximized';
plot(lunghezze_t,T(:,2))
hold on
for i=3:n
    plot(lunghezze_t,T(:,i))
end
title(['Shear stress results for the ' this.ancorage])
xlabel('Length(m)')
ylabel('Shear stress (Mpa)')
legend(this.legendarray(2:n),'Location','northeast',
      'NumColumns',2)
grid on
set(gca,'Fontsize',20)
whereToStore=fullfile(this.Directorypath,['Shear stress
             results for the ' this.ancorage '.fig']);
saveas(gcf, whereToStore);
hold off



a_and_b=zeros(2,m(2)-1);

prompt="Where is the initial point of the interpolation?";
L1_fit=input(prompt);
values_to_fit=T(:,1)>L1_fit;
values=find(values_to_fit);
n_values=length(values);
T_fit=zeros(n_values,m(2));
T_fit(:,1)=lunghezze_t(values);
for i=2:m(2)
    p=T(values,i);
    f=fit(T_fit(:,1),p,'exp1');
    t1=feval(f,T_fit(:,1));
    T_fit(:,i)=t1;
    ab=coeffvalues(f);
    a_and_b(:,i-1)=ab;
end


f5=figure(5);
f5.WindowState = 'maximized';
plot(lunghezze_t(values),T_fit(:,2))
hold on
```

```
    for i=3:n
        plot(lunghezze_t(values),T_fit(:,i))

    end
    title(['Shear stress fitting results for the ' this.ancorage])
    plot(lunghezze_t,T(:,2),':')

    for i=3:n
        plot(lunghezze_t,T(:,i),':')
    end
    xlabel('Length(m)')
    ylabel('Shear stress (Mpa)')
    legend(vettore_legenda,'Location','northeast','NumColumns',3)
    grid on
    set(gca,'Fontsize',20)
    whereToStore=fullfile(this.Directorypath,['Shear stress
                fitting results for the ' this.ancorage '.fig']);
    saveas(gcf, whereToStore);
    hold off
end

%-----------------------------------------------------------------

%-----------------------Effort displacement-----------------------
function [real_disp]=real_displacement(this)
    %displacement_steel=this.effort*(((this.Matrice_FO(1,1))*1000)
                        /(this.Area*this.Es));
    displacement_steel=this.effort*(((this.Lengthfree)*1000)/
                       (this.Area*this.Es));
    % now we consider that from 0kN to the first charge the
    % displacement is linear and with the steel stiffness we
    % calcule this displacement and then add it to all the other
    % points
    linear_displacement= this.effort(1)*(((this.Lengthfree)*1000)/
                        (this.Area*this.Es));
    corrected_displacement=this.displacement+linear_displacement;
    real_disp=corrected_displacement-displacement_steel;

    figure(6)
    plot(corrected_displacement,this.effort)
    hold on
    plot(displacement_steel,this.effort)
    plot(real_disp,this.effort)
    prompt = 'What is the Lower Boundary for the linear
             approximation :';
    LB = input(prompt)
    prompt = 'What is the Upper Boundary for the linear :';
    UB = input(prompt)
```

```
            disp_max=max(real_disp);
            eff_max=max(this.effort);
            entry=find(eff_max==this.effort);
            growing_displacement=real_disp;
            sizevector=length(growing_displacement);    % questo é fatto
                                                         perché a volte
                                                         indicando un
                                                         intervallo si
                                                         prende anche il
                                                        tratto decrescente
            growing_displacement(entry:sizevector)=0;
            FI=find(((growing_displacement>LB).*(
                    growing_displacement<UB))>0);
            p=polyfit(growing_displacement(FI,1),this.effort(FI,1),1);
            displacements_for_linear_interpolation=linspace(0,disp_max,20);
            efforts_for_linear_interpolation=
                                displacements_for_linear_interpolation*p(1);

            plot(displacements_for_linear_interpolation,
                 efforts_for_linear_interpolation)
            title(['Effort displacement for the ' this.ancorage])
            xlabel('Displacement (mm)')
            ylabel('Effort (kN)')
            legend('Gross displacement','Theoretical steel displacement',
                  'Net displacement','Linear approximation')
            whereToStore=fullfile(this.Directorypath,['Effort displacement
                         for the ' this.ancorage '.fig']);
            saveas(gcf, whereToStore);
            hold off
        end
        %-------------------------------------------------------------------
    end

    %-----------------------------------------------------------------------

end
```

15 Bibliography

References

[1] Benmokrane, B., Chennouf, A. & Mitri, H.S., (1995) Laboratory evaluation of cement-based grouts and grouted rock anchors. *International Journal of Rock Mechanics and Mining Sciences & Geomechanics Abstracts*, 32(7), pp.633–642.

[2] Blanco Martín, L., (2012) *Ph.D. thesis: Theorical and experimental study of fully grouted rockbolts and cablebolts under axial loads*. Ecole nationale supérieure des mines de Paris.

[3] BS 8081, (1989) *Code of practice for ground anchorages*, BSI.

[4] Chunlin Li, (2017) *Rockbolting principles and applications*.

[5] Ducan C. Wyllie, (2018) *Rock Slope Engineering, Civil Applications* .

[6] Eligehausen, Popov & Bertéro, (1983). Local bond stress-slip relationships of deformed bars under generalized excitations. *Proceedings of the 7th European Conference on Earthquake Engineering*.

[7] Farmer, I.W., (1975) Stress distribution along a resin grouted rock anchor. *International Journal of Rock Mechanics and Mining Sciences & Geomechanics Abstracts*.

[8] Fib (1993) *Model Code 1990*, Thomas Telford Ltd.

[9] Fib (2000) *Bond of Reinforcement in Concrete: State-of-the-art report*, International Federation for structural Concrete(fib), 2000.

[10] Fib (2013) *Model Code for Concrete structures 2010*, International Federation for structural Concrete(fib), 2012.

[11] Ho Dac An, (2017) *Ph.D. thesis: Comportement axial des ancrages passifs scellés au rocher : étude de l'interface barre-scellement et modélisation*. IFSTTAR.

[12] Hoek, E. & Brown, E.T., (1980). Empirical strength criterion for rock masses. *Journal of Geotechnical and Geoenvironmental Engineering*.

[13] Hyett A.J., Bawden W.F., Macsporran G.R., and Moosavi M., (1995) A Constitutive Law for Bond Failure of Fully-grouted Cable Bolts Using a Modified Hoek Cell. *International Journal of Rock Mechanics and Mining Sciences & Geomechanics Abstracts*.

[14] Hyett, A.J., Bawden, W.F. & Reichert, R.D., (1992). The effect of rock mass confinement on the bond strength of fully grouted cable bolts. *International Journal of Rock Mechanics and Mining Sciences & Geomechanics Abstracts*.

[15] Haberfield, C.M. & Baycan, S., (1997). Field Performance of the Grout/Rock Interface in Anchors. *In Ground anchorages and anchored structures*.

[16] Kılıc, A., Yasar, E. & Atis, C.., (2003). Effect of bar shape on the pull-out capacity of fully-grouted rockbolts. *Tunnelling and Underground Space Technology.*

[17] Li, C. & Stillborg, (1999). Analytical models for rock bolts. *International Journal of Rock Mechanics and Mining Sciences.*

[18] Moosavi, M. & Bawden, W.F., (2003). Shear strength of Portland cement grout. *Cement and Concrete Composites.*

[19] Moosavi, M., Jafari, A. & Khosravi, A., (2005). Bond of cement grouted reinforcing bars under constant radial pressure. *Cement and Concrete Composites.*

[20] NF P 94-444, (2002). *Essai statique d'arrachement, sous un effort axial de traction, d'un ancrage scellé dans un massifs rocheux*, AFNOR.

[21] Pellet, F. & Egger, (1996).Analytical Model for the Mechanical Behaviour of Bolted Rock Joints Subjected to Shearing. *Rock Mechanics and Rock Engineering.*

[22] Tepfers, R., (1979). Cracking of concrete cover along anchored deformed reinforcing bars. *Magazine of Concrete Research.*

[23] Windsor, C.R., (1979). Rock reinforcement systems. *International Journal of Rock Mechanics and Mining Sciences.*